



5-2020

## Thermochemical Conversion of Biomass to Renewable Fuels

Naijia Hao

*University of Tennessee*, [nhao@vols.utk.edu](mailto:nhao@vols.utk.edu)

Follow this and additional works at: [https://trace.tennessee.edu/utk\\_graddiss](https://trace.tennessee.edu/utk_graddiss)

---

### Recommended Citation

Hao, Naijia, "Thermochemical Conversion of Biomass to Renewable Fuels. " PhD diss., University of Tennessee, 2020.

[https://trace.tennessee.edu/utk\\_graddiss/5827](https://trace.tennessee.edu/utk_graddiss/5827)

This Dissertation is brought to you for free and open access by the Graduate School at TRACE: Tennessee Research and Creative Exchange. It has been accepted for inclusion in Doctoral Dissertations by an authorized administrator of TRACE: Tennessee Research and Creative Exchange. For more information, please contact [trace@utk.edu](mailto:trace@utk.edu).

To the Graduate Council:

I am submitting herewith a dissertation written by Naijia Hao entitled "Thermochemical Conversion of Biomass to Renewable Fuels." I have examined the final electronic copy of this dissertation for form and content and recommend that it be accepted in partial fulfillment of the requirements for the degree of Doctor of Philosophy, with a major in Chemical Engineering.

Arthur J. Ragauskas, Major Professor

We have read this dissertation and recommend its acceptance:

Bamin Khomami, Nourredine Abdoulmoumine, Paul Frymier

Accepted for the Council:

Dixie L. Thompson

Vice Provost and Dean of the Graduate School

(Original signatures are on file with official student records.)

**Thermochemical Conversion of Biomass to Renewable Fuels**

**A Dissertation Presented for the**

**Doctor of Philosophy**

**Degree**

**The University of Tennessee, Knoxville**

**Naijia Hao**

**May 2020**

To my beloved husband, Dr. Lingyun Ren, without whom this dissertation  
would have been completed earlier.

## ACKNOWLEDGEMENTS

First I would like to thank my advisor Dr. Arthur J. Ragauskas, for his support and encouragement during the past five years. Without his thoughtful mind, vast knowledge, and patient guidance, this dissertation will not be possible. The attitude towards research I learned from him will greatly help me in my future career. I would also appreciate my committee members Dr. Bamin Khomami, Dr. Paul Frymier, and Dr. Nour Abdoulmoumine, for their thoughtful advice and comments to my PhD studies.

I want to thank my colleagues at University of Tennessee and Oak Ridge National Laboratory, especially Dr. Yunqiao Pu, Dr. Chang Geun Yoo, Dr. Mi Li, Dr. Qining Sun, Dr. Xianzhi Meng, Dr. Thomas Moore, Dr. Somnath Shinde, Dr. Rosemary Le, Dr. Yun-Yan Wang, Dr. Qiong Wu, Dr. Jia Wang, Dr. Chen Huang, Luna Liang, Shuyang Zhang, and Nathan Byrant. Without your support and help on my research projects, I could not finish this PhD dissertation.

I also appreciate my collaborators Dr. Zhi-Hua Liu from Texas A&M University, Dr. Kristina Iisa from National Renewable Energy Laboratory, Dr. Selhan Karagoz and Dr. Kubiley Tekin from Karabük University, Dr. Sushil Adhikari from Auburn University, for their insightful support on the research projects during the past years.

I want to express my deepest gratitude to my husband Dr. Lingyun Ren and my parents Lin Wang and Jinghao Hao. The love, understanding, and support from family makes this dissertation possible.

I would especially like to appreciate sisters and brothers from Chinese Christian Fellowship at University of Tennessee for the strong support all the time and the wonderful time we shared together.

Finally, I would like to acknowledge the Chemical and Biomolecular Engineering department at University of Tennessee for the support during the past years. Go Vols!

## ABSTRACT

Valorization of lignocellulosic biomass to renewable biofuels provides a promising solution to address growing concerns regarding energy security and environmental issues. Researchers are breaking the chemical & engineering barriers to efficiently convert lignocellulosic biomass to liquid fuels. The thermochemical deconstruction strategies can be classified into three categories: gasification, pyrolysis, and liquefaction. Pyrolysis and liquefaction are called selective thermal processing which generate liquid products via depolymerization and fragmentation of biomass feedstocks. This dissertation focuses on the pyrolysis and liquefaction of whole lignocellulosic biomass. The liquid products (called bio-oil) are inherently chemical complex, of high oxygen content, low heating values compared to commercial heavy fuels, thus need treatments towards the thermal process to enhance the bio-oil's properties.

This dissertation thoroughly examined thermochemical conversion strategies to generate high quality bio-oils as a fuel precursor. Two major aspects in this dissertation include 1) the biomass pyrolysis and 2) solvent liquefaction. Two strategies have been examined to promote the pyrolysis oils' qualities, including pretreatment and *ex-situ* catalysis. Two different strategies have been studied during the one-pot liquefaction including the metal chloride additive and a bi-catalyst system of Pd/C and water tolerant Lewis acid.

The major objectives in this dissertation are listed below:

- Investigated the pretreatment effect on the biomass structure and the subsequent pyrolysis oil's properties (Chapter III)

- Optimized the auto-hydrolysis pretreatment on biomass towards the “optimal” pyrolysis oils as a fuel precursor (Chapter IV)
- Accomplished the *ex-situ* upgrading of the pyrolysis oils using metal oxide catalysts (Chapter V)
- Evaluate the structures of the *ex-situ* catalytic upgraded pyrolysis vapors from a bench-scale unit (Chapter VI)
- Examined the one-step liquefaction of biomass in solvent to produce bio-oils using metal chlorides (Chapter VII)
- Explored the bi-catalyst system performance in one-step liquefaction of biomass (Chapter VIII)



# TABLE OF CONTENTS

|   |    |
|---|----|
| CHAPTER I: LITERARURE REVIEW .....  | 1  |
| 1.1 Problem statement.....  | 2  |
| 1.2 Thermochemical conversion of biomass .....  | 4  |
| 1.2.1 Overview of pyrolysis oils .....  | 4  |
| 1.2.2 Upgrading technologies applied in pyrolysis.....  | 5  |
| 1.2.3 One-pot liquefaction approach.....  | 7  |
| 1.3 Characterization methods of bio-oils .....  | 25 |
| 1.3.1 NMR analysis of bio-oils .....  | 25 |
| 1.3.2 GC-MS analysis of bio-oils .....  | 40 |
| 1.3.3 GPC analysis of bio-oils .....  | 42 |
| 1.3.3 Elemental composition, heating value and other analysis techniques of bio-oils<br>..... | 43 |
| CHAPTER II: EXPERIMENTAL METHODS AND MATERIALS .....  | 44 |
| 2.1 Materials and chemicals.....  | 45 |
| 2.1.1 Biomass feedstocks.....   | 45 |
| 2.1.2 Reagents.....   | 46 |
| 2.2 Experimental procedure .....  | 46 |
| 2.2.1 Autohydrolysis pretreatment of biomass .....  | 46 |
| 2.2.2 Small scale pyrolysis.....  | 47 |
| 2.2.3 Large scale pyrolysis.....  | 47 |
| 2.2.4 Hydrothermal liquefaction in water and organic solvents .....                           | 49 |

|  |    |
|--|----|
| 2.2.5 Catalyst preparation .....                                       | 50 |
| 2.2.6 Upgrading reaction of the bio-oil.....                           | 50 |
| 2.3 Analytical instrumentation.....                                    | 51 |
| 2.3.1 Characterization of biomass feedstocks.....                      | 51 |
| 2.3.2 SEM analysis of char .....                                       | 52 |
| 2.3.3 Characterization of bio-oils.....                                | 52 |
| 2.3.4 XRD analysis of catalyst.....                                    | 55 |
| <br>CHAPTER III: INITIAL EXAMINATION OF AUTOHYDROLYSIS                 |    |
| PRETREATMENT EFFECT ON BIOMASS FEEDSTOCKS.....                         | 56 |
| 3.1 Introduction.....  | 57 |
| 3.2 Experimental methods .....   | 60 |
| 3.2.1 Material and sample preparation.....                             | 60 |
| 3.2.2 Equipments and experimental procedures .....                     | 60 |
| 3.2.3 Characterization of biomass and bio-oils.....                    | 61 |
| 3.3 Results and discussion .....                                       | 61 |
| 3.3.1 Compositional analysis of pine wood feedstocks .....             | 61 |
| 3.3.2 CP/MAS <sup>13</sup> C NMR analysis of pine wood feedstocks..... | 62 |
| 3.3.3 FT-IR analysis of pine wood feedstocks.....                      | 63 |
| 3.3.4 Yields of pyrolysis products .....                               | 64 |
| 3.3.5 <sup>31</sup> P NMR analysis of heavy oils .....                 | 65 |
| 3.3.6 HSQC NMR analysis of heavy oils .....                            | 67 |
| 3.4 Conclusion .....   | 67 |

|   |        |
|---|--------|
| CHAPTER IV: EXPERIMENTAL CONDITION OPTIMIZATION OF<br>AUTOHYDROLYSIS PRETREATMENT EFFECT ON BIOMASS FEEDSTOCKS .. | 69     |
| 4.1 Introduction.....   | 70     |
| 4.2 Experimental methods .....  | 72     |
| 4.2.1 Material and sample preparation.....  | 72     |
| 4.2.2 Equipments and experimental procedures .....  | 72     |
| 4.2.3 Characterization of biomass and bio-oils.....   | 72     |
| 4.3 Results and discussion .....  | 73     |
| 4.3.1 Chemical composition analysis.....  | 73     |
| 4.3.2 CP/MAS <sup>13</sup> C NMR analysis .....   | 74     |
| 4.3.3 Yield distribution of the pyrolysis products.....   | 75     |
| 4.3.4 Molecular weight analysis of the bio-oils.....  | 76     |
| 4.3.5 <sup>31</sup> P NMR analysis of the bio-oils .....  | 77     |
| 4.3.6 HSQC NMR analysis of the bio-oils .....   | 78     |
| 4.4 Conclusion .....  | 79     |
| <br>CHAPTER V: EX-SITU UPGRADING OF BIO-OILS OVER METAL OXIDE<br>CATALYSTS .....                                  | <br>80 |
| 5.1 Introduction.....   | 81     |
| 5.2 Experimental methods .....  | 83     |
| 5.2.1 Material and sample preparation.....  | 83     |
| 5.2.2 Equipments and experimental procedures .....  | 83     |
| 5.2.3 Characterization of biomass and bio-oils.....   | 83     |

|  |     |
|--|-----|
| 5.3 Results and discussion .....   | 83  |
| 5.3.1 Effect of reaction temperature .....                               | 83  |
| 5.3.2 Effect of reaction time and catalyst loading .....                 | 86  |
| 5.3.3 Molecular weight distribution and hydroxyl group distribution..... | 87  |
| 5.4 Conclusion .....   | 88  |
| <br>CHAPTER VI: EX-SITU CATALYTIC UPGRADING OF PYROLYSIS VAPORS          |     |
| OVER H-ZSM5 .....  | 89  |
| 6.1 Introduction.....  | 90  |
| 6.2 Experimental methods .....   | 93  |
| 6.2.1 Material and sample preparation.....                               | 93  |
| 6.2.2 Equipments and experimental procedures .....                       | 93  |
| 6.2.3 Characterization of biomass and bio-oils.....                      | 93  |
| 6.3 Results and discussion .....   | 94  |
| 6.3.1 Oil yields and oxygen content.....                                 | 94  |
| 6.3.2 Oil analysis.....  | 97  |
| 6.4 Conclusion .....   | 104 |
| <br>CHAPTER VII: ONE-POT TRANSFORMATION OF BIOMASS TO BIO-OILS OVER      |     |
| METAL CHLORIDES .....  | 106 |
| 7.1 Introduction.....  | 107 |
| 7.2 Experimental methods .....   | 110 |
| 7.2.1 Material and sample preparation.....                               | 110 |
| 7.2.2 Equipments and experimental procedures .....                       | 110 |

|   |     |
|---|-----|
| 7.2.3 Characterization of biomass and bio-oils.....   | 110 |
| 7.3 Results and discussion .....  | 110 |
| 7.3.1 Deconstruction product distributions.....   | 110 |
| 7.3.2 GC-MS analysis of bio-oil composition .....   | 113 |
| 7.3.3 HSQC NMR analysis of bio-oils .....   | 114 |
| 7.3.4 <sup>31</sup> P NMR analysis of bio-oils .....  | 116 |
| 7.3.5 Elemental analysis of feedstocks, bio-oils, and solid residues .....  | 117 |
| 7.3.6 Boiling point distributions of bio-oils.....  | 118 |
| 7.4 Conclusion .....  | 118 |
| <br>CHAPTER VIII: ONE-POT TRANSFORMATION OF BIOMASS TO BIO-OILS<br>OVER Pd/C AND WATER TOLERANT LEWIS ACIDS ..... |     |
| 8.1 Introduction.....   | 121 |
| 8.2 Experimental methods .....  | 124 |
| 8.2.1 Material and sample preparation.....  | 124 |
| 8.2.2 Equipments and experimental procedures .....  | 124 |
| 8.2.3 Characterization of biomass and bio-oils.....   | 124 |
| 8.3 Results and discussion .....  | 124 |
| 8.3.1 Product yields from the liquefaction in water and ethanol .....   | 124 |
| 8.3.3 Boiling point distribution of bio-oils .....  | 128 |
| 8.3.4 GC-MS analysis of bio-crudes.....   | 129 |
| 8.4 Conclusion .....  | 133 |
| <br>CHAPTER IX: OVERALL CONCLUSIONS .....   |     |
|   | 134 |

|  |     |
|--|-----|
| CHAPTER X: RECOMMENDATIONS FOR FUTURE WORKS..... | 139 |
| LIST OF REFERENCES.....                          | 142 |
| APPENDIX .....                                   | 194 |
| VITA.....  | 324 |

## LIST OF TABLES

|  |     |
|--|-----|
| Table 1. Comparison of physical properties of bio-oils from thermal processing and heavy fuel oils. <sup>9-11</sup> .....  | 195 |
| Table 2. Characteristics of bio-oil and challenges for its applications. <sup>10, 12, 14-15</sup> .....  | 196 |
| Table 3. Typical bio-oil upgrading methods and characteristics. <sup>22, 28-31</sup> .....   | 197 |
| Table 4. Summary of non-catalytic and catalytic degradation of lignin in ethanol. ....   | 198 |
| Table 5. Yields (mg/g of lignin) of the products from ethanol degradation without and with Kraft lignin added at 280 °C for 240 min over 0.5 g Mo/Al <sub>2</sub> O <sub>3</sub> catalyst with initial 0.1 MPa of N <sub>2</sub> and 100 mL of ethanol. <sup>65</sup> (Adapted from Ref.65 with the permission from American Chemistry Society.) ..... | 200 |
| Table 6. Summary of non-catalytic and catalytic degradation of lignocellulosic biomass in ethanol.....   | 201 |
| Table 7. NMR techniques applied in bio-oil analysis.....   | 202 |
| Table 8. Composition of the <sup>1</sup> H NMR Chemical Shift Integration Regions of Bio-oil. <sup>98, 102, 104-105</sup> .....  | 210 |
| Table 9. Comparison of <sup>13</sup> C NMR Chemical Shift Integration Regions of Bio-oil. <sup>102, 104</sup> .....  | 211 |
| Table 10. Chemical Shift Assignments for Bio-oils after Derivatization with TMDP Using NHND as an Internal Standard in a <sup>31</sup> P NMR Spectrum. <sup>119</sup> .....  | 212 |
| Table 11. The detected monomeric phenols from the decomposition of lignin in ethanol at 350 °C. <sup>51</sup> .....  | 213 |

|  |     |
|--|-----|
| Table 12. Molecular weight of bio-oils from pyrolysis and liquefaction reported in the literature.....   | 214 |
| Table 13. The proximate and ultimate analyses of the grape seeds.....  | 215 |
| Table 14. The proximate and ultimate analyses of the fir woods.....  | 216 |
| Table 15. An example of the relation between the temperature and pressure during the autohydrolysis pretreatment.....  | 217 |
| Table 16. Comparison of the lignin and carbohydrates contents of untreated (control) and autohydrolysis pretreated pine wood (wt%). .....  | 218 |
| Table 17. Assignment of FT-IR spectra in a region of 1750 – 1000 cm <sup>-1</sup> for pine wood samples.....   | 219 |
| Table 18. Structural detection of the individual compounds in bio-oils by GC-MS analysis.....  | 220 |
| Table 19. Effect of B:C ratio and upgrading temperature on MW distribution of bio-oil. ....  | 223 |
| Table 20. Identified compounds in bio-oils from the hydrothermal processing of grape seed without and with additive (MgCl <sub>2</sub> :TiCl <sub>4</sub> ). (T=300 °C, t=30 min, PH <sub>2int</sub> =2 MPa).....          | 224 |
| Table 21. Identified compounds in bio-oils from the supercritical ethanol processing of grape seed without and with additive (MgCl <sub>2</sub> :TiCl <sub>4</sub> ). (T=300 °C, t=30 min, PH <sub>2int</sub> =2 MPa)..... | 226 |
| Table 22. Quantitative analysis of hydroxyl groups in bio-oils produced from hydrothermal and supercritical ethanol processing.....  | 230 |



|  |     |
|--|-----|
| Table 23. Elemental composition (wt% and atomic ratio) of raw material, bio-oils and solid residues from the hydrothermal liquefaction of grape seed with (MgCl <sub>2</sub> :TiCl <sub>4</sub> ). (T:300 °C, t=30 min, PH <sub>2</sub> int.=2 MPa) .....                          | 231 |
| Table 24. Elemental composition (wt% and atomic ratio) of raw material, bio-oils, and solid residues from supercritical ethanol processing of grape seed without and with additive (MgCl <sub>2</sub> :TiCl <sub>4</sub> ). (T=300 °C, t=30 min, PH <sub>2</sub> int.=2 MPa) ..... | 232 |
| Table 25. Boiling point distributions (wt%) of the crude bio-oils obtained from hydrothermal liquefaction and supercritical ethanol processing of grape seed without and with the additives. (T=300 °C, t=30 min, PH <sub>2</sub> int.=2 MPa).....                                 | 233 |
| Table 26. Bio-oil and solid residue yields produced from fir wood without and with catalyst at different concentrations of the raw material through HTL and SCEL processing. (T=300 °C, t=30 min) .....  | 234 |
| Table 27. Elemental composition (wt% and atomic ratio) of raw metarial, bio-oils and solid residues from the HTL of fir wood without and with catalysts. (T=300 °C, t=30 min).....   | 235 |
| Table 28. Elemental composition (wt% and atomic ratio) of raw metarial, bio-oils and solid residues from SCEL processing of fir wood without and with catalysts. (T=300 °C, t=30 min) .....  | 236 |
| Table 29. Boiling point distributions (wt%) of the crude bio-oils obtained from HTL and SCEL processing of fir wood without and with catalysts. (T=300 °C, t=30 min)..   | 237 |
| Table 30. Identified compounds in bio-oils from the HTL of fir wood without and with catalysts. (T=300 °C, t=30 min).....  | 238 |

Table 31. Identified compounds in bio-oils from the SCEL processing of fir wood  
without and with catalysts. (T=300 °C, t=30 min, PH<sub>2</sub>int.=2 MPa)..... 240

## LIST OF FIGURES

|  |     |
|--|-----|
| Figure 1. The main components of lignocellulosic biomass. <sup>6</sup> (Reproduced from Ref.6 with permission from John Wiley & Sons).....   | 243 |
| Figure 2. Monomeric phenols from degradation of lignin in ethanol. <sup>6</sup> (Reproduced from Ref.6 with permission from John Wiley & Sons).....  | 244 |
| Figure 3. Schematic representation of the Guerbet reaction for primary alcohols. <sup>71</sup> (Reproduced from Ref. 71 with permission from The Royal Society of Chemistry) .....   | 245 |
| Figure 4. Acid-catalyzed decomposition of cellulose in ethanol. <sup>78</sup> (Reproduced from Ref. 78 with permission from Elsevier).....   | 246 |
| Figure 5. <sup>1</sup> H NMR spectra of a) oxidized bio-oil, b) partially deoxygenated bio-oil, c) fully deoxygenated bio-oil, and d) a commercial gasoline-jet fuel-diesel mixture. <sup>107</sup> (Reproduced from Ref. 107 with permission from Elsevier) ..... | 247 |
| Figure 6. <sup>13</sup> C NMR spectra of the crude bio-oil, water-soluble extract, neutral extract, phenolic extract, and organic acids extract. <sup>115</sup> (Reproduced from Ref. 115 with the permission from The Royal Society of Chemistry) .....           | 248 |
| Figure 7. Reactions between TMDP and various hydroxyl functional groups and the <sup>31</sup> P NMR assignment of phosphitylated compounds. <sup>119</sup> (Reprinted from Ref. 119 with permission from American Chemistry Society) .....                         | 249 |
| Figure 8. Quantitative <sup>31</sup> P NMR spectra of a) the crude oil, b) the bio-oil upgraded at 250 °C and c) the bio-oil upgraded at 300 °C. <sup>122</sup> (Reproduced from Ref. 122 with permission from The Royal Society of Chemistry) .....               | 250 |

|   |     |
|---|-----|
| Figure 9. HSQC spectra of bio-oil, sugar monomer standards, and anhydrosugar standards. Gray: bio-oil; Red: sugar monomer standards (i.e., glucose, galactose, mannose, xylose, and arabinose; Green: anhydrosugars (i.e., levoglucosan, cellobiosan, and celotriosan). <sup>131</sup> (Reprinted from Ref. 131 with the permission from American Chemical Society) ..... | 251 |
| Figure 10. HSQC spectra of bio-oil and its fractions. (a) raw bio-oil; (b) water-insoluble fraction; (c) water-insoluble and CH <sub>2</sub> Cl <sub>2</sub> -soluble fraction; (d) water-insoluble and CH <sub>2</sub> Cl <sub>2</sub> -insoluble fraction. <sup>131</sup> (Reprinted from Ref. 131 with the permission from American Chemical Society) .....            | 252 |
| Figure 11. Total ion chromatogram of bio-oil produced after 30 min at 350 °C with a formic acid to lignin mass ratio of 1.5. The lignin source was CSAHL. <sup>59</sup> (Reprinted from Ref. 59 with permission from Elsevier) .....  | 253 |
| Figure 12. Illustration of the bench-top small scale pyrolysis unit. <sup>136</sup> (Adapted from Ref. 136 with permission from American Chemistry Society) .....   | 254 |
| Figure 13. Illustration of the fluidized bed reactor system. <sup>137</sup> (Reproduced from Ref. 137 with permission from American Chemistry Society) .....  | 255 |
| Figure 14. CP/MAS <sup>13</sup> C NMR spectra of untreated pine wood (bottom) and autohydrolysis pretreated pine wood (top) samples.....  | 256 |
| Figure 15. FTIR spectra of untreated pine wood and autohydrolysis pretreated pine wood samples.....   | 257 |
| Figure 16. Yields distributions of pyrolysis products obtained from untreated and autohydrolysis pretreated pine wood samples under 400 °C, 500 °C, and 600 °C (wt%).....   | 258 |

|  |     |
|--|-----|
| Figure 17. $^{31}\text{P}$ NMR spectra of heavy oils produced from untreated and autohydrolysis pretreated pine wood at 400 °C, 500 °C, and 600 °C. (the c denotes control, the p denotes pretreatment).....   | 259 |
| Figure 18. Acid-OH contents in heavy oils obtained from untreated and autohydrolysis pretreated pine wood samples under 400 °C, 500 °C, and 600 °C. ....   | 260 |
| Figure 19. Aliphatic-OH contents in heavy oils obtained from untreated and autohydrolysis pretreated pine wood samples under 400 °C, 500 °C, and 600 °C. ....  | 261 |
| Figure 20. Non-condensed hydroxyl group contents in heavy oils obtained from untreated and autohydrolysis pretreated pine wood samples under 400 °C, 500 °C, and 600 °C. ( <sup>a</sup> : G: guaiacyl type phenolic OH; C: catechol type phenolic OH; P: <i>p</i> -hydroxy-phenyl OH).....               | 262 |
| Figure 21. C <sub>5</sub> substituted condensed hydroxyl group contents in heavy oils obtained from untreated and autohydrolysis pretreated pine wood samples under 400 °C, 500 °C, and 600 °C. ....   | 263 |
| Figure 22. HSQC spectra of levoglucosan contents in bio-oils.....  | 264 |
| Figure 23. HSQC spectra of methoxy groups in bio-oils.....   | 265 |
| Figure 24. Compositional analysis of the sugarcane bagasse before and after the autohydrolysis pretreatment.....   | 266 |
| Figure 25. CP/MAS $^{13}\text{C}$ NMR spectra (from bottom to top) of untreated sugarcane bagasse and sugarcane bagasse samples pretreated for 180 °C -10 min, 180 °C -40 min, 200 °C -40 min. (*the signals in cellulose region 105-62 ppm overlap with the signals from lignin and hemicellulose)..... | 267 |

|  |     |
|--|-----|
| Figure 26. Yield distribution of the bio-oils from the untreated and pretreated sugarcane bagasse pyrolyzed at 400, 500, and 600 °C based on the mass of pretreated biomass.<br>.....  | 268 |
| Figure 27. Yield distribution of the bio-oils from untreated and pretreated sugarcane bagasse pyrolyzed at 400, 500, and 600 °C based on the mass of original biomass.<br>(mass yields of the three pretreatment conditions 180 °C – 10 min, 180 °C - 40 min, 200 °C - 40 min are 72.50%, 64.40%, and 57.29%, respectively)..... | 269 |
| Figure 28. Molecular weight distribution of the bio-oils pyrolyzed from the untreated and pretreated sugarcane bagasse. ....   | 270 |
| Figure 29. Aliphatic OH contents in the bio-oils pyrolyzed from the untreated and pretreated sugarcane bagasse. ....   | 271 |
| Figure 30. C <sub>5</sub> substituted phenolic OH contents in the bio-oils pyrolyzed from the untreated and pretreated sugarcane bagasse. ....   | 272 |
| Figure 31. Non-condensed phenolic OH contents in the bio-oils pyrolyzed from the untreated and pretreated sugarcane. ....  | 273 |
| Figure 32. Acid contents in the bio-oils pyrolyzed from the untreated and pretreated sugarcane bagasse. ....   | 274 |
| Figure 33. HSQC NMR spectra and assignments of methoxy groups in the sugarcane bagasse bio-oils pyrolyzed at 500 °C. (black area: unassigned).....   | 275 |
| Figure 34. HSQC NMR spectra and assignments of each C-H bond of levoglucosan in the sugarcane bagasse bio-oils pyrolyzed at 500 °C. (black area: unassigned).....  | 276 |
| Figure 35. HSQC NMR spectra and assignments of aliphatic C-H bonds in the sugarcane bagasse bio-oils pyrolyzed at 500 °C. (black area: unassigned).....  | 277 |

|   |     |
|---|-----|
| Figure 36. HSQC NMR spectra and assignments of aromatic C-H bonds in the sugarcane bagasse bio-oils pyrolyzed at 500 °C. (black area: unassigned).....  | 278 |
| Figure 37. X-ray spectra of the copper doped hydrotalcite precursor. ....   | 279 |
| Figure 38. Effect of (a) varied reaction temperature, 8 h, B:C = 1:1; (b) varied reaction time, 275 °C, B:C = 1:1; (c) varied B:C ratio, 275 °C, 8h. ....   | 280 |
| Figure 39. GC-MS results of the bio-oils at 250 °C and 300 °C (8 h, B:C = 1:1).....   | 282 |
| Figure 40. An example of the GC spectra of the upgraded bio-oil. (300 °C, 8 h, B:C = 1:1).....  | 283 |
| Figure 41. <sup>1</sup> H NMR analysis of bio-oils. (8 h, B:C = 1:1).....   | 284 |
| Figure 42. <sup>1</sup> H NMR integration results of bio-oils. (8 h, B:C = 1:1).....  | 285 |
| Figure 43. HSQC NMR analysis of bio-oils. (8 h, B:C = 1:1).....   | 286 |
| Figure 44. <sup>31</sup> P NMR analysis of bio-oils. (275 °C, B:C = 1:1).....   | 287 |
| Figure 45. <sup>31</sup> P NMR integration results of bio-oils (a) 8 h, B:C = 1:1; (b) 275 °C, B:C = 1:1; (c) 275 °C, 4h.....   | 288 |
| Figure 46. Non-condensed OH of bio-oils. (275 °C, B:C = 1:1, 4h).....   | 290 |
| Figure 47. <sup>31</sup> P NMR integration results of non-condensed OH (a) 8 h, B:C = 1:1; (b) 275 °C, B:C = 1:1; (c) 275 °C, 4h. ....  | 291 |
| Figure 48. GPC curve of bio-oils. (275 °C, B:C = 1:1, 4h).....  | 293 |
| Figure 49. GPC curve of bio-oils (a) 8 h, B:C = 1:1; (b) 275 °C, B:C = 1:1; (c) 275 °C, 4h. ....  | 294 |
| Figure 50. Carbon yields (g C in product/g C in feed) for CFP products and oil organic oxygen content. (a) function of the biomass-to-catalyst mass (B:C) ratio with upgrading temperature of 550°C, and b) function of the upgrading temperature ratio |     |

|   |     |
|---|-----|
| with B:C of 1.4. Two of the experiments were repeated (550° and 600°C at B:C 1.4) and the average is shown for these experiments. The replicate carbon yields for all products were within one percentage point of the average. ....  | 296 |
| Figure 51. a) GC-MS analysis and b) <sup>13</sup> C NMR analysis of the oils. The values are weight-averaged results of analyses of bottom and top oils. The GC-MS analysis shows the mass selectivity of the identified fraction, and the identified compounds constituted 25-43% of the oil. Other in GC-MS includes peaks for furans and ketones. .... | 297 |
| Figure 52. The effect of (a) upgrading temperature, and (b) B:C ratio on various hydroxyl groups of bio-oil. The values are weight-averaged results of analyses of bottom and top oils. ....  | 298 |
| Figure 53. The effect of (a) upgrading temperature, and (b) B:C ratio on total aromatic hydroxyl groups in bio-oil. The values are weight-averaged results of analyses of bottom and top oils. ....   | 299 |
| Figure 54. Molecular weight distributions for non-catalytic fast pyrolysis oil (FP) and bottom CFP oils. (a) different upgrading temperatures, and (b) for different biomass:catalyst (B:C) ratios. ....  | 300 |
| Figure 55. Detailed structures of assignments for HSQC-NMR analysis of bio-oil .....  | 301 |
| Figure 56. The aliphatic C-H bonds in the HSQC NMR spectra for selected bottom fractions of CFP oils. (a) 500°C B:C 1.4 bottom, (b) 600°C B:C 1.4 bottom, (c) 550°C B:C 1.0 bottom, (d) 550°C B:C 1.8 bottom. ....  | 302 |
| Figure 57. Aromatic C-H bonds in the HSQC NMR spectra. (a) 500°C B:C 1.4 bottom, (b) 600°C B:C 1.4 bottom, (c) 550°C B:C 1.0 bottom, (d) 550°C B:C 1.8 bottom.  | 303 |



|  |     |
|--|-----|
| Figure 58. Methoxyl group in the HSQC NMR spectra. (a) 500°C B:C 1.4 bottom, (b) 600°C B:C 1.4 bottom, (c) 550°C B:C 1.0 bottom, (d) 550°C B:C 1.8 bottom. ....  | 304 |
| Figure 59. Bio-oil and solid residue yields obtained in hydrothermal medium. (a) residence time=30 min, without additives; (b) T=300 °C, without additives; (c) T=300 °C, residence time=30 min, with and without additives .....  | 305 |
| Figure 60. Bio-oil and solid residue yields obtained in supercritical ethanol.(a) residence time=30 min, without additives; (b) T=300 °C, without additives; (c) T=300 °C, residence time=30 min, with and without additives .....   | 307 |
| Figure 61. Chemical class composition of identified compounds in bio-oils from the hydrothermal processing of grape seed without and with MgCl <sub>2</sub> :TiCl <sub>4</sub> . (T=300 °C, t=30 min, PH <sub>2int.</sub> =2 MPa) .....  | 309 |
| Figure 62. Chemical class composition of identified compounds in bio-oils from the supercritical ethanol processing of grape seed without and with MgCl <sub>2</sub> :TiCl <sub>4</sub> . (T=300 °C, t=30 min, PH <sub>2int.</sub> =2 MPa).....  | 310 |
| Figure 63. Comparison of the aromatic regions of the HSQC NMR spectra of the deconstruction products. (a) non-additive ethanol processing; (b) non-additive hydrothermal processing; (c) ethanol processing with 4 mmol MgCl <sub>2</sub> /TiCl <sub>4</sub> ; (d) hydrothermal processing with 4 mmol MgCl <sub>2</sub> /TiCl <sub>4</sub> .....  | 311 |
| Figure 64. Comparison of the aliphatic regions of the HSQC NMR spectra of the deconstruction products. (a) non-additive ethanol processing; (b) non-additive hydrothermal processing; (c) ethanol processing with 4 mmol MgCl <sub>2</sub> /TiCl <sub>4</sub> ; (d) hydrothermal processing with 4 mmol MgCl <sub>2</sub> /TiCl <sub>4</sub> ..... | 312 |

|  |     |
|--|-----|
| Figure 65. Effect of liquefaction temperature on bio-oil and solid residue yields derived from non-catalytic liquefaction of fir wood. (a) HTL media, and (b) SCEL media (PH <sub>2int.</sub> =2 MPa, t=30 min)..... | 313 |
| Figure 66. Effect of residence time on bio-oil and solid residue yields derived from non-catalytic liquefaction of fir wood. (a) HTL media, and (b) SCEL media. (T=300 °C, PH <sub>2int.</sub> =2 MPa).....          | 314 |
| Figure 67. Chemical class composition of the identified compounds in the bio-crudes from HTL.....  | 315 |
| Figure 68. Chemical class composition of the identified compounds in the bio-crudes from SCEL.....   | 316 |
| Figure 69. Plausible major reaction pathways for the liquefaction of lignocellulose in water and ethanol.....  | 317 |
| Figure 70. Aromatic C-H bonds in bio-oils from control HTL.....  | 318 |
| Figure 71. Aromatic C-H bonds in bio-oils from control SCEL.....   | 319 |
| Figure 72. Aromatic C-H bonds in bio-oils from HTL over Pd/C.....  | 320 |
| Figure 73. Aromatic C-H bonds in bio-oils from SCEL over Pd/C.....   | 321 |
| Figure 74. Aromatic C-H bonds in bio-oils from HTL over Pd/C + Sm(OTf) <sub>3</sub> .....  | 322 |
| Figure 75. Aromatic C-H bonds in bio-oils from SCEL over Pd/C + Sm(OTf) <sub>3</sub> .....   | 323 |

## CHAPTER I: LITERATURE REVIEW

Sections 1.1, 1.2.1, and 1.3.1 of the Chapter I was originally published by Naijia Hao, Haoxi Ben, Chang Geun Yoo, Sushil Adhikari, and Arthur J. Ragauskas and reprinted with permission from American Chemistry Society:

Hao, N.; Ben, H.; Yoo, C. G.; Adhikari, S.; Ragauskas, A. J., Review of NMR Characterization of Pyrolysis Oils. *Energy & Fuels* **2016**, 30 (9), 6863-6880.

The author Haoxi Ben is from Southeast University. The author Chang Geun Yoo is from Oak Ridge National Laboratory. The author Sushil Adhikari is from Auburn University. The author Arthur J. Ragauskas is from University of Tennessee and Oak Ridge National Laboratory. Naijia Hao drafted the review manuscript. Haoxi Ben, Chang Geun Yoo, Sushil Adhikari, and Arthur J. Ragauskas revised the review manuscript.

Section 1.2.3 of the Chapter I was originally published by Kubilay Tekin, Naijia Hao, Selhan Karagoz, and Arthur J. Ragauskas and reprinted with permission from Wiley:

Tekin, K.; Hao, N.; Karagoz, S.; Ragauskas, A. J., Ethanol: A Promising Green Solvent for the Deconstruction of Lignocellulose. *ChemSusChem* **2018**, 11 (20), 3559-3575.

The authors Kubilay Tekin and Selhan Karagoz are from Karabük University. The author Arthur J. Ragauskas is from University of Tennessee and Oak Ridge National Laboratory. Naijia Hao drafted the part regarding the characterization of the liquefaction products from biomass.

## 1.1 Problem statement

Developing viable green energy technologies is imperative because of environmental issues related to fossil fuel usage.<sup>1-3</sup> Utilization of biomass has been introduced as a solution towards the development of sustainable and green energy platforms.<sup>4</sup> Lignocellulosic biomass is a complex composite primarily comprising three principle components: cellulose (35-50%), hemicellulose (20-35%), and lignin (10-25%).<sup>5</sup> Figure 1 presents the typical structure of these components.<sup>6</sup> All the figures and tables in this dissertation are presented in the Appendix.

Besides these three main components, biomass also has minor components including ash, protein, and other extractives, whose concentrations widely vary depending on the feedstocks. Lignocellulosic biomass is an attractive feedstock for biofuels because it is relatively inexpensive, abundant, avoids the “food or fuel” argument and is a renewable source of carbon. Typical bio-resources for biofuels include energy crops, such as switchgrass, miscanthus, poplar, and energy cane, or biomass residues from agriculture and forestry operations.<sup>7</sup> The U.S. Department of Energy and U.S. Department of Agriculture established a national goal that lignocellulosic biomass will supply 5% of the nation’s power by 2020 and 20% of its transportation fuels and 25% of its chemicals by 2030. This goal is approximately equivalent to 30% of the petroleum consumption in the year 2005.<sup>8</sup> There are three major biomass deconstruction approaches: gasification, hydrolysis and selective thermal processing. Unlike the former two approaches, selective thermal processing creates liquid bio-oil products with high complexity. The physical properties of bio-oils from pyrolysis and liquefaction are compared with that of heavy fuel oils and the information are summarized in Table 1.<sup>9-11</sup> The major limitations of the pyrolysis oils and

liquefaction oils are due to the high oxygen content. The high oxygen content leads to two problems regarding bio-oil's applications as a transportation fuel substitute. First the high oxygen content resulted in the lower heating values of the bio-oils, especially for the pyrolysis oils. Second the high acidity of the bio-oils makes the oils hard to be processed in the current biorefinery infrastructure as the corrosion of the steels can not be avoided. To reduce the oxygen numbers in the bio-oils, numerous efforts have been put forwarded and challenges could be lumped into four aspects:

- Lowering the oxygen content in bio-oils has always been the center of research regarding thermal processing of biomass. For example, down-stream catalytic hydrodeoxygenation of the bio-oils has been performed under high pressures (>2000 psi) and subsequently cracking in a fluidized reactor. More efficient strategies towards hydrodeoxygenations need to be proposed and designed.
- Techno-economic evaluation of the thermal processing need to be addressed. The large quantity of the hydrogen consumed during the hydrodeoxygenation reactions needs to be considered. The high cost of noble catalysts and catalyst deactivation problems call for the development of catalysts with a low cost and recycle ability.
- The intrinsic characteristics of the selective thermal processing makes it a challenge for the existing biorefinery infrastructure, for example the high pressure required by the liquefaction and hydrotreating reaction.
- The complexity of the pyrolysis and liquefaction makes it a real challenge to fully understand the underlying mechanisms during the processing. The deep

insight understanding requires advanced wet chemistry characterization techniques and micro kinetic modeling studies.

In this dissertation, we focus on developing chemical strategies to promote the bio-oil's qualities from the selective thermal processing, from bench top reactors to fluidized bed reactors. The detailed chemistry analysis of the bio-oils is another emphasis in this dissertation, to provide a deep understanding regarding the thermal processing instead of empirical evaluation.

## **1.2 Thermochemical conversion of biomass**

### **1.2.1 Overview of pyrolysis oils**

Pyrolysis oil, also known as bio-oil, is a dark-brown, free-flowing liquid product from biomass obtained using assorted pyrolysis processes. The oil is a very complex mixture containing phenolic compounds, carbohydrates, furans, ketones, aldehydes, carboxylic acids, and water.<sup>12-13</sup> Although pyrolysis oil has considerable potential as an alternative fuel, it still has some technical barriers to be overcome. Characteristics of the bio-oil and challenges of its applications are summarized in Table 2.<sup>10, 12, 14-15</sup> Polar oxygen-containing components (e.g., carboxylic acids, hydroxyl groups) cause bio-oils to be immiscible with non-polar transportation fuels. Water from feedstock participates in the pyrolysis reaction and affects the product yields and structures. The water contents of fast pyrolysis oils vary between 15 and 30 wt%, and the presence of water lowers the oil's heating value and causes the delay problem in ignition engines.<sup>15-16</sup> Corrosion problems of the bio-oils are primarily due to carboxylic acids and phenolic compounds, which cause storage and transportation problems.<sup>17</sup> Ortega et al.<sup>18</sup> and others<sup>19-21</sup> have investigated the aging process of bio-oils and have analyzed how their chemical and physical properties

change during aging. Aging experiments resulted in the increase of viscosity, molecular weight, and non-volatile contents of bio-oil samples, because the etherification, esterification, and olefin condensation occurred during aging process.<sup>21</sup> For these reasons, upgrading is a necessary step to convert bio-oils into refinery products (e.g., gasoline, diesel, jet fuel, olefins).

### **1.2.2 Upgrading technologies applied in pyrolysis**

As summarized in section 1.2.1, the pyrolysis oils are subjected to multiple physical and chemical property limitations to be used as a fuel precursor. In the past decade, research works have been focused on the upgrading strategies to solve the bio-oil's problems such high oxygen content and low stability. Bridgwater<sup>22</sup> and others<sup>23-27</sup> have discussed bio-oil upgrading methods. Typical upgrading methods and their characteristics are presented in Table 3.<sup>22, 28-31</sup>

Aforementioned bio-oil upgrading methods are potential solutions for overcoming the challenges of bio-oil applications; however, these methods still need further developments. Structure characteristics of bio-oil products can reveal insight for subsequent upgrading methods; therefore, understanding and selecting a proper analysis method is as important as developing the upgrading methods. In this section, two major upgrading techniques developed in the past decade (hydrotreating and catalytic cracking of the pyrolysis vapors) will be reviewed and discussed.

The hydrotreating reaction of the pyrolysis oils usually requires a separate process carried out after the fast pyrolysis. The reactions involved high temperature (up to 400 °C) and high pressure (up to 20 MPa) and a hydrogen source.<sup>32</sup> The hydrogen is typically

supplied externally or from solvents in a supercritical environment. The oxygen in the bio-oils will be rejected as water in the presence of the catalysts in a hydrotreating reaction.

The catalysts initially tested in the hydrotreating of bio-oils are mainly sulfide CoMo and NiMo with aluminum support. For example, Zhang et al. used Co-Mo-P in upgrading of pyrolysis oils from a fluidized bed reactor. The liquid products were generated from the pyrolysis bed reactor and separated into oil phase and water phase. The oil phase was later subjected into the hydrotreating reaction (360 °C, 2 MPa). The Co-Mo-P treated bio-oil exhibited oil-soluble characteristics.<sup>33</sup> Tang et al. applied Pd/SO<sub>4</sub><sup>2-</sup>/ZrO<sub>2</sub>/SBA-15 catalyst in the hydrotreatment of crude bio-oil in supercritical ethanol.<sup>34</sup> The heating value of the bio-oil was promoted to 20.1 MJ/Kg and only trace amount of char was observed during the reaction. Significant amount of research works are focused on the

The catalysts applied in the catalytic vapor cracking of the pyrolysis vapors could be classified into two categories: mesoporous materials and microporous materials. Zeolite is the most common catalysts applied in the vapor cracking. The zeolite cracking could be coupled inside the pyrolysis operation unit through an *ex-situ* upgrader. Several typical micro- and meso-porous catalysts are discussed below. On-going research works are trying to solve the deactivation of the catalysts and improving the deoxygenation performance of the bio-oil upgrading. Huber's group applied the zeolite in the biomass pyrolysis. With the zeolite participated, the organic vapors went through a series of reactions (e.g., dehydration, isomerization, oligomerization) and gasoline range aromatics were obtained.<sup>35</sup> Almeida's research group studied the ZSM-5' performance on the model compounds representing the oxygenated bio-oil components, such as acetic acid, phenol, and hydroxyacetone.<sup>36</sup> Peng et al. performed the HZSM-5 upgrading of the rice husk pyrolysis oils in supercritical



ethanol.<sup>37</sup> The amount of the acids in the upgraded bio-oils decreased significantly while the ester fractions increased evidently.

### **1.2.3 One-pot liquefaction approach**

Ethanol has been widely applied as a viable solvent for the decomposition of lignocellulosic biomass over the last few decades and is classified as an environmentally preferable green solvent as it is produced by fermenting renewable sources including sugars, starches and lignocellulosics.<sup>38</sup> In comparison with other solvents, ethanol is a relatively low-cost solvent and readily available when incorporated into a second-generation cellulosic ethanol production facility. Substitution of organic solvents with an environmentally favorable solvent for the deconstruction of lignocellulosic biomass is indeed of importance in terms of green chemistry and sustainability. Ethanol has a pronounced enhancement of solubility at the supercritical state, which makes an excellent reaction medium for the decomposition of lignocellulose.<sup>39</sup> The critical temperature and pressure for ethanol are as follows:  $T_c = 240.9\text{ }^\circ\text{C}$ ,  $P_c = 6.14\text{ MPa}$ . Furthermore, supercritical ethanol (Sc-EtOH) is less corrosive and more reactive when compared with supercritical water (SCW).<sup>39</sup> The depolymerization of lignocellulosic biomass in Sc-EtOH benefits from its hydrogen donation ability, high heat transfer efficiency, and it hinders the re-polymerization of unstable fragments of biomass which results in less char formation.<sup>40-</sup>  
<sup>41</sup> Studies regarding the decomposition of lignocellulosic biomass in subcritical/supercritical EtOH without and with catalysts has become a research focus area and herein, non-catalytic and catalytic decomposition of lignocellulosic biomass and its components in ethanol processing are reviewed.

### 1.2.3.1 Deconstruction of lignin in ethanol

Lignin is a natural polymer that is composed of phenylpropane units including coniferyl, sinapyl, or *p*-coumaryl alcohol linked through aryl ether bonds ( $\beta$ -O-4-aryl ether,  $\alpha$ -O-4-aryl ether), and carbon-carbon bonds ( $\beta$ -5-phenylcoumaran, 5-5-biphenyl,  $\beta$ -1-(1,2-diarylpropane) and  $\beta$ - $\beta$ -(Resinol)).<sup>42</sup> Lignin, the most significant non-carbohydrate component in biomass, is found in most terrestrial plants with a content of 15~40%.<sup>43</sup> Wood contains lignin in an approximate range of 25–35 %.<sup>44</sup> The composition and amount of lignin in softwood, hardwood and even in different parts from the same plant is dissimilar.<sup>45</sup> Nonetheless, it is well recognized as a significant future source of renewable oxygenated aromatic hydrocarbons.<sup>46</sup>

Lignin has a rigid and amorphous structure and it is difficult to decompose upon the thermal treatment in the absence of oxygen with thermal degradation studies reporting a broad decomposition range between 350 to 600 °C.<sup>47</sup> Thermal degradation of lignin yields aromatic oxygenates that are being actively investigated as a feedstock for chemical industry or blending with conventional transportation fuels.<sup>48</sup> Jet fuel, a type of aviation fuel, is composed of mixtures of naphtha (C<sub>5</sub>–C<sub>15</sub>) and kerosene (C<sub>9</sub>–C<sub>16</sub>); lignin-derived bio-oil has a high potential to meet the requirements of the carbon chain length of jet fuel.<sup>48</sup> Degradation of lignin in Sc-EtOH produces mainly monomeric phenols. Figure 2 presents examples of the monomeric phenols formed from ethanol processing.<sup>6</sup> Table 4 summarizes the results of Kim et al. investigation into depolymerization of Organosolv lignin produced from poplar wood and the effects of several parameters including temperature (200, 275, and 350 °C), residence time (20, 40, and 60 min), lignin/solvent ratios (50, 100, and 150

g/mL) and initial hydrogen gas pressures (2 and 3 MPa) on the decomposition of lignin. The highest bio-oil yield (94.9 wt%) was obtained at the lowest reaction temperature (200 °C) with a residence time of 20 min and solvent ratio of 100 ml /g lignin, the highest amounts of monomeric phenols were obtained at 350 °C and 40 min and 100 mL/ g lignin (Table 4, entry 1). Depolymerization of Protobind lignin in ethanol was carried out at 200, 250 and 280 °C with residence times of 15, 30 and 45 min under autogenic pressures.<sup>49</sup> The highest bio-oil yield (~81wt%) was obtained at 200 °C for all tested residence times (Table 4, entry 2), increasing the reaction temperature resulted in a decrease in bio-oils. The liquefaction of laboratory prepared lignin from the hydrolysis of red pine sawdust using concentrated sulfuric acid was carried out in EtOH at 293, 300, 333 and 350 °C with a fixed residence time (30 min).<sup>50</sup> The highest bio-oil yield was approximately 30 wt% and obtained at 293 °C (Table 4, entry 3). The bio-oil yield was almost same at between 300 and 333 °C and lower than that of the temperature of 293 °C. The lowest bio-oil yield was obtained at the highest temperature. One can conclude that the temperature of 200 °C is optimal for the high bio-oil yields for the liquefaction of lignin in ethanol. However, these bio-oils are mainly composed of oligomer-rich components rather than a monomer-rich fraction at this temperature. The bio-oil yield from the liquefaction of poplar wood derived Organosolv lignin does not change significantly between 265 and 350 °C in ethanol whereas the monomeric products increase with increasing the temperature when at relatively short residence times are employed (15-45 min).<sup>51</sup> At the temperatures higher than 350 °C, a great deal of reactive free radicals can be formed in the reaction medium; these free radicals come together to form oligomers/polymers which results in an increased amount of char formation. In contrast to aforementioned studies, Nielsen and co-workers

found the optimum temperature for the liquefaction of lignin from wheat straw was 400 °C for the highest bio-oil yield.<sup>52</sup> The authors used lignin which was acid insoluble and obtained from wheat straw via enzymatic hydrolysis. The lignin was processed at 250-450 °C, and residence time (0-8 h). The highest bio-oil yield from lignin was approximately 40 wt% which was obtained at a temperature of 400 °C with a residence time of 4 h (Table 4, entry 4). Notably, the optimum temperature for high bio-oil yields depends strongly on the type of lignin employed. The differences in starting lignin structure have significant effects on the yields of bio-oils and the products of lignin subcritical/supercritical ethanol processing. Park et al. investigated the relationship between the structure of lignin and its depolymerization behavior.<sup>53</sup> Six types of lignin samples were obtained from oak and pine wood using three different delignification techniques (ethanosolv, formosolv, and Klason). As oak wood has a higher content of sinapyl alcohol unit, ether linkage in the lignins derived from oak wood found three times higher than the lignins derived from pinewood. The ether linkages in the lignin samples were as follows: formosolv > ethanosolv > Klason. The lignin samples were treated in scEtOH and formic acid at 250–350 °C. Depolymerization studies showed that both the plant source and lignin isolation method have an effect on subsequent bio-oil yields and product compositions upon Sc-EtOH treatment especially at temperatures between 250 and 300 °C.<sup>53</sup>

### **1.2.3.2 Catalytic liquefaction of lignin**

Most recent Sc-EtOH studies have focused on the role of catalysts for the decomposition of lignin. The catalytic decomposition of lignin in ethanol significantly changes bio-oil compositions when it is compared to noncatalytic decomposition of lignin. Several homogenous and heterogeneous catalysts have been tested for the deconstruction

of lignin in Sc-EtOH. Heterogeneous catalysts are more attractive than homogeneous catalysts for the decomposition of lignocellulosic materials in ethanol as they can be easily separated and re-used. However, a high catalyst to biomass ratio might be required for the efficient decomposition of lignocellulose in ethanol. Guo and co-workers investigated autocatalytic depolymerization of alkali wet straw lignin impregnated with NaOH at subcritical/supercritical EtOH ( $T=150-300\text{ }^{\circ}\text{C}$ ,  $t=1-8\text{ h}$ ).<sup>41</sup> The highest lignin conversion yield and bio-oil yield (obtained at the temperature of  $240\text{ }^{\circ}\text{C}$  and a residence time of 4 h with a pressure of 7.2 MPa) were 74.88% and 67.58%, respectively (Table 4, entry 5). Miller and co-workers investigated the depolymerization of Kraft- and organosolv-derived lignins in Sc-EtOH using various bases including KOH, NaOH, CsOH, LiOH,  $\text{Ca}(\text{OH})_2$ , and  $\text{Na}_2\text{CO}_3$  at  $290\text{ }^{\circ}\text{C}$  for 1h.<sup>54</sup> It was reported that stronger bases were found to be more effective for the deconstruction of lignin under Sc-EtOH conditions. In the case of KOH, the conversion of lignin was 93% (Table 4, entry 6).

The positive synergistic effect of co-catalyst (a combination of metal supported carbon and solid-base catalysts) to produce monophenol-rich bio-oil from lignin in ethanol was demonstrated by Limarta and co-workers.<sup>55</sup> Kraft lignin was depolymerized in ethanol at  $350\text{ }^{\circ}\text{C}$  for 60 min without and with catalysts (i.e., MgO/C, MgO/ $\text{Al}_2\text{O}_3$ , MgO/ $\text{ZrO}_2$ , Ru/C, Ru/C+ MgO/C, Ru/C+ MgO/ $\text{Al}_2\text{O}_3$ , and Ru/C+ MgO/ $\text{ZrO}_2$ ). All tested catalyst produced more bio-oil than that of the non-catalytic run. Although the highest bio-oil yield (88.1 wt%) was obtained with Ru/C, the use of co-catalyst (i.e., mixture of Ru/C and MgO/ $\text{ZrO}_2$ ) increased the monomeric phenols (Table 4, entry 7).<sup>55</sup> It was suggested that ethanol acted as a nucleophilic reagent for C-O-C cleavage through alcoholysis reactions, while Ru/C and MgO are mainly responsible for the depolymerization of

fragmented species into monomeric and smaller products. The above-mentioned lignin depolymerization reactions were solvolysis-based carried out under nitrogen atmosphere. The authors also investigated lignin depolymerization through hydrogenolysis, the catalytic reactions using Ru/C+ MgO/ZrO<sub>2</sub> were carried out at 350 °C for 60 min under H<sub>2</sub> atmosphere. The use of H<sub>2</sub> instead of N<sub>2</sub>, led to the slight reduction of the bio-oil yield but molecular weight of bio-oil was decreased from 861 g/mol to 784 g/mol.

Kuznetsov and co-workers investigated the effects of sulfated ZrO<sub>2</sub>, sulfated ZrO<sub>2</sub> supported Al<sub>2</sub>O<sub>3</sub> catalysts, and acidic zeolite catalysts for the decomposition of alkali lignin from Aspen wood in ScEtOH at 350 and 400°C.<sup>56</sup> Alkali lignin was depolymerized without and with the use of sulfated ZrO<sub>2</sub>, sulfated ZrO<sub>2</sub> supported Al<sub>2</sub>O<sub>3</sub>, and various laboratory synthesized high\_silica zeolites [in H\_form with Si/Al = 100 (HHSZ\_100) and Si/Al = 30 (HHSZ\_30)] and a commercial zeolite [with Si/Al = 4.9 (HY)] catalysts at 300, 350 and 400 °C and a residence time of 60 min. The tested catalysts gave higher conversion than that of the control trial with no catalyst. The highest bio-oil yield was 62.5 wt% employing the sulfated ZrO<sub>2</sub> catalyst (Table 4, entry 8). The bio-oil yield contained a wide range of organic compounds including esters, ethers, phenols, aldehydes, ketones, alkanes, and alkenes. The relative yield of ethers significantly increased with all tested catalysts. Notably, ethanol itself was degraded without and with the use of a catalyst under the reaction conditions. However, the conversion of ethanol from the non-catalytic run was low and increased with the use of catalyst.<sup>56</sup> The primary product from ethanol conversion was 1,1-diethoxyethane for all tested catalysts.

It is well known that Formic acid generates in-situ hydrogen at elevated temperatures above 200 °C and its use in lignin solvolysis/hydrogenolysis reactions in

ethanol yield higher bio-oils as the addition of formic acid suppress the formation of char, increases bio-oil yields and hinders the recombination of reaction intermediates<sup>57</sup>. Notably, ethanol also acts as an effective hydrogen donor by hydride transfer of its  $\alpha$ -hydrogen.<sup>58</sup> The combine effect of ethanol and formic acid enhances the yields of de-polymerized lignin. Riaz and co-workers demonstrated that the use of formic acid with lignin under Sc-EtOH conditions provided a high conversion (92%) and bio-oil yield (85 wt%) at 350 °C with a residence time of 30 min and a formic acid-to-lignin mass ratio of 1.5 (Table 4, entry 9).<sup>59</sup> The crude bio-oil contained phenols, esters, alcohols, and traces of aliphatic compounds. The relative content of the detectable hydrocarbons by gas chromatography coupled with mass spectrometry (GC-MS) changed depending on the reaction conditions employed (i.e., residence time, pressure, and catalyst to lignin ratio). Phenols and esters were dominant products in catalytic runs. Among the phenolic compounds, phenol was the major product but methyl, methoxy, and ethyl groups bonded to the aromatic ring were also observed. The phenolic compounds with different substitution patterns are mainly formed from monomers lignin fragments under acid catalyzed ethanol processing conditions.<sup>44</sup> The formation of ethyl esters takes place under Sc-EtOH reaction conditions. Although the exact mechanism for the acid-catalyzed depolymerization of lignin in ethanol is not fully known, the cleavage of etheric bonds in lignin is considered to have an important effect on the product compositions. In most native lignocellulosics, the amount of ether linked inter-unit linkages are much higher than carbon-carbon interunit linkages. These etheric bonds are less stable and readily ruptured under elevated Sc-EtOH conditions. The depolymerization of lignin in ethanol is enhanced with the use of an acidic catalyst leading to the rupture of ether and carbon-carbon bonds are cleaved producing

monomeric and oligomeric reactive free radicals. Some of these radicals are stabilized by ethanol and subsequently quenched but repolymerization still occurs.<sup>60</sup> These possible two pathways competitively occur depending on operating conditions (i.e., temperature, residence time, catalyst amount, and strength of acid).

Zeolites, especially ZSM-5, are known as aromatization and cracking catalysts due to their ideal pore structure and acid sites for the reaction.<sup>35</sup> Jeong et al. examined the depolymerization of Protobind lignin in the presence of metal supported ZSM-5 catalysts (Co, Ni, and Cu) using ethanol as a solvent at 440 °C for 5 h.<sup>61</sup> The type of metal, as well as Si/Al<sub>2</sub> ratio, played an crucial role on the yields of monoaromatic products. The highest monoaromatic yield was 98.2 wt% obtained with the use of 10 wt% Cu loaded on ZSM-5 with a Si/Al<sub>2</sub> ratio of 30 (Table 4, entry 10). It was demonstrated that there is a linear correlation between the yield of monoaromatic compounds and the acid density of Cu/ZSM-5 with various Si/Al<sub>2</sub> ratios. The aluminum content of extra framework increased with decreasing in the Si/Al<sub>2</sub> ratio, which resulted in an increase of the acidity of the catalyst which increased the yield of monoaromatic under Sc-EtOH conditions. Selected monoaromatic compounds from catalytic runs were determined and were shown to be mainly composed of benzaldehyde, ethylbenzene, *m*-xylene, toluene together with some minor compounds such as *o*-cresol, 2-ethylphenol, and syringol.

Heterogeneous catalysts such as Raney Ni, Pd/C, Rh/C have been used for the lignin hydrogenation reactions and earlier studies were mainly aimed at the structural elucidation of the lignin.<sup>62</sup> Guo et al. carried out the depolymerization of alkali lignin from wheat straw in subcritical/supercritical EtOH using either Raney/Ni or Rh/C catalysts. The use of Raney/Ni or Rh/C catalysts increased bio-oils yields at all tested temperatures (180-



300 °C) and residence times (1-8 h).<sup>63</sup> The use of either Raney/Ni or Rh/C catalysts promoted the hydrogenation of the fragmented intermediates, which inhibits repolymerization reactions. The highest bio-oil yield of 75wt% ca. was obtained with Raney-Ni catalyst at 240 °C and a residence time of 4 h (Table 4, entry 11). Analysis of the bio-oils detected the presence of esters, ketones, acids, and phenols. The use of either Raney/Ni or Rh/C catalyst increased the relative content of phenols under all tested temperature (i.e., 180, 240 and 300 °C) and residence times (i.e., 1, 4, and 8 h). The use of the catalyst increased the amount of de-polymerized lignin, which resulted higher yields of phenolics as the phenol is the basic entity of lignin structure. Although the char yield decreased in the catalytic runs, char formation was observed in both non-catalytic and catalytic runs. Li's group at Tianjin University demonstrated that the Kraft lignin could be completely converted into bio-oil with the help of a molybdenum carbide catalyst at 280 °C for 6 h.<sup>64</sup> The bio-oil consisted of C<sub>6</sub>–C<sub>10</sub> esters, alcohols, arenes, phenols, and benzyl alcohols in remarkably high yield without any tar or char formation. Ethanol formed a complex on the surface of the catalyst which served as the active site and facilitated the formation of reactive intermediates, which then functionalized the lignin fragments formed during the Sc-EtOH reaction. The same group also investigated the decomposition of Kraft lignin over various molybdenum-based catalysts (i.e., MoO<sub>3</sub>/Al<sub>2</sub>O<sub>3</sub>, Mo/Al<sub>2</sub>O<sub>3</sub>, Mo<sub>2</sub>N/Al<sub>2</sub>O<sub>3</sub>, and α-MoC<sub>1-x</sub>/AC) at 280 °C in Sc-EtOH for 6 h and an initial nitrogen pressure of 0.5 MPa.<sup>65</sup> It was demonstrated that Mo-based catalysts showed remarkable catalytic performance for the decomposition of lignin in Sc-EtOH producing promising overall yields of high-valued chemicals without tar and char formation. The suggested reaction steps involve the formation of lignin fragments by the noncatalytic decomposition

of the lignin and interactions of these fragments with the radicals generated from ethanol in the presence of Mo-based catalysts. It was also mentioned that ethanol itself was degraded and incorporated into the fragments from lignin that are present in the reaction medium during Sc-EtOH process. The authors investigated the conversion of EtOH with a selected catalyst (Mo/Al<sub>2</sub>O<sub>3</sub>) under same conditions and the results were compared with the processing of lignin and EtOH together with the catalyst. The compounds that are believed to be released from the degradation of EtOH in the presence of Mo/Al<sub>2</sub>O<sub>3</sub> are shown in Table 5.<sup>65</sup> The degradation of EtOH with Mo/Al<sub>2</sub>O<sub>3</sub> produced mainly acetaldehyde, ethyl acetate, butanol, and 1,1-diethoxyethane with amounts of 879, 1615, 917, and 651 mg per g of lignin, respectively. When a Sc-EtOH treatment was conducted with the catalyst and lignin the product mixture contained acetaldehyde, ethyl acetate, butanol, and 2-butenol were the main compounds attributed to ethanol in the amounts of 566, 526, 982, and 410 mg/g of lignin applied, respectively. Hensen's group at the Eindhoven University of Technology investigated transition metal (i.e., Ti, Mo, Nb, W) nitrides and TiO<sub>2</sub> catalyst for lignin depolymerization in Sc-EtOH at 300 and 340 °C for 1 h.<sup>66</sup> The highest THF soluble fraction (61 wt%) was obtained with the use of W<sub>2</sub>N (urea glass) at 340 °C for 1 h. The highest aromatic monomer yield was 19 wt% and this was obtained with the use of TiN (urea glass). The products obtained with TiN were classified as hydrogenated cyclics, oxygen-free aromatics, and oxygen-containing aromatics. The metallic character of TiN facilitated hydrogen transfer reactions of the solvent, which were attributed to the presence of hydrogenated cyclics (mostly cyclohexenes). Of significance, alkylated aromatic products were obtained in bio-oils. Studies regarding the use hydrotalcite-like catalyst (Cu–MgAlOy) for the depolymerization of lignin in Sc-EtOH has

attracted much attention from the scientific community and used for processing of lignin in ethanol.<sup>67-70</sup>

Hensen's group tested Cu-Mg-Al mixed oxide catalysts for the depolymerization of lignin in Sc-EtOH.<sup>70</sup> They tested the depolymerization of lignin at the temperatures 300 and 380 °C and residence times of 4 and 8 h.<sup>70</sup> The highest THF soluble fraction (bio-oil) was 73 wt% obtained at 300 °C and 4 h. Formation of repolymerized products (solid residue containing char and catalyst) was a result of a balance between depolymerization, and repolymerization, reactions that suppress repolymerization, that was, alkylation.<sup>69</sup> C-alkylation and O-alkylation of the products were confirmed using model compounds (i.e., o-cresol, 2,4,6-trimethylphenol, and anisole) at 300 °C for 1 h over a CuMgAlO<sub>x</sub> catalyst. In a subsequent paper by the same group, the same catalyst (CuMgAlO<sub>x</sub>) was used, but the effect of Cu content and (Cu+Mg)/Al ratio on the product distribution from the decomposition of alkali lignin from the hydrolysis of wheat straw was investigated.<sup>67</sup> The catalyst samples were denoted as Cu<sub>x</sub>MgAl<sub>(y)</sub>, where x referred to as the Cu content (by weight), and y was the atomic ratio of (Cu+Mg)/Al. The optimum catalyst, which has the highest total basic sites (0.35 mmol/CO<sub>2</sub>), was found to be as Cu<sub>20</sub>MgAl<sub>(4)</sub> and produced 36 wt % monomers without formation of char at 340 °C for 4 h. Total basic sites of the tested catalyst strongly affected THF soluble yields, monomer yields and their contents at 340 °C for 4 h. All the tested catalysts produced high yields of C<sub>4+</sub> alcohols and esters. It was mentioned that these products were formed via Guerbet-type reactions as well as esterification reactions. As shown in Figure 3, the Guerbet reaction is a condensation reaction of primary or secondary alcohols to the branched alcohols.<sup>71</sup> The higher the

basicity of the catalyst gave higher amounts of alcohols and esters via Guerbet-type and esterification reactions.<sup>67, 72</sup>

As mentioned above, alkylation reactions play an essential role for suppressing char formation. The authors used phenol as a model compound to determine the alkylation degree of phenol in ethanol at 340 °C for 4 h over the mixed oxide catalysts using <sup>1</sup>H–<sup>13</sup>C heteronuclear single quantum coherence (HSQC) NMR spectrometry.<sup>67</sup> The highest degree of alkylation for phenol was 8.1 and was obtained with Cu<sub>20</sub>/γ-Al<sub>2</sub>O<sub>3</sub>. Alkylation from ethanol was also observed during the decomposition of lignin in Sc-EtOH using homogenous Lewis acids.<sup>73</sup> The studies above focused on either alkylated products and alkylation degree or ethanol self-degradation with catalysts under the conditions that lignin depolymerized.<sup>65, 67, 70, 73</sup> Reactions of ethanol via alkylation and esterification reactions were frequently determined using HSQC NMR data.<sup>67, 69</sup> In an earlier published work by Miller and co-workers, the authors demonstrated the incorporation of EtOH-derived products into the bio-oil attributed to the presence of base catalysts using model compounds at 290 °C for 1 h in the presence of KOH.<sup>54</sup> The studies with model compounds (i.e., phenyl ether, phenol, catechols, etc.) showed that ethanol participated in the reactions of phenyl ethers and led to phenols and ethyl ethers that were subject to further reactions. Also, phenols and catechols were alkylated by ethanol or one of its products and produced ethyl phenol and catechols. The experiments using alcohol and base demonstrated that ethanol was primarily converted into acetic acid and 1-butanol. As stated earlier, incorporation of ethanol into the products derived from lignin may also occur during non-catalytic Sc-EtOH processing, but this is limited.<sup>52, 56, 74</sup> The most important question is the amount of EtOH derived products, which were incorporated into bio-oils after Sc-EtOH processing of lignin.

The best way to assess the amount of EtOH derived products is to determine the overall carbon balances as EtOH itself can transform into the bio-oil as well as gaseous products.<sup>75</sup> Carbon balances that exceed 100 % can provide an estimate on the quantity of EtOH-derived products incorporated into the bio-oils. In a very recent study, Hensen's group at the Eindhoven University of Technology estimated the amount of ethanol derived products in the bio-oils using carbon-14 dating analysis of the bio-oils.<sup>68</sup> The carbon-14 dating technique can distinguish carbon from biomass and carbon from petroleum derived sources. Biomass includes a fixed amount of  $^{14}\text{C}$  which is close of the  $^{14}\text{C}$  content of atmospheric  $\text{CO}_2$ ; on the other hand, fossil fuel derived ethanol contains only very small amounts of  $^{14}\text{C}$  due to its radioactive decay (half-life of 5730 years). For this purpose, the authors carried out their experiments with ethanol derived from petroleum.<sup>68</sup> The results demonstrated that the amount of incorporated carbon atoms was 18% at 200 °C. Remarkably at 380 and 420 °C, the values were reported to be 60 and 61 %, respectively. As expected, more degradation products from ethanol take place at higher reaction temperatures, which results in increased participation of fragments from ethanol into the bio-oil. The method used by Huang et al. is interesting as well as tedious.<sup>68</sup> For future studies, it would be interesting to compare the results from carbon balance, and the results from the  $^{14}\text{C}$  technique for the estimation of ethanol derived carbon amounts attached into the bio-oils after the deconstruction of lignin in ethanol medium.

### **1.2.3.3 Deconstruction of cellulose in ethanol**

In contrast to lignin subcritical/supercritical EtOH studies there are only a few studies which examine the reactivity of cellulose under these conditions. Brand and Kim reported the liquefaction of cellulose at the temperatures of 265, 280, 300 and 350 °C with

ethanol under an initial nitrogen pressure of 2 MPa.<sup>50</sup> In case of cellulose, the bio-oil yield was only 1.6 wt% at 265 °C. It was raised to 48.4 wt% when the temperature was increased to 350 °C. The gas product mainly consisted of carbon monoxide (CO) and carbon dioxide (CO<sub>2</sub>). Except at the temperature of 265 °C, the mole yield of CO was higher than the mole yield of CO<sub>2</sub>. The cracking of the glycosidic linkage of cellulose is believed to lead to the formation of CO. Trace amounts of C<sub>2</sub> gases (C<sub>2</sub>H<sub>4</sub> and C<sub>2</sub>H<sub>6</sub>) were detected in gas phase from cellulose decomposition in ethanol. The compounds detected by GC-MS from the decomposition of cellulose in ethanol were esters, acids, furans, glucose, ethers, ketones, and cyclopentanones. At 350 °C, the total relative yield of esters was the highest.<sup>50</sup> Ester compounds in bio-oils help to reduce some of the unwelcome properties of typical bio-oils such as high acidity, corrosiveness, and thermal instability.<sup>50, 76</sup> Hong-Xiu and co-workers carried out the decomposition of cellulose in ethanol at 320 °C for 60 min.<sup>77</sup> They investigated the effect of ethanol to cellulose ratio on the bio-oil yield and its composition. The highest conversion and bio-oil yield were approximately 86% and 55wt%, respectively and this was obtained at the solvent to cellulose ratio of 10:7. The bio-oil is composed of ketones, acids, esters, alcohols, and furans. An increase in solvent to cellulose ratio increased the formed ketones.

#### **1.2.3.4 Catalytic liquefaction of cellulose**

The generally accepted mechanism for the cellulose decomposition with an acid catalyst in ethanol starts with the conversion of cellulose into ethyl glucosides followed by formation of furan intermediates via dehydration of ethyl glucosides units. Further decomposition of furans produces esters (as shown in Figure 4).<sup>78</sup> Sels' group at the University of Leuven converted cellulose into ethyl levulinate sulfonated hyperbranched

poly(arylene oxindole)s catalyst (5-Cl-SHPAO) in ethanol at the temperatures of 150, 160, 170, 180 and 190 °C and for 2, 3, 4, 6, and 10 h.<sup>79</sup> The highest ethyl levulinate yields were 60 % obtained at 160 °C for 6 h with a complete conversion of cellulose. Notably, the formation of humins occurred as a side product which accounted for the major carbon loss in the reaction. It is probable that some furan intermediates from cellulose were transformed into humins. In a previous report, it was demonstrated that humins are produced from furan via primarily aldol addition and condensation reactions.<sup>80</sup> Huber's group at the University Wisconsin also proposed that humins could also be produced from oligosaccharide intermediates during aqueous phase acid-catalyzed decomposition of cellulose.<sup>81</sup> In another study, cellulose obtained from cotton was treated with hydrochloric acid either in ethanol or water at the temperatures of 45 and 65 °C for 1–5 h.<sup>82</sup> Soluble sugar contents were the highest at 65 °C for 5 h using ethanol as a solvent.

### **1.2.3.5 Deconstruction of lignocellulosic biomass in ethanol**

Lignocellulosic biomass has been used as a raw material in biomass processing studies using ethanol as a supercritical solvent. Efficient conversion of lignocellulosic biomass into biofuels in ethanol is remains a challenging process. Akalin et al. investigated the effects of process parameters on the bio-oil yield (wt%) and biomass conversion (%) produced from the liquefaction of the beech wood in ethanol media at different temperatures (from 265 to 320 °C), residences times (from 37 to 143 min) and biomass loadings (from 4 to 16 wt%).<sup>83</sup> The individual and interaction effects of process parameters were investigated statically. The most significant factor on the bio-oil yield and biomass conversion was found to be the reaction temperature. The highest bio-oil yield from beech wood was obtained at 300 °C and it was about 40 wt% of the starting biomass (Table 6,

entry1). Subsequently, the decomposition of Hawthorn stones (separated from the fruits) was carried out in ethanol at different temperatures (from 280 to 320 °C), residence times (60, 90 and 120 min) and biomass loading (8-12 wt%).<sup>84</sup> The statistical investigation by a chemometric approach demonstrated that the most significant factor was the temperature which affected bio-oil yields as well as biomass conversions. The highest crude bio-oil yield was approximately 41 wt% (Table 6, entry 2). Another important study investigated effects of operating parameters (i.e., temperature, residence time, initial nitrogen pressure, biomass/solvent ratio) for the liquefaction of pine wood in ethanol. The tested temperatures, residence times, pressures, and biomass/solvent ratio were 280-400 °C, 0-240 min, 0.4-7.5 MPa, and 0.06-0.25 g/g, respectively.<sup>85</sup> Brand et al. demonstrated that the reaction temperature and residence time had pronounced effects on the bio-oil yields as well as biomass conversions from pine wood using ethanol as a solvent.<sup>85</sup> An increase of the temperature from 280 to 400 °C led to an increase in the bio-oil yield and the maximum bio-oil yield was observed to be 59.9 wt% at 400 °C (Table 6, entry 3). Biomass conversion also increased from ~34 to 98% with increasing the temperature from 280 to 400 °C. Almost 100% conversion of solid biomass into liquid and gaseous products was reported at 400 °C. Notably, 90% of beech wood decomposes in Sc-EtOH at 350 °C with a residence time of 30 min.<sup>86</sup> A two-step process for the liquefaction of lignocellulosic biomass in ethanol has also been proposed.<sup>87</sup> Rice straw was first pretreated at 200 °C for 10 min with CO<sub>2</sub> and then liquefied at 275–345 °C for either 15 or 30 min. The highest biomass conversion and bio-oil yield was ~80 % and 48 wt %, respectively and obtained at 345 °C and 15 min residence time (Table 6, entry 4). In a subsequent work reported by Li et al., rice stalk was torrefied in a fixed-bed reactor at 200, 240, and 280 °C, respectively.<sup>88</sup> The



torrefied rice stalk was depolymerized at 325 °C in ethanol for 60 min. The torrefaction process led to a decrease in bio-oil yields and biomass conversion. The increase in torrefaction temperature decreased bio-oil yield and increased solid residue yield. The highest biomass conversion and bio-oil yields were ~78% and ~55 wt% and obtained from non-torrefied rice stalk. However, the highest ester content and heating value were obtained with torrefied rice stalk at 200 °C.

#### **1.2.3.6 Catalytic liquefaction of whole biomass**

All aforementioned studies demonstrated that the temperature is the most significant factor which affects bio-oil yields and biomass conversions. The second important parameter is the residence time. The initial pressures have little effect on the resulting bio-oils and biomass conversions. The type of biomass used is important for the determination of the optimal conditions for the highest bio-oil yields. Because, the yields are affected by the structure of the various biopolymers. It seems to be the temperature range from 300 - 400 °C is the optimum temperature for the liquefaction of lignocellulose in ethanol.<sup>89</sup>

The use of homogeneous and heterogeneous catalysts will also change optimum process conditions including temperature, time, initial pressure, biomass/solvent ratio for the highest crude bio-oil and biomass conversion. In earlier studies, various heterogeneous catalysts were tested for the conversion of lignocellulosic biomass in ethanol. Xu and Etcheverry investigated iron-based catalysts (FeS or FeSO<sub>4</sub>) for the deconstruction of Jack pine powder in subcritical/supercritical EtOH.<sup>58</sup> The tested operating conditions were as follows: the temperature at between 200 and 350 °C, initial hydrogen pressures at between 2.0 and 10.0 MPa, reaction times 15 and 60 min, 5 wt% of catalyst loading. The highest oil

yield from the non-catalytic run was about 44 wt% at 350 °C employing a residence time of 40 min and an initial hydrogen pressure of 2 MPa. The use of FeSO<sub>4</sub> increased the crude bio-oil yield to 63 wt% at 350 °C and 40 min and an initial hydrogen pressure of 5 MPa (Table 6, entry 6). The use of catalyst decreased the heating values of crude oils. The heating values of crude bio-oil was 31.8 MJ/kg with no catalysts. It was 29.3 MJ/kg with FeSO<sub>4</sub> and 18.5 MJ/kg with FeS. Phenolic compounds were dominant in all oils regardless of the type of catalyst or whether the catalyst was used or not. The use of high-pressure hydrogen and Sc-EtOH promoted the formation of long-chain alkanes. Recently, Liu and co-workers used a combination of 1-butyl-3-methylimidazolium chloride ([BMIM]Cl) and nickel (II) chloride (NiCl<sub>2</sub>) for the liquefaction of wood chips in ethanol.<sup>90</sup> The experiments were carried out at the temperature ranging from 300 to 400 °C and initial hydrogen pressures varying from 2 to 10 MPa and a residence time of 40 min without and with co-catalyst (1.2 wt% [BMIM]Cl and 300 µg/g NiCl<sub>2</sub>). The bio-oil yield from the non-catalytic run was about 32.6 wt% and it was increased to 49.5 wt% using [BMIM]Cl/NiCl<sub>2</sub> catalyst (Table 6, entry 7). The identified compounds in light and heavy bio-oils from the liquefaction of wood chips were mainly composed of ester, phenols and carboxylic acids. No information was provided whether these compounds are generated from the catalytic or non-catalytic run. The same group synthesized silica-supported monoclinic molybdenum dioxide (MoO<sub>2</sub>/SiO<sub>2</sub>) catalyst for the liquefaction of wood in the form of sawdust in ethanol at 340 °C for 40 min.<sup>91</sup> The crude bio-oil yield was 47 wt% at 320 °C for 40 min using an initial hydrogen pressure of 2 MPa. The use of the catalyst increased the bio-oil yield to ~60 wt% under same conditions (Table 6, entry 8).

An increase of the initial pressure of hydrogen from 2 to 6 MPa, increased the crude bio-oil yield from ~60 to 72 wt%. The metallic sites of MoO<sub>2</sub> can dissociate hydrogen and can produce active hydrogen atoms.<sup>92</sup> It is proposed that active hydrogen atoms aids to decompose lignocellulose in ethanol. Increasing the initial hydrogen pressure produce more active hydrogen which resulted in more bio-oil and less bio-char.<sup>91</sup> In a very recent study, Akalin et al. investigated the decomposition of beech wood was carried out in ethanol without with the use of hydrated cerium (III) chloride at 300 °C with residence times from 10 to 120 min.<sup>78</sup> The bio-oil yields from catalytic runs were higher than those of bio-oils from the non-catalytic runs under identical conditions. The highest bio-oil yield was ~48 wt% and obtained at 300 °C using 5 mmol of hydrated cerium (III) chloride at a residence time of 90 min in ethanol. In the non-catalytic run, phenols and esters were the dominant component in the bio-oil. With the use of the catalyst, the relative content of acids significantly increased and phenols decreased. It was proposed that condensation reactions were dominating for the long residence times, which affected the bio-oil compositions in the catalytic run.

### **1.3 Characterization methods of bio-oils**

#### **1.3.1 NMR analysis of bio-oils**

Various instrumental analytical techniques including gas chromatography (GC), liquid chromatography (LC), high-resolution mass spectrometry (HRMS), Fourier transform infrared spectroscopy (FT-IR), thermo gravimetric analysis (TGA), and NMR were introduced for characterization of bio-oils in the previous studies.<sup>93-97</sup> One of the most comprehensive spectroscopic experiments suited for the comprehensive elucidation of bio-oil components is NMR spectroscopy. Various NMR experiments have been employed to

better understand the components and structures of thermally generated bio-oils.  $^1\text{H}$  and  $^{13}\text{C}$  NMR have been widely used to investigate the structural hydrogen-carbon framework of bio-oils.<sup>98</sup> Moreover, selective analysis of the functional groups in the pyrolysis oils through other NMR analysis techniques allows a deep understanding the characteristics of pyrolysis oils. For instance, hydroxyl functional groups of bio-oils can be measured by phosphorylation followed by  $^{31}\text{P}$  NMR.<sup>99</sup> Likewise, derivatization of bio-oils with 4-(trifluoromethyl)phenylhydrazine followed by  $^{19}\text{F}$  NMR provides a quantitative and comprehensive understanding of carbonyl groups, which lead to corrosion and aging problems during upgrading.<sup>100</sup> 2D-NMR experiments, such as  $^1\text{H}$ - $^{13}\text{C}$  HSQC, are used to infer likely functional groups and substructures present in the oil by detecting one bond correlations between heteronuclear chemical shifts.<sup>101</sup>

Mullen et al.<sup>98</sup> discussed the characteristics of analytical techniques applied to bio-oils, including GC, high-performance liquid chromatography (HPLC), gel permeation chromatography (GPC), FT-IR, and NMR. Among the characterization methods mentioned above, NMR techniques have been widely used for the structural elucidation of bio-oils. Table 7 summarizes applications of NMR characterization of various bio-oil products reported over the past decade. Diverse NMR methods provided structural information of the bio-oil products and assisted understanding the effects of diverse pyrolysis processes and post-pyrolysis upgrading methods.

The main advantages of the application of NMR to the analysis of bio-oils are 1) the whole bio-oil can be dissolved in an appropriate solvent and information about the whole functional groups can be obtained, which does not depend on the volatility of the components in the bio-oils; and 2) the chemical-shift ranges for functional groups have

been well studied, and quantitative analysis of functional groups can be achieved by integration of peaks based on the proposed chemical shift assignment ranges. For example, Joseph et al.<sup>102</sup> proposed revised chemical shift ranges for the assignment of <sup>13</sup>C NMR and <sup>1</sup>H NMR data and discussed uncertainties of the functional group assignments because of the OH contents in bio-oils, incomplete relaxation, and nuclear Overhauser effects by analyzing 54 pyrolysis oil model compounds. However, NMR analysis of bio-oils still has several limitations. It is challenging to integrate online NMR analysis into pyrolysis production lines and hence remains primarily a laboratory research tool. In addition, NMR analysis is well known to be an insensitive research tool and for bio-oils it is often difficult to identify individual compounds and better suited to analyze changes in functional group composition. Practically, researchers need to apply several characterization techniques together to fully analyze bio-oils, to get thorough understanding of bio-oil components. In the following contents, the chemical shift assignments and applications of various NMR analysis methods will be thoroughly discussed.

Proton NMR is widely applied in bio-oil characterization. The <sup>1</sup>H nucleus is abundant; thus proton NMR allows rapid detection with a high signal-to-noise (S/N) ratio. However, unambiguous assignment of the NMR chemical shifts caused by severe spectral overlapping makes this analysis challenging.<sup>103</sup> Joseph et al.<sup>102</sup> reported <sup>1</sup>H NMR signal overlapping from different bio-oil model compounds in DMSO-*d*<sub>6</sub>. The proton shifts in non-conjugated alkenes (6.0-4.0 ppm) overlap those in aliphatic OH groups (6.5-4.0 ppm) and ether groups (5.5-3.0 ppm). The signals between 3.0 and 2.0 ppm can be assigned to both aliphatic protons and protons on carbons attached to a carbonyl group. Table 8 compares typical <sup>1</sup>H NMR chemical shift integration regions reported in the literature and

proposes a revised integration region.<sup>98, 102, 104-105</sup> Aldehydes and carboxylic acids are assigned in the downfield regions of 10.0-8.3 ppm. Aliphatic protons are assigned to 3.0-0.5 ppm; however, primary, secondary, and tertiary protons cannot be distinguished by <sup>1</sup>H NMR.<sup>102</sup> The chemical shift range of 8.3-5.7 ppm is assigned to aromatics and alkenes, and that of 5.7-3.0 ppm is assigned to protons on carbons  $\alpha$  to an oxygen atom. These chemical shift ranges are not distinguished further because of severe overlaps in the <sup>1</sup>H NMR spectrum. Phenols and aliphatic hydroxyl groups are not specified in the revised chemical shift integration regions because hydroxyl protons shift widely in different solvents and concentrations because of strong hydrogen bonding in polar solvents.

<sup>1</sup>H NMR has been used to elucidate the structures of bio-oils obtained under different pyrolysis conditions and upgrading methods as well as those of chemicals extracted from bio-oils. Tessarolo et al.<sup>106</sup> used <sup>1</sup>H NMR to analyze bio-oils from pine wood and sugarcane bagasse. The bio-oils were obtained from non-catalytic and ZSM-5-catalyzed pyrolysis at different temperatures (450 °C, 500 °C, and 550 °C). The bio-oil from sugarcane bagasse pyrolyzed with ZSM-5 showed an increase of aromatic and conjugated alkene hydrogen contents (8.2-6.0 ppm) and a decrease of hydrogen contents from oxygen-containing groups (12.5-8.2 ppm, 6.0-3.0 ppm) compared to non-catalytic sugarcane bagasse bio-oil. The same ZSM-5 catalyst effect was observed on pine wood bio-oils, i.e., an increase of aromatic and conjugated alkene hydrogen contents and a decrease of hydrogen contents from oxygen-containing groups. However, pine wood bio-oil catalytically pyrolyzed at 500 °C contained more hydrogen from ethers (4.2-3.0 ppm) compared to the noncatalyzed pyrolysis oil. This unusual tendency was due to the spectral overlap between the water region (3.7-3.3 ppm) and hydrogens related to ethers (4.2-3.0

ppm). The spectral overlap of aliphatic hydrogens and hydrogens  $\alpha$  to carbonyl groups in the region from 3.0 to 2.0 ppm made the quantification of aliphatic hydrogens difficult.

Tanneru and Steele performed catalytic deoxygenation to convert pretreated pine wood bio-oil into partially deoxygenated products in the presence of syngas.<sup>107</sup> The pretreatment was an oxidation step to convert aldehydes in the crude bio-oil to carboxylic acids, which are more conducive to catalytic hydrotreating. The partially deoxygenated product was then fully deoxygenated to hydrocarbons. Figure 5 presents the <sup>1</sup>H NMR spectra of a) oxidized bio-oil, b) partially deoxygenated bio-oil, c) fully deoxygenated bio-oil, and d) a commercial gasoline-jet fuel-diesel mixture.<sup>107</sup> A comparison of Figure 5a with Figure 5b reveals that protons in the region 5.2-3.2 ppm (esters, ethers, lignin-derived methoxy phenols) were almost eliminated by partial deoxygenation. Partial deoxygenation also increased the aliphatic hydrocarbon content (1.8-0.8 ppm). A comparison of Figure 5b with Figure 5c indicates that the full deoxygenation reduced the content of phenols, substituted phenols, and aromatic compounds (7.5-5.0 ppm). Figure 5c and Figure 5d show that the fully deoxygenated product exhibited a spectrum similar to that of the commercial gasoline-jet fuel-diesel mixture.

Mancini et al.<sup>108</sup> used quantitative <sup>1</sup>H NMR to detect the selective production of (1*R*,5*S*)-1-hydroxy-3,6-dioxo-bicyclo[3.2.1]octan-2-one (LAC) in cellulose pyrolysis oils. LAC has the potential to be applied in the organic synthesis of tetrahydrofuran structures found in natural products.<sup>109</sup> Cellulose pyrolysis was performed using the catalysts aluminum-titanate (AlTi), montmorillonite K10 (MK10), Sn-MCM-41, or recycled Sn-MCM-41. The quantitative <sup>1</sup>H NMR detection of LAC in bio-oils was achieved using a NMR standard-addition method.<sup>110</sup> The quantitative <sup>1</sup>H NMR results showed that the LAC

concentrations in bio-oils using Sn-MCM-41 and recycled Sn-MCM-41 were 27.6 wt% and 26.8 wt%, respectively. The  $^1\text{H}$  NMR results indicated that catalyst Sn-MCM-41 exhibited high efficiency to achieve LAC selective production in cellulose pyrolysis process.

$^{13}\text{C}$  NMR spectroscopy provides carbon information of bio-oil components. In comparison to an  $^1\text{H}$  NMR spectrum, a  $^{13}\text{C}$  NMR spectrum benefits from a broader chemical shift range, which means less spectral overlap.<sup>111</sup> The limitation of quantitative  $^{13}\text{C}$  NMR is its low sensitivity and long experiment time due to the low natural abundance of  $^{13}\text{C}$  nuclei. Table 9 compares two typical  $^{13}\text{C}$  NMR chemical shift integration ranges measured in DMSO- $d_6$ , as proposed by Ingram et al.<sup>104</sup> and Joseph et al.<sup>102</sup> Joseph et al. reported that primary carbons overlapped with secondary and tertiary carbons extensively in the region 34-24 ppm of  $^{13}\text{C}$  NMR from bio-oil model compounds.<sup>102</sup> Thus, the alkyl region (54-0 ppm) could not be subdivided into primary, secondary, and tertiary carbons. Methoxy/hydroxyl groups and carbohydrates were assigned to 70-54 ppm and 103-70 ppm, respectively, which was slightly different from the assignments proposed by Ingram et al.<sup>104</sup> In the study of model compounds, aromatic and alkene carbons overlapped completely in the region 163-103 ppm. Moreover, carbonyl carbons were easily distinguished in the region of 215-163 ppm in the studies of both Ingram et al. and Joseph et al.<sup>102, 104</sup>

Tarves et al.<sup>112</sup> investigated the effects of reactive gas atmospheres on the properties of switchgrass bio-oils produced by microwave pyrolysis. Bio-oils produced under various gaseous atmospheres ( $\text{CO}$ ,  $\text{CH}_4$ , and  $\text{H}_2$ ) and a model pyrolysis gas mixture (PyGas) were analyzed by  $^{13}\text{C}$  NMR spectroscopy and compared with bio-oils obtained under an  $\text{N}_2$



atmosphere. Compared to the bio-oils obtained under an N<sub>2</sub> atmosphere (control group), the oils produced under CO and H<sub>2</sub> atmospheres contained 18.6% and 27.6% greater concentrations of aliphatic compounds (55-0 ppm), respectively. The CO, H<sub>2</sub>, and PyGas atmospheres also produced higher percentages of aromatic compounds (165-95 ppm) and lower percentages of ketones, aldehydes, acids, and esters (215-165 ppm). In addition, the oils obtained under reactive gas atmospheres (CO, CH<sub>4</sub>, H<sub>2</sub>, and PyGas) contained approximately half of the percentage of alcohols and carbohydrates (95-55 ppm) compared to the N<sub>2</sub> atmosphere control group. The <sup>13</sup>C NMR integration results indicated that the reactive gas atmospheres resulted in lower contents of oxygen-containing compounds and higher contents of deoxygenated products in bio-oils.

Mante et al.<sup>113</sup> hydrothermally treated fluid catalytic cracking (FCC) catalysts and ZSM-5 additives and studied the effects of the treatments on bio-oils obtained from catalytic pyrolysis of poplar wood by <sup>13</sup>C NMR analysis. One commercial FCC catalyst and two commercial ZSM-5 additives were tested in the study. The <sup>13</sup>C NMR integration results indicated that the bio-oil obtained with silica sand via non-catalytic pyrolysis contained the highest amounts of oxygenated compounds (220-180, 180-160, 105-60, and 57-55 ppm). In general, the use of FCC catalysts and ZSM-5 additives decreased the concentrations of oxygenated compounds and increased the aromatic contents (160-105 ppm) in bio-oil products. A comparison of the products obtained using fresh FCC catalyst (FCC-1) with those obtained using FCC catalyst hydrothermally treated at 732 °C (FCC-2) revealed that the contents of oxygen-containing compounds in the regions of 220-160, 105-60, and 57-55 ppm decreased 47.2% with FCC-2. This result indicated that the selectivity and activity of the FCC catalyst was promoted upon steaming. Conversely, the

FCC catalyst steamed at 788 °C (FCC-3) did not decrease the oxygen content of the products compared to those obtained with the fresh FCC catalyst (FCC-1), which suggested that the severe treatment temperature (788 °C) led to diminished effectiveness of the catalysts for deoxygenation reactions (e.g., demethoxylation, decarboxylation, and decarbonylation). In contrast to the <sup>13</sup>C NMR analysis results for the products obtained using the FCC catalyst, those for the bio-oil showed that steaming of the ZSM-5 additives did not substantially lower the oxygen content in bio-oils. For example, in the case of phosphorous-impregnated ZSM-5 additive steam treated at 732 °C (PZSM5-2), the methoxy carbons from lignin decomposition products (57-55 ppm) were decreased by 9.9% and the carbons in alcohols, ethers, anhydrosugars, and levoglucosan (105-60 ppm) were decreased by 17.1%; however, carbonyl groups (220-160 ppm) in the bio-oil increased by 43.7% compared to the product obtained using fresh phosphorous-impregnated ZSM-5 additives (PZSM5-1).

Liu et al.<sup>114</sup> reported a method to upgrade bio-oils using zero-valent metals at ambient temperature and pressure. The effects of zero-valent metals were investigated on both model compounds and a bio-oil from rice husk. According to the <sup>13</sup>C NMR integration results, carbonyl groups (215-170 ppm) in the upgraded bio-oil decreased by 68.4% compared to their contents in the raw bio-oil. This significant change was accompanied by an increase of the contents of alcohols and ethers (90-50 ppm) in the upgraded bio-oil. Selective conversion of benzaldehyde, which was used as a model compound, into benzyl alcohol in the presence of zero-valent zinc powders was consistent with the results for bio-oils from rice husk.

Alwehaibi et al.<sup>115</sup> characterized the phenolic compounds of the bio-oil obtained from spruce wood and used the bio-oil and its subfractions to stabilize biodiesel against autoxidation. The <sup>13</sup>C NMR spectra of the crude bio-oil and its isolated extracts are shown in Figure 6.<sup>115</sup> As evident from the <sup>13</sup>C NMR spectra, multi-solvent extraction clearly separated the bio-oil into two major families: carbohydrates (95-55 ppm) in the water-soluble extract and phenolic compounds (165-95 ppm) in the phenolic extract. The sharp peak at approximately 56 ppm indicated that the majority of the phenolic compounds have a methoxy substitution.

Recently, researchers combined NMR spectroscopy with modeling techniques to predict the chemical properties of bio-oils. Strahan et al.<sup>116</sup> summarized the <sup>13</sup>C NMR data for 73 different samples, including 55 bio-oils, two commercial fuels, and 16 small-molecule standards. The bio-oils were produced from various feedstocks, pyrolysis processes, and post-pyrolysis treatments. Partial least squares (PLS) models were created to correlate the <sup>13</sup>C NMR data with the samples' other chemical properties including their phenol concentration, cresol concentration, total acid number, elemental composition, and higher heating value. The chemical properties were predicted from the models and compared with the experimental values. These models can provide researchers a method for estimating pyrolysis oil's chemical properties using only <sup>13</sup>C NMR.

<sup>31</sup>P NMR method has attracted increasing interest in bio-oil characterizations in recent years. It involves phosphitylation of hydroxyl groups with a <sup>31</sup>P reagent followed by quantitative <sup>31</sup>P NMR analysis. This method provides quantitative information about various hydroxyl functional groups in bio-oils and complements <sup>1</sup>H NMR and <sup>13</sup>C NMR analysis, especially in cases where there are strong signals overlapping and dynamic range

problems in the  $^1\text{H}$  NMR spectra or long relaxation time issues in the  $^{13}\text{C}$  NMR experiments. Pu et al.<sup>117</sup> reviewed the applications of  $^{31}\text{P}$  NMR in lignin and lignin-derived products and stated that 2-chloro-4,4,5,5-tetramethyl-1,3,2-dioxaphospholane (TMDP) is the most common phosphitylating reagent for lignin and its derivatives. Wroblewski et al.<sup>118</sup> examined five trivalent  $^{31}\text{P}$  reagents to derivatize organic model compounds including phenols, aliphatic acids, aromatic acids, aliphatic alcohols, amines, and thiols. TMDP has emerged as an optimum reagent because most hydroxyl groups containing compounds derivatized with this reagent showed non-overlapped chemical shifts. Figure 7 shows reactions between TMDP and various hydroxyl function groups in bio-oils and the  $^{31}\text{P}$  NMR assignments of the phosphitylated compounds.<sup>119</sup> The reactions between TMDP and hydroxyl groups require an organic base, such as pyridine. Pyridine has the ability to capture the liberated hydrogen chloride and drive the overall phosphitylation reaction to total conversion.<sup>117</sup>  $^{31}\text{P}$  NMR also requires an internal standard for quantitative assessment of hydroxyl groups in bio-oils.<sup>120</sup> *endo-N*-Hydroxyl-5-norborene-2,3-dicarboximide (NHND) has been selected as a suitable internal standard because it has a chemical shift (152.8-151.0 ppm) that is well-separated from those of the bio-oil components.<sup>120</sup>

Recently, Ben and Ferrell<sup>121</sup> examined the time-dependent changes of several commonly used internal standards for the  $^{31}\text{P}$  NMR analysis of bio-oil. Their results showed that NHND is not stable after 12 h of storage or experiment, whereas cyclohexanol and triphenylphosphine oxide (TPPO) can be used as internal standards for long experiment or storage times. Moreover, the chemical shifts and integration regions for bio-oils after derivatization with TMDP have been studied; typical chemical shift assignments are presented in Table 10.<sup>119</sup>

David et al.<sup>99</sup> compared bio-oils from pine wood, sweetgum, softwood lignin, and cellulose isolated from pine wood using <sup>31</sup>P NMR spectroscopy. David et al.<sup>99</sup> derivatized the bio-oils by TMDP and assessed the quantitative analysis against cyclohexanol as an internal standard. Their quantitative <sup>31</sup>P NMR results showed that the total hydroxyl contents in the pine wood bio-oil (2.62 mmol/g) were higher than the total hydroxyl contents in the sweetgum bio-oil (1.54 mmol/g). The bio-oil obtained from cellulose contained the highest aliphatic hydroxyl contents (2.95 mmol/g) and the lowest contents of phenolic hydroxyl groups and carboxylic acids. The bio-oil from softwood lignin contained only 0.10 mmol/g aliphatic hydroxyl groups, whereas the contents of the phenolic hydroxyls (2.53 mmol/g) and carboxylic acids (0.26 mmol/g) were the highest in the bio-oil from softwood lignin.

Naik et al.<sup>122</sup> upgraded the bio-oil obtained from *Jatropha* by catalytic cracking with vacuum gas oil. They used quantitative <sup>31</sup>P NMR spectroscopy to analyze the crude oil and the oils catalytically cracked at 250 °C and 300 °C. Figure 8 shows the quantitative <sup>31</sup>P NMR spectra of the crude and upgraded bio-oils.<sup>122</sup> The bio-oils were analyzed by <sup>31</sup>P NMR spectroscopy after derivatization with TMDP, and NHND was selected as an internal standard. In this study, the aliphatic OH, C5-substituted β-5 phenolic OH, guaiacyl phenolic OH, and *p*-hydroxyphenyl OH were assigned to the regions 150.02-145.07, 145.07-140.42, 140.42-138.20, and 138.20-136.96 ppm, respectively. A comparison of Figure 8a and Figure 8b indicates that the aliphatic OH (150.02-145.07 ppm) and C<sub>5</sub>-substituted β-5 phenolic OH (145.07-140.42 ppm) were almost eliminated after the deoxygenation. The deoxygenation upgrading process at 250 °C also reduced the guaiacyl phenolic OH contents in the bio-oil. Figure 8c shows that deoxygenation at 300 °C

completely removed the hydroxyl contents in bio-oils obtained from the fast pyrolysis of *Jatropha*.

Fu et al.<sup>123</sup> reported a method to extract phenolic compounds as a mixture from lignin pyrolysis oil using switchable hydrophilicity solvents (SHS). The <sup>31</sup>P NMR integration results showed that the guaiacyl phenolic signal (140.2-139.0 ppm) was dominant for the three subfractions. The majority of hydroxyl groups were concentrated in the phenolic compounds extract (fraction 3). For instance, the phenolic extract (fraction 3) contained 90.5% aliphatic OH (150.0-145.5) and 57.4% catechol type OH (139.0-138.2 ppm) among the three subfractions. The <sup>31</sup>P NMR analysis after derivatization with TMDP validated that fractionation using SHS is a useful method to extract phenolic compounds from bio-oils.

<sup>19</sup>F comprises 100% of naturally-occurring fluorine, and this isotope is highly responsive to NMR measurement. Similar to the <sup>31</sup>P NMR analysis, <sup>19</sup>F NMR technology provides an efficient method to detect a specific type of functional group. In contrast to <sup>31</sup>P NMR, <sup>19</sup>F NMR follows treatment of bio-oils with 4-(tri-fluoromethyl)phenylhydrazine to analyze carbonyl functional groups. Carbonyl groups have been reported to play an important role in corrosion and aging problems of pyrolysis oil; however, because of the complexity of the bio-oil composition, quantitative identifying carbonyl groups is difficult. Huang et al. first studied the application of <sup>19</sup>F NMR in detecting the carbonyl groups of pyrolysis oil derivatives.<sup>100</sup> They treated the pyrolysis samples with 4-(tri-fluoromethyl)phenylhydrazine as described in the published work.<sup>100</sup> For the quantitation of carbonyl contents using <sup>19</sup>F NMR method, 2-fluoroguaiacyl benzoate ( $\delta = -57.2$  ppm) is used as an internal standard, which allows the quantitative assessment of carbonyl contents.

In a  $^{19}\text{F}$  NMR spectrum, the chemical shift range of -60.60 to -62.00 ppm is assigned to the quinone 4-(trifluoromethyl)phenylhydrazine derivative, whereas the range of -58.50 to -60.60 ppm is assigned to the aldehyde and ketone 4-(trifluoromethyl)phenyl-hydrazine derivatives.

Huang et al.<sup>100</sup> quantitatively analyzed different pyrolysis oils by  $^{19}\text{F}$  NMR after derivatization with 4-(tri-fluoromethyl)phenylhydrazine. The  $^{19}\text{F}$  NMR results were then compared with the results obtained by an oximation method.<sup>124</sup> The results showed that the carbonyl contents of bio-oils analyzed by  $^{19}\text{F}$  NMR ranged from 1.38-4.54 mmol g<sup>-1</sup>, which was in agreement with the values from the oximation method. The  $^{19}\text{F}$  NMR analysis results were slightly higher than the oximation analysis results. The difference could be attributed to the incomplete reaction of the quinonic groups during the oximation process. One of the advantages of the  $^{19}\text{F}$  NMR analysis of carbonyl groups is the ability to detect the quinoid content as well as the aldehyde/ketone content separately. Moreover, the  $^{19}\text{F}$  NMR method is more efficient than the traditional oximation method due to its short reaction time (24 h vs. 48 h), simpler operational procedure, and smaller sample amount requirement.

Traditional one-dimensional (1-D)  $^1\text{H}$  and  $^{13}\text{C}$  NMR analysis can provide valuable structural information for bio-oils. The 1-D NMR characterization techniques are quantitative essentially; however, these techniques usually suffer from spectral overlapping problems or long relaxation time issues when applied in the bio-oil analysis. 2-D NMR techniques have emerged as attractive methods to compensate the limitations of 1-D NMR techniques. In a 2-D spectrum, the chances of overlapping problems are reduced because the signals are spread out into two dimensions.<sup>125</sup> HSQC is a proton-detected 2-D

heteronuclear correlation experiment.<sup>126-127</sup> In an HSQC experiment, the detected proton is labeled with the frequency of the heteroatom attached to.  $^1\text{H}$ - $^{13}\text{C}$  HSQC uses successive insensitive nuclei enhanced by polarization (INEPT) transfers that exploit the strong one-bond  $J_{\text{HC}}$  on either side of the  $^{13}\text{C}$  evolution period.<sup>125</sup> The HSQC is more sensitive than the traditional heteronuclear correlation (HECTOR) experiment, because the HSQC starts and ends on the sensitive  $^1\text{H}$  nucleus whereas the HECTOR detects the insensitive nucleus.<sup>128</sup> Modern HSQC sequences also use z-axis gradient pulse for coherence selection, which is a benefit for sensitivity-enhancement.<sup>129</sup> Ben and Ragauskas<sup>101</sup> applied  $^1\text{H}$ - $^{13}\text{C}$  HSQC NMR method to investigate carbon-hydrogen bonding in bio-oils and proposed assignments for the oils from slow pyrolysis of lignin, cellulose, and pine wood. Fortin et al.<sup>130</sup> used  $^1\text{H}$ - $^{13}\text{C}$  HSQC NMR to analyze pyrolytic lignin extracted from a switchgrass pyrolysis oil. The HSQC NMR spectra showed that aryl methoxy groups and guaiacyl units were still present in the pyrolytic lignin after the thermal conversion. The peaks of xylose and arabinose units also existed in the HSQC spectra of pyrolytic lignin.

Recently, Yu et al.<sup>131</sup> characterized pyrolytic sugars in bio-oil samples. Figure 9 showed the HSQC spectra of bio-oil samples and assignments of pyrolytic sugars. The assignments of pyrolytic sugars were proposed by characterizing of sugar standards, including sugar monomers (i.e., glucose, galactose, mannose, xylose, and arabinose) and anhydrosugars (i.e., levoglucosan, cellobiosan, and cellotriosan), as shown in Figure 9. In Figure 10, the HSQC spectra indicated that the intensity of sugar peaks in the raw bio-oil was considerably higher, compared to those in the water-insoluble bio-oil fraction.<sup>131</sup> The sugar contents in  $\text{CH}_2\text{Cl}_2$ -soluble and  $\text{CH}_2\text{Cl}_2$ -insoluble fractions did not exhibit significant difference. From the HSQC spectra, the  $\text{CH}_2\text{Cl}_2$ -soluble fraction contained the higher



intensity of aliphatic, methoxy, and guaiacyl groups compared to CH<sub>2</sub>Cl<sub>2</sub>-insoluble fraction.

The NMR technologies presented provide a facile way to analyze pyrolysis oil. Since most pyrolysis research focuses on reducing the oxygen contents in bio-oils through optimizing the pyrolysis experiment parameters (e.g., temperature, gas atmosphere), adding catalysts during pyrolysis, and post-pyrolysis treatments, <sup>1</sup>H, <sup>13</sup>C, <sup>31</sup>P, and <sup>19</sup>F NMR are powerful tools for obtaining structure information about the whole fraction of bio-oils. Moreover, post pyrolysis fractionation and chemical extraction have attracted increasing interest; in this area, NMR analysis also provides structural information about the bio-oil subfractions and extracted compounds. Hydroxyl and carbonyl groups, which are the primarily groups that limit the ability of bio-oils to blend with commercial fuels, can be detected by <sup>31</sup>P and <sup>19</sup>F NMR methods after derivatization. <sup>1</sup>H-<sup>13</sup>C HSQC NMR provides carbon-hydrogen information, which is useful for elucidating possible reactive pathways during pyrolysis reactions. The 1-D NMR techniques are quantitative in nature, however, the spectral overlap problems usually occur because of the complex constitution of bio-oils. Researchers should carefully select appropriate NMR experiment parameters to let nucleus fully relaxed. Quantitative HSQC analysis of the bio-oil could be an interesting application in the future. Other 2-D NMR analysis could also bring benefit for the bio-oil studies, such as heteronuclear single quantum coherence-total correlation spectroscopy (HSQC-TOCSY).

Moreover, researchers are now focusing on several challenges of bio-oil characterization by NMR methods. For example, limited information is available about hemicellulose pyrolysis distribution because of its less well-defined structures and less

mature isolation techniques. Deducing more assignments for hemicellulose pyrolysis oil in  $^{13}\text{C}$  and 2D NMR spectra will provide further insight into hemicellulose pyrolysis behavior.<sup>132</sup>

$^1\text{H}$  diffusion-ordered NMR spectroscopy (DOSY) is also considered for measuring the molecular weights of polymers and macromolecules and for investigating the interactions of small molecules. The application of  $^1\text{H}$  DOSY to bio-oil molecular weight measurement to obtain shorter experiment times and achieve greater accuracy would be interesting.<sup>133</sup>

### **1.3.2 GC-MS analysis of bio-oils**

Gas chromatography coupled with mass spectrometry (GC-MS) is a commonly used analytical technique for the qualitative and semi-quantitative analysis organic compounds in bio-oils from the liquefaction of lignocellulosic biomass in ethanol. A wide range of organic compounds in bio-oils arise from the decomposition of lignocellulosics or its lignin and cellulose components. The main features of GC-MS instrument are the injector (which is heated), mass detector, transfer lines, allowed programmed temperature of the column. At first, the bio-oil sample is volatilized in a heated injector port of the gas chromatograph. With the help of carrier gas such as Helium, the sample in the gas phase is transferred from the injector port to capillary column packed with a stationary (solid) phase at which separation of components of sample takes place. The components in the analyte is separated. The separated components in the analyte elute from the column at different times (refer to residence time). After the components leave the column, the components are ionized by the mass spectrometry and identified using a library of mass spectra for different compounds. In a typical GC-MS analysis, about 1  $\mu\text{g}$  of bio-oil sample is

dissolved in an appropriate organic solvent such as dichloromethane. The dissolved sample in organic solvent is injected. The injector port temperature is generally set at between 250 and 300 °C. The GC oven temperature is programmed before the starting the analysis. The volatilized sample flows from the injector port to the column with a carrier gas such as helium (as a mobile phase). The components of the bio-oils are separated in the column. The end of the column is directly introduced into the ion source of a mass selective detector. The compounds in bio-oils that is light enough to elute from the GC column are identified in comparison with peak patterns of different compounds in the library.

The detected monomeric compounds from the decomposition of lignin in ethanol are shown in Table 11.<sup>51</sup> The bio-oil from the decomposition of lignin in ethanol mainly contains monomeric phenols, acids, ketones and esters.<sup>51, 63</sup> The amount of each compound changes depending on the type of lignin employed as well as operating conditions. Notably, the use of catalyst has a significant effect on the composition of lignin-derived bio-oil and may change the content and relative yield of organic compounds depending on the type and amount of catalyst. Figure 11 shows total ion chromatogram of bio-oil produced from concentrated sulfuric acid hydrolysis lignin (CSAHL) treated at 350 °C for 30 min with formic acid to lignin mass ratio of 1.5.<sup>59</sup> The main compounds detected by GC-MS from the liquefaction of cellulose in ethanol are esters, alcohols, ethers, ketones, acids, furans, cyclopentanones, and aromatic compounds.<sup>50</sup>

GC-MS is an efficient analytical technology to identify the individual compound existing in bio-oils. Although GC-MS is being most commonly applied in the analysis of bio-oils, this technology still has challenges to accurately quantify all the compounds in the bio-oils. Usually the injector temperature for GC is set to around 250 °C, which means

the chemical species with a high boiling point will not be able to enter the GC columns (e.g., phenolic oligomers). The absolute quantification of important individual compounds requires calibration curves obtained from internal standards of the chemical compounds of interest. This quantification method with internal standard can be expensive and time consuming; thus, most research efforts only calculate the relative percentage of chemical species (e.g., hydrocarbons, alcohols, esters) or an individual compound of interest based on the total identified compounds. To complement GC-MS and achieve a thorough analysis of the chemical components of the bio-oils, NMR has been widely employed in this research field.

### **1.3.3 GPC analysis of bio-oils**

Gel permeation chromatography (GPC), also known as size exclusion chromatography (SEC) is a commonly used technique to determine the molecular weight of the bio-oils derived from thermochemical processing. The molecular weight of the bio-oils could be used as an important reference to determine the degree of the depolymerisation of biomass. Typically, there are two major methods applied in the GPC characterization: absolute value determination and relative value determination using a calibration curve.<sup>134</sup> The bio-oils could be dissolved in organic solvents (e.g., THF) easily and without derivatization which makes GPC a practical and feasible method for bio-oil's molecular weight characterization. Ben et al. performed catalytic pyrolysis and prepared bio-oils with a low molecular weight of ~ 100 g/mol which falls into the gasoline range (80~120 g/mol). It should be noted that since the molecular weight of the bio-oils are typically below limitation Table 12 summarized the molecular weight values of bio-oils from pyrolysis and liquefaction during the past three years.

### 1.3.3 Elemental composition, heating value and other analysis techniques of bio-oils

Elemental analysis is a useful technique to determine carbon, hydrogen and oxygen content of bio-oils produced from the decomposition of lignocellulose in ethanol. Previous studies regarding the decomposition of lignocellulose demonstrated that bio-oil contain more carbon and less hydrogen than that of raw biomass.<sup>78, 83</sup> Depending on the temperature and catalyst used, the carbon content can be increased and oxygen content decreased in comparison with the non-catalytic run, which corresponds to higher heating values.<sup>50, 52, 135</sup> Heating values of bio-oils can be estimated from elemental composition of bio-oils using an empirical formula.<sup>52, 78</sup> Elemental analysis provides the atomic ratios of O/C and H/C in bio-oils. We can estimate the de-oxygenation degree in bio-oil from O/C atomic ratios. The previous studies demonstrated that the liquefaction of lignocellulose in ethanol resulting in lower O/C ratio in comparison with raw material. The O/C ratio of bio-oils changes depending on the operating conditions and can be significantly lowered using catalysts.<sup>78, 135</sup> The H/C ratio can provide clues regarding the aromatic content of bio-oils. If the H/C ratio of bio-oils and/or bio-chars is high, then the aromatic content is low.

# **CHAPTER II: EXPERIMENTAL METHODS AND MATERIALS**

## **2.1 Materials and chemicals**

### **2.1.1 Biomass feedstocks**

In this dissertation work, five types of biomass feedstocks were used for investigating the thermochemical processing and derived bio-oil products. The information of the southeastern pine wood, southern yellow pine, sugarcane bagasse, grape seeds, and fir wood are provided here.

Southeastern pine wood, secured from a pulp mill located in Georgia state, was used for the study in Chapter III. After manual debarking, the woodchips were milled through a 0.4 mm screen. The pine sawdust was then Soxhlet extracted with dichloromethane for 24 h. After air-drying in a fume hood, the milled pine wood sample was stored at 0 °C.

Southern yellow pine was studied in Chapter V and provided by Idaho National Laboratory and ground to <0.5 mm. The composition by ultimate analysis was 49.6 wt% C, 6.3 wt% H, 43.5 wt% O, 0.1 wt% N, <0.1 wt% S, and 0.3 wt% ash, and the moisture content was 2.3%.

Sugarcane bagasse used in Chapter IV and Chapter VI was grown and harvested in Egypt. The samples of sugarcane bagasse were air dried in the fume hood for 24 h. After air drying, the sugarcane bagasse samples were milled through a 2 mm sieve using a Wiley mill. The milled sugarcane bagasse samples were Soxhlet extracted by the mixture of toluene and ethanol (v/v = 2:1) for 8 h, followed by the acetone for 4 h. After Soxhlet extraction, the sugarcane bagasse samples were air dried in the fume hood. After air drying, the extractive free sugarcane bagasse samples were collected and stored in the fridge at 0 °C.

The red grape seeds were acquired from a local market in Karabuk, Turkey and used in Chapter VII. The grape seeds were ground and used as received from the consumer source. The proximate and ultimate analyses of the grape seeds are shown in Table 13.

The fir wood feedstocks were acquired from a local market in Karabuk, Turkey and used in Chapter VIII. The fir wood were ground and used as received from the consumer source. Proximate analysis, ultimate analysis and component analysis of the fir wood feedstock were performed and the results were listed in Table 14.

### **2.1.2 Reagents**

The ZSM-5 used in Chapter V was purchased from Zeolyst (CBV 3024E) with silica-to-alumina ratio of 30. The original extrudates were ground and sieved, and the experiments were performed with the 300-1000  $\mu\text{m}$  particle size fraction. The acid site density of the fresh catalyst was determined to be  $\sim 960 \mu\text{mol/g}$  by ammonia temperature-programmed desorption. Fresh catalyst was used for the experiments, with once-through flow without catalyst reuse or regeneration. The silica sand of 300-500  $\mu\text{m}$  in the pyrolyzer was purchased from Black Lab, LLC (Chardon, OH). All the other chemicals and reagents were purchased from Sigma-Aldrich and used as received. Gases used in this dissertation were purchased from Airgas.

## **2.2 Experimental procedure**

### **2.2.1 Autohydrolysis pretreatment of biomass**

Extractive-free milled biomass samples ( $\sim 6.5 \text{ g}$ ,  $\sim 7.0 \%$  moisture content) were used in the pretreatment. Different conditions were applied in the autohydrolysis reactions, for example  $180 \text{ }^\circ\text{C} - 10 \text{ min}$ ,  $180 \text{ }^\circ\text{C} - 40 \text{ min}$ ,  $200 \text{ }^\circ\text{C} - 40 \text{ min}$ . A mixture of biomass sample and water was loaded into a 200 mL Parr reactor, with a solid to liquid ratio of 1:20



(v/v). An example of the corresponding temperature-pressure information is presented in Table 15. After the pretreatment reactions, the reactor was cooled to room temperature (RT) using an ice bath. The solid product was filtered and washed with deionized water before collection. The biomass samples pretreated at the same condition were well mixed up together before storing at 0 °C.

### **2.2.2 Small scale pyrolysis**

Briefly, the Soxhlet extracted biomass sample was oven dried at 105 °C before pyrolysis. The oven dried pyrolysis sample (around 3 g) was placed in a quartz sample boat that was positioned in the center of a pyrolysis tube. The pyrolysis tube was connected with two condensers and flushed with nitrogen gas (0.5 L/min), then inserted into the furnace preheated to 400, 500, or 600 °C. The heating rate was ~2.7 °C/s and was measured by immersing a K-type thermocouple into the sample powders. The condensers were immersed in liquid nitrogen. The pyrolysis outflow passed through the tube and condensers. The pyrolysis process was lasted for 30 min. Upon the pyrolysis was completed, the tube and the condensers were removed from the furnace and liquid nitrogen respectively, and were cooled down to RT under constant nitrogen flow. The pyrolysis char and oil were collected for analysis. The liquid products were recovered by acetone wash followed by evaporation under reduced pressure. Char yield was determined gravimetrically, and gas formation was calculated by mass difference.<sup>119</sup> A diagram illustrating the small scale pyrolysis unit is provided in Figure 12.<sup>136</sup>

### **2.2.3 Large scale pyrolysis**

*Ex situ* catalytic pyrolysis experiments were conducted in a dual fluidized bed reactor system with two bubbling fluidized bed reactors. The illustration of the fluidized

bed reactor system is presented in Figure 13.<sup>137</sup> Char was separated in a cyclone and the pyrolysis vapors entered the second, upgrading reactor (5.2 cm inner diameter x 15 cm tall lower section and a 7.8-cm diameter x 35.6 cm disengagement section). Catalyst was dropped into the upgrading reactor twice per minute and removed continuously via an overflow tube. The upgraded vapors and gases were filtered in a stainless-steel mesh hot gas filter and the vapors were condensed in a system comprised of an air-cooled condenser, an electrostatic precipitator, dry-ice traps, and a coalescing filter.<sup>137</sup>

The pyrolysis temperature was 500°C in all experiments and the upgrading temperature was varied in the range of 500-600°C. The biomass-to-catalyst (B:C) mass ratios were varied by adjusting the catalyst feed rate. Gas bag samples were taken from the exit gases and they were analyzed by a GC-MS/FID (Agilent 7890B with a 5977A MS and FID) for condensable organic vapors.

The liquids from the condensation train receivers were combined and they spontaneously separated into three phases: top organic oil, middle aqueous liquid, and bottom organic oil. The fractions were separated by decanting and weighed.

The total liquid yield was determined from the mass gain in the condensation train, and the yields of the individual liquid fractions from the distribution of the separated liquids. The char yield was calculated from the mass gains in the cyclone char receiver and the pyrolysis reactor sand bed, and the coke yield from the TGA analysis of the spent catalyst and the mass of catalyst solids fed. For yields on biomass basis, this mass was subtracted from the aqueous yield. The gas yields were determined from the gas analysis by the micro-GC and the gas flow rate.

#### 2.2.4 Hydrothermal liquefaction in water and organic solvents

Hydrothermal (HTL) and supercritical ethanol (SCE) liquefaction experiments were carried out using a benchtop reactor-model 4848 (Illinois, USA). In a typical run, around 15 g of biomass (on a dry basis) and 150 mL solvent (ultrapure water or ethanol) were placed into the reactor, which was then closed, purged with hydrogen three times to remove the inside air and purged with an initial H<sub>2</sub> pressure of 2 MPa. In the experimental runs with additives, the feed was the same, and the required amount of MgCl<sub>2</sub>:TiCl<sub>4</sub> was added, and the same procedure was applied. After charging the autoclave and pressurizing with H<sub>2</sub>, the reactor was heated to the desired temperatures (from 250 to 350 °C) under continuous stirring (250 rpm) and held at the desired temperatures for 15, 30 and 60 min. The experimental runs with MgCl<sub>2</sub>:TiCl<sub>4</sub> were carried out at the optimum temperature (300 °C) for 30 min. Different amounts of MgCl<sub>2</sub>:TiCl<sub>4</sub> (1mmol:1mmol, 2 mmol:2mmol, 4mmol:4mmol) was used for the hydrothermal and supercritical ethanol processing of grape seeds.

All experiments were conducted in triplicate. The standard deviation values are shown as error bars in the product distributions. After the reactions were completed, the reactor was cooled to room temperature by an internal stainless-steel water cooling loop. Once the gas products were released, the reactor was cooled, the reaction contents and the walls of the reactor were rinsed with dichloromethane. The solid and liquid products were separated by vacuum filtration. The liquid portion was extracted with an equal amount of dichloromethane (300 mL) in the hydrothermal processing runs. The resulting solution was dried over anhydrous sodium sulfate (Na<sub>2</sub>SO<sub>4</sub>), filtered, and evaporated in a rotary evaporator at room temperature. Upon removal of the dichloromethane, the remaining

fraction was quantified and labeled as bio-oil. In the case of ethanol processing, after autoclaving, the reactor was opened, and the reactor contents and the walls of the reactor were rinsed with dichloromethane. The solid and liquid products were separated by vacuum filtration. The liquid portion was dried with anhydrous  $\text{Na}_2\text{SO}_4$  and then filtered. Upon removal of the solvent, the remaining fraction was quantified and labeled as bio-oil. After separation of the liquid and solid products, the solids remaining on the filter paper were dried at  $105\text{ }^\circ\text{C}$  in an oven for 4 h. These solid products were defined as solid residues.

### **2.2.5 Catalyst preparation**

The preparation of copper doped metal oxide catalyst was modified according to the published procedure<sup>138</sup> and described below: Hydrotalcite like metal oxide ( $\text{CuMgAlO}_x$ ) catalyst was prepared by the co-precipitation method with a 20 wt% Cu and a fixed  $\text{M}^{2+}/\text{M}^{3+}$  atomic ratio of 2.  $\text{Cu}(\text{NO}_3)_2 \cdot 2.5\text{H}_2\text{O}$  (0.019 M),  $\text{Mg}(\text{NO}_3)_2 \cdot 6\text{H}_2\text{O}$  (0.061 M), and  $\text{Al}(\text{NO}_3)_3 \cdot 9\text{H}_2\text{O}$  (0.04 M) were well mixed in 100 mL de-ionized water. The mixed solution was added into 150 mL  $\text{Na}_2\text{CO}_3$  (0.048 M) solution together with 100 mL NaOH solution while keeping the pH around 10. The milk like blue slurry was aged at  $60\text{ }^\circ\text{C}$  under stirring overnight. The precipitation was filtered and washed until the filtrate reached neutral condition. The precipitates were dried under  $105\text{ }^\circ\text{C}$  overnight and the solid catalysts were ground, sieved through a  $125\text{ }\mu\text{m}$  screen, and stored in a desiccator with desiccants.

### **2.2.6 Upgrading reaction of the bio-oil**

Parr reactor (higher pressure, compact, series 5500, 30 mL) was used in this study to explore the catalytic activity towards the biomass derived pyrolysis oils. Typically, 500 mg of  $\text{CuMgAlO}_x$  catalyst, 500 mg of bio-oil, and 10 mL methanol were mixed and added to the Parr reactor vessel. The Parr reactor was sealed and purged with  $\text{N}_2$  to remove

oxygen. Reactors were heated to a specific temperature (i.e., 250, 275, 300 °C) for a specific reaction time (i.e., 2, 4, 8, 16 h). After the reaction, the Parr reactors were quenched in water to cool down to room temperature. The product mixture was taken from the reactor vessel and collected after filtering through a 0.45 µm syringe filter. An aliquot of 0.5 mL was taken from this collected mixture and directly analyzed by GC-MS. The filter cake and the reactor vessel were washed by MeOH by multiple times and the MeOH containing residual oils were combined with the product mixture. The total product mixture was collected in a 20-mL vial and placed in the fume hood overnight until a constant weight is obtained. The sticky dark oil samples were weighted for the yield determination and subjected to further characterization.<sup>138</sup>

## **2.3 Analytical instrumentation**

### **2.3.1 Characterization of biomass feedstocks**

#### **2.3.1.1 Compositional analysis of biomass feedstocks**

Klason lignin and structural carbohydrates contents were analyzed according to the laboratory analytical procedure (NREL/TP-510-42618).<sup>139</sup> In brief, around 0.175 g extracted biomass sample was hydrolyzed using 72 wt% sulfuric acid for 60 min at 30 °C. Then the mixture was diluted to 3 wt% sulfuric acid and then autoclaved for 60 min at 121 °C. The resulting mixture was cooled down to RT then filtered; the precipitate was weighted to determine the Klason lignin content. The filtrate was used to determine the carbohydrate composition by high performance anion exchange chromatography using Dionex ICS-3000. The eluent was 0.20 M NaOH and post-column rinsing effluent was 0.40 M NaOH. Fucose was used as internal standards. Standard solutions of glucose, xylose, arabinose, mannose, and galactose were used to build a calibration curve.

### **2.3.1.2 FT-IR analysis of biomass feedstocks**

Surface functionality of the pine wood feedstock was assessed using a PerkinElmer Spectrum One FT-IR spectrometer with universal attenuated total reflection. The spectra were obtained at a  $4\text{ cm}^{-1}$  resolution with a total of 64 scans for each sample from  $4000\text{ cm}^{-1}$  to  $800\text{ cm}^{-1}$ .

### **2.3.1.3 $^{13}\text{C}$ CP/MAS NMR analysis of biomass feedstocks**

For the solid state NMR analysis, the pine wood samples were packed in 4 mm  $\text{ZrO}_2$  rotors. The solid state CP/MAS  $^{13}\text{C}$  NMR was performed using a Bruker 400 MHz spectrometer operating at a frequency of 75.48 MHz for  $^{13}\text{C}$ . The experiment was carried out at ambient temperature with a Bruker 4mm MAS probe. The CP/MAS  $^{13}\text{C}$  NMR spectra were acquired with 3072 scans,  $90^\circ$  proton pulse, 1.5 ms contact pulse, and 4 s recycle delay.<sup>140</sup>

### **2.3.2 SEM analysis of char**

The surface morphology of biochars produced from SCE and HTL processing was carried out using an FEI Quanta 450 FEG scanning electron microscope (SEM). All samples were gold coated before examined with SEM using an applied voltage of 15 kV.

### **2.3.3 Characterization of bio-oils**

#### **2.3.3.1 GC-MS analysis of bio-oils**

Characterization of bio-oil components was conducted using Agilent 7890A/5795C GC/MS with a HP-5 MS capillary column ( $30\text{ m} \times 0.32\text{ mm}$  and  $0.25\mu\text{m}$  thickness) under Helium gas flow. GC samples were prepared by mixing bio-oil with methanol (bio-oil: methanol = 1: 10 w/w). An injection of  $0.5\ \mu\text{L}$  with a split ratio of 20:1 and injector temperature of  $250\text{ }^\circ\text{C}$  was used for each sample. The GC oven was held at  $40\text{ }^\circ\text{C}$  for 3 min

and started heating at 5 °C /min to 260 °C and held for 3 min. The molecular mass range (m/z) of MS detector was set at 40-400 to avoid methanol peak in spectra. Chemical compounds of bio-oil were identified by comparing their spectra with the standard spectra in the National Institute of Standards and Technology (NIST) library and from previous literature.<sup>141-142</sup>

### **2.3.3.2 Molecular weight distribution analysis of bio-oils**

The weight average molecular weight (Mw), molar average molecular weight (Mn), and molecular weight polydispersity (PDI) of the heavy pyrolysis oils are determined by GPC following the literature.<sup>136</sup> Before GPC analysis, the heavy oil samples were dissolved in tetrahydrofuran (THF) (1 mg/mL). The mixture was then filtered through a 0.2 µm filter and injected into the HPLC vials. THF was used as the mobile phase (1.0 mL/min) with injection volumes of 30 µL. Polystyrene standards (i.e.,  $1.53 \times 10^3$ ,  $1.11 \times 10^3$  Da), dioctyl phthalate (Mw = 390 g/mol), 2,2'-dihydroxy-4,4'-dimethoxyl-benzophenone (Mw = 274 g/mol), phenol (Mw = 94 g/mol), and acetone (Mw = 58 g/mol) were used as standards to build a calibration curve by fitting a polynomial equation to the retention volumes. The Mw and Mn were calibrated against the calibration curve. The polynomial order of the standard calibration curve is 3. The R<sup>2</sup> of the calibration curve is 0.997.

### **2.3.3.3 Elemental analysis of bio-oils**

Elemental analyses were carried out using a LECO CHNS 932 instrument and the results reported are the mean values of these two analyses. The Dulong formula ( $HHV = 0.338C + 1.428(H-O/8) + 0.095S$ ) was used to estimate heating values of bio-oils and bio-chars produced from the HTL and SCE processing of grape seeds.

#### **2.3.3.4 Boiling point distribution analysis of bio-oils**

A thermal gravimetric analyzer (TGA, 7200 system SII NanoTechnology Inc., Chiba, Japan) was used to estimate of boiling distributions of hydrocarbons in bio-oils.<sup>143</sup>

#### **2.3.3.5 NMR analysis of bio-oils**

##### **2.3.3.5.1 <sup>1</sup>H NMR analysis of bio-oils**

The Quantitative proton NMR analysis of bio-oils was acquired on a Bruker 500 MHz spectrometer with 1s pulse delay and 16 scans at ambient environment.

##### **2.3.3.5.2 <sup>13</sup>C NMR analysis of bio-oils**

For <sup>13</sup>C NMR analysis, the oils were dissolved in dimethylsulfoxide (DMSO)-d<sub>6</sub>. The <sup>13</sup>C NMR spectra were acquired on a Bruker III Avance 600 MHz spectrometer at 150.92 MHz with inverse gated coupling, a recycle delay of 10 s, 90° pulse angle, 300 ppm sweep width, and 4096 averaged scans. The assignments were based on those developed by Ben and Ragauskas<sup>144</sup> and later modified by Happs et al.<sup>145</sup> for CFP oils.

##### **2.3.3.5.3 <sup>31</sup>P NMR analysis of bio-oils**

The <sup>31</sup>P NMR was acquired using the methods in the published analytical laboratory procedure (NREL/TP-5100-65887).<sup>146</sup> A stock solution of pyridine/CDCl<sub>3</sub> (v/v = 1.6/1) was prepared first. The chromium acetylacetonate (relaxation reagent) and *endo-N*-hydroxy-5-norbornene-2,3-dicarboximide (internal standard) were then added to the stock solution. About 25 mg bio-oil was dissolved in the solution mixture, and then derivatized using 2-chloro-4,4,5,5-tetramethyl-1,3,2-dioxaphospholane (TMDP). The <sup>31</sup>P NMR spectra were acquired on a Bruker 500 MHz spectrometer. The following parameters were employed in the NMR experiments: inverse-gated decoupling pulse sequence, 1.2 s



acquisition time, 25 s pulse delay, 90° pulse angle, and 64 scans. The data were analyzed using Mestrenova software.

#### **2.3.3.5.4 HSQC analysis of bio-oils**

The HSQC NMR spectra were acquired on a Bruker 500 MHz spectrometer. Around 50 mg heavy oil was dissolved in 0.6 mL dimethylsulfoxide (DMSO)-*d*<sub>6</sub>. The following parameters were employed in the HSQC experiments: 1.5 s pulse delay, 0.11s acquisition time, 24 scans, <sup>1</sup>*J*<sub>C-H</sub> of 145 Hz, 716 data points for <sup>1</sup>H, and 256 data points for <sup>13</sup>C. The <sup>1</sup>H and <sup>13</sup>C widths are 13 ppm and 220 ppm, respectively. The data was analyzed using the software Mestrenova. δ<sub>C/H</sub> = 39.50/2.49 ppm was used to reference the central solvent peak. The automatic phase and baseline correction were accomplished using the software.<sup>105</sup>

#### **2.3.4 XRD analysis of catalyst**

XRD was performed at the Joint Institute for Advanced Materials (JIAM) Diffraction Facility, located at the University of Tennessee, Knoxville. Powder X-ray experiments were recorded on a Panalytical Empyrean XRD diffractometer using CuKα radiation and the spectra were recorded in the 2θ angle range of 10–70°.

# **CHAPTER III: INITIAL EXAMINATION OF AUTOHYDROLYSIS PRETREATMENT EFFECT ON BIOMASS FEEDSTOCKS**

A version of this chapter was originally published by Naijia Hao, Tais Bezerra, Qiong Wu, Haoxi Ben, Qining Sun, Sushil Adhikari, and Arthur J. Ragauskas; reprinted with permission from Elsevier:

“Hao, N.; Bezerra, T. L.; Wu, Q.; Ben, H.; Sun, Q.; Adhikari, S.; Ragauskas, A. J., Effect of autohydrolysis pretreatment on biomass structure and the resulting bio-oil from a pyrolysis process. *Fuel* **2017**, 206, 494-503.”

The authors Tais Bezerra, Qiong Wu, Haoxi Ben, Qining Sun were from University of Tennessee. The author Sushil Adhikari is from Auburn University. The author Arthur J. Ragauskas is from University of Tennessee and Oak Ridge National Laboratory. Naijia Hao, Sushil Adhikari, and Arthur Ragauskas designed the study. Naijia Hao performed the experiments and draft the manuscript. Tais Bezerra, Qiong Wu, and Qining Sun assisted with the experiments. Haoxi Ben, Sushil Adhikari, and Arthur Ragauskas revised the manuscripts.

### 3.1 Introduction

Energy security and environmental issues have driven the research and development of renewable energy.<sup>147</sup> According to the U.S. Energy Information Administration (EIA) monthly energy review, renewable energy consumption constituted 9.92% of the total energy consumption in the year 2015.<sup>148</sup> In the same year, among the renewable energy sources (e.g., hydro-electric, geothermal, solar, wind, biomass), biomass contributed 48.64% of the total renewable energy production.<sup>148</sup> Biomass is mainly comprised of three components: lignin, cellulose, and hemicellulose. Lignin is a complex aromatic substance mainly comprising of guaiacyl, syringyl, and *p*-hydroxyphenyl units. Lignin is a complex aromatic substance of phenyl propane units, formed by the dehydrogenation of hydroxyl cinnamyl alcohols such as coniferyl and sinapyl alcohols.<sup>149</sup> Cellulose is a linear structure composed of  $\beta$  (1-4) linked anhydroglucose subunits. The inter- and intra- chain hydrogen bonding system makes the cellulose partly crystalline. The crystalline part of cellulose shows much higher resistance to hydrolysis than the amorphous part.<sup>150-151</sup> Hemicellulose is a family of polysaccharides composed of different 5- and 6-carbon monosaccharide units, interacts with cellulose micro-fibrils and cross-links with lignin.<sup>150, 152</sup> The microfibrils assemble as macrofibril, which plays an important role in a plant cell wall's structural stability.<sup>152</sup> Pyrolysis is a promising technology to convert biomass to biofuels. The pyrolysis process breaks down biomass into smaller molecules, generating bio-oil, char, and gas, respectively.<sup>12</sup> Bio-oil has several similar physicochemical properties similar to fossil fuels (e.g., specific gravity); thus, upgraded bio-oil has the potential to be distributed to the existing facilities with minor modifications in the future.<sup>153</sup> Bio-oil contains negligible sulfur content and is carbon-neutral, hence it

has a broad potential as a clean alternative fuel.<sup>10</sup> Bio-oil usually contains hundreds of compounds, such as phenolic compounds, alcohols, sugars, aldehydes, and acids.<sup>17</sup> The extraction of value-added chemicals from bio-oil is also a promising research trend. However, as a fuel, the bio-oil still suffers from several limitations. For example, the high acid content of bio-oil leads to the corrosion problems in vehicle engines.<sup>154</sup> Oxygen-rich species (e.g., aldehyde groups) make bio-oil unstable and result in aging problems, causing phase separation and increasing the oil's viscosity.<sup>155</sup> In addition, polar molecular components (e.g., hydroxyl groups) make bio-oil immiscible with current commercial transportation fuels.<sup>156</sup> Thus, solving these limitations and enhancing the performance of bio-oil as a fuel have become critical research topics.

Researchers are putting forth efforts to find solutions to the current fuel limitations of bio-oil. These solutions include catalytic hydrodeoxygenation, integrated catalytic pyrolysis, the co-processing of bio-oil with fossil fuels, pyrolysis operation parameters optimization, and addition of pretreatment prior to pyrolysis.<sup>32, 157-162</sup> Recently, research studies have highlighted the opportunities to address some of the detrimental properties of bio-oils by modifying chemical properties of biomass prior to pyrolysis. A thermal and chemical pretreatment of biomass usually alters the chemical structures of the biomass materials and partially overcomes the recalcitrance to some extent.<sup>163</sup> For example, Neupane et al. performed torrefaction on pine wood. For the bio-oil from non-catalyzed pyrolysis, the torrefaction decreased furan concentration and increased phenolic compounds selectivity. For the H<sup>+</sup>ZSM-5 catalyzed pyrolysis, the torrefaction increased the aromatic hydrocarbon and total carbon yield.<sup>164</sup> Mahadevan et al. torrefied pine wood and switchgrass, found that the torrefaction pretreatment promoted the selectivity of

benzene-toluene-xylene compounds from bio-oils.<sup>149</sup> Among a variety of pretreatment techniques, autohydrolysis (also called hydrothermal pretreatment or hot water pretreatment) is a promising pretreatment process carried out at a high temperature (140-220 °C) using water in the liquid phase.<sup>165</sup> At the first stage of the autohydrolysis, water releases the hydronium ion and this acts as a weak acid to mainly depolymerize hemicelluloses (e.g., the selective hydrolysis of glycosidic linkages, the release of acetyl groups from hemicellulose fraction).<sup>166</sup> Acetic acid is formed during the hydration of the acetyl groups, which further accelerates the hydrolysis process.<sup>167-168</sup> The autohydrolysis process is environmentally friendly because the process uses only water without additional chemicals or catalysts. Autohydrolysis is applied in the cellulosic ethanol fermentation process. It is one of the key tools to make the biomass matrix more accessible to enzymes and to reduce the cost of the biotechnology to make biofuels.<sup>5</sup> It would be promising to integrate the autohydrolysis pretreatment technology into both biological and thermal conversion (pyrolysis) approach to biofuels. Stephanidis et al.<sup>169</sup> performed hydrothermal pretreatment of beech wood, and demonstrated that carboxylic acids, phenols, and ketones were reduced in the bio-oil produced from pretreated beech wood compared to the oil from untreated beech wood. Du et al.<sup>170</sup> analyzed pyrolysis oil from hydrothermally pretreated microalgae and found that hydrothermal pretreatment significantly reduced N-containing compounds in the bio-oil products. These findings indicated that the autohydrolysis pretreatment offers a method to promote the qualities of the bio-oils obtained from hardwood and algae. However, the effects of autohydrolysis pretreatment on softwood and the subsequent pyrolysis process have not been investigated, and the underlying chemistry is not understood.

The objective of this study is to characterize the effects of autohydrolysis pretreatment on pine wood and examine the applicability of this material for pyrolysis. The proposed study seeks to determine if autohydrolysis pretreatment technology could have a beneficial impact on pyrolysis oil generation. Especially in-light of the known effects on biomass structure during autohydrolysis which could improve bio-oil properties.<sup>165</sup> Depending on the benefits of this pretreatment technology on pyrolysis oil generation, it could facilitate the introduction of thermal conversion technologies at a biological biorefining operation by an incremental increase in autohydrolysis production facilities along with a pyrolysis unit. In this study, pine wood was pretreated at  $175\pm 3$  °C for 40 min and this material was pyrolyzed at 400, 500, and 600 °C. As a control, a sample of native wood was also characterized and pyrolyzed, the resulting products were also examined. The structural transformation of the pine wood feedstocks was analyzed using compositional analysis, CP/MAS <sup>13</sup>C NMR, and FT-IR spectroscopy. The yield distribution, GPC, <sup>31</sup>P NMR, and <sup>1</sup>H-<sup>13</sup>C HSQC NMR results of the bio-oil samples were compared and discussed to fully understand the effects of autohydrolysis pretreatment on the bio-oil quality.

## **3.2 Experimental methods**

### **3.2.1 Material and sample preparation**

Chemicals and biomass used in this chapter was presented in the sections 2.1.1 and 2.1.2 in this dissertation.

### **3.2.2 Equipments and experimental procedures**

Autohydrolysis and pyrolysis set-ups and processing details were presented in sections 2.2.1 and 2.2.2.

### 3.2.3 Characterization of biomass and bio-oils

Detailed characterization techniques were presented in sections 2.3.1.1, 2.3.1.2, 2.3.1.3, 2.3.3.5.3, and 2.3.3.5.4.

## 3.3 Results and discussion

### 3.3.1 Compositional analysis of pine wood feedstocks

Table 16 presents the compositional analysis of the pine wood feedstock before and after the autohydrolysis pretreatment. The hemicellulosic sugars decreased significantly after the autohydrolysis pretreatment. The xylose, galactose, arabinose, and mannose were removed by 39.23%, 96.21%, 53.6%, and 68.18%, respectively. For southern USA softwood, the primary hemicellulose is *O*-acetyl-galacto-glucomannan and arabino-4-*O*-methyl-glucurono-xylan is a minor component.<sup>171</sup> The acidic environment of the autohydrolysis process results in hydrolysis of glycosidic linkages of hemicellulose fractions. Hemicellulose are mainly solubilized into its corresponding sugar monomers and partially converted to other degradation products such as furfural.<sup>163</sup> In this study, the glucan percentage of pretreated solid slightly increased from 39.88% to 42.54% after pretreatment. The phenomenon was probably attributed to that the loss of hemicellulose which caused the other two fractions (i.e., lignin, cellulose) to increase relatively. The acid insoluble lignin represents mainly Klason lignin, but also includes ash and condensation products of polysaccharide degradation known as pseudo-lignin.<sup>172</sup> The acid insoluble lignin increased from 32.06% to 46.11%, which can be attributed to 1) the hemicellulose loss; 2) the formation of pseudo-lignin during autohydrolysis process.<sup>164, 172-173</sup>

### 3.3.2 CP/MAS $^{13}\text{C}$ NMR analysis of pine wood feedstocks

CP/MAS  $^{13}\text{C}$  NMR analysis was employed to fully characterize the effect of autohydrolysis pretreatment on the biomass structure of the pine wood, as shown in Figure 14. The assignment of the chemical shifts was followed according to the literature.<sup>174</sup> The peak at ~21 ppm was assigned to the acetyl  $\text{CH}_3$  groups of hemicellulose and the intensity of the peak significantly decreased after the autohydrolysis pretreatment. The decreased peak intensities indicated that the acetyl groups of softwood galactoglucomannan were significantly solubilized in the presence of the acidic hydronium ions. The peak at 55 ppm represented the methoxy groups of lignin in the various pine samples. Similar peak intensities for this signal were observed in the untreated and pretreated pine wood samples indicating that the hydrothermal pretreatment had the minimal effect on the lignin methoxy group content. The peak centered at 65-62 ppm was assigned to C-6 of cellulose and the peak centered at 75-72 was assigned to C-2, C-3, C-4 of cellulose. The peaks at ~84 ppm and ~89 ppm were attributed to amorphous and crystalline C-4 of cellulose, but also overlapped with the hemicellulose carbons and lignin side chain carbons. The ratio of the crystalline to amorphous cellulose increased. This observation can be attributed to the change of cellulose crystallinity and the removal of the hemicellulose.<sup>165</sup> The peak at 105 ppm mainly represented C-1 of cellulose and overlapped with signals for hemicellulose. The peaks ranged from 137-131 ppm and 120-112 ppm were attributed to the aromatic C-C bonds and C2, C5, C6 of guaiacyl C-H bonds in lignin, respectively. The increased intensity of these peaks indicated that the higher lignin content in the autohydrolysis pretreated pine wood. The carbohydrates degradation components could also form aromatic C-H and C-C bonds. The peak at ~153 ppm was attributed the aromatic C-3 or C-



4 in the etherified guaiacyl units which was decreased. Meanwhile, the intensity of the peak at 148 ppm increased, which was attributed to the aromatic C-3 or C-4 in the guaiacyl units with free phenolic groups. Furthermore, the pretreated pine wood showed lower intensity of the carboxyl carbons (~173 ppm), which indicated that some of the acid moieties has been removed during the autohydrolysis process. In the previous study about the biomass torrefaction pretreatment, CP/MAS  $^{13}\text{C}$  NMR results showed an increased intensity of the carboxyl peak after torrefaction, which was in contrast of the autohydrolysis pretreatment<sup>174</sup>.

### 3.3.3 FT-IR analysis of pine wood feedstocks

The FT-IR spectra of both untreated and pretreated pine sawdust feedstocks are shown in Figure 15. The assignments of FT-IR spectroscopy peaks are based on the literature.<sup>175-178</sup> The region  $1800 - 800\text{ cm}^{-1}$  of the spectra was ascribed for lignin, cellulose, and hemicellulose units. Major peaks in this region are labeled and the peak assignments are summarized in Table 17. As shown in Table 17, the peak 1 has been assigned to the C=O in hemicellulose. The peaks in the region of  $1600 - 1250\text{ cm}^{-1}$  are mainly ascribed to the lignin units. In Figure 14, it was clearly observed that the intensity of peak 1 decreased while the intensity of peaks 3 – 9 increased. This qualitative observation concluded that the ratio of lignin to hemicellulose was increased for the pine wood sample after the pretreatment. Yan et al.<sup>176</sup> characterized dilute acid pretreated poplar wood using FT-IR spectroscopy and reported a similar result. The FT-IR spectroscopy qualitative results were consistent with the  $^{13}\text{C}$  CP/MAS NMR results, showed that mild autohydrolysis pretreatment largely removed hemicellulose, while had much smaller impact on cellulose and lignin.

### 3.3.4 Yields of pyrolysis products

The pyrolysis process breaks down biomass into three phase products: gas, oil, and char. Figure 16 presents the pyrolysis products yield distribution from both untreated and pretreated pine wood samples. For the oils produced at all the three temperatures (400 °C, 500 °C, 600 °C), the autohydrolysis pretreatment resulted in less light oil yields especially at 600 °C. According to the literature, the major components in light oil include water, acetic acid, methanol, and catechol.<sup>119</sup> The light oil yields proved that autohydrolysis can effectively remove the unfavorable water-soluble contents of the bio-oil, which is beneficial to the overall pyrolysis process. Conversely, the pretreatment led to the higher yields of the heavy oils. The heavy oil refers to the water-insoluble fraction and is primarily comprised of aromatic compounds. The heavy oil yields increased by 14.73%, 22.56%, 40.12% after the autohydrolysis pretreatment, at elevated pyrolysis temperature, respectively. It can be attributed to that the autohydrolysis pretreatment increased the lignin content percentage and lignin decomposed to the aromatic products during the pyrolysis process. For the pyrolysis process at 400 °C and 500 °C, the autohydrolysis pretreated biomass gave higher total oil yields, which was consistent with Chang et al.'s report.<sup>179</sup> However, for the pyrolysis process at 600 °C, the pretreated pine wood led to 13.27% reduction of total oil yield compared to the untreated pine wood. Previous literature reported that at a higher temperature, the pyrolysis oil experiences a secondary decomposition process.<sup>12, 119</sup> The pyrolysis oil components undergo self-decomposition process and form non-condensable gases, such as H<sub>2</sub>, CO, CH<sub>4</sub>, CO<sub>2</sub>, C<sub>2</sub>H<sub>4</sub>, and C<sub>2</sub>H<sub>6</sub>. Comparing the pyrolysis of untreated pine wood at 500 °C and 600 °C, total oil yield decreased from 58.44% to 50.40%, while the gas yield increased from 16.96% to 27.70%.

The pretreated pine wood produced 64.11% and 43.71% total oil, 12.86% and 36.18% gas, at 500 °C and 600 °C, respectively. The yield results indicated that the secondary decomposition had more severe impact on pretreated pine wood than original pine wood. As for the solid products, the pretreatment led to lower char yields for all the three pyrolysis temperatures. Previous studies pointed out that another pretreatment method, torrefaction, caused higher char yields and reduced liquid pyrolysis product yields.<sup>180-182</sup> The char and bio-oil yield results in this study proved that the autohydrolysis pretreatment did not suffer from the same problem.

### **3.3.5 <sup>31</sup>P NMR analysis of heavy oils**

To examine the effect of autohydrolysis pretreatment on the hydroxyl groups in bio-oils, <sup>31</sup>P NMR analysis was employed in this study. The <sup>31</sup>P NMR spectra of derivatized heavy oils from untreated and pretreated pine wood feedstocks are listed in Figure 17 and the assignment of chemical shifts was followed according to the literature.<sup>119, 122, 183</sup> Figure 18 compares the acid hydroxyl contents in the heavy oils from pyrolysis of untreated and pretreated pine wood samples. The acid-OH groups exhibit peaks at 136.6-134.6 ppm in a <sup>31</sup>P NMR spectrum. For the pyrolysis temperatures at 400, 500, and 600°C, the acid-OH contents decreased by 48.53%, 70.96%, and 78.18%, respectively. The removal of acetyl groups and acid moieties of hemicellulose could be a potential reason causing the decrease of acid-OH contents. The reduction of acid contents can significantly decrease the corrosiveness of bio-oil. Figure 19 presents the aliphatic hydroxyl groups in the heavy oils from pine wood feedstocks before and after the pretreatment. The chemical shift assignment of aliphatic hydroxyl groups is 150.0 ppm – 145.0 ppm. Fu et al.<sup>184</sup> reported the <sup>31</sup>P NMR analysis results of the bio-oil from untreated southern pine wood. Their results

indicated that the aliphatic hydroxyl group contents ranged from 6.36 mmol/g to 7.08 mmol/g and made up the majority of the total hydroxyl groups, which was very consistent with our results for the heavy oils from untreated pine wood. Figure 19 indicates that the autohydrolysis pretreatment increased the aliphatic hydroxyl groups in the heavy oils. The sharp peak signals at 148.70 ppm, 147.27 ppm, and 147.22 ppm in Figure 19 were assigned to the three phosphitylated hydroxyl groups from a levoglucosan molecule.<sup>184</sup> The non-condensed and C<sub>5</sub> substituted condensed phenolic hydroxyl group contents are shown in Figure 20 and Figure 21, respectively. The <sup>31</sup>P NMR results showed that the pretreated pine wood produced higher guaiacyl, catechol, and *p*-hydroxy-phenyl OH contents in the heavy oils, with an exception that the pretreatment led to a 22.86% reduction of catechol type OH content at a pyrolysis temperature of 600 °C. Similarly, Neupane et al. claimed that the torrefaction pretreatment increased the carbon yield of phenolic compounds in bio-oils from 0.99% to at most 3.45%.<sup>164</sup> Neupane et al. proposed that these phenolic compounds can be dehydrated to form aromatic hydrocarbons in a H<sup>+</sup>ZSM-5 catalyzed pyrolysis process, which will promote the bio-oil's quality as a fuel.<sup>164</sup> Figure 21 indicated that the pretreated pine wood produced higher C<sub>5</sub> substituted condensed phenolic contents at a pyrolysis temperature of 400 °C and 500 °C. Although the CP/MAS <sup>13</sup>C NMR results suggested that the autohydrolysis partly broke down the ether bonds in lignin, the relative total lignin percentage increased and the condensed poly-aromatic structures formed during the autohydrolysis pretreatment, which led to higher C<sub>5</sub> substituted condensed phenolic contents in heavy oils. However, at a pyrolysis temperature of 600 °C, the autohydrolysis pretreatment removed 92.70±1.69%, 92.00±5.03%, and 15.18±4.51% of the β-5, 4-O-5, 5-5 type C<sub>5</sub> substituted condensed phenolic compounds in heavy oils. The <sup>31</sup>P NMR results

indicated that at a high pyrolysis temperature (e.g., 600 °C), the autohydrolysis pretreatment had a significant effect on minimizing the presence of C<sub>5</sub> substituted phenolics.

### 3.3.6 HSQC NMR analysis of heavy oils

HSQC provides a facile way to elucidate the component structures in the bio-oil. Figure 22 shows the HSQC spectra of levoglucosan in the bio-oils and the assignments of C-H bonds in levoglucosan. It is clear that under all the three pyrolysis temperatures, the autohydrolysis pretreated pine wood produced higher yields of levoglucosan, which was consistent with the <sup>31</sup>P NMR analysis results. Figure 23 indicates the methoxy group contents in the bio-oils produced from both untreated and pretreated pine wood. The HSQC spectra shows that under the pyrolysis temperature 400 °C and 500 °C, the methoxy groups in bio-oils produced from untreated and pretreated pine wood feedstocks were comparable. At the higher pyrolysis temperature (600 °C), the autohydrolysis pretreatment led to a reduction of methoxy groups in the bio-oil.

## 3.4 Conclusion

In this study, the effects of autohydrolysis pretreatment on pine sawdust and the resulting pyrolysis oils were fully investigated. The autohydrolysis pretreatment effectively removed acetyl groups from the pine wood. The autohydrolysis pretreatment led to up to 40.12% increase of the heavy fraction in the bio-oil product. The pretreatment resulted in 48.53%, 70.96%, and 78.18% reduction of acids from the bio-oil produced at a pyrolysis temperature of 400, 500, and 600°C. At the higher temperature, the autohydrolysis pretreatment also removed condensed hydroxyl groups and methoxy groups from the bio-

oil, which is a benefit for the bio-oil as a fuel. Further condition optimization will be studied in the next chapter.

**CHAPTER IV: EXPERIMENTAL CONDITION**

**OPTIMIZATION OF AUTOHYDROLYSIS**

**PRETREATMENT EFFECT ON BIOMASS FEEDSTOCKS**

A version of this chapter was originally published by Naijia Hao, Konyu Lu, Haoxi Ben, Sushil Adhikari, Tais Bezerra, and Arthur J. Ragauskas; reprinted with permission from Wiley:

“Hao, N.; Lu, K.; Ben, H.; Adhikari, S.; Lacerda, T. B.; Ragauskas, A. J., Effect of Autohydrolysis Pretreatment Conditions on Sugarcane Bagasse Structures and Product Distribution Resulting from Pyrolysis. *Energy Technology* **2018**, 6 (4), 640-648.”

The author Tais Bezerra is from University of Tennessee. The author Haoxi Ben is from Southeast University. The author Sushil Adhikari is from Auburn University. The author Arthur J. Ragauskas is from University of Tennessee and Oak Ridge National Laboratory. Naijia Hao, Sushil Adhikari, and Arthur Ragauskas designed the study. Naijia Hao performed the experiments and drafted the manuscript. Konyu Lu assisted with the GC-MS analysis of bio-oils. Tais Bezerra, Haoxi Ben, Sushil Adhikari, and Arthur Ragauskas revised the manuscripts.

## 4.1 Introduction

According to the U.S. Energy Information Administration (EIA), global energy consumption is projected to increase to 858 exajoules in 2040 compared with 549 exajoules in 2012.<sup>185</sup> While fossil fuels remain the dominant transportation fuel, renewable energy sources are trending upward. The U.S. Department of Energy (DOE) reported that the renewable energy consumption has increased steadily since 2001 and the total renewable energy consumption has expanded by ~82% from 2001 to 2014.<sup>186</sup> Among the renewable energy resources, biomass-based resources play a critical role. Lignocellulosic bioresources are broadly applied to the generation of power, heat, and fuels from home use to industrial production.

Biomass resources include woody feedstocks, energy crops, crop residues, and waste resources. These feedstocks are low-cost and typically avoid direct competition with the use of agriculture land for food crops. Sugarcane bagasse is a typical biomass feedstock from agriculture waste; it is estimated that each ton of sugarcane can yield ~0.14 tons of bagasse on a dry basis.<sup>186</sup> The large-volume production of the sugarcane bagasse has attracted significant attention for its use in the biorefinery scenario, especially for its conversion to bioethanol and biopower.<sup>187</sup>

Pyrolysis is one of the promising biomass conversion techniques to produce biofuel precursors. Researchers have conducted pyrolysis on the sugarcane bagasse and examined the properties of the bio-oils.<sup>188-190</sup> These results showed that the pyrolysis oils from sugarcane bagasse exhibited low pH values, low heating values, and high water content, which were comparable to the bio-oils generated from other biomass feedstocks.<sup>191</sup>



Pretreatment of biomass is one of the methods currently under investigation to address the unfavorable characteristics of the bio-oils. Researchers have been focused on both thermal pretreatment (i.e., torrefaction) and chemical pretreatment (e.g., leaching/washing, acid pretreatment, autohydrolysis pretreatment) to achieve the optimum feedstocks prior to the pyrolysis.<sup>158</sup> Davidsson et al. conducted water washing and acid leaching on wheat straw, wood waste, and cellulose and pyrolyzed the pretreated feedstocks, which improved the combustion properties of the resulting bio-oils by removing alkali components.<sup>192</sup> Neupane et al. performed both non-catalytic and catalytic pyrolysis on torrefied pine wood; the torrefied pine wood with a reduced content of hemicelluloses achieved a higher yield of aromatic hydrocarbons.<sup>164</sup> Wang et al. compared acid, alkali, and steam explosion pretreatments on the pine wood prior to pyrolysis; here, the results showed that a dilute acid pretreatment resulted in the highest heating value of the bio-oil.<sup>193</sup>

Among pyrolysis pretreatment technologies, an autohydrolysis pretreatment is free of chemical additives using the elevated reaction temperature (140 – 220 °C), to generate acetic acid from the acetyl groups of hemicellulose which catalyzes autohydrolysis reactions.<sup>194</sup> When compared with the pretreatments involving acids or alkali, the autohydrolysis pretreatment process does not require a large amount of chemicals to neutralize the hydrolyzed products. Another benefit of this pretreatment process is low reactor corrosion requirement.<sup>195</sup> This pretreatment process has been applied to bioethanol production as a convenient methodology to reduce the recalcitrance of biomass; researchers are now seeking opportunities to combine this technology together with the pyrolysis process to test if the

autohydrolysis pretreatment could achieve higher quality of bio-oils. Zheng et al. performed autohydrolysis pretreatment on the eucalyptus wood and showed that the pretreatment lowered reactive components (i.e., ketones, aldehydes, acids) in the bio-oils.<sup>196</sup> Du et al. conducted autohydrolysis pretreatment on microalgae and concluded that the resulting bio-oil yielded less N-containing compound.<sup>170</sup> However, at the present time, no knowledge exists about the effect of autohydrolysis pretreatment on the resulting pyrolysis oils derived from sugarcane bagasse. In this study, we performed the autohydrolysis pretreatment on sugarcane bagasse using three different conditions: 180 °C - 10 min, 180 °C - 40 min, 200 °C - 40 min. Compositional analysis and <sup>13</sup>C CP/MAS NMR were used to investigate the structural changes in the sugarcane bagasse feedstocks. The product distribution and the properties of the bio-oils were characterized by HSQC, phosphorylation followed by <sup>31</sup>P NMR, and GPC.

## **4.2 Experimental methods**

### **4.2.1 Material and sample preparation**

Chemicals and biomass used in this chapter was presented in the sections 2.1.1 and 2.1.2 in this dissertation.

### **4.2.2 Equipments and experimental procedures**

Autohydrolysis and pyrolysis set-ups and processing details were presented in sections 2.2.1 and 2.2.2.

### **4.2.3 Characterization of biomass and bio-oils**

Detailed characterization techniques were presented in sections 2.3.1.1, 2.3.1.3, 2.3.3.1, 2.3.3.2, 2.3.3.5.3, and 2.3.3.5.4.

## 4.3 Results and discussion

### 4.3.1 Chemical composition analysis

Autohydrolysis pretreatment of sugarcane bagasse was conducted at three reaction conditions: 180 °C – 10 min, 180 °C – 40 min, and 200 °C – 40 min. Figure 24 presents the chemical composition of sugarcane bagasse both before and after the autohydrolysis pretreatment. The untreated sugarcane bagasse was mainly comprised of four monosaccharides: glucose, xylose, arabinose, and galactose. Xylose made up to 22.08% and represented the major hemicellulosic monosaccharide from the untreated feedstock. The autohydrolysis pretreatment significantly removed the hemicellulose fraction in sugarcane bagasse. The pretreatment at 180 °C for 10 min removed 23.96% xylose, 86.00% arabinose, and almost 100% galactose. Prolonging the pretreatment time to 40 min enhanced the removal of xylose up to 73.87% and led to complete removal of arabinose. Under the most severe pretreatment conditions (200 °C – 40 min), it was observed that nearly 100% of the hemicellulosic components were removed. Klason lignin, also known as acid insoluble lignin, showed an increasing trend after the pretreatment at 180 °C for 10 min and 40 min, and a reduction after the pretreatment at 200 °C for 40 min. The relative increase of the lignin fraction could be attributed to the removal of other components (mainly hemicellulose) as well as “pseudo-lignin” formation.<sup>172</sup> Under the acidic conditions employed, autohydrolysis can lead to hydrolysis of lignin carbohydrate complexes and depolymerization of lignin via  $\alpha$ -O-4 and  $\beta$ -O-4 bond rupture and these reactive components can undergo a series of reactions including dehydration and condensation reactions resulting in solubilization of lignin fragments and the modification of lignin in the plant cell wall.<sup>197</sup> These competing reaction pathways presumably

contribute to the observed changes in the content of lignin of the autohydrolyzed products at differing severity conditions.<sup>198</sup> As for cellulose, the pretreatments increased the cellulose content, reaching a maximum value of 64.57%. This trend was attributed to the substantial removal of hemicellulose. It has been reported that a longer reaction time did not significantly increase the removal of cellulose due to the crystallinity of cellulose.<sup>199</sup>

#### 4.3.2 CP/MAS <sup>13</sup>C NMR analysis

The most significant changes in solid-state <sup>13</sup>C NMR spectral data of the starting and autohydrolyzed bagasse samples (see Figure 25) can be found around 21 and 173 ppm. These two peaks were assigned to the acetyl methyl and carboxyl carbons in hemicellulose, respectively.<sup>200</sup> These two peaks were relatively intense in the untreated sugarcane bagasse; it was clearly observed that the intensity of these two peaks decreased with increasing pretreatment condition severities. After pretreatment at 200 °C for 40 min, the carboxyl and acetyl groups in the hemicellulose were almost eliminated. Another major change can be observed in the lignin region centered about 148 and 152 ppm, which were assigned to the non-ether linked and ether linked guaiacyl carbons, respectively. The peak intensity of the ether linked guaiacyl carbons decreased after the pretreatment, whereas the peak intensity of the non-ether linked guaiacyl carbons increased. This result indicated the cleavage of the ether linkages lignin presumably leading to the formation of free phenolic groups. The chemical shift region of 105 – 62 ppm was assigned to the cellulose carbons which overlapped with lignin and hemicellulose signals. The peak at 89 ppm contains the C-4 signal for crystalline cellulose, along with other structural components. The peak at 84 ppm was assigned to C-4 of amorphous cellulose and overlapped with signals from lignin and hemicellulose. As the severity of the pretreatment condition increased, the peak

intensity ratio of the peaks at 89 and 84 ppm also increased. This result suggested that the autohydrolysis pretreatment enhanced the cellulose crystallinity component in the pretreated sugarcane bagasse.

#### **4.3.3 Yield distribution of the pyrolysis products**

Figure 26 and Figure 27 summarize the product yield distribution from the sugarcane bagasse pretreated at different conditions, based on the mass of pretreated biomass and original biomass, respectively. Figure 26 shows that at a pyrolysis temperature of 400 °C, bio-oils generated from the pretreated sugarcane bagasse were all observed to have higher yields than bio-oil from the control group. However, the most severe pretreatment condition (200 °C - 40 min) resulted in decreased bio-oil yields than the milder pretreatment conditions (180 °C - 10 min, 180 °C - 40 min), with a char yield increase of around 4%. This observation may indicate that at a lower pyrolysis temperature (i.e., 400 °C), the severe pretreatment condition caused the sugarcane bagasse to suffer from more carbonization reactions. At a pyrolysis temperature of 500 and 600 °C, the sugarcane bagasse samples that were pretreated at 180 °C - 10 min and 200 °C - 40 min generated higher bio-oil yields (up to 59.86%) when compared to the control group, while the pretreatment condition 180 °C - 40 min showed a negative effect on the oil yields. The lower oil yields from the pretreatment at 180 °C - 40 min corresponded to lower char yields and the highest gas yields. This phenomenon suggests that the pyrolysis of the 180 °C - 40 min pretreated sugarcane bagasse at higher temperatures (i.e., 500 and 600 °C) leads to secondary decomposition reactions of pyrolysis oils. During secondary decomposition reactions, parts of liquid products were fragmented into gases.<sup>201</sup> Past pyrolysis studies of biomass indicated that carbon monoxide, carbon dioxide, methane, ethane, and ethene are

some of the most common components in the gas phase.<sup>202</sup> As shown in Figure 3(b), the autohydrolysis pretreatment lowered the bio-oil yield based on the mass of original biomass due to the mass loss during the pretreatment process. At a pyrolysis temperature of 400 °C, the bio-oils produced from both untreated and 180 °C - 10 min pretreated sugarcane bagasse had the similar yields ~ 40% based on the mass of original biomass. Considering the energy consumption during the autohydrolysis pretreatment and pyrolysis process, the pretreatment condition of 180 °C - 10 min was recommended for achieving higher bio-oil yield.

#### **4.3.4 Molecular weight analysis of the bio-oils**

The weight average molecular weight (Mw), number average molecular weight (Mn), and polydispersity (PDI) of bio-oils produced from the control and pretreated sugarcane bagasse are presented in Figure 28. Gasoline range products have a number molecular weight around 80~120 g/mol.<sup>203</sup> Usually bio-oils have much higher average molecular weight values, which is not a preferred characteristic for pyrolysis oils. At a pyrolysis temperature of 400 and 500 °C, the bio-oils produced from 180 °C - 40 min pretreated sugarcane bagasse exhibited the highest average molecular weights among the oils. At a pyrolysis temperature of 600 °C, the pretreatments at 180 °C (both 10 min and 40 min) yielded comparable higher average molecular weights (Mn=136.01 and 138.97 g/mol). Bio-oil produced from the 200 °C - 40 min pretreated and 400 °C pyrolyzed sugarcane bagasse showed the lowest average molecular weight (Mn=121.88 g/mol), which was close to the range of gasoline products. The bio-oil produced from this condition also yielded the lowest polydispersity value of 1.42. This could be attributed to

the fact that in the bio-oil produced under these conditions had the most favorable thermal fragmentation and secondary reactions.<sup>119</sup>

#### 4.3.5 <sup>31</sup>P NMR analysis of the bio-oils

Figure 29-32 present the quantitative integration results of <sup>31</sup>P NMR analysis of the phosphitylated bio-oils produced from various sugarcane bagasse feedstocks. The chemical shift assignments are based on the literature.<sup>183</sup> The aliphatic OH groups were assigned to 150.5-144.5 ppm. Figure 29 shows that at all three pyrolysis temperatures, the bio-oils from the pretreated sugar bagasse exhibited similar trends: pretreatments of moderate conditions (180 °C, 10 or 40 min) increased the aliphatic OH groups compared to the control group. For the 40 min pretreatments increasing the pretreatment temperature from 180 °C to 200 °C lowered the aliphatic OH content. Most of the aliphatic OH groups came from levoglucosan, which were assigned to signals at 148.68, 147.26, and 147.21 ppm. Figure 30 presents the C<sub>5</sub> substituted phenolic OH groups; β-5 and 5-5 phenolic OH groups were generated less in the pretreated sugarcane bagasse bio-oils, while pretreatment resulted in more 4-O-5 phenolic OH groups. Non-condensed phenolic OH groups are shown in Figure 31. It is clear the pretreatment at all conditions led to a reduced production of guaiacyl and catechol OH groups. Most importantly, as shown in Figure 32, the significant reduction of the acids in bio-oils was presumably due to the pretreatment hydrolysis of acetylated hemicelluloses. At a pyrolysis temperature of 400 °C with bagasse pretreated at 180 °C for 40 min, the resulting bio-oil is produced the least amount of acids (0.34 mmol/g), while at a pyrolysis temperature of 500 or 600 °C, the most severe pretreatments led to the least amount of acids (0.47, 0.34 mmol/g). The GC-MS data in Table 18 showed the similar trends regarding the acids removal.

#### 4.3.6 HSQC NMR analysis of the bio-oils

Figures 33-36 present the 2D HSQC spectra and assignments of C-H bonds in bio-oils pyrolyzed from untreated and pretreated sugarcane bagasse at 500 °C. The chemical shift assignments are based on the published literature.<sup>101</sup> Figure 33 shows the two different methoxy groups in the bio-oils. The C1 type of methoxy group does not exist in native sugarcane bagasse lignin and could be rearranged from C2. At all three pyrolysis temperatures, the intensity of both C1 and C2 type of methoxy groups slightly decreased after the autohydrolysis. Figure 34 presents the 2-D maps of the C-H bonds of levoglucosan in the bio-oils. The intensity of levoglucosan contents increased especially in the high severity conditions, which are consistent with the <sup>31</sup>P NMR results. The aliphatic regions of the HSQC spectra are shown in Figure 35. The content of compound F (5-methylfurfural) increased significantly with the increasing pretreatment severity. Like levoglucosan, the 5-methylfurfural is a major degradation product from cellulose. The increased percentage of cellulose after the pretreatment resulted in the increased amount of levoglucosan and 5-methylfurfural. The oxygenated compound G (aldehyde type) was slightly removed by the pretreatment while part of the hydrocarbon products D4 (aromatic type) and D5 (aliphatic type) were partially eliminated. Figure 36 presents the aromatic region of the HSQC spectra of the bio-oils. From these data, it could be observed that the pretreatments partially reduced the phenol type oxygenated compounds A1 and B1. However, the pretreatment severity does not have a significant effect on the contents of these oxygenated compounds. The contents of the phenol type oxygenated compounds B3 also decreased after the pretreatment and achieved the minimum quantity by the most severe pretreatment condition.



#### **4.4 Conclusion**

The three different conditions of autohydrolysis pretreatments (180 °C - 10 min, 180 °C - 40 min, 200 °C - 40 min) were conducted on the sugarcane bagasse and the resulting bio-oils were analyzed. The autohydrolysis pretreatment led to an optimum bio-oil yield of 59.86%, and bio-oils of the lowest molecular weight were generated from the most severe condition pretreated sugarcane bagasse at a pyrolysis temperature of 400 °C. The autohydrolysis pretreatment effectively reduced the presence of acids and oxygenated aromatic compounds in the bio-oils, while the yields of undesired levoglucosan and 5-methylfurfural increased. Overall, considering both the undesired products reduction and lower pyrolysis conditions, a mild pretreatment condition (180 °C - 10 min) is suggested to be applied to enhance the bio-oil property.

## **CHAPTER V: EX-SITU UPGRADING OF BIO-OILS OVER METAL OXIDE CATALYSTS**

A version of this chapter was under preparation by Najjia Hao, Xianzhi Meng, Chang Geun Yoo, Charles Cai, Charles Wyman, and Arthur J. Ragauskas.

Hao, N.; Meng, X.; Yoo, C.; Cai, C.; Wyman, C.; Ragauskas, A.J., Upgrading of bio-oils from sugarcane bagasse via hydrogen transfer in supercritical methanol using Copper doped porous metal oxide.

The author Xianzhi Meng is from University of Tennessee. The author Chang Geun Yoo is from Oak Ridge National Laboratory. The authors Charles Cai and Charles Wyman are from University of California, Riverside. The author Arthur J. Ragauskas is from University of Tennessee and Oak Ridge National Laboratory. Najjia Hao and Arthur J. Ragauskas designed the study. Najjia Hao performed the experiments and drafted the manuscript. Xianzhi Meng and Charles Cai assisted with the catalyst preparation. Charles Wyman and Arthur J. Ragauskas revised the manuscript.

## 5.1 Introduction

Pyrolysis is a single-step process to transform lignocellulosic biomass feedstocks to liquid bio-crudes.<sup>204</sup> The method of pyrolysis distinguished from a variety of biomass conversion routes to bioenergy and value-added chemicals as pyrolysis benefits from the low processing cost and requires one single reactor system and short residence times.<sup>205-206</sup> The potential of co-processing of biomass derived drop-in fuels with petroleum refinery in current infrastructure could possibly reduce capital cost, hence make pyrolysis of biomass a route with high technical and economic advantages.<sup>207</sup>

Bio-crudes (bio-oils) from pyrolysis of whole biomass typically contain oxygenated species including acids, aldehydes, ketones, phenols, furans, and anhydrosugars.<sup>208</sup> These highly-oxygenated species make the bio-oils of a high oxygen content (35~40%) and cause the poor qualities of bio-oils to be blended with current liquid transportation fuels.<sup>26</sup> The higher heating value (HHV) of the crude bio-oils are typically 16-19 MJ/kg compared with 40 MJ/Kg of the commercial heavy fuels.<sup>26</sup> The acidic contents in bio-oils result in the corrosion problem of the engine or the pipeworks. The aldehyde and hydroxyl contents are highly reactive, thus the continuation of secondary reactions cause the aging problems of bio-oils.<sup>105</sup> The high reactivity of these species at a high temperature even make the distillation for separation not applicable. Research efforts have been put forward into the hydrodeoxygenation (HDO) of bio-oils to two different categories of value-added products: liquid hydrocarbons as fuel precursors and chemical building blocks. The representative research efforts include Huber and co-worker's strategy demonstrating a combinatorial process to produce liquid alkanes ranging from C<sub>7</sub> to C<sub>15</sub> using acid and solid base catalysts.<sup>209</sup> Huber and co-workers also outlined a strategy

converting bio-oils to commodity chemical feedstocks (e.g., benzene, toluene, xylene) using catalytic hydro processing followed by zeolite catalysis.<sup>210</sup>

Ford and co-workers were inspired by the KOH promoted hydrogenolysis of dihydrobenzofuran (DHBF) in supercritical conditions and dedicated to developing a solid base catalyst that could transfer hydrogen from supercritical methanol to cleave the aromatic ether bond.<sup>211</sup> A copper-doped porous metal oxide (PMO) derived from Mg-Al hydrotalcite-like (HTL) precursors was synthesized and applied to convert DHBF to ethylcyclohexanol (selectivity of 67.7%). This copper-doped PMO catalyst benefits from the cheap price and can be easily prepared. The characteristic of transferring hydrogen from supercritical alcohol of this catalyst was further applied to hydrogenolysis and hydrogenation of real lignin since lignin consists large amount of phenyl ether bonds which can be represented by the model compound DHBF. Ford's group and Hensen's group applied the copper-doped PMO in the depolymerization of lignin in supercritical methanol/ethanol and found the char formation was largely suppressed at a moderate reaction temperature depending on the feedstock sources.<sup>138, 212-215</sup> Huber's group depolymerized cellulose in supercritical methanol and used model compounds to elucidate that the reaction pathway primarily consisting of retro-aldol condensation and recondensation with the methanol.<sup>216</sup> However, very limited studies were focused on the catalytic upgrading of bio-oils using a CuMgAl mixed metal oxide catalyst. Wang et al. valorized sugar fractions from fast pyrolysis oils in supercritical alcohols using Cu doped PMO catalyst.<sup>217</sup> The obtained product profile was quite complicated and consisted mainly mono-alcohols, diols, ethers, esters, and furans.<sup>217</sup> Research works to date have not studied the role of Cu doped PMO

catalyst in upgrading of real bio-oils and the complex underlying reaction pathways have not been revealed in this bio-oil catalytic upgrading system.

Here we demonstrated a strategy to upgrade sugarcane bagasse bio-oils via hydrogen transfer in supercritical methanol to achieve the hydrodeoxygenation of bio-oils. The experiments were performed in a batch reactor for the bio-oil catalytic upgrading. The upgraded bio-crudes were thoroughly analyzed by a variety of analytical methods, including  $^1\text{H}$  NMR,  $^{31}\text{P}$  NMR, HSQC NMR, GC-MS, and GPC. The results demonstrated the significant reaction condition impact on the hydrogenation degree of the bio-oils.

## **5.2 Experimental methods**

### **5.2.1 Material and sample preparation**

Chemicals and biomass used in this chapter was presented in the sections 2.1.1 and 2.1.2 in this dissertation.

### **5.2.2 Equipments and experimental procedures**

Pyrolysis set-ups and catalyst preparation details were presented in sections 2.2.2 and 2.2.5.

### **5.2.3 Characterization of biomass and bio-oils**

Detailed characterization techniques were presented in sections 2.3.3.1, 2.3.3.2, 2.3.3.5.1, 2.3.3.5.3, 2.3.3.5.4, and 2.3.4.

## **5.3 Results and discussion**

### **5.3.1 Effect of reaction temperature**

The Copper doped hydrotalcite precursor was prepared by a co-precipitation method based on the published work.<sup>211-212</sup> The hydrotalcite layered structure was confirmed by XRD, as shown in Figure 37. Peaks close to  $2\theta = 38^\circ, 46^\circ, 60^\circ$  were attributed

to diffraction by planes confirm the layered structure of hydrotalcite.<sup>138</sup> The hydrotalcite precursor was further calcinated to porous metal oxide powders, which was denoted as CuMgAlO<sub>x</sub>.

Experiments of the sugarcane bagasse bio-oil upgrading was performed in a batch reactor. The temperature, reaction time, and catalyst loading were tested. The corresponding yield distribution of the upgraded bio-crudes were illustrated in Figure 38 a-c. Temperatures (250 °C, 275 °C, 300 °C) were tested with the reaction time of 8 h and a B:C of 1:1. The highest yield of 43.99 wt% occurs at 275 °C, which was calculated based on the mass of the bio-oil subjected into the reactor. The reaction at 250 °C resulted only 16.75%, which may be partially due to that the hydrogen not fully donated from methanol under this condition. The yield and quality of the bio-oils from catalytic upgrading were usually a trade-off. Compared with the previous research works, Cheng et al. performed the hydrodeoxygenation of bio-oils over 15%Ni-5%Zn/Al<sub>2</sub>O<sub>3</sub> and the highest upgraded bio-oil yield was 44.64 wt%.<sup>218</sup> Duan et al. upgraded the pretreated algae bio-oil over zeolite in supercritical water and found that the highest bio-oil yield was 54.45 wt% over MCM-41.<sup>219</sup>

The initial GC-MS analysis results of reaction profile at varied temperature was presented in Figure 39. The aliphatic alcohol was not identified in the original bio-oil whereas the 250 °C upgrading reaction resulted in a 30.70 area% of the aliphatic alcohol. It should be noted that the anhydrosugars (i.e., levoglucosan) was not categorized as ether or alcohol in Figure 39, and the anhydrosugar content in the original bio-oil was 33.58 area%. The carbonyl content (ketone/aldehyde) was significantly increased with higher the reaction severity. The total hydrocarbon content became prevalent as upgrading

temperature increased. The hydrocarbon compounds were not detected in original bio-oil, as upgrading increased to 300 °C, the hydrocarbon shared 14.19 area% of the total GC identified compounds.

Figure 40 listed the aliphatic alcohol and hydrocarbon compounds in the bio-oil upgraded from 300 °C, 8h, B:C = 1:1 g/g. There are three main categories of the hydrocarbon compounds identified by GC under this condition: benzene derivatives, cyclohydrocarbon, and unsaturated chains. For the alcohols, most comprised of short chain alcohols, but hydrogenated cyclo-alcohol existed as well, for example, 2,6,6-trimethylcyclohex-2-en-1-ol, 2,4-dimethylcyclopentan-1-ol, and 3-methylcyclopentane-1,2-diol. GC-MS provides a detailed compound identification but GC-MS could not detect the bio-oil fraction with a high boiling point and lowest boiling point fraction may be covered by the solvent delay either.<sup>220</sup>

To compensate the GC limitations regarding the bio-oil characterization, proton NMR was applied for a detailed structural elucidation. Figure 41 provides an example of the <sup>1</sup>H NMR spectra of the bio-oil upgraded from the reaction with 300 °C, 8 h, B:C = 1:1. The figure was split into four regions: aldehyde and carboxyl acids (-CHO, -COOH), aromatic proton or protons adjacent to an unsaturated chain (ArH, HC=C-), proton adjacent to an oxygen (-CH<sub>n</sub>-O-, CH<sub>3</sub>-O-), and aliphatic protons (-CH<sub>3</sub>, -CH<sub>n</sub>-). The detailed integration results were shown in Figure 42. Consistent with GC-MS results, the aliphatic protons were increased with higher reaction temperature. The aromatic/alkene proton integration results from upgraded bio-oils decreased compared with the original bio-oils, whereas the 275 °C was observed with the highest aromatic/alkene protons among the

upgrading reactions. To further evidence the aromatic structural changes during the upgrading reactions, 2-D HSQC NMR was selected to characterize the bio-oils.

An example of the HSQC analysis of the aromatic structures in the bio-oil before and after upgrading reactions was shown in Figure 43. The HSQC NMR signals were assigned to four proton types in aromatic structures (A-D) and furfural structure (E and F).<sup>119, 221</sup> It was clearly found that E type aromatic proton and E&F type proton in furfural derivatives were eliminated by the upgrading reaction at all temperatures (250 °C, 275 °C, 300 °C). Compare the original bio-oil and upgraded bio-oil, the intensity of A type and C type aromatic structures including phenols and methoxylated phenols were significantly reduced by the upgrading; nevertheless, the temperature impact on the phenols and methoxy groups were not detected.

### **5.3.2 Effect of reaction time and catalyst loading**

To further optimize the reaction conditions and promote both the yield and qualities of the sugarcane bagasse yield. Figure 38 (b) and Figure 38 (c) presents the yield distribution based on the varied reaction time and catalyst loading. It was found that 43.99 wt% appeared to be the highest bio-oil yield for 8 h. Due to the pressure limitation of the batch reactor, the reaction could only be prolonged to 16 h. It should be noted that in Figure 38 (c), the reaction was performed for 4 h, because the reactor pressure limitation did not allow for a B:C ratio less than 1 for higher than 4 h. To make the comparison of the B:C reasonable and explore the lower B:C ratio impact on the bio-oils, the reaction time was set to 4 h. It was suggested that higher catalyst loading did not have a positive impact on the bio-oil yield. Lowering the B:C ratio from 1:1 to 1:2 resulted in a 11.88% decrease of the upgraded bio-oil.



To evaluate the reaction time and catalyst loading impact on the upgrading, a quantitative evaluation of hydroxyl groups was performed by  $^{31}\text{P}$  NMR, as shown in Figure 44 and Figure 45. The hydroxyl group was usually considered a most significant structure resulting the aging problem. The peaks were assigned to four categories: aliphatic OH,  $\text{C}_5$  substituted aromatic OH, non-condensed aromatic OH, and carboxylic acid OH. An example was illustrated in Figure 44, shown the reaction time impact on the OH contents in the bio-oils. Considering the quantitative integration of the hydroxyl groups, it was found that the severe reaction condition typically correlated to the lower non-condensed OH groups. However, the condensed OH groups did not show a strong correlation with the upgrading condition severity.

### 5.3.3 Molecular weight distribution and hydroxyl group distribution

The non-condensed OH groups include guaiacyl, catechol, and *p*-hydroxyphenyl type OH groups. The detailed chemical shift assignment was illustrated in Figure 46, shown in different colors. Figure 47 summarized the quantitative integration results of the three OH groups, along with the varied temperature, time and catalyst loading. As shown in Figure 47 (a) and Figure 47 (b), guaiacyl and *p*-hydroxylphenyl groups were eliminated under the most severe conditions: 300 °C and 16 h. Lowering the B:C ratio from 1:1 to 1:2 did not show the positive impact on the elimination of the catechol OH groups.

Molecular weight distribution was measure by GPC (Figure 48 and Figure 49). The weight average molecular weight of original bio-oil was 228.03, and the curve was significantly shifted to higher molecular weight. For the catalyst loading of 0.1 g (B:C = 5:1), there was two major proportions: > 800 Da and < 800 Da. This could be attributed to that the catalyst deactivates and more oxygenates formed higher molecular products.<sup>222</sup>

## 5.4 Conclusion

This was a follow-up study of Chapter IV to further promote the sugarcane bagasse bio-oil's quality as a fuel precursor. The porous metal oxide (Cu-PMO) was demonstrated to be a highly active catalyst for hydrogenation of oxygenated chemical species. A yield of 43.99 wt% of upgraded products was achieved based on the original bio-oils. A hydrocarbon selectivity of 14.1% in the upgraded bio-oil was obtained through the batch reactor upgrading. Non-condensed phenolic hydroxyl contents were almost eliminated under the most severe reaction conditions. *Ex-situ* upgrading of the bio-oils in a bench scale reactor will be discussed in the next chapter.

## CHAPTER VI: EX-SITU CATALYTIC UPGRADING OF PYROLYSIS VAPORS OVER H-ZSM5

A version of this chapter was published by ACS Sustainable Chemistry & Engineering by Himanshu Patel<sup>#</sup>, Naijia Hao<sup>#</sup>, Kristiina Iisa, Richard J. French, Kellene A. Orton, Calvin Mukarakate, Arthur J. Ragauskas, and Mark R. Nimlos. Reprinted with permission from Wiley:

Patel, H.<sup>#</sup>; Hao, N.<sup>#</sup>; Iisa, K.; French R.; Orton, K.; Mukarakate, C.; Ragauskas, A., Nimlos, M., Detailed Oil Compositional Analysis Enables Evaluation of Impact of Temperature and Biomass-to-Catalyst Ratio on ex Situ Catalytic Fast Pyrolysis of Pine Vapors over ZSM-5. *ACS Sustainable Chemistry & Engineering* **2020**, 8 (4), 1762-1773.

(#: Co-first author)

The author Patel Himanshu and Naijia Hao are from University of Tennessee. The authors Kristiina Iisa, Richard J. French, Kellene A. Orton, Calvin Mukarakate, and Mark R. Nimlos are from National Renewable Energy Laboratory. The author Arthur J. Ragauskas is from University of Tennessee and Oak Ridge National Laboratory. Kristiina Iisa designed the study, performed the pyrolysis experiments & GC-MS/<sup>13</sup>C NMR characterization, and drafted the manuscript. Naijia Hao and Himanshu Patel performed the <sup>31</sup>P NMR / HSQC NMR / GPC experiments and drafted the manuscript. Richard J. French, Kellene A. Orton, Calvin Mukarakate, Mark R. Nimlos, and Arthur Ragauskas revised the manuscripts.

## 6.1 INTRODUCTION

Biomass can be used to produce liquid transportation fuels to ensure indigenous feedstock sources for transportation and to reduce greenhouse gas emissions. High liquid yields can be obtained via fast pyrolysis – heating biomass rapidly to 450-600°C in an inert gas atmosphere - but, as well known, the product liquid has high oxygen and water content and is acidic, corrosive, immiscible with hydrocarbons, thermally unstable and reactive and thus unsuitable for use as a liquid transportation fuel.<sup>10, 12</sup> The properties of pyrolysis oils can be enhanced by catalytically upgrading the vapors prior to condensation in a process called catalytic fast pyrolysis (CFP) or vapor phase upgrading. The catalyst may be located in the pyrolysis reactor (*in situ* CFP) or in a separate down-stream reactor (*ex situ* CFP). *Ex situ* CFP allows separate optimization of the conditions for pyrolysis and upgrading, and it reduces the contact of the catalyst with biomass char and ash components, thereby reducing catalyst poisoning.

HZSM-5 has been widely tested for CFP because of its ability to deoxygenate pyrolysis vapors and produce aromatic molecules at relatively high yields.<sup>223-227</sup> The yield and composition of the liquid product is impacted by a variety of factors, including the upgrading temperature, the ratio of biomass to catalyst, weight-hourly space velocity, and catalyst properties. Mukarakate et al.<sup>228</sup> compiled data from fixed bed reactors and showed that the product oil yield and oxygen content for CFP over ZSM-5 at a given temperature could be correlated to the mass ratio of biomass fed to the catalyst, i.e. biomass-to-catalyst (B:C) ratio. At low B:C ratios, when the catalyst is very active, aromatic hydrocarbons are formed. As the B:C ratio increases, the catalyst deactivates due to coking and oxygenates

are formed. Initially, the oxygenates are phenols and furans, but as the catalyst becomes more coked, primary pyrolysis vapors such as methoxyphenols break through.<sup>222, 228-229</sup>

The impact of operating parameters has been investigated in the bench or pilot scale for *in situ* CFP over ZSM-5. Under conditions with low or negligible contents of oxygenated compounds in the CFP oil, a maximum in aromatic hydrocarbon yields has been reported around 600°C, with the highest conversion of biomass carbon to aromatic compounds (aromatics carbon yield) around 14%.<sup>225, 230</sup> Increasing the temperature enhanced gas yields and reduced solids (char and coke) yields. Among the aromatic hydrocarbons, benzene selectivity increased as temperature increased as did the selectivity of ethene compared to higher alkenes. The fraction of biomass converted to coke (coke yield) decreased as the B:C ratio decreased but the gas yields or selectivities were not impacted.<sup>230</sup> Under conditions with mainly oxygenated organic liquid products, Lappas et al.<sup>231</sup> showed in a circulating fluidized bed reactor that decreasing the B:C ratio increased organic liquid yields. Coke on catalyst increased as the B:C ratio increased though coke yields decreased. Char yields decreased but gas yields remained relatively constant as the catalyst-to-biomass ratio increased. Based on *in situ* CFP experiments in a circulating fluidized bed reactor, Paasikallio et al.<sup>232</sup> reported that decreasing the B:C ratio enhanced the conversion of pyrolysis vapors but did not result in a continuous improvement in bio-oil quality.

While *ex situ* CFP oils have been produced over ZSM-5 catalysts in the bench scale and oil properties evaluated<sup>137, 233-234</sup> there are few systematic studies on the impact of changing operating conditions in that scale or larger. In the micro scale with analytical pyrolysis (Py-GC-MS), increasing the upgrading temperature has been reported to increase

the aromatic hydrocarbon yields up to temperatures of 500-600°C in studies with low B:C ratios, decrease coke formation and increase light gas formation.<sup>235-236</sup> Higher upgrading temperatures enhanced the selectivity of benzene compared to alkylated one-ring aromatics, and this change in selectivity has been attributed to increased dealkylation reactions at higher temperatures.<sup>235</sup> Changing the B:C ratio during Py-GC-MS experiments of *ex situ* CFP has been reported not to have a significant impact on product yields or selectivities in studies with sufficient catalyst present to completely or almost completely deoxygenate pyrolysis vapors under all conditions<sup>235, 237</sup> but aromatic hydrocarbon yields decrease as the B:C ratio is further increased.<sup>228, 234, 237</sup> Most studies have reported significant increases in oxygenates as the B:C ratio increases<sup>228, 234</sup> while one study reported only modest increases in oxygenates and decreases in the total liquid carbon yields as the B:C ratio increased.<sup>238</sup> Hernando et al.<sup>239</sup> assessed the impacts of pyrolysis temperature, upgrading temperature, and B:C ratio in a laboratory-scale fixed bed system. Increasing the upgrading temperature from 400 to 500°C reduced oil yield and increased gas yields. Decreasing the B:C ratio decreased oil yields and increased gas and coke yields. Semi-batch experiments in the bench scale similarly showed that increasing the B:C ratio increased oil yields, decreased coke and gas yields and led to increases in oil oxygen content and the variety of oxygenated compounds.<sup>240</sup>

CFP oil can be further upgraded via hydrotreating or co-processed in a petroleum refinery.<sup>241-243</sup> Compared to hydrotreating of non-catalytic fast pyrolysis oils, CFP oils offer the possibility for one-stage hydrotreating if the CFP oil is sufficiently deoxygenated instead of the two or more stages required for fast pyrolysis oils.<sup>243-244</sup> The highest CFP oil oxygen content that allows one-stage hydrotreating may depend on the content of specific

oxygenate groups in the CFP oil, for example, acids or carbonyls. This makes it important to understand the composition of CFP oils in detail. Specific oxygen functional groups in the CFP oil could also be utilized in coupling reactions to improve yields of higher-value compounds.<sup>245</sup>

The current study was undertaken to assess the impacts of upgrading temperature and biomass-to-catalyst (B:C) ratio on oil composition for *ex situ* CFP over ZSM-5 in the bench scale. The experiments were performed for pine pyrolysis vapor upgrading in a dual fluidized bed reactor system. The oils were analyzed by a variety of techniques, including GC-MS, <sup>13</sup>C NMR, <sup>31</sup>P NMR, heteronuclear single-quantum correlation (HSQC) NMR analysis, and gel permeation chromatography (GPC) to assess the impacts on oil quality. The results show significant impacts on the composition and the molecular weight distribution.

## **6.2 Experimental methods**

### **6.2.1 Material and sample preparation**

Chemicals and biomass used in this chapter was presented in the sections 2.1.1 and 2.1.2 in this dissertation.

### **6.2.2 Equipments and experimental procedures**

Pyrolysis set-ups and processing details were presented in sections 2.2.3.

### **6.2.3 Characterization of biomass and bio-oils**

Detailed characterization techniques were presented in sections 2.3.3.1, 2.3.3.2, 2.3.3.5.2, 2.3.3.5.3, and 2.3.3.5.4.

## 6.3 Results and discussion

### 6.3.1 Oil yields and oxygen content

Experiments of *ex situ* CFP were performed in the dual fluidized bed system with a constant pyrolysis temperature of 500°C and a constant biomass feed rate. Either the upgrading temperature - temperature of the second fluidized bed reactor – or the rate of catalyst feed to the upgrading reactor was varied. The impacts of upgrading temperature and the biomass-to-catalyst feed mass ratio (B:C) on the carbon yields of the major products and the oil oxygen content are illustrated in Figure 50.

Low B:C ratios correspond to a relatively fresh catalyst with good vapor upgrading capability, and oil with a low oxygen content of 9 wt% oxygen on dry basis was produced at B:C of 1.0. As the B:C ratio increased, the deoxygenation capability of the catalyst decreased, and the oil oxygen content increased to 17 wt% at B:C ratio of 1.8. At the same time the oil carbon yield (g C in oil/g C in biomass) increased. The increases in oil yield and oxygen content are consistent with several earlier research results.<sup>228-229, 231, 240</sup> The carbon yield in the aqueous phase also increased as the B:C ratio increased. The increase in the aqueous phase carbon can be attributed to the formation of more oxygenated compounds as the B:C ratio increases and the higher solubility of the more polar oxygenates compounds in water. Overall 3% or less of the feed carbon was collected in the aqueous liquid.

The char yield remained constant as would be expected since char formation is not impacted by the downstream upgrading process. The coke carbon yield decreased from 16 to 13% (Figure 50). Even though a higher fraction of carbon in the biomass was converted to coke on a fresh catalyst than a deactivated catalyst, the amount of coke on catalyst



increased as the B:C ratio increased; here from 0.09 to 0.12 g coke/g catalyst. The majority of coke was, therefore, formed on a fresh catalyst (here with B:C < 1) and significantly less coke is formed on a more deactivated catalyst as shown in the literature as well.<sup>228, 232, 240</sup> A fresh uncoked catalyst has a high fraction of available active sites, leading to efficient vapor upgrading but also high coke formation on these active sites. As the active sites become blocked by coke, the upgrading efficiency of the catalyst decreases but this also reduces additional coke formation.

Increasing the upgrading temperature decreased the oil carbon yield but produced oil with a lower oxygen content. The gas carbon yields increased significantly (from 25% to 34%) as the upgrading temperature increased, and the main impact of upgrading temperature was the transfer of carbon from oil into gases. Coke formation remained relatively constant or slightly decreased as the upgrading temperature increased. The carbon in the aqueous phase decreased as the oil oxygen content decreased, as a result of the lower solubility of hydrocarbons in the aqueous phase as already discussed.

Overall, the results suggest that, within the range studied here, increasing the B:C ratio reduced deoxygenation and increased oil yield while lowering coke and light gas formation. Increasing the upgrading temperature enhanced deoxygenation and the transformation of the products from liquid-range compounds to light gases.

The efficiency of converting carbon in the biomass into oil and the quality of the product oil are key factors impacting the economics of biofuels production via catalytic fast pyrolysis.<sup>240</sup> Under all cases, the largest source of carbon inefficiencies was light gases. CO had the largest contribution and accounted for 13-17% of the biomass carbon; C<sub>2</sub>-C<sub>4</sub> alkenes gave the second highest loss (6-9%), followed by CO<sub>2</sub> (5-6%). The gas yields

increased as the upgrading temperature was increased and slightly decreased as B:C increased. In addition to CO, the formation of methane and light alkenes increased with increasing upgrading temperature. This is consistent with increased cracking and dealkylation at higher temperatures.

The loss of carbon in gases for non-catalytic fast pyrolysis (FP) is included as a comparison. All of the gas carbon yields were higher for CFP than for FP. The difference was highest for CO, which increased by 11-16 percentage points. CO<sub>2</sub> is a more desirable product for deoxygenation than CO due to the higher O:C molar ratio. The formation of CO<sub>2</sub> may, however, be limited by the amount of functional groups that are likely to form CO<sub>2</sub> during upgrading. Decarboxylation is a feasible reaction pathway for acids and esters, which have two oxygen atoms connected to a carbon atom, but for the majority of oxygen functional groups present in pyrolysis vapors, decarbonylation or dehydration is more likely. The formation of CO<sub>2</sub> during the upgrading (difference between CO<sub>2</sub> during FP and CFP) corresponds well with the conversion of acid detected in the FP oil to CO<sub>2</sub>. The carboxylic acid number (CAN) of the FP oil was 76 mg KOH/g oil, which, taking into account the yield of the biomass oil, corresponds to 1.2 mol of acid per kg of biomass fed. The highest difference in the CO<sub>2</sub> yield between CFP and FP was 5.5%, which corresponds to 1.3 mol of CO<sub>2</sub> per kg of biomass fed. The close correspondence of the moles of acids in the pyrolysis vapors and the moles of CO<sub>2</sub> formed during upgrading suggests that acids are the source of CO<sub>2</sub> and that CO<sub>2</sub> formation during CFP using ZSM-5 is limited by the amount of acids in the pyrolysis vapors. This explains the reported higher enhancements in CO than CO<sub>2</sub> when comparing catalytic and non-catalytic pyrolysis<sup>137, 239-240, 246</sup> or changing operating conditions, in particular the upgrading temperature.<sup>225, 230, 235, 238-239</sup>

### 6.3.2 Oil analysis

The GC-MS and the  $^{13}\text{C}$  NMR analysis results for the oils are summarized in Figure 51. Aromatic hydrocarbons constituted the majority of the GC-MS detectable compounds in all CFP oils except the oil produced at 500°C, which had the highest oxygen content. Within the GC-MS-detected aromatics, 2- and 1-ring compounds were the most prevalent. Consistent with the oil oxygen contents, the hydrocarbon fractions decreased as the B:C ratio increased or the upgrading temperature decreased. The oxygenates included aromatic compounds with hydroxyl groups (phenols, naphthols, and indenols), furans, methoxyphenols, and also levoglucosan, which was detected in the oils produced at the highest B:C and at the lowest upgrading temperature. In particular, the oil upgraded at 500°C had low aromatic hydrocarbon and high oxygenate contents. At that temperature, there were few completely deoxygenated molecules and a high fraction of primary pyrolysis vapors (methoxyphenols and anhydrosugars). Conversely, few primary pyrolysis vapor compounds were identified in the oil upgraded at 600°C, and the identified compounds consisted of aromatic hydrocarbons and partially deoxygenated compounds. GC-MS cannot identify high-boiling compounds that do not vaporize in the GC column; some early eluting compounds may have also been covered by the solvent delay. The oil prepared at B:C 1.8 at 550°C had the lowest fraction identified by GC-MS (25%) while the identified fractions ranged from 34 to 43% for the rest of the CFP oils. The top oils had by far a higher fraction of the mass identified (on average 65%) than the bottom oils did, which suggests that a large fraction of the unidentified compounds were high boiling. The  $^{13}\text{C}$  NMR analysis in Figure 38b indicates overall similar trends. The fractions of oxygenated functional groups increased, as the B:C ratio increased or upgrading temperature decreased,

consistent with the oil oxygen contents. The largest oxygenated group was aromatic C-O, which includes hydroxyl groups attached to aromatics (phenols, naphthols, indenols, and methoxyphenols) but also the C-O bonds in furan rings. Carbonyl groups (C=O present in ketones, aldehydes, and acids), aliphatic C-O (present in e.g. levoglucosan), and methoxy groups all became more prevalent as the B:C ratio increased or upgrading temperature decreased, and they were highest for the oil vapors upgraded at 500°C. The largest identified groups were aromatic C-H and C-C, which indicates that the oil was highly aromatic; however, aromatic hydrocarbons may not have been the most prevalent compound type. Each aromatic C-O bond is associated with a high fraction of aromatic C-C or C-H bonds, e.g., phenol contains five aromatic C-H carbons and only one aromatic C-O carbon. Therefore, a significant fraction of the aromatic C-C and C-C groups present in the oils were likely associated with the phenolic compounds.

Methoxy groups constituted overall a very small fraction the carbon atoms, 2% at highest for the 500°C oil; nevertheless, methoxyphenols constitute a significantly higher portion of the compounds in the oil due to the high fraction of other carbons in methoxyphenols; for example, 2-methoxyphenol (guaiacol) contains four aromatic C-H, two aromatic C-O, and one methoxyl carbon. The presence of 2% of methoxy groups, therefore, suggests that at least 14% of the carbons was in methoxyphenols. In contrast, for a carbohydrate-derived compound such as levoglucosan, five of the six carbons fall within the range of aliphatic C-O bonds, and the highest content of 4% of aliphatic C-O would translate to less than 5% levoglucosan. The relatively low fraction of compounds with aliphatic C-O bonds and high fraction of compounds with aromatic C-O bonds suggests that a large fraction of the compounds non-identifiable by GC-MS consisted of lignin-

derived material, i.e. pyrolytic lignin, instead of carbohydrate-derived molecules such as anhydrosugars.

There was in general very good agreement between the types of molecules detected by GC-MS and the functional groups measured by  $^{13}\text{C}$  NMR. An exception was carbonyls, which were identified in higher abundance by  $^{13}\text{C}$  NMR than by GC-MS. The carbonyls likely included small molecules such as acetaldehyde, acetone, and acetic acid, which were not detectable by GC-MS due to overlap with the solvent peak. In addition, some of the compounds categorized as methoxyphenols in the GC-MS analysis also included carbonyl groups (e.g., 4-hydroxy-2-methoxycinnamaldehyde).

Overall, both the GC-MS and  $^{13}\text{C}$  NMR results suggest that the majority of the oils consisted of aromatic compounds, including aromatic hydrocarbons, simple phenols, and methoxyphenols. The fraction of hydrocarbons decreased as the B:C ratio increased or the upgrading temperature decreased. Conversely, the fraction of oxygenated compounds increased and the variety of oxygenated compounds also increased as B:C increased.

The GC-MS and  $^{13}\text{C}$  NMR analyses indicated the presence of both aliphatic and aromatic -OH groups in the CFP oils, and  $^{31}\text{P}$  C NMR can be used to further differentiate the types of -OH groups and to quantify their concentrations.<sup>247-248</sup> As shown in Figure 52, aliphatic -OH groups in the bio-oil decreased with increasing upgrading temperature, and the decrease was most significant from 500 to 550°C. The decrease in the aliphatic -OH group can be attributed to elimination of -OH groups in cellulose- and hemicellulose-derived compounds, e.g. levoglucosan, and it is consistent with the drop in aliphatic C-O by  $^{13}\text{C}$  NMR and the decrease in levoglucosan by GC-MS. Another source for -OH groups are side chains in lignin. The cleavage of -OH groups leads to the formation of water and

unsaturated bonds through dehydration of aliphatic -OH groups. Guaiacyl, catechol and *p*-hydroxyphenyl type -OH groups also decreased as upgrading temperature increased as shown Figure 52. Thermal decomposition of ether bonds in lignin structure and methoxyl-aromatic compounds results in the formation of catechol and *p*-hydroxyphenyl type -OH groups during pyrolysis.<sup>144, 247</sup> With increasing upgrading temperature, the total concentration of aromatic -OH groups decreased in bio-oil (Figure 52). Total aromatic -OH group includes C<sub>5</sub>-substituted condensed phenolic hydroxyls ( $\beta$ -5, 4-O-5, and 5-5) in addition to the guaiacyl, catechol and *p*-hydroxyphenyl type -OH groups. The secondary cleavage of the -OH groups becomes promoted more by the ZSM-5 catalyst at higher upgrading temperatures, which leads to lower concentrations. The carboxylic acid concentrations corresponded to <17 mg KOH/g (carboxylic acid number or CAN) in the CFP oils, which is in line with CAN values determined for CFP oils with similar oxygen contents.<sup>240</sup>

All -OH groups increased in the bio-oil as the B:C ratio increased from 1.0 to 1.8 (Figure 52). The increase was significant for the aliphatic -OH group, consistent with the increase in aliphatic C-O by <sup>13</sup>C NMR and levoglucosan by GC-MS (Figure 51). ZSM-5 promotes dehydration reactions, which lead to lower yields of aliphatic -OH groups.<sup>249</sup> The same trend was observed with C<sub>5</sub>-substituted condensed phenolic hydroxyls though the effect was less significant compared to that of aliphatic -OH group. Guaiacyl, catechol, and *p*-hydroxyphenyl concentrations also increased as B:C increased. The increase in the aromatic -OH is consistent with the increase of phenolics and higher hydroxyaromatics by GC-MS and aromatic C-O bonds by <sup>13</sup>C NMR (Figure 51). Dehydration and decarboxylation reactions are promoted by ZSM-5<sup>250-255</sup>, which explains the decrease in

aliphatic and aromatic -OH groups as B:C ratio decreased. The total aromatic -OH yield increased as B:C ratio increased.

Molecular weight distributions for both bottom and top oils were measured by GPC (Figure 54 and Table 19). A dramatic shift towards lower molecular weight compounds can be seen for all CFP oils compared to the non-catalytic fast pyrolysis (FP) oil (Figure 54) with a reduction in the proportion of species with molecular weights >100 Dalton and formation of new species with molecular weights <100 Dalton. 1-ring aromatics, such as benzene and toluene, and phenol are examples of compounds with <100 Dalton present in the CFP oils. The molecular weight decreased for both bottom as well as top fractions of the CFP oils as upgrading temperature increased. Higher upgrading temperatures promoted cracking by ZSM-5 resulting in relatively lower  $M_w$  products as evidenced by the decrease in the relative abundance of the higher molecular weight compounds and in the decrease the weight and number average molecular weights  $M_w$  and  $M_n$ . The polydispersity index (PDI), which is the ratio of  $M_w$  to  $M_n$  ( $M_w/M_n$ ), can be used to determine the molecular homogeneity of a bio-oil). The PDI is always  $\geq 1$ , and a higher value of PDI indicates lower molecular homogeneity. PDI decreased with increasing upgrading temperature; in other words, the molecular homogeneity improved at higher upgrading temperatures, which was observed with both bottom and top fractions of the CFP oils. For each bio-oil sample, the top fraction was more molecularly homogeneous than the bottom fraction. With decreasing B:C ratio,  $M_w$  and  $M_n$  decreased for bottom fraction of the bio-oil which indicates that ZSM-5 promoted cracking and resulted in lower  $M_w$  products. For each bio-oil sample,  $M_w$  and  $M_n$  were significantly lower for the top fraction compared to that for bottom fraction. The GPC suggests that catalytic upgrading using ZSM-5 reduces the average  $M_w$

into gasoline range (80 to 120 g mol<sup>-1</sup>). For the bottom fraction, the PDI decreased with decreasing B:C ratio (Table S2) indicating higher molecular homogeneity with decreased B:C ratio.

For bio-oil characterization 2-D HSQC NMR was employed. The HSQC spectra were classified into three regions: aliphatic region covering compound groups A, B, C, D, E, G in Figure 55 aromatic region including F, J, I, K, L in Figure 42 and methoxyl group region including M, O in Figure 42. The peak assignments were accomplished based on literature.<sup>221, 249, 256</sup>

Aliphatic C-H bonds in HSQC-NMR for selected bottom fractions of the CFP oils are shown in Figure 56, aromatic C-H bonds in Figure 57, and methoxyl groups in Figure 58. The relative abundance of aliphatic C-H bonds dropped significantly as the upgrading temperature increased (in Figure 56). This was true for aliphatic C-H bonds in the side chains of aromatic compounds (A, B, C, D in Figure 55) as well as for aliphatic compounds (E and G in Figure 55). The decrease in aliphatic C-H bonds is consistent with an increase in light hydrocarbons observed in the gas phase as the upgrading temperature increased and with enhanced dealkylation reported in the literature.<sup>257-259</sup> As the B:C ratio increased, aliphatic C-H bonds decreased (in Figure 56). It has been shown that aromatic hydrocarbon products are more alkylated at low B:C ratios (high ZSM-5 loadings) and the degree of dealkylation decreases as the B:C ratio increases for cellulose-derived compounds.<sup>260</sup> This suggests that the decrease in the aliphatic C-H bonds as B:C increased may be due to the presence of less alkylated aromatics as the catalyst becomes more deactivated.

Aromatic C-H bonds were shown to be prevalent in all CFP oils by HSQC-NMR (Figure 57). The relative abundance of C-H bonds in phenols and methoxyphenols (F and



J in Figure 55) and naphthols (K in Figure 55) decreased with rising upgrading temperature (Figure 57), which agrees with the decrease in aromatic -OH groups (Figure 53). Multiring selectivity decreased with upgrading temperature (see e.g. K and L). The trend is consistent with literature findings<sup>237, 257</sup> and it may be due to faster desorption of upgrading products from ZSM-5 at higher temperatures before they have time to react further to multiring compounds.<sup>257</sup> The abundance of all types of aromatic C-H bonds decreased as the B:C ratio increased (Figure 57). ZSM-5 promoted polyaromatic formation, which is consistent with the literature.<sup>249</sup> The formation of polyaromatics (L and K) decreased as B:C increased, as has also been reported in the literature.<sup>260-261</sup>

Methoxyl group compounds decreased as upgrading temperature increased as observed also by GC-MS and <sup>13</sup>C NMR analysis (Figure 51). The bottom fractions of the CFP oils were richer in terms of methoxyl groups compared to the top fractions, which was consistent within the entire upgrading temperature range. The top fraction of bio-oil obtained at 600°C was free from methoxyl group compounds. No significant change in methoxyl group abundance was observed with changing the B:C ratio (Figure 58). The GC-MS and <sup>13</sup>C NMR analyses also suggested only modest impacts of B:C ratio on the methoxyl groups in the range studied.

The results overall indicate that the quality of the oils improved as either the B:C decreased or upgrading temperature increased (Figures 51-53). At the same time, the yields of the pyrolysis oils decreased (Figure 50). For successful production of biofuels, a proper balance of yield and oil quality needs to be achieved; <sup>262</sup> too efficient deoxygenation leads to low yields and high fuel costs but too low deoxygenation produces oil with low quality requiring complicated hydrotreating processes. Aldehydes and anhydrosugars are very

reactive and their presence in pyrolysis oils has been shown to cause catalyst fouling during hydrotreating and lead to requirements of additional stabilization stages prior to hydrotreating.<sup>263</sup> The concentration of anhydrosugars were highest in the oil produced at 500°C (Figure 51) and none were detected in the oils from higher upgrading temperatures, which suggests that 550°C may be an optimal temperature for this system since it gave a high carbon yield without detected anhydrosugars. For the catalyst and conditions utilized here, B:C ratios of 1.4 may be best due to the increase in anhydrosugars and higher molecular weight compounds at the higher B:C ratio. It should be noted that the desired B:C ratio depends on the activity of the catalyst. The catalyst in these experiments had a very high acid site density (1116  $\mu\text{mol/g}$ ); the activity of commercial ZSM-5 catalysts may be an order of magnitude lower<sup>264</sup> and, consequently, the desired B:C ratio in circulating riser reactors may be significantly lower.

#### **6.4 Conclusion**

The oxygen content in catalytic fast pyrolysis oil was reduced by 7 wt% with increasing upgrading temperature from 500°C to 600°C or it was decreased by 8 wt% with decreasing the biomass-to-catalyst (B:C) ratio from 1.8 to 1, and both changes also decreased the oil yield. Changes in upgrading temperature had a large impact on carbon losses in light gases, which was increased from 25 wt% at 500°C to 34 wt% at 600°C. A rise of 3 wt% in coke carbon yield was observed with the decrease in B:C ratio from 1.8 to 1. Increasing the B:C ratio (decreasing catalyst loading) decreased the fraction of aliphatic C-H bonds suggesting less alkylated hydrocarbon products as the catalyst became more deactivated. The fraction of polyaromatics also decreased as B:C ratio increased and the fractions of both aliphatic and aromatic OH groups increased, indicating decreased

dehydration and C-C bond formation. Increasing the upgrading temperature enhanced cracking by ZSM-5 leading to oil with lower molecular weight, enhanced dealkylation and formation of light hydrocarbon gases, enhanced demethoxylation and decreased polyaromatics formation. Aliphatic and aromatic OH decreased in particular from 500 to 550°C, but there was less impact when the temperature was further increased to 600°C.

## **CHAPTER VII: ONE-POT TRANSFORMATION OF BIOMASS TO BIO-OILS OVER METAL CHLORIDES**

A version of this chapter was published by Naijia Hao, Koray Alper, Kubilay Tekin, Selhan Karagoz, and Arthur J. Ragauskas and reprinted with permission from Elsevier:

“Hao, N.; Alper, K.; Tekin, K.; Karagoz, S.; Ragauskas, A.J., One-pot transformation of lignocellulosic biomass into crude bio-oil with metal chlorides via hydrothermal and supercritical ethanol processing. *Bioresource Technology* **2019**, 288, 121500.”

The authors Koray Alper, Kubilay Tekin, Selhan Karagoz are from Karabük University. The author Arthur J. Ragauskas is from University of Tennessee and Oak Ridge National Laboratory. Naijia Hao, Kubilay Tekin, Selhan Karagoz, and Arthur J. Ragauskas designed the study. Koray Alper and Naijia Hao performed the experiments. Naijia Hao drafted the manuscript. Kubilay Tekin, Selhan Karagoz, and Arthur J. Ragauskas revised the manuscript.

## 7.1 Introduction

There is an increasing demand for the sustainable fuels and chemicals to alleviate energy insecurity and achieve proposed carbon emission reduction targets. Lignocellulosic biomass resources are contributing to the current renewable energy consumption targets and benefit from their abundant quantity and low price.<sup>147</sup> Ethanol produced from corn grain dominates the bio-based fuel production in the current bioeconomy with a 87.64% share. Gasoline blendstock/bio-naphtha derived from a variety lignocellulosic feedstocks, such as agricultural residue and forest residue, only has a share of 0.075% in the bio-based fuel production.<sup>186</sup> Thus, two significant limitations in biofuel production need to be addressed: how to effectively utilize the non-food biomass sources and how to fully utilize each biomass component including lignin.

A one-step conversion of lignocellulosic biomass to liquid fuel precursor in a solvent media becomes a promising solution. This strategy avoids the fractionation of lignocellulosic biomass and effectively utilize lignin instead of merely burning it to generate power. Numerous studies have focused on the deconstruction of biomass in a high-temperature water media.<sup>265-267</sup> Tekin et al. used colemanite, a natural calcium borate mineral in water to liquefy the beech wood. The highest obtained bio-oil yield was 40.1 wt%, and the highest higher heating value (HHV) was 27.53 MJ/kg with the use of the natural calcium borate mineral.<sup>268</sup> Zheng et al. deconstructed swine carcasses in high-temperature water with sodium hydroxide and achieved an HHV of 32.35 MJ/kg and the highest mass yield was 62.2 wt%.<sup>269</sup> Bach et al. used potassium hydroxide as an additive to deconstruct a Norwegian macro-alga. It was found that the addition of potassium hydroxide reduced the formation of gas and did not have a remarkable change on the bio-

oil yield.<sup>270</sup> Besides high-temperature water, the use supercritical organic solvent is attracting attention for the catalytic deconstruction of lignocellulosic biomass.<sup>271-273</sup> Matson et al. used a Cu-Mg-Al mixed oxide to convert wood sawdust to alcohols and esters. The Cu-Mg-Al mixed oxide was found to be useful to minimize unreacted wood sawdust and the formation of the char.<sup>215</sup> Like supercritical methanol, supercritical ethanol is one of the most popular organic solvent media for conversion of lignocellulosics to biofuels in a supercritical state. Importantly, ethanol is a preferred environmental chemical and can be biologically derived from biomass to achieve sustainable requirements. Huang et al. used a Cu-Mg-Al mixed oxide to depolymerize pine wood in supercritical ethanol. A 54 wt% yield of the aromatic and long chain aliphatic products based on the biomass weight was achieved.<sup>214</sup> Xu et al. depolymerized pinewood sawdust in supercritical ethanol using an iron-based catalyst. A 43.18 wt% yield of the bio-oil was obtained compared to the depolymerization without a catalyst.<sup>274</sup> Chumpoo, and Prasassarakich also converted bagasse in supercritical ethanol using an iron-based catalyst. The same conclusion was made that iron-based catalyst significantly promoted bio-oil yield.<sup>275</sup> Most of the previous works regarding the degradation of lignin and lignocellulosic biomass in hot-compressed water and ethanol focused on the effect of the base and basic salts catalysts on bio-oil yields and properties as they have high reactivity to lignocellulose.<sup>276-281</sup>

Research efforts regarding applications of metal chlorides in biomass conversion have been focused on converting carbohydrates to platform chemicals (e.g., 5-hydroxymethylfurfural (HMF)).<sup>282-286</sup> A limited number of studies examined the catalytic effect of typical metal chloride Lewis acids (i.e., FeCl<sub>3</sub>, AlCl<sub>3</sub>, ZnCl<sub>2</sub>, and NiCl<sub>2</sub>) on bio-oil yields from the deconstruction of lignin in water and ethanol.<sup>287-288</sup> Hepditch and Thring

studied the degradation of lignin in hydrothermal media using Lewis acids ( $\text{NiCl}_2$  and  $\text{FeCl}_3$ ) at 255, 280, and 305 °C for 0, 60 and 120 min.<sup>287</sup> The highest ether soluble products (17.5 wt%) were obtained at 305 °C and 120 min by using  $\text{NiCl}_2$ . The yield of ether-soluble products from the experimental runs without  $\text{NiCl}_2$  was 9.2 wt% under the same conditions. Zhang et al. investigated the depolymerization of lignin in water, methanol, ethanol, butanol and octane using several metal halides acids (i.e.,  $\text{NiCl}_2$ ,  $\text{ZnCl}_2$ ,  $\text{AlCl}_3$ , and  $\text{CuCl}_2$ ) at between 220 and 340 °C and at reaction times from 1 to 8 h. The yield of bio-oil from the non-catalytic processing of lignin was about 45 wt% and increased to app. 55.0 wt% by using  $\text{ZnCl}_2$  at 260 °C and 2 h.<sup>288</sup> In 2007, Kaminsky and Zorriquetta used a combination of  $\text{TiCl}_4$  and  $\text{AlCl}_3$ , in the pyrolysis reactions of polypropylene. The use of the  $\text{TiCl}_4/\text{AlCl}_3$  significantly reduced the pyrolysis reaction temperature for the optimum production of light oils (i.e., carbon number less than 13) from polypropylene.<sup>289</sup> Considering that lignocellulose deconstruction to liquid fuels requires effective cleavage of existing C-C and C-O bonds in individual fractions (i.e., lignin, cellulose, and hemicellulose) and the lignin-carbohydrate complex, the authors are eager to know that if the combination of  $\text{TiCl}_4$  and  $\text{MgCl}_2$  can provide an effective and facile way to deconstruct lignocellulosics to liquid fuel precursors.

Here, we selected a combination of two Lewis acids,  $\text{TiCl}_4$  and  $\text{MgCl}_2$ , in lignocellulosic biomass deconstruction in both hydrothermal and supercritical ethanol deconstruction reactions. Grape seeds, as a residue of wine and grape juice industry, represent up to 15% of the solid wastes from wine industry.<sup>290-291</sup> In this study, waste grape seeds were subjected to hydrothermal and supercritical ethanol media at a temperature of 250, 300, and 350 °C and a residence time of 15, 60, and 90 min. The optimum reaction

temperature and time were determined based on the yields of the liquid products from deconstruction reactions. Both solid and liquid products were analyzed for insight into the structural composition. Scanning electron microscope (SEM) was used to characterize the solid products from the catalytic deconstruction; GC-MS,  $^{31}\text{P}$  NMR, and HSQC NMR were employed to analyze the structural components in bio-oils for a deeper insight into the catalytic deconstruction pathway. To our best knowledge, this work first investigated the role of the metal chloride additives in the whole biomass deconstruction reactions. The characteristics and structures of the crude liquid products (bio-oils) were the focus in this work.

## **7.2 Experimental methods**

### **7.2.1 Material and sample preparation**

Chemicals and biomass used in this chapter was presented in the sections 2.1.1 and 2.1.2 in this dissertation.

### **7.2.2 Equipments and experimental procedures**

Liquefaction procedures were presented in sections 2.2.4.

### **7.2.3 Characterization of biomass and bio-oils**

Detailed characterization techniques were presented in sections 2.3.1.1, 2.3.2, 2.3.3.1, 2.3.3.3, 2.3.3.4, 2.3.3.5.3, 2.3.3.5.4.

## **7.3 Results and discussion**

### **7.3.1 Deconstruction product distributions**

The deconstruction reactions of grape seeds were conducted in two different liquid media: hot compressed water and supercritical ethanol. Figure 59a to 59c present the effect of reaction temperature, time, and catalyst loading on the yields of liquid product (bio-oil)



and solid residue from the hydrothermal processing. The highest solid residue yield was obtained at 250 °C. With increasing the reaction temperature, the solid residue yield decreased. The reaction (at 350 °C and 30 min) in a hydrothermal media produced the lowest solid residue yield (31.9 wt%). While prolonging the reaction time from 15 min to 60 min only slightly reduced the percentage of solid residue. This phenomenon suggests that the deconstruction reactions were likely incomplete under the lowest temperature and time-tested in this work. As for the bio-oil yield, an inflection point was found when investigating the optimum reaction temperature and time. The highest bio-oil yield (13.4 wt%) was found operating at 300 °C and 30 min in hydrothermal media. This could be explained that under a more severe reaction conditions, part of the liquid products was further decomposed to gas products. Another possible reason for the decline of bio-oil yield at 350 °C was that lignin and hemicellulose degradation reactions were exothermic at a higher temperature which was thermodynamically unfavourable.<sup>292</sup> Figure 59c showed the additive loading effect on the product yield distribution from the hydrothermal processing at 300 °C for 30 min. It was found that higher additive loading had a detrimental impact on the bio-oil yield when using high-temperature water as the liquid media.

Similarly, Figure 60a and 60b showed the effect of reaction temperature and time on the bio-oil and solid residue from supercritical ethanol deconstruction. Temperature has a nearly linear relation with the bio-oil and solid residue yield. Higher temperature suppressed the solid residue while promoted the bio-oil yield up to 39.2 wt% (at 350 °C). Figure 60c presents the effect of additive loading on the product yields. In contrast to the reactions with additives in hydrothermal media, the solvolysis products from  $\text{MgCl}_2:\text{TiCl}_4$  had a remarkably positive impact on the bio-oil yield from supercritical ethanol processing.

At 300 °C for 30 min, the highest additive loading ( $\text{MgCl}_2/\text{TiCl}_4=4\text{mmol}/4\text{mmol}$ ) promoted the bio-oil yield by 49.2 wt%, compared to the yield from the reaction without an additive. It should be noted that previous studies regarding ethanol processing of lignocellulose demonstrated that increases in the mass yields for of bio-oils were due to the incorporation of some ethanol-derived products into bio-oils.<sup>6</sup> The degradation of ethanol takes place with the help of an additive and some of the degraded products from ethanol were incorporated into the bio-oils during ethanol deconstruction reactions. The ethanol incorporated compounds will be summarized in the GC-MS analysis studies. Comparing the deconstruction reactions in hot compressed water and supercritical ethanol, there were two significant differences: 1) without the additives, supercritical ethanol exhibited better bio-oil production performance: deconstruction in water led to a bio-oil yield up to 13.4 wt% while deconstruction in supercritical achieved up to 39.2 wt%; 2) The solvolysis products of  $\text{MgCl}_2:\text{TiCl}_4$  were effective for promoting bio-oil yield in supercritical ethanol while it played a negative role in hydrothermal media. This could be explained by the fact that supercritical ethanol acted as a hydrogen donor and promoted the hydrogen transfer to the unreacted biomass feedstock.<sup>293</sup> It is well known that  $\text{TiCl}_4$  is water sensitive and can be easily hydrolysed to titanium dioxide ( $\text{TiO}_2$ ). This is also valid for supercritical ethanol processing as where is could react either with ethanol or trace amounts of water. It has been suggested that the acidic pH is responsible for the formation of the catalytically active metal species to facilitate the deconstruction of lignocellulose.<sup>283, 294</sup> The catalytic activity of metal species is related to the ionic radius of metal cations.

### 7.3.2 GC-MS analysis of bio-oil composition

To reveal the volatile fractions present in the bio-oils, GC-MS analysis was conducted on the bio-oils obtained from hydrothermal and supercritical ethanol media. Table 20 and Table 21 listed all the GC-MS detected compounds in hydrothermal and supercritical ethanol media at 300 °C for 30 min, respectively. Figures 61 and 62 summarize the structures in bio-oils into several categories: ketones, hydrocarbons, phenols, acids, aldehydes, esters, and others. From hydrothermal processing, the acids dominated the structures in bio-oils. The detected prominent fatty acids in bio-oils from the hydrothermal liquefaction of lignocellulose are n-hexadecanoic acid, linoleic acid and octadecanoic acid (Table 20). It is considered that these fatty acids were formed from the decomposition of extractives in lignocellulose.<sup>295</sup> The additive loading (TiCl<sub>4</sub>/MgCl<sub>2</sub>=2mmol/2mmol) resulted in the highest acid percentage (78.23%). Akalin et al. used hydrated cerium (III) chloride to deconstruct lignocellulose in high-temperature water and observed the same trend that acids are the most favorable products in bio-oils.<sup>296</sup> The higher additive loading corresponded to a lower phenolic content. This result could be explained by that non-condensed aromatic hydroxyl groups were reduced during the liquefaction, which was consistent with the NMR results. In Figure 62, the ethanol processing exhibited a remarkably different effect on the bio-oil composition. The esters instead of acids dominated the bio-oil structures. This result could be attributed to the esterification reactions between the formatted acids and ethanol which was both a solvent and a reactant in the deconstruction. In the bio-oil composition analysis of supercritical ethanol liquefaction without an additive (in Table 21), 2-ethoxyethanol, 1,1-diethoxyethane, 1-ethoxy-2-propanol, 2-ethoxyphenol, and 2-ethoxy-4-methylphenol only

made up to 0.17% of the total compounds; while in catalytic runs, the relative yields of these compound increased with the catalyst loading and made up to 2.34% during the 4mmol/4mmol MgCl<sub>2</sub>:TiCl<sub>4</sub> run. This finding may suggest that with the help of MgCl<sub>2</sub>/TiCl<sub>4</sub>, ethanol was incorporated into the deconstruction products. GC-MS analysis can only provide the relative yields of the identified compounds in the bio-oils that were light enough to elute from the GC column. Thus, we further carried out HSQC and <sup>31</sup>P-NMR analyses of the crude bio-oils and these results are discussed in the following subsections.

### 7.3.3 HSQC NMR analysis of bio-oils

Two-dimensional HSQC NMR was employed for characterizing the structures in bio-oils from the hydrothermal and ethanol processing of grape seeds with the metal chloride additives. The HSQC spectra were divided into two regions (i.e., aromatic region and aliphatic region), and the specific peak assignment was based on the published research works.<sup>297-300</sup> Figures 63a and 63b present the major aromatic structures in bio-oils from ethanol/hydrothermal processing without an additive, respectively. Signals of guaiacyl (G), catechol (C), and *p*-hydroxyphenyl (H) lignin units can be clearly observed in the deconstruction products from non-additive ethanol processing (Figure 63a). While the majority of the catechol lignin units were etherified, a trace amount of non-etherified catechol lignin units existed. Furan derivatives and alkyl unsaturated chains were detected in the ethanol deconstruction products. Figure 63b presents the aromatic signals detected in the bio-oils from non-additive hydrothermal deconstruction. Both ethanol and hydrothermal processing yielded a comparable amount of guaiacyl, etherified catechol, *p*-hydroxyphenyl lignin units, and alkyl unsaturated chains as shown in Figure 63a and Figure

63b. In contrast to the ethanol processing, furan derivatives and non-etherified catechol lignin units were not detected in the bio-oils from hydrothermal processing due to their low abundance.

Figure 63c presents the aromatic signals in the bio-oils from ethanol processing with the highest additive loading ( $\text{MgCl}_2:\text{TiCl}_4 = 4\text{mmol}:4\text{mmol}$ ). It was concluded that guaiacyl lignin units were almost eliminated at the highest additive loading as well as the furan derivatives and catechol type units. The higher catalyst loading significantly promoted the removal of guaiacyl lignin units while the 1 mmol loading of the additive exhibited comparable ability compared with 4 mmol loading towards removal of catechol and furan derivatives. The additive effect in a hydrothermal environment was examined by HSQC, as shown in Figure 63d. These effects imply that the additive slightly decreased the intensity of the G/C/H contents in bio-oils. Different from the bio-oils from ethanol processing, the incrementing additive loading did not result in a higher level of removal of G/C/H.

Figures 64a and 64b present the HSQC aliphatic regions of the deconstruction products from non-additive ethanol and hydrothermal processing. The major differences between non-additive ethanol/hydrothermal processing were the extent of the O-alkylated structures. In the non-additive ethanol deconstructed products (Figure 65a), O-methylated, O-ethylated, acetylated  $\gamma$  carbon in lignin sub-units, and C<sub>1</sub>/H<sub>1</sub> in  $\beta$ -O-4 ether linkage was the major O-alkylated structures. In the non-additive water deconstructed products (Figure 65b), methoxy group was the only O-alkylated structure with a high abundance. Both ethanol and hydrothermal processing yielded comparable C-alkylated structures as shown in Figure 64a and 64b.

Figure 64c shows the HSQC aliphatic side chain changes with the incrementing additive loading in SCE. O-methylated, O-ethylated, and C/H<sub>γ</sub> in β-O-4 ether linkage were eliminated with the highest additive loading (4 mmol), while the acetylated γ carbon in lignin sub-units remains. The higher additive loading exhibited a stronger ability to cleave the C-O bonds in bio-oils. The complete removal of methoxy groups was consistent with the removal of guaiacyl structures revealed in the partial HSQC spectra of aromatic regions. Different from the ethanol processing, the additive in hydrothermal processing slightly removed the methoxy structures in bio-oils while kept the C-alkylated structures intact.

#### 7.3.4 <sup>31</sup>P NMR analysis of bio-oils

The quantitative analysis of hydroxyl group contents in the bio-oils obtained from both hydrothermal/supercritical ethanol processing are shown in Table 22. The hydroxyl groups in the bio-oils were reacted with the 2-chloro-4,4,5,5-tetramethyl-1,3,2-dioxaphospholane and the quantitative calculations were based on the internal standard of *endo* N-hydroxy-5-norbornene-2,3-dicarboxylic acid imide (NHND). The chemical shift assignments were based on published research works.<sup>117, 119, 183</sup> The addition of MgCl<sub>2</sub>:TiCl<sub>4</sub> significantly lowered the aliphatic hydroxyl groups in the bio-oils produced from ethanol processing. The highest additive loading (4 mmol) removed 65.17% aliphatic OH contents while the additive loading of 1 mmol and 2 mmol lowered the aliphatic OH content by 34.83% and 39.32%, respectively. Although the summation of aliphatic alcohol contents (e.g., ethoxyethanol, methyl butanol, ethoxy-propanol) determined by GC-MS did not show a significant reduction with the addition of MgCl<sub>2</sub>:TiCl<sub>4</sub>, it should be noted that <sup>31</sup>P NMR quantified all the aliphatic hydroxyl groups in the bio-oils, including the alcohol

fractions with higher boiling points which could not be detected by GC-MS. As for the C<sub>5</sub> substituted condensed phenolic, approximately a 70% reduction of 5-5 inter-unit linkages were achieved by the addition of 2:2 mmol or 4:4 mmol MgCl<sub>2</sub>:TiCl<sub>4</sub>. This result may prove that the additives have the ability to cleave 5-5 lignin interunit linkages. A significant reduction of guaiacyl structures was found in both hydrothermal and supercritical ethanol processing with the addition of the additives. There was a 76.4% and 51.85% reduction of guaiacyl hydroxyl groups observed in ethanol/hydrothermal processing, respectively. This phenomenon was consistent with HSQC results, and the decrease in guaiacyl groups could be attributed to the cleavage of methoxy groups in guaiacyl units. The reduction of catechol hydroxyl groups from 0.29 mmol/g bio-oil to 0.13 mmol/g bio-oil in ethanol processing with 4 mmol addition level of additives was consistent with the results that catechol signals were almost eliminated in HSQC spectra.

### **7.3.5 Elemental analysis of feedstocks, bio-oils, and solid residues**

Tables 23 and 24 present the elemental analysis results of the bio-oils and biochars obtained from the deconstruction reactions in water and ethanol, respectively. In comparison with raw material, bio-oils from both hydrothermal and ethanol processing of lignocellulose increased the carbon content and decreased the oxygen contents. O/C atomic ratio of bio-oil from non-additive ethanol processing was 0.26, and it was reduced to the level of 0.17 with the use of the additive. This data shows that the additive de-oxygenates the bio-oils in case of supercritical ethanol processing. Higher additive loading resulted in a decrease in carbon contents of biochars for both reaction medium. It is considered that most of the additives were accumulated in char matrix, which lowered carbon contents of biochars for catalytic runs. The solid residues from hydrothermal processing had an HHV

range of 20.25 to 24.88 MJ/kg, which were slightly higher than the solid residues from supercritical ethanol processing. Importantly, both hydrothermal and ethanol processing with the highest additive loading produced bio-oils with a high HHV of 35.05 and 35.00 MJ/kg. These values are comparable to the commercial heavy fuel oils (~40 MJ/kg).<sup>12</sup>

### **7.3.6 Boiling point distributions of bio-oils**

A miniature distillation apparatus was used to estimate the boiling point distribution of hydrocarbons in the crude bio-oils, which are shown in Table 25. Hydrocarbons are classified (according to petroleum fractions) as light naphtha (<B.P: 93 °C), heavy naphtha (B.P: 93–204 °C), light gas oil (B.P: 204–343 °C) and heavy gas oil (>343 °C). The amount of light gas oil fraction in bio-oils from hydrothermal processing was higher than those of supercritical ethanol processing. It was reverse for heavy naphtha fraction. Most fractions for supercritical ethanol and hydrothermal processing was in the range between at 93 and 343 °C.

## **7.4 Conclusion**

In this study, both hydrothermal and supercritical ethanol liquefaction were applied on grape seed with the additive  $\text{MgCl}_2:\text{TiCl}_4$ . The additive has detrimental effects on bio-oil yields in hydrothermal media while the bio-oil yields were significantly improved by using the additive in supercritical ethanol media. The O/C atomic ratio of the raw lignocellulose was 0.56 and it was decreased to the level of 0.17 by using  $\text{MgCl}_2/\text{TiCl}_4$  (4:4 mmol) in both hydrothermal and supercritical ethanol media suggesting that de-oxygenation reactions are facilitated by the catalyst. H/C atomic ratios of bio-oils from SCE and hydrothermal processing of lignocellulose was significantly decreased in comparison with that of the raw material indicating that dehydration reactions. The use of



the  $\text{MgCl}_2/\text{TiCl}_4$  effectively promoted the heating values of the liquefaction products (bio-oils) to 35 MJ/Kg. The structural analysis of bio-oils revealed that the additives could facilitate the C-O bond cleavage and reduced the non-condensed aromatic hydroxyl groups during supercritical ethanol liquefaction.

# **CHAPTER VIII: ONE-POT TRANSFORMATION OF BIOMASS TO BIO-OILS OVER Pd/C AND WATER TOLERANT LEWIS ACIDS**

A version of this chapter was submitted to a peer-reviewed journal by Naijia Hao, Koray Alper, Kubilay Tekin, Selhan Karagoz, and Arthur J. Ragauskas:

Hao, N.; Alper, K.; Patel, H; Tekin, K; Karagoz, S; Ragauskas, A.J., One-step Transformation of Biomass to Fuel Precursors Using a Bifunctional Combination of Pd/C and Water Tolerant Lewis Acid.

The author Patel Himanshu is from University of Tennessee. The authors Koray Alper, Kubilay Tekin, Selhan Karagoz are from Karabük University. The author Arthur J. Ragauskas is from University of Tennessee and Oak Ridge National Laboratory. Naijia Hao, Kubilay Tekin, Selhan Karagoz, and Arthur J. Ragauskas designed the study. Koray Alper, Naijia Hao, and Himanshu Patel performed the experiments. Naijia Hao drafted the manuscript. Kubilay Tekin, Selhan Karagoz, and Arthur J. Ragauskas revised the manuscript.

## 8.1 Introduction

Lignocellulosic biomass is a valuable resource for generating renewable fuels and value-added products and benefits from its large quantity and low price.<sup>147</sup> Current biological biorefinery technologies towards cellulose have been commercialized (primarily cellulosic ethanol production). However, lignin, which is found ~15 wt% to 40 wt% (dry weight) in terrestrial plants, is underutilized in the current biorefinery industry.<sup>147,301</sup> Thus, creating a conversion route for effective utilization of lignin or whole biomass is of research interests. Recent research works focus on the one-step direct liquefaction of lignocellulosic biomass feedstocks to bio-crudes with high yields and high heating values comparable with commercial diesel fuels. One-pot catalytic liquefaction of whole biomass in environmental friendly solvents (e.g., water, ethanol) has been examined in the literature recently. A variety of catalysts, including Lewis acids, strong bases and basic salts, metal oxides, and mineral materials, have been screened to enhance the bio-oil yield from liquefaction and to promote the bio-oil product's property as a fuel precursor.<sup>214, 268-269, 288, 302</sup> The obtained bio-oils from catalytic liquefaction has a yield ranging from 40.1~62.2 wt% and a HHV value ranging from 27.5 ~ 35.0 MJ/Kg.<sup>268-269, 302</sup> Thus, one of the key point for effective conversion of biomass relies on development of catalysts suitable for the water or alcohol media.

Precious metal catalysts have been widely studied in the biomass renewable conversion area. The precious metal catalysts are typically supported on (e.g., carbon, Al<sub>2</sub>O<sub>3</sub>) which usually leads to a lower coking.<sup>303</sup> In addition, these non-sulfided precious metal catalysts avoid some deactivation problems caused by the sulfur compared to the commercial base-metal sulfide catalysts.<sup>304</sup> Palladium is one of the most studied precious

metal catalysts and it is widely chosen as a catalyst for hydro-treating of bio-oils and related representative model compounds. Studies with Pd/C catalysts performed on either crude pyrolysis oils or hydrothermal derived crude oils reported a HHV value range between 37.4 MJ/kg and 43.8MJ/kg of Pd/C hydro-treated oils.<sup>305-308</sup> Hydrotreating of crude bio-oils<sup>306-309</sup> or CFP oils<sup>304</sup> in these studies used external hydrogen for the Pd/C hydrotreating experiments and achieved deoxygenation level up to 90 wt%. Several research groups selected supercritical water or hydrogen donor solvents as *in-situ* hydrogen source to test the hydrodeoxygenation performance of Pd/C catalysts.<sup>310-311</sup> For example, Tan et al. selected formic acid and acetic acid as *in-situ* reforming reagents and performed hydrogenation of bio-oil model compounds (phenol and furfural) over Pd/C using the *in-situ* generated H<sub>2</sub>.<sup>311</sup> Peter et al.<sup>312</sup> tested a wide range of catalysts including reduced noble metal catalysts, and proved that Pd/C is active towards the deoxygenation of phenol, which is a representative model compound for biomass derived oils.

Recent research efforts have been exploring a bifunctional catalyst system consisting of Pd/C and acidic reagents to facilitate hydrodeoxygenation conversion of biomass or biomass derived compounds to hydrocarbons or high-value chemicals.<sup>313-320</sup> Lercher's group selected a mineral acid H<sub>3</sub>PO<sub>4</sub> to assist with the Pd/C catalyzed hydrodeoxygenation of phenol. Phenol was converted to cyclohexane with a high yield (> 90 %) where cyclohexanol was dehydrated to cyclohexene in the presence of the mineral acid in the transition step.<sup>313</sup> Liu et al used Pd/C with H<sub>3</sub>PO<sub>4</sub> to achieve complete transformation of 5,5'-di(hydroxymethyl)furoin (DHMF) to linear C<sub>10</sub>-C<sub>12</sub> hydrocarbons.<sup>314</sup> These studies suggested that a bifunctional catalyst system of Pd/C and acids would effectively convert oxygenated biomass derived compounds to saturated

hydrocarbons through the synergy of hydrogenation/ring opening/dehydration/hydrogenation (ring opening step may be neglected for the phenol type model compounds).<sup>314</sup> This bifunctional catalyst system allows the HDO reaction in a water-based system and makes the separation of hydrocarbon products from water medium efficient. In addition to the mineral acids (e.g., H<sub>3</sub>PO<sub>4</sub>), water-tolerant Lewis acids have been studied in biomass hydrodeoxygenation conversion in the past five years.<sup>315-320</sup> Water-tolerant Lewis acid (e.g., metal triflate complex) avoids the hydrolysis problems of some conventional Lewis acids in water and offers recyclability and air stability.<sup>315</sup> Li et al. screened a series of metal triflates to test the C-O hydrogenolysis performance on alcohol and ether type model compounds.<sup>315</sup> The result suggested that a tandem combination of dehydration mediated by triflates in the first step and a following hydrogenation step by Pd/C could achieve near complete conversion to hydrocarbons on selected reactant model compounds.<sup>315</sup> Other studies used metal triflates and Pd/C to convert bio-derived furan type compounds in one-pot through hydrodeoxygenation reactions and high yields (>90%) of hydrocarbon products were obtained.<sup>316, 318</sup> Another study used Hf(OTf)<sub>4</sub> and Pd/C to selectively deoxygenate levulinic acid to valeric acid.<sup>320</sup> A 99% conversion and 92% selectivity were obtained in a mild reaction condition (150 °C, 6h).<sup>320</sup> Hensen's group applied the Pd/C and metal triflates catalyzed depolymerization on woody biomass and achieved a high yield of aromatic monomers (55 wt%).<sup>317</sup>

In this chapter, a bifunctional catalyst system of a hydrogenation catalyst 5% Pd/C and a metal triflate was developed and applied in the one-pot depolymerization of fir wood. Metal triflates with three different metal center (i.e., Sm(OTf)<sub>3</sub>, La(OTf)<sub>3</sub>, and Cu(OTf)<sub>2</sub>) were used in this study to explore the synergy between Pd/C and a metal triflate. The main

focus of this study is to evaluate the bifunctional catalyst system's effect on the bio-oils and discuss the plausible reaction mechanisms based on the structure analysis of bio-oil products. The physical properties of obtained bio-oils were evaluated by the yields, higher heating values and total carbon recovered values. The detailed structures of bio-oils were thoroughly analyzed by GC-MS and HSQC.

## **8.2 Experimental methods**

### **8.2.1 Material and sample preparation**

Chemicals and biomass used in this chapter was presented in the sections 2.1.1 and 2.1.2 in this dissertation.

### **8.2.2 Equipments and experimental procedures**

Liquefaction procedures were presented in sections 2.2.4.

### **8.2.3 Characterization of biomass and bio-oils**

Detailed characterization techniques were presented in sections 2.3.1.1, 2.3.2, 2.3.3.1, 2.3.3.3, 2.3.3.4, 2.3.3.5.3, 2.3.3.5.4.

## **8.3 Results and discussion**

### **8.3.1 Product yields from the liquefaction in water and ethanol**

The effect of liquefaction temperature and conversion type on bio-oil and solid residue yields produced from non-catalytic liquefaction of fir wood was first investigated, as shown in Figure 65. Initially, with an increase in HTL temperature from 250 °C to 300 °C bio-oil yield was marginally increased, a further increase in temperature resulted in a drop regarding bio-oil yield. The reduced bio-oil yield at higher HTL temperature can be attributed to conversion of bio-oil into gaseous species.<sup>321</sup> However, for SCEL bio-oil yield increased exponentially with increasing liquefaction temperature. For fir wood, at all the

tested liquefaction temperatures, SCEL processing resulted into more bio-oil yield than HTL, which was consistent with the previous experimental findings with oak wood.<sup>322</sup> The yield of solid residue decreased with increasing liquefaction temperature, which was consistent with both the conversion types. However, the drop in solid residue yield was more intense with SCEL. With the change in liquefaction temperature from 250 °C to 350 °C, yield of solid residue dropped by 66.81 % with SCEL processing, whereas that was dropped by 23.37 % with HTL.

Figure 66 illustrates the effect of residence time and effect of conversion type on yield of bio-oil and solid residue produced from liquefaction of fir wood without catalyst. A marginal rise in bio-oil yield was observed with increase in residence time from 15 to 30 mins. However, the further increase in residence time lead to a drop regarding bio-oil yield, which was observed with both the conversion types. The suppressed bio-oil yield at a higher residence time can be attributed to the secondary decomposition of bio-oil into gaseous products.<sup>323</sup> The maximum bio-oil yield was obtained at residence time of 30 mins. for both the conversion types. A constant drop in solid residue yield was observed at a prolonged residence time for both the conversion types. This is attributed to extended thermochemical decomposition of feedstock experienced at higher residence time.

For maximizing bio-oil yield, it was decided to perform catalytic liquefaction at 300 °C and at residence time of 30 mins. As these conditions were found optimum with non-catalytic liquefaction of fir wood. Heterogeneous catalyst like, palladium on activated charcoal (5 wt% Pd/C), various transition metal triflates and the combination of metal triflates with palladium on activated charcoal were examined in the present work.

Table 26 compares yield distribution of bio-oil and solid residues obtained after catalytic and non-catalytic liquefaction of fir wood via HTL and SCEL. Catalytic liquefaction leads to higher bio-oil yield than non-catalytic liquefaction, which was observed with all the tested catalysts with both the conversion types. With HTL, a maximum bio-oil yield of 10.47 wt% was obtained with 5 wt% Pd/C, which was more than double the yield obtained with non-catalytic HTL. Compared to HTL, SCEL resulted in better bio-oil yield and lower solid residue yield, which was consistent with all the studied cases. Reduced solid yield and improved bio-oil yield with SCEL at all the tested liquefaction conditions can be attributed to higher hydrogen donating tendency of ethanol, which ultimately leads to better thermochemical decomposition of lignocellulose.<sup>50, 55</sup> The maximum bio-oil yield of 49.71 wt% was achieved with 0.04 mmol 5 wt% Pd/C and La(OTf)<sub>3</sub> in SCEL at a liquefaction temperature of 300 °C and residence time of 30 min. Catalytic liquefaction with metal triflates along with Pd/C yielded higher bio-oil and lower solid residue compared to that attained with metal triflates alone, which was observed with both the conversion types. For example, bio-oil yield of 6.94 wt% was obtained with HTL using 0.04mmol La(OTf)<sub>3</sub> which was increased to 10.22 wt% with 0.04mmol 5 wt% Pd/C and La(OTf)<sub>3</sub>.

### **8.3.2 Elemental composition of bio-crudes**

It can be observed from Table 27 that the HHV of bio-oil obtained after HTL was much improved than the HHV of raw material (i.e. fir wood). Additionally, compared to non-catalytic HTL, catalytic HTL of fir wood resulted in improved HHV of bio-oil and it was consistent with all the tested catalysts. Solid residue obtained from catalytic HTL exhibited improved HHV than that obtained from non-catalytic HTL except catalytic HTL



with 0.04mmol 5 wt% Pd/C and Sm(OTf)<sub>3</sub>. Bio-oil with the highest HHV of 30.46 MJ/kg was obtained from catalytic HTL with a catalyst mixture of 0.04 mmol 5 wt% Pd/C and Cu(OTf)<sub>2</sub>. The improved HHV of bio-oil and solid residue can be attributed to decline in oxygen content. All the tested catalysts promoted deoxygenating reactions that resulted into lower O/C ratio in obtained bio-oil, which ultimately lead to improved HHV.

Table 28 shows the elemental composition of raw material, bio-oil and solid residue from SCEL of fir wood without and with catalyst. The carbon and hydrogen content of bio-oil was significantly improved over the starting raw material, whereas the oxygen content was dropped notably which was consistent with both the conversion types (see Table 27 and Table 28). However, no clear trend with nitrogen content in bio-oil was observed. In comparison to raw material, the oxygen and hydrogen content in solid residue declined, whereas the carbon content was increased, which was observed with both the conversion types. This result can be attributed to deoxygenation via dehydration reaction favored during catalytic and non-catalytic liquefaction.<sup>323</sup> Catalytic HTL produced bio-oil with less oxygen content than the bio-oil produced via non-catalytic HTL (see Table 27). However, the same trend was not observed with SCEL. For SCEL, catalytic liquefaction with metal triflates resulted into bio-oil with relatively inferior HHV than non-catalytic liquefaction. For SCEL, catalytic liquefaction with Pd/C and Pd/C along with metal triflates yielded bio-oil with better HHV compared to that attained by non-catalytic liquefaction. Additionally, bio-oil derived from catalytic liquefaction with Pd/C and Pd/C along with metal triflates via SCEL showed improved HHV than via catalytic HTL with the same catalysts. For example, bio-oil derived from catalytic liquefaction with 5 wt% Pd/C through SCEL showed HHV of 32.38 MJ/kg, which was higher than the HHV of bio-oil derived with the

same catalyst via HTL. Bio-oil with the maximum HHV of 32.39 MJ/kg was obtained from catalytic liquefaction in SCEL media with a catalyst mixture of 0.04 mmol 5 wt% Pd/C and Sm(OTf)<sub>3</sub>. In comparison with HTL, bio-oil obtained through SCEL showed higher H/C ratio for all the liquefaction experiments. Which indicates relatively lower aromatic content in bio-oil derived with SCEL than that obtained with HTL.<sup>324</sup>

### 8.3.3 Boiling point distribution of bio-oils

The boiling point distribution of hydrocarbons available in crude bio-oil has been further measured using thermogravimetric analysis in N<sub>2</sub> atmosphere and presented in Table 29. According to petroleum fractions, hydrocarbons present in bio-oil were classified in four categories: (1) light naphtha (BP < 93 °C), (2) heavy naphtha (BP 93-204 °C), (3) light gas oil (BP 204-343 °C), and (4) heavy gas oil (BP > 343 °C). For SCEL processing, the fraction of light naphtha decreased in bio-oil derived from catalytic liquefaction than that in the bio-oil derived via non-catalytic liquefaction. However, for catalytic HTL no such clear trend was observed with variation in light naphtha fraction. Catalytic liquefaction with metal triflates along with Pd/C reduced heavy naphtha fraction in bio-oil compared to that attained with metal triflates alone, which was observed with both the conversion types. The fraction of light gas oil in obtained bio-oil increased with catalytic liquefaction compared to non-catalytic liquefaction in SCEL processing. However, for catalytic HTL no such clear trend was observed with change in light gas oil fraction. In comparison with non-catalytic HTL, catalytic liquefaction using all the catalyst had increased fraction of heavy gas oil in bio-oil except with 0.04 mmol La(OTf)<sub>3</sub>. The same trend was observed with SCEL processing except with 0.04 mmol Cu(OTf)<sub>2</sub>.

### 8.3.4 GC-MS analysis of bio-crudes

To gain further information into the detailed chemical composition of the bio-oils, summarize the major chemical species in the bio-crudes from the HTL and SCEL process are summarized in Figure 67 and Figure 68, respectively. Acid, ketone, cyclopentenone, alcohol, phenol, and furan type compounds were found in both the HTL and SCEL processes. Ethers and esters were only produced from the SCEL process, where ester type compounds shared an area% in the GC-MS results up to 13.16% employing well established methodologies. From both the HTL and SCEL processes, aromatic compounds represent the most abundant chemical species, with a GC area% up to 52.77% and 46.86%, respectively. Due to the natural complexity of the biomass derived bio-crudes, the number of detected depolymerized products are typically more than 60 and the information provided by the GC-MS data are valuable but complex. Table 30 and Table 31 provide lists of the detailed major compounds in the depolymerized products from HTL and SCEL process. For simplicity, each chemical species is discussed in separate paragraphs, which is inspired by the original work by Brand and Kim.<sup>32</sup> The emphasis is on the similarity and differences of the products from HTL and SCEL processes, as well as the catalytic effect on the detailed product composition. The formation of certain chemical species will also be discussed to understand the possible reaction pathways during the depolymerization reactions in water and supercritical ethanol.

From both HTL and SCEL processes, cyclopentenone and its derivatives (i.e., hydrogenated, hydroxylated, and alkylated type derivatives) comprised a major chemical species in the bio-oil products. Specifically, the area% of the total cyclopentenone/cyclopentanone type compounds from the non-catalytic HTL process was

14.23%; whereas the non-catalytic SCEL process resulted in 4.65 area% of the cyclopentenone/cyclopentanone type compounds. Polysaccharides could be transformed to furfural and alkylated furfural during the liquefactions by the isomerization and dehydration reactions (step [B] in Figure 69). Hronec et al. studied the influence of water and alcohol media on the transformation of furfural to cyclopentanone over Pd/C.<sup>325</sup> It was reported that the yield of cyclopentanone and cyclopentanol was 76.46 mol% in total using water as a solvent. When the n-butanol was applied as a solvent and other reaction conditions were kept consistent, the major products shifted to furfuryl alcohol and 2-methylfuran, with yields of 47.86 mol% and 40.43 mol%, respectively. These findings may imply that the transformation of furanic compounds to cyclopentenone/cyclopentanone type compounds favors the hydrothermal media rather than the alcohol solvent, which is consistent with the results in this study. It should be noted that for the SCEL process, the hydrogenated derivative cyclopentanone type compounds only existed in the catalytic derived products. For examples, 2-methylcyclopentanone, 1-hydroxy-2-pentanone, and 2-ethylcyclopentanone were not detected from the control SCEL process. After the addition of the Pd/C and metal triflates in the SCEL process, several cyclopentenone type compounds were completely eliminated, specifically, including 2-cyclopentenone, 2-methyl-2-cyclopentenone, 3-methyl-2-cyclopentenone, 2-hydroxy-3-methyl-2-cyclopentenone, and 2-hydroxy-3-propyl-2-cyclopentenone. In contrast, for the HTL cyclopentenone and cyclopentanone both exist in the control reaction. This finding may suggest that for the HTL, the ring conversion of the cyclopentenone to cyclopentanone could happen without the addition of Pd/C or metal triflates (step [D] in Figure 69). For the SCEL process the addition of Pd/C or a combination of Pd/C and metal triflates could

strongly promote the hydrogenation of the C=C of the cyclopentenone type compounds (step [F] in Figure 69). Several research groups have converted furfural to cyclopentanone and studied the selectivity of the products from different levels of hydrogenation.<sup>326-328</sup> In contrast to these reported work, the excessive hydrogenated product cyclopentanol was not detected in either HTL or SCEL process under the conditions in this work. In Figure 69, steps A-F summarized the major conversions from carbohydrate to cyclopentenone/cyclopentanone type compounds. For the steps D and E illustrating the funanics to cyclopentenone type products, furanmethanol and tetrahydrofurfuryl alcohol could be the intermediate formed during the transformation based on Guo et al.'s model compound study.<sup>328</sup>

Aromatic compounds were shown as the most abundant chemical species in the bio-crude from both HTL and SCEL process. For simplicity of the discussion only the aromatic compounds with an area% higher than 1% are discussed here. For the bio-crude from control HTL process, 2-methoxyphenol and vanillin made up the major aromatic products with an area% of 25.10% and 4.26%, respectively. For the catalytic runs, the content of 2-methoxyphenol was reduced to the level of 10.85 wt%~12.24%. Vanillin was completely removed for the catalytic from HTL. In contrast, the content of alkylated methoxyphenol compounds (i.e., 2-Methoxy-4-methylphenol, 4-Ethyl-2-methoxyphenol, 2-Methoxy-4-propylphenol) increased drastically. For example, from the control HTL, the total area% of these three alkylated methoxyphenols were 9.19%; from the HTL over Pd/C and Cu(OTf)<sub>2</sub> this value was increased to 36.49%. Taken together, these findings suggest that the bi-functional catalyst is capable of the alkylation on the aromatic compounds during HTL. For the bio-crudes from SCEL process, the major aromatic product was 4-

hydroxy-3-methoxybenzeneacetic acid with an area% of 16.80%~28.99% in the catalytic runs. The catalytic effect on the alkylation reactions were not observed for the SCEL process. In Figure 69, two major routes to form aromatic compounds were summarized: step [J] denotes the the depolymerization of lignin to aromatic fragments; steps [H] and [I] demonstrates the possible aldol and Michael condensation of C2, C3, and C4 ketone/aldehyde intermediates to form aromatic structures in HTL and SCEL process.<sup>329-333</sup> Additionally, Figure 69 demonstrates the plausible reaction pathways for forming ketone/aldehydes in step [G] and esterification specifically occurring in SCEL process in step [K].

### 8.3.5 HSQC analysis of bio-crudes

To examine the structural change during the bi-functional catalyst assisted HTL and SCEL of fir wood, two-dimensional HSQC NMR analysis was further employed to analyze the aromatic and aliphatic C-H bonds in the bio-oils. Figures 70-75 report the aromatic and aliphatic C-H information of the bio-oils from depolymerization of fir wood in water and ethanol. The chemical shift assignment of the C-H bonds in bio-oils was assigned according to the published literature.<sup>302</sup> Compare Figure 70 and Figure 72, it was observed clearly that H<sub>2/6</sub>/C<sub>2/6</sub> in *p*-hydroxyphenyl units [ $\delta_C/\delta_H=128.0\text{ppm}/7.2\text{ppm}$ ] was completely removed by HTL over Pd/C. Contrast to the *p*-hydroxyphenyl type lignin sub-units, guaiacyl type and catechol type units remained constant after the Pd/C catalyzed hot water pretreatment. For the bi-functional system of Pd/C and Sm(OTf)<sub>3</sub> as illustrated by Figure 74, this bi-catalyst exhibited similar performance regarding the *p*-hydroxyphenyl unit removal when compared to the sole use of Pd/C. Compare Figure 71 and Figure 73, it was observed that guaiacyl type C-H was partially removed by Pd/C in ethanol. It should be

noted that this observation was determined by the  $C_6/H_6$  [ $\delta_C/\delta_H=119.1/6.8$ ] since  $C_2/H_2$  and  $C_6/H_6$  were largely overlapped with other signals. Compare the Figure 70 and Figure 71, it was found that H type structure existed in the HTL generated bio-oils, however H type structure was not found in the deconstruction products from SCEL.

#### 8.4 Conclusion

A bi-functional catalyst system of Pd/C and water tolerant Lewis acid (i.e.,  $Sm(OTf)_3$ ,  $La(OTf)_3$ ,  $Cu(OTf)_2$ ) were demonstrated to be effective for producing fuel precursors from biomass liquefaction in both water and ethanol. Specifically, the highest bio-oil yield of 49.71 wt% was observed from supercritical ethanol liquefaction over Pd/C and  $La(OTf)_3$  under the condition of 300 °C and 30 min. The highest higher heating value of ~32 MJ/Kg was observed from the supercritical ethanol liquefactions over Pd/C, Pd/C +  $Sm(OTf)_3$ , and Pd/C +  $Cu(OTf)_2$ . Additionally, the structures in the biomass liquefied products were studied by GC-MS and NMR allowing for postulating reaction pathways. The Pd/C-metal triflate catalytic system facilitated the hydrogenation of cyclopentenone ring and alkylation of the aromatic rings, especially for the hydrothermal liquefaction. The synergy of the Pd/C and metal triflate catalytic system regarding the liquefaction performance was not observed under the conditions tested and reaction condition optimization was recommended for further study.

## CHAPTER IX: OVERALL CONCLUSIONS

This dissertation work accomplished the thermochemical conversion of biomass to value-added fuel precursors with improved qualities compared with original biomass derived oils. Three major aspects of the renewable transformation of biomass to liquid fuel feedstocks have been focused: pretreatment of the biomass feedstocks prior to the pyrolysis, ex-situ catalytic upgrading of the pyrolysis oils, and one-pot liquefaction of biomass using additives.

Pyrolysis is a promising method for converting biomass to biofuels. However, some of pyrolysis oil's physiochemical properties still limit its commercial applications. In this study, the autohydrolysis pretreatment at  $175\pm 3$  °C for 40 min was conducted to improve the resulting pine pyrolysis oil's properties as a fuel. During autohydrolysis, deacetylation and decomposition of hemicellulose was observed by ion-exchange chromatography and Fourier transform infrared spectroscopy (FT-IR). In addition, the cleavage of lignin ether bonds was clearly determined by  $^{13}\text{C}$  cross-polarization/magic angle spinning (CP/MAS) nuclear magnetic resonance (NMR). Phosphitylation followed by  $^{31}\text{P}$  NMR analysis of the heavy oils gave detailed structural information of the hydroxyl groups; the results revealed that autohydrolysis pretreatment led to a reduction of carboxyl acids in the heavy oils generated at all three pyrolysis temperatures (400, 500, and 600 °C). The  $^{31}\text{P}$  NMR analysis also revealed that autohydrolysis pretreatment led to a reduction of condensed phenolic hydroxyl groups in the heavy oils produced at 600 °C.  $^1\text{H}$ - $^{13}\text{C}$  heteronuclear single-quantum correlation (HSQC) NMR analysis showed that at a pyrolysis temperature of 600 °C, the pretreated pine produced lower methoxy group constituents. Both  $^{31}\text{P}$  and HSQC



NMR results indicated that autohydrolysis pretreatment increased levoglucosan yields in the bio-oils.

Pyrolysis has been increasingly perceived as a promising technology to produce biofuel precursors (bio-oil) from agricultural residuals; however, there is a significant quality gap between a bio-oil and the fuels used for transportation. In this study, we autohydrolyzed pretreated sugarcane bagasse at three different conditions (180 °C - 10 min, 180 °C - 40 min, 200 °C - 40 min), then we investigated the effect of this pretreatment on a subsequent pyrolysis stage. High-pressure ion-exchange chromatography (HPIC) and the <sup>13</sup>C cross-polarization/magic angle spinning (CP/MAS) solid state nuclear magnetic resonance (NMR) revealed that the autohydrolysis pretreatment significantly disrupted the hemicellulose fractions in the sugarcane bagasse and caused the breakage of lignin ether linkages in the sugarcane bagasse feedstocks. As the <sup>31</sup>P NMR results indicated, the autohydrolysis pretreatment removed carboxylic acid groups up to 66.7%, which could significantly address the corrosion problem of bio-oils. Heteronuclear single quantum correlation (HSQC) analysis suggested that the autohydrolysis pretreatment effectively lowered the presence of the oxygenated aromatic compounds in the bio-oils. Gel permeation chromatography (GPC) analysis of the bio-oils indicated that the oils from severely pretreated sugarcane bagasse pyrolyzed at a low temperature (i.e., 400 °C) had lower molecular weights components similar to those present gasoline products.

The impact of upgrading temperature and biomass-to-catalyst mass ratio on upgrading of pine pyrolysis vapors over HZSM-5 was studied in a dual fluidized bed reactor system. Increasing the upgrading temperature or reducing the biomass-to-catalyst ratio enhanced deoxygenation but decreased organic oil yields. Higher upgrading

temperatures enhanced transformation of carbon into gaseous products whereas reduced biomass-to-catalyst ratio increased the conversion of biomass vapors to coke. While oxygen was removed as CO, H<sub>2</sub>O, and CO<sub>2</sub>, decarboxylation was limited by the amount of acids in the pyrolysis vapors. Bio-oil with molecular weight in gasoline range was derived via catalytic upgrading. The molecular homogeneity was improved at higher catalytic upgrading temperature and lower biomass-to-catalyst (B:C) ratio. Increasing the B:C ratio decreased the fraction of aliphatic C-H bonds and of polyaromatics and increased the retention of both aliphatic and aromatic OH groups. Increasing the upgrading temperature enhanced cracking by ZSM-5 leading to oil with lower molecular weight, enhanced dealkylation and formation of light hydrocarbon gases, enhanced demethoxylation and decreased polyaromatics formation. Aliphatic and aromatic OH decreased as upgrading temperature was increased from 500 to 550°C, but there was less impact when the temperature was further increased to 600°C.

Lignocellulosic biomass (grape seeds) was deconstructed in both hydrothermal and supercritical ethanol media with a combination of two metal chlorides (TiCl<sub>4</sub>/MgCl<sub>2</sub>) to produce bio-oils. The use of this metal chlorides additive in supercritical ethanol achieved the highest bio-oil yield of 49.2 wt% at 300 °C with a residence time of 30 min, which was 35.8 % higher than the bio-oil yield obtained from the same reaction conditions with no additive added in. Both the hydrothermal and supercritical ethanol deconstruction reactions with the highest additive loading (TiCl<sub>4</sub>/MgCl<sub>2</sub>=4mmol/4mmol) produced the bio-oils with a higher heating values (HHV) of 35 MJ/Kg which was comparable of the HHV of petroleum-based liquid fuels. As for the structural changes of bio-oils, gas chromatography-mass spectrometry (GC-MS) analysis of the bio-oils showed that the

major products in bio-oils from the hydrothermal deconstruction were acids while the majority products in bio-oils from the supercritical ethanol deconstruction were esters. <sup>31</sup>P Nuclear magnetic resonance (NMR) data of the phosphorylation bio-oils suggested that both hydrothermal and supercritical ethanol deconstruction reactions with metal chlorides significantly reduced the non-condensed OH in bio-oils while only supercritical ethanol deconstruction with metal chlorides reduced the aliphatic OH in bio-oils. Heteronuclear single quantum coherence (HSQC) NMR revealed that deconstruction in both supercritical ethanol and hydrothermal media largely removed oxygenated lignin sub-units while the removal of O-alkylated structures was only found in the catalytic ethanol deconstruction.

To further study the one-pot depolymerization of biomass, a bi-functional catalyst system consisting of palladium supported on carbon (Pd/C) and metal triflates (i.e., Sm(OTf)<sub>3</sub>, La(OTf)<sub>3</sub>, and Cu(OTf)<sub>2</sub>) were shown to promote the biomass liquefaction in both water and supercritical ethanol medium, converting fir wood into oxygenated compounds. The highest bio-oil yield from hydrothermal liquefaction (HTL) was 10.47 wt% over Pd/C whereas the highest bio-oil yield of 49.71 wt% was achieved from supercritical ethanol liquefaction (SCEL) over the bi-functional catalyst system of Pd/C and La(OTf)<sub>3</sub>. Higher heating values, carbon recovered values and boiling point distributions were further determined for elucidating the physical properties of the bio-oils. Gas chromatography mass spectrometry (GC-MS) analysis of the bio-oils revealed the chemical composition of the bio-oils. Substituted phenols and cyclopentenone/cyclopentanone type compounds consisted of more than 60 of the total products from HTL as determined by from SCEL process. The major reaction pathways

are proposed based on the GC-MS results, which include depolymerization, isomerization, dehydration, condensation, and hydrogenation.

## **CHAPTER X: RECOMMENDATIONS FOR FUTURE WORKS**

The development of efficient lignocellulose conversion pathways to value-added fuel products and platform chemicals is a significant global challenge targeted at addressing future energy and sustainability challenges. The utility of ethanol as a solvent provides an environmentally friendly approach to overcome lignocellulose recalcitrance and obtain attractive depolymerized structures that are the precursors of fuel substituents and functionalized chemicals. Complex structures of the main constituents of lignocellulose offer tremendous potential for the desired sustainable production of fuels and chemicals. Both a fundamental understanding of the chemistry involved in supercritical and near-supercritical ethanolysis reactions, and the creation of innovative biorefinery processing technologies on micro/large scales are desired for fully utilizing the potential of the lignocellulose constituent structures. Future studies on the deconstruction of lignocellulose to value-added products include selectively converting biomass into desired functionalized structures, employing the whole biomass as a starting source, developing economically viable catalysts suitable for ethanolysis processing, minimizing condensation and repolymerization reactions during deconstruction with ethanol, a deeper understanding of the mechanisms of the deconstruction reactions, and technoeconomic analyses, as outlined in more detail below.

Current biomass deconstruction research focuses on two lignocellulose conversion strategies: convergent pathways to generate hydrocarbons as liquid transportation fuel precursors and divergent functionalization to produce chemical building blocks.<sup>[62]</sup> The

convergent pathways usually require deoxygenation and hydrogenation to obtain saturated chains and deoxygenated aromatic structures. This pathway involving depolymerization, deoxygenation, and chain elongation is promising for reducing fossil fuel dependence.<sup>[7a]</sup> Deconstruction of biomass in ethanol also contributes to the production of bulk chemicals (i.e., C2, C3, C4, and BTX) if followed by hydroprocessing steps.<sup>[63]</sup> Future research may focus on finding pathways to deconstruct biomass in ethanol to produce chemical building blocks directly by keeping selected functional structures intact.

The use of whole biomass as a feed material, instead of pretreatment and separation of the three main constituents before deconstruction reactions in ethanol, is of growing interest. For example, Sun et al. recently designed an integrated catalyst recycling system to obtain amine and alkane precursors from biomass deconstruction products in alcoholic solvent.<sup>[62]</sup> This concept of full conversion of the whole biomass could be adopted in future studies on catalytic biomass deconstruction reactions in ethanol.

The design of suitable catalysts for deconstruction reactions in ethanol is a high priority and challenging target. The catalysts need to be environmentally friendly, noble metal free, low cost, and exhibit the ability to be recycled.<sup>[64]</sup> The suitability of the catalyst to function in ethanol should also be taken into consideration, for example, the deconstruction of biomass in ethanol by using CuMgAl catalyst successfully suppresses undesired side reactions (i.e., char forming) and shifts the reactions towards depolymerization.

If deconstructing lignin in ethanol, the repolymerization and condensation of reactive fragments significantly suppress the yields of monomers. Barret et al. used dimethyl carbonate as a cosolvent to successfully promote the yields of the stable,

depolymerized aromatic species upon disassembling lignin in supercritical alcohol with CuMgAl catalyst.<sup>[65]</sup> The idea of using protection and stabilization reagents may inspire future research into the deconstruction of lignin in ethanol for higher yields of monomers.<sup>[66]</sup>

Deeper insights into the reaction mechanisms during lignocellulose deconstruction reactions in ethanol are needed. More complex model compounds of biomass constituents should be developed and applied in mechanistic studies.<sup>[64]</sup> In addition, advanced techniques, including isotopic labeling and in situ NMR spectroscopy, for analyzing the deconstruction products should also be applied in this research area.<sup>[67]</sup>

Technoeconomic analysis needs to be incorporated into future research studies regarding ethanol-assisted biomass deconstruction. The direct conversion of lignocellulose into biofuels in ethanol is an attractive technology because much of the ethanol can be recovered and reused in the process. Moreover, if all deconstructed products from lignocellulose, namely, biofuels, biochars, and gases, are effectively used, it can lead to improved capital effectiveness for the overall process. Nonetheless, as this technology begins to mature, technoeconomic analysis of the overall process now needs to be assessed.

## **LIST OF REFERENCES**



1. Hoffert, M. I.; Caldeira, K.; Benford, G.; Criswell, D. R.; Green, C.; Herzog, H.; Jain, A. K.; Kheshgi, H. S.; Lackner, K. S.; Lewis, J. S., Advanced technology paths to global climate stability: energy for a greenhouse planet. *Science* **2002**, *298* (5595), 981-987.
2. Pacala, S.; Socolow, R., Stabilization wedges: solving the climate problem for the next 50 years with current technologies. *Science* **2004**, *305* (5686), 968-972.
3. Quadrelli, E. A., 25 years of energy and green chemistry: saving, storing, distributing and using energy responsibly. *Green Chem.* **2016**, *18* (2), 328-330.
4. Ghoniem, A. F., Needs, resources and climate change: clean and efficient conversion technologies. *Prog. Energ. Combust. Sci.* **2011**, *37* (1), 15-51.
5. Ragauskas, A. J.; Williams, C. K.; Davison, B. H.; Britovsek, G.; Cairney, J.; Eckert, C. A.; Frederick, W. J.; Hallett, J. P.; Leak, D. J.; Liotta, C. L., The path forward for biofuels and biomaterials. *Science* **2006**, *311* (5760), 484-489.
6. Tekin, K.; Hao, N.; Karagoz, S.; Ragauskas, A. J., Ethanol: A Promising Green Solvent for the Deconstruction of Lignocellulose. *ChemSusChem* **2018**, *11* (20), 3559-3575.
7. Huber, G. W.; Iborra, S.; Corma, A., Synthesis of Transportation Fuels from Biomass: Chemistry, Catalysts, and Engineering. *Chem. Rev. (Washington, DC, U. S.)* **2006**, *106* (9), 4044-4098.
8. Perlack, R. D.; Wright, L. L.; Turhollow, A. F.; Graham, R. L.; Stokes, B. J.; Erbach, D. C. *Biomass as feedstock for a bioenergy and bioproducts industry: the technical feasibility of a billion-ton annual supply*; DTIC Document: 2005.

9. Ed. George W. Huber, U. o. M. A. N. S. F. C., Bioengineering,, NSF. 2008. Breaking the Chemical and Engineering Barriers to Lignocellulosic Biofuels: Next Generation Hydrocarbon Biorefineries. *Environmental, and Transport Systems Division*. **2008**, Washington D.C., 180 p.
10. Czernik, S.; Bridgwater, A. V., Overview of Applications of Biomass Fast Pyrolysis Oil. *Energy Fuels* **2004**, *18* (2), 590-598.
11. Douglas Elliott, G. S., liquid hydrocarbon fuels from biomass. *Amer. Chem. Soc., Fuel Chem. Reports* **1989**, *34* (4), 1160-1166.
12. Mohan, D.; Pittman, C. U., Jr.; Steele, P. H., Pyrolysis of Wood/Biomass for Bio-oil: A Critical Review. *Energy Fuels* **2006**, *20* (3), 848-889.
13. Mullen, C. A.; Boateng, A. A., Chemical Composition of Bio-oils Produced by Fast Pyrolysis of Two Energy Crops. *Energy Fuels* **2008**, *22* (3), 2104-2109.
14. Bridgwater, A. V., Renewable fuels and chemicals by thermal processing of biomass. *Chem. Eng. J. (Amsterdam, Neth.)* **2003**, *91* (2-3), 87-102.
15. Lu, Q.; Li, W.-Z.; Zhu, X.-F., Overview of fuel properties of biomass fast pyrolysis oils. *Energy Convers. Manage.* **2009**, *50* (5), 1376-1383.
16. Oasmaa, A.; van de Beld, B.; Saari, P.; Elliott, D. C.; Solantausta, Y., Norms, Standards, and Legislation for Fast Pyrolysis Bio-oils from Lignocellulosic Biomass. *Energy Fuels* **2015**, *29* (4), 2471-2484.
17. Talmadge, M. S.; Baldwin, R. M.; Bidy, M. J.; McCormick, R. L.; Beckham, G. T.; Ferguson, G. A.; Czernik, S.; Magrini-Bair, K. A.; Foust, T. D.; Metelski, P. D.; Hetrick, C.; Nimlos, M. R., A perspective on oxygenated species in the refinery integration of pyrolysis oil. *Green Chem.* **2014**, *16* (2), 407-453.

18. Ortega, J. V.; Renehan, A. M.; Liberatore, M. W.; Herring, A. M., Physical and chemical characteristics of aging pyrolysis oils produced from hardwood and softwood feedstocks. *J. Anal. Appl. Pyrolysis* **2011**, *91* (1), 190-198.
19. Nolte, M. W.; Liberatore, M. W., Real-Time Viscosity Measurements during the Accelerated Aging of Biomass Pyrolysis Oil. *Energy Fuels* **2011**, *25* (7), 3314-3317.
20. Naske, C. D.; Polk, P.; Wynne, P. Z.; Speed, J.; Holmes, W. E.; Walters, K. B., Postcondensation Filtration of Pine and Cottonwood Pyrolysis Oil and Impacts on Accelerated Aging Reactions. *Energy Fuels* **2012**, *26* (2), 1284-1297.
21. Alsbou, E.; Helleur, B., Accelerated Aging of Bio-oil from Fast Pyrolysis of Hardwood. *Energy Fuels* **2014**, *28* (5), 3224-3235.
22. Bridgwater, A. V., Review of fast pyrolysis of biomass and product upgrading. *Biomass Bioenerg.* **2012**, *38*, 68-94.
23. Mu, W.; Ben, H.; Ragauskas, A.; Deng, Y., Lignin Pyrolysis Components and Upgrading-Technology Review. *BioEnergy Res.* **2013**, *6* (4), 1183-1204.
24. Mortensen, P. M.; Grunwaldt, J. D.; Jensen, P. A.; Knudsen, K. G.; Jensen, A. D., A review of catalytic upgrading of bio-oil to engine fuels. *Appl. Catal. A* **2011**, *407* (1-2), 1-19.
25. Huber, G. W.; Corma, A., Synergies between bio- and oil refineries for the production of fuels from biomass. *Angew. Chem. Int. Ed.* **2007**, *46* (38), 7184-7201.
26. Zhang, Q.; Chang, J.; Wang, T.; Xu, Y., Review of biomass pyrolysis oil properties and upgrading research. *Energy Convers. Manage.* **2006**, *48* (1), 87-92.
27. Xiu, S.; Shahbazi, A., Bio-oil production and upgrading research: A review. *Renew. Sustain. Energ. Rev.* **2012**, *16* (7), 4406-4414.

28. Chen, G.; Yao, J.; Liu, J.; Yan, B.; Shan, R., Biomass to hydrogen-rich syngas via catalytic steam reforming of bio-oil. *Renew. Energ.* **2016**, *91*, 315-322.
29. Tanneru, S. K.; Parapati, D. R.; Steele, P. H., Pretreatment of bio-oil followed by upgrading via esterification to boiler fuel. *Energy (Oxford, U. K.)* **2014**, *73*, 214-220.
30. Xu, J.; Jiang, J.; Dai, W.; Zhang, T.; Xu, Y., Bio-Oil Upgrading by Means of Ozone Oxidation and Esterification to Remove Water and to Improve Fuel Characteristics. *Energy Fuels* **2011**, *25* (4), 1798-1801.
31. Li, Q.; Hu, G., Supply chain design under uncertainty for advanced biofuel production based on bio-oil gasification. *Energy (Oxford, U. K.)* **2014**, *74*, 576-584.
32. Bridgwater, A. V., Review of fast pyrolysis of biomass and product upgrading. *Biomass Bioenergy* **2012**, *38*, 68-94.
33. Zhang, S.; Yan, Y.; Li, T.; Ren, Z., Upgrading of liquid fuel from the pyrolysis of biomass. *Bioresour. Technol.* **2005**, *96* (5), 545-50.
34. Tang, Z.; Lu, Q.; Zhang, Y.; Zhu, X.; Guo, Q., One Step Bio-Oil Upgrading through Hydrotreatment, Esterification, and Cracking. *Industrial & Engineering Chemistry Research* **2009**, *48* (15), 6923-6929.
35. Carlson, T. R.; Vispute, T. P.; Huber, G. W., Green Gasoline by Catalytic Fast Pyrolysis of Solid Biomass Derived Compounds. *ChemSusChem* **2008**, *1* (5), 397-400.
36. Graça, I.; Ribeiro, F. R.; Cerqueira, H. S.; Lam, Y. L.; de Almeida, M. B. B., Catalytic cracking of mixtures of model bio-oil compounds and gasoil. *Appl. Catal B: Environ.* **2009**, *90* (3), 556-563.
37. Peng, J.; Chen, P.; Lou, H.; Zheng, X., Catalytic upgrading of bio-oil by HZSM-5 in sub- and super-critical ethanol. *Bioresour. Technol.* **2009**, *100* (13), 3415-8.

38. Capello, C.; Fischer, U.; Hungerbühler, K., What is a green solvent? A comprehensive framework for the environmental assessment of solvents. *Green Chem.* **2007**, *9* (9), 927-934.
39. Lu, J.; Boughner, E. C.; Liotta, C. L.; Eckert, C. A., Nearcritical and supercritical ethanol as a benign solvent: polarity and hydrogen-bonding. *Fluid Phase Equilib.* **2002**, *198* (1), 37-49.
40. Vasilakos, N. P.; Austgen, D. M., Hydrogen-donor solvents in biomass liquefaction. *Ind. Eng. Chem. Process Des. Dev.* **1985**, *24* (2), 304-311.
41. Guo, D.; Liu, B.; Tang, Y.; Zhang, J.; Xia, X., Autocatalytic Depolymerization of Alkali Lignin by Organic Bound Sodium in Supercritical Ethanol. *Energy Fuels* **2017**, *31* (10), 10842-10849.
42. Yoo, C. G.; Pu, Y.; Li, M.; Ragauskas, A. J., Elucidating Structural Characteristics of Biomass using Solution-State 2 D NMR with a Mixture of Deuterated Dimethylsulfoxide and Hexamethylphosphoramide. *ChemSusChem* **2016**, *9* (10), 1090-1095.
43. Ragauskas, A. J.; Beckham, G. T.; Biddy, M. J.; Chandra, R.; Chen, F.; Davis, M. F.; Davison, B. H.; Dixon, R. A.; Gilna, P.; Keller, M., Lignin valorization: improving lignin processing in the biorefinery. *Science* **2014**, *344* (6185), 1246843.
44. Kleinert, M.; Barth, T., Phenols from lignin. *Chem. Eng. Technol.* **2008**, *31* (5), 736-745.
45. Pandey, M. P.; Kim, C. S., Lignin depolymerization and conversion: a review of thermochemical methods. *Chem. Eng. Technol.* **2011**, *34* (1), 29-41.

46. Deuss, P. J.; Scott, M.; Tran, F.; Westwood, N. J.; de Vries, J. G.; Barta, K., Aromatic monomers by in situ conversion of reactive intermediates in the acid-catalyzed depolymerization of lignin. *J. Am. Chem. Soc.* **2015**, *137* (23), 7456-7467.
47. Brebu, M.; Vasile, C., Thermal degradation of lignin—a review. *Cell. Chem. Technol.* **2010**, *44* (9), 353.
48. Zeng, J.; Yoo, C. G.; Wang, F.; Pan, X.; Vermerris, W.; Tong, Z., Biomimetic Fenton-Catalyzed Lignin Depolymerization to High-Value Aromatics and Dicarboxylic Acids. *ChemSusChem* **2015**, *8* (5), 861-871.
49. Singh, R.; Prakash, A.; Dhiman, S. K.; Balagurumurthy, B.; Arora, A. K.; Puri, S.; Bhaskar, T., Hydrothermal conversion of lignin to substituted phenols and aromatic ethers. *Bioresour. Technol.* **2014**, *165*, 319-322.
50. Brand, S.; Kim, J., Liquefaction of major lignocellulosic biomass constituents in supercritical ethanol. *Energy* **2015**, *80*, 64-74.
51. Kim, J.-Y.; Oh, S.; Hwang, H.; Cho, T.-s.; Choi, I.-G.; Choi, J. W., Effects of various reaction parameters on solvolytical depolymerization of lignin in sub-and supercritical ethanol. *Chemosphere* **2013**, *93* (9), 1755-1764.
52. Nielsen, J. B.; Jensen, A.; Madsen, L. R.; Larsen, F. H.; Felby, C.; Jensen, A. D., Noncatalytic Direct Liquefaction of Biorefinery Lignin by Ethanol. *Energy Fuels* **2017**, *31* (7), 7223-7233.
53. Park, J.; Riaz, A.; Insyani, R.; Kim, J., Understanding the relationship between the structure and depolymerization behavior of lignin. *Fuel* **2018**, *217*, 202-210.

54. Miller, J.; Evans, L.; Littlewolf, A.; Trudell, D., Batch microreactor studies of lignin and lignin model compound depolymerization by bases in alcohol solvents. *Fuel* **1999**, *78* (11), 1363-1366.
55. Limarta, S. O.; Ha, J.-M.; Park, Y.-K.; Lee, H.; Suh, D. J.; Jae, J., Efficient depolymerization of lignin in supercritical ethanol by a combination of metal and base catalysts. *J. Ind. Eng. Chem.* **2018**, *57*, 45-54.
56. Kuznetsov, B.; Sharypov, V.; Chesnokov, N.; Beregovtsova, N.; Baryshnikov, S.; Lavrenov, A.; Vosmerikov, A.; Agabekov, V., Lignin conversion in supercritical ethanol in the presence of solid acid catalysts. *Kinet. Catal.* **2015**, *56* (4), 434-441.
57. Huang, S.; Mahmood, N.; Tymchyshyn, M.; Yuan, Z.; Xu, C. C., Reductive depolymerization of kraft lignin for chemicals and fuels using formic acid as an in-situ hydrogen source. *Bioresour. Technol.* **2014**, *171*, 95-102.
58. Xu, C.; Etcheverry, T., Hydro-liquefaction of woody biomass in sub-and supercritical ethanol with iron-based catalysts. *Fuel* **2008**, *87* (3), 335-345.
59. Riaz, A.; Kim, C. S.; Kim, Y.; Kim, J., High-yield and high-calorific bio-oil production from concentrated sulfuric acid hydrolysis lignin in supercritical ethanol. *Fuel* **2016**, *172*, 238-247.
60. Cabrera, Y.; Cabrera, A.; Jensen, A.; Felby, C., Purification of biorefinery lignin with alcohols. *J. Wood Chem. Technol.* **2016**, *36* (5), 339-352.
61. Jeong, S.; Yang, S.; Kim, D. H., Depolymerization of Protobind lignin to produce monoaromatic compounds over Cu/ZSM-5 catalyst in supercritical ethanol. *Mol. Catal.* **2017**, *442*, 140-146.

62. Zakzeski, J.; Bruijninx, P. C.; Jongerius, A. L.; Weckhuysen, B. M., The catalytic valorization of lignin for the production of renewable chemicals. *Chem. Rev.* **2010**, *110* (6), 3552-3599.
63. Guo, D.; Liu, B.; Tang, Y.; Zhang, J.; Xia, X.; Tong, S., Catalytic Depolymerization of Alkali Lignin in Sub-and Super-critical Ethanol. *BioResources* **2017**, *12* (3), 5001-5016.
64. Ma, R.; Hao, W.; Ma, X.; Tian, Y.; Li, Y., Catalytic Ethanolysis of Kraft Lignin into High-Value Small-Molecular Chemicals over a Nanostructured  $\alpha$ -Molybdenum Carbide Catalyst. *Angew. Chem. Int. Ed.* **2014**, *53* (28), 7310-7315.
65. Ma, X.; Ma, R.; Hao, W.; Chen, M.; Yan, F.; Cui, K.; Tian, Y.; Li, Y., Common pathways in ethanolysis of kraft lignin to platform chemicals over molybdenum-based catalysts. *ACS Catal.* **2015**, *5* (8), 4803-4813.
66. Chen, L.; Korányi, T. I.; Hensen, E. J., Transition metal (Ti, Mo, Nb, W) nitride catalysts for lignin depolymerisation. *Chem. Commun.* **2016**, *52* (60), 9375-9378.
67. Huang, X.; Atay, C.; Korányi, T. s. I.; Boot, M. D.; Hensen, E. J., Role of Cu–Mg–Al mixed oxide catalysts in lignin depolymerization in supercritical ethanol. *ACS Catal.* **2015**, *5* (12), 7359-7370.
68. Huang, X.; Atay, C.; Zhu, J.; Palstra, S. W.; Korányi, T. I.; Boot, M. D.; Hensen, E. J., Catalytic depolymerization of lignin and woody biomass in supercritical Ethanol: influence of reaction temperature and feedstock. *ACS Sustain. Chem. Eng.* **2017**, *5* (11), 10864-10874.
69. Huang, X.; Korányi, T. I.; Boot, M. D.; Hensen, E. J., Catalytic depolymerization of lignin in supercritical ethanol. *ChemSusChem* **2014**, *7* (8), 2276-2288.



70. Huang, X.; Korányi, T. I.; Boot, M. D.; Hensen, E. J., Ethanol as capping agent and formaldehyde scavenger for efficient depolymerization of lignin to aromatics. *Green Chem.* **2015**, *17* (11), 4941-4950.
71. Gabriëls, D.; Hernández, W. Y.; Sels, B.; Van Der Voort, P.; Verberckmoes, A., Review of catalytic systems and thermodynamics for the Guerbet condensation reaction and challenges for biomass valorization. *Catal. Sci. Technol.* **2015**, *5* (8), 3876-3902.
72. Sad, M. E.; Neurock, M.; Iglesia, E., Formation of C–C and C–O Bonds and Oxygen Removal in Reactions of Alkanediols, Alkanols, and Alkanals on Copper Catalysts. *J. Am. Chem. Soc.* **2011**, *133* (50), 20384-20398.
73. Güvenatam, B.; Heeres, E. H.; Pidko, E. A.; Hensen, E. J., Lewis-acid catalyzed depolymerization of Protobind lignin in supercritical water and ethanol. *Catal. Today* **2016**, *259*, 460-466.
74. Jiang, W.; Wu, S., Mechanism Study on Depolymerization of the  $\alpha$ -O-4 Linkage Lignin Model Compound in Supercritical Ethanol System. *Waste Biomass Valori.* **2017**, 1-8.
75. Zeb, H.; Choi, J.; Kim, Y.; Kim, J., A new role of supercritical ethanol in macroalgae liquefaction (*Saccharina japonica*): Understanding ethanol participation, yield, and energy efficiency. *Energy* **2017**, *118*, 116-126.
76. Peng, J.; Chen, P.; Lou, H.; Zheng, X., Upgrading of Bio-oil over Aluminum Silicate in Supercritical Ethanol. *Energy Fuels* **2008**, *22* (5), 3489-3492.
77. TAO, H.-x.; XIE, X.-a.; TANG, C.-z.; TIAN, W.-g., Mechanism of ketones formation from cellulose liquefaction in sub-and supercritical ethanol. *J. Fuel Chem. Technol.* **2013**, *41* (1), 60-66.

78. Akalin, M. K.; Das, P.; Alper, K.; Tekin, K.; Ragauskas, A. J.; Karagöz, S., Deconstruction of lignocellulosic biomass with hydrated cerium (III) chloride in water and ethanol. *Appl. Catal. A: Gen.* **2017**, *546*, 67-78.
79. Yu, F.; Zhong, R.; Chong, H.; Smet, M.; Dehaen, W.; Sels, B. F., Fast catalytic conversion of recalcitrant cellulose into alkyl levulinates and levulinic acid in the presence of soluble and recoverable sulfonated hyperbranched poly (arylene oxindole) s. *Green Chem.* **2017**, *19* (1), 153-163.
80. Patil, S. K.; Lund, C. R., Formation and growth of humins via aldol addition and condensation during acid-catalyzed conversion of 5-hydroxymethylfurfural. *Energy Fuels* **2011**, *25* (10), 4745-4755.
81. Weingarten, R.; Conner, W. C.; Huber, G. W., Production of levulinic acid from cellulose by hydrothermal decomposition combined with aqueous phase dehydration with a solid acid catalyst. *Energy Environ. Sci.* **2012**, *5* (6), 7559-7574.
82. Lin, J.-H.; Chang, Y.-H.; Hsu, Y.-H., Degradation of cotton cellulose treated with hydrochloric acid either in water or in ethanol. *Food Hydrocoll.* **2009**, *23* (6), 1548-1553.
83. Akalin, M. K.; Karagöz, S.; Akyüz, M., Supercritical ethanol extraction of bio-oils from German beech wood: design of experiments. *Ind. Crops. Prod.* **2013**, *49*, 720-729.
84. Akalin, M. K.; Akyüz, M.; Karagöz, S., Supercritical Fluid Extraction of Bio-oils from Hawthorn Stones: A Box–Behnken Design for the Extraction Parameters. *Energy Technol.* **2015**, *3* (1), 40-47.
85. Brand, S.; Susanti, R. F.; Kim, S. K.; Lee, H.-s.; Kim, J.; Sang, B.-I., Supercritical ethanol as an enhanced medium for lignocellulosic biomass liquefaction: influence of physical process parameters. *Energy* **2013**, *59*, 173-182.

86. Yamazaki, J.; Minami, E.; Saka, S., Liquefaction of beech wood in various supercritical alcohols. *J. Wood Sci.* **2006**, *52* (6), 527-532.
87. Yang, T.; Wang, J.; Li, B.; Kai, X.; Li, R., Effect of residence time on two-step liquefaction of rice straw in a CO<sub>2</sub> atmosphere: Differences between subcritical water and supercritical ethanol. *Bioresour. Technol.* **2017**, *229*, 143-151.
88. Li, R.; Li, B.; Yang, T.; Xie, Y.; Kai, X., Production of bio-oil from rice stalk supercritical ethanol liquefaction combined with the torrefaction process. *Energy Fuels* **2014**, *28* (3), 1948-1955.
89. Brand, S.; Hardi, F.; Kim, J.; Suh, D. J., Effect of heating rate on biomass liquefaction: differences between subcritical water and supercritical ethanol. *Energy* **2014**, *68*, 420-427.
90. Liu, D.; Li, Q.; Zhao, A.; Song, L.; Wu, P.; Yan, Z., Hydro-liquefaction of sawdust and its three components in supercritical ethanol with [BMIM] Cl/NiCl<sub>2</sub> catalyst. *Chem. Eng. J.* **2015**, *279*, 921-928.
91. Li, M.; Liu, D.; Wu, P.-P.; Cong, X.-S.; Song, L.-H.; Chen, Q.-T.; Liu, J.; Wu, H.; Yan, Z.-F., Efficient Hydroliquefaction of Sawdust over a Novel Silica-Supported Monoclinic Molybdenum Dioxide Catalyst. *Energy Fuels* **2016**, *30* (8), 6495-6499.
92. Flores, O. G. M.; Ha, S., Activity and stability studies of MoO<sub>2</sub> catalyst for the partial oxidation of gasoline. *Appl. Catal. A: Gen.* **2009**, *352* (1-2), 124-132.
93. Fan, Y.; Cai, Y.; Li, X.; Yin, H.; Yu, N.; Zhang, R.; Zhao, W., Rape straw as a source of bio-oil via vacuum pyrolysis: Optimization of bio-oil yield using orthogonal design method and characterization of bio-oil. *J. Anal. Appl. Pyrolysis* **2014**, *106*, 63-70.

94. Tessarolo, N. S.; dos Santos, L. R.; Silva, R. S.; Azevedo, D. A., Chemical characterization of bio-oils using comprehensive two-dimensional gas chromatography with time-of-flight mass spectrometry. *J. Chromatogr. A* **2013**, *1279*, 68-75.
95. Demiral, İ.; Eryazıcı, A.; Şensöz, S., Bio-oil production from pyrolysis of corncob (*Zea mays* L.). *Biomass Bioenergy* **2012**, *36*, 43-49.
96. Stas, M.; Kubicka, D.; Chudoba, J.; Pospisil, M., Overview of Analytical Methods Used for Chemical Characterization of Pyrolysis Bio-oil. *Energy Fuels* **2014**, *28* (1), 385-402.
97. Kanaujia, P. K.; Sharma, Y. K.; Garg, M. O.; Tripathi, D.; Singh, R., Review of analytical strategies in the production and upgrading of bio-oils derived from lignocellulosic biomass. *J. Anal. Appl. Pyrolysis* **2014**, *105*, 55-74.
98. Mullen, C. A.; Strahan, G. D.; Boateng, A. A., Characterization of Various Fast-Pyrolysis Bio-Oils by NMR Spectroscopy. *Energy Fuels* **2009**, *23* (5), 2707-2718.
99. David, K.; Kosa, M.; Williams, A.; Mayor, R.; Realff, M.; Muzzy, J.; Ragauskas, A., <sup>31</sup>P-NMR analysis of bio-oils obtained from the pyrolysis of biomass. *Biofuels* **2010**, *1* (6), 839-845.
100. Huang, F.; Pan, S.; Pu, Y.; Ben, H.; Ragauskas, A. J., <sup>19</sup>F NMR spectroscopy for the quantitative analysis of carbonyl groups in bio-oils. *RSC Adv.* **2014**, *4* (34), 17743-17747.
101. Ben, H.; Ragauskas, A. J., Heteronuclear Single-Quantum Correlation-Nuclear Magnetic Resonance (HSQC-NMR) Fingerprint Analysis of Pyrolysis Oils. *Energy Fuels* **2011**, *25* (12), 5791-5801.

102. Joseph, J.; Baker, C.; Mukkamala, S.; Beis, S. H.; Wheeler, M. C.; De Sisto, W. J.; Jensen, B. L.; Frederick, B. G., Chemical Shifts and Lifetimes for Nuclear Magnetic Resonance (NMR) Analysis of Biofuels. *Energy Fuels* **2010**, *24* (9), 5153-5162.
103. Lundquist, K. In *Proton (<sup>1</sup>H) NMR spectroscopy [of lignin in solution]*, Springer: 1992; pp 242-9.
104. Ingram, L.; Mohan, D.; Bricka, M.; Steele, P.; Strobel, D.; Crocker, D.; Mitchell, B.; Mohammad, J.; Cantrell, K.; Pittman, C. U., Pyrolysis of Wood and Bark in an Auger Reactor: Physical Properties and Chemical Analysis of the Produced Bio-oils. *Energy Fuels* **2008**, *22* (1), 614-625.
105. Ben, H.; Ragauskas, A. J., In Situ NMR Characterization of Pyrolysis Oil during Accelerated Aging. *ChemSusChem* **2012**, *5* (9), 1687-1693, S1687/1-S1687/5.
106. Tessarolo, N. S.; Silva, R. V. S.; Vanini, G.; Casilli, A.; Ximenes, V. L.; Mendes, F. L.; de Rezende Pinho, A.; Romao, W.; de Castro, E. V. R.; Kaiser, C. R.; Azevedo, D. A., Characterization of thermal and catalytic pyrolysis bio-oils by high-resolution techniques: <sup>1</sup>H NMR, GC × GC-TOFMS and FT-ICR MS. *J. Anal. Appl. Pyrolysis* **2016**, *117*, 257-267.
107. Tanneru, S. K.; Steele, P. H., Production of liquid hydrocarbons from pretreated bio-oil via catalytic deoxygenation with syngas. *Renew. Energ.* **2015**, *80*, 251-258.
108. Mancini, I.; Dosi, F.; Defant, A.; Crea, F.; Miotello, A., Upgraded production of (1R,5S)-1-hydroxy-3,6-dioxabicyclo[3.2.1]octan-2-one from cellulose catalytic pyrolysis and its detection in bio-oils by spectroscopic methods. *J. Anal. Appl. Pyrolysis* **2014**, *110*, 285-290.

109. Fabbri, D.; Torri, C.; Mancini, I., Pyrolysis of cellulose catalyzed by nanopowder metal oxides: production and characterization of a chiral hydroxylactone and its role as building block. *Green Chem.* **2007**, *9* (12), 1374-1379.
110. Bharti, S. K.; Roy, R., Quantitative <sup>1</sup>H NMR spectroscopy. *Trends Anal. Chem.* **2012**, *35*, 5-26.
111. Charles E. Wyman (Editor), *Aqueous Pretreatment of Plant Biomass for Biological and Chemical Conversion to Fuels and Chemicals*. Wiley: Chichester, West Sussex, United Kingdom, **2013**; p 538 pp.
112. Tarves, P. C.; Mullen, C. A.; Boateng, A. A. Effects of Various Reactive Gas Atmospheres on the Properties of Bio-Oils Produced Using Microwave Pyrolysis. *ACS Sustainable Chem. Eng.* **2016**, *4* (3), 930-936.
113. Mante, O. D.; Agblevor, F. A.; Oyama, S. T.; McClung, R., The effect of hydrothermal treatment of FCC catalysts and ZSM-5 additives in catalytic conversion of biomass. *Appl. Catal. A* **2012**, *445-446*, 312-320.
114. Liu, W.-J.; Zhang, X.-S.; Qv, Y.-C.; Jiang, H.; Yu, H.-Q., Bio-oil upgrading at ambient pressure and temperature using zero valent metals. *Green Chem.* **2012**, *14* (8), 2226-2233.
115. Alwehaibi, A. S.; Macquarrie, D. J.; Stark, M. S. Effect of spruce-derived phenolics extracted using microwave enhanced pyrolysis on the oxidative stability of biodiesel. *Green Chem.* **2016**, *18*, 2762-2774.
116. Strahan, G. D.; Mullen, C. A.; Boateng, A. A. Prediction of Properties and Elemental Composition of Biomass Pyrolysis Oils by NMR and Partial Least Squares Analysis. *Energy Fuels* **2016**, *30* (1), 423-433.

117. Pu, Y.; Cao, S.; Ragauskas, A. J., Application of quantitative  $^{31}\text{P}$  NMR in biomass lignin and biofuel precursors characterization. *Energy Environ. Sci.* **2011**, *4* (9), 3154-3166.
118. Wroblewski, A. E.; Lensink, C.; Markuszewski, R.; Verkade, J. G., Phosphorus-31 NMR spectroscopic analysis of coal pyrolysis condensates and extracts for heteroatom functionalities possessing labile hydrogen. *Energy Fuels* **1988**, *2* (6), 765-74.
119. Ben, H.; Ragauskas, A. J., NMR Characterization of Pyrolysis Oils from Kraft Lignin. *Energy Fuels* **2011**, *25* (5), 2322-2332.
120. Balakshin, M.; Capanema, E., On the quantification of lignin hydroxyl groups With  $^{31}\text{P}$  and  $^{13}\text{C}$  NMR spectroscopy. *J. Wood Chem. Technol.* **2015**, *35* (3), 220-237.
121. Ben, H.; Ferrell Iii, J. R., In-depth investigation on quantitative characterization of pyrolysis oil by  $^{31}\text{P}$  NMR. *RSC Adv.* **2016**, *6* (21), 17567-17573.
122. Naik, D. V.; Kumar, V.; Prasad, B.; Poddar, M. K.; Behera, B.; Bal, R.; Khatri, O. P.; Adhikari, D. K.; Garg, M. O., Catalytic cracking of jatropha-derived fast pyrolysis oils with VGO and their NMR characterization. *RSC Adv.* **2015**, *5* (1), 398-409.
123. Fu, D.; Farag, S.; Chaouki, J.; Jessop, P. G., Extraction of phenols from lignin microwave-pyrolysis oil using a switchable hydrophilicity solvent. *Bioresour. Technol.* **2014**, *154*, 101-108.
124. Lin, S. Y.; Dence, C. W., *Methods in Lignin Chemistry*. Springer-Verlag: Berlin, 1992.
125. Jacobsen, N. E., *NMR spectroscopy explained: simplified theory, applications and examples for organic chemistry and structural biology*. John Wiley & Sons: 2007.

126. Palmer, A. G., III; Cavanagh, J.; Wright, P. E.; Rance, M., Sensitivity improvement in proton-detected two-dimensional heteronuclear correlation NMR spectroscopy. *J. Magn. Reson.* **1991**, *93* (1), 151-70.
127. Mori, S.; Abeygunawardana, C.; Johnson, M. O. N.; van Zijl, P. C. M., Improved sensitivity of HSQC spectra of exchanging protons at short interscan delays using a new fast HSQC (FHSQC) detection scheme that avoids water saturation. *J. Magn. Reson., Ser. B* **1995**, *108* (1), 94-8.
128. Maudsley, A. A.; Ernst, R. R., Indirect detection of magnetic resonance by heteronuclear two-dimensional spectroscopy. *Chem. Phys. Lett.* **1977**, *50* (3), 368-72.
129. Dayie, K. T.; Wagner, G., Relaxation-rate measurements for <sup>15</sup>N-<sup>1</sup>H groups with pulsed-field gradients and preservation of coherence pathways. *J. Magn. Reson., Ser. A* **1994**, *111* (1), 121-6.
130. Fortin, M.; Mohadjer Beromi, M.; Lai, A.; Tarves, P. C.; Mullen, C. A.; Boateng, A. A.; West, N. M., Structural Analysis of Pyrolytic Lignins Isolated from Switchgrass Fast-Pyrolysis Oil. *Energy Fuels* **2015**, *29* (12), 8017-8026.
131. Yu, Y.; Chua, Y. W.; Wu, H., Characterization of Pyrolytic Sugars in Bio-Oil Produced from Biomass Fast Pyrolysis. *Energy Fuels* **2016**, Ahead of Print.
132. Patwardhan, PhD Dissertation, Iowa State University, 2010.
133. Li, W.; Chung, H.; Daeffler, C.; Johnson, J. A.; Grubbs, R. H., Application of <sup>1</sup>H DOSY for Facile Measurement of Polymer Molecular Weights. *Macromolecules* **2012**, *45* (24), 9595-9603.



134. Tolbert, A.; Akinosho, H.; Khunsupat, R.; Naskar, A. K.; Ragauskas, A. J., Characterization and analysis of the molecular weight of lignin for biorefining studies. *Biofuels, Bioprod. Biorefin.* **2014**, *8* (6), 836-856.
135. Korányi, T. s. I.; Huang, X.; Coumans, A. E.; Hensen, E. J., Synergy in lignin upgrading by a combination of Cu-based mixed oxide and Ni-phosphide catalysts in supercritical ethanol. *ACS Sustain. Chem. Eng.* **2017**, *5* (4), 3535-3543.
136. Ben, H.; Ragauskas, A. J., Pyrolysis of Kraft Lignin with Additives. *Energy Fuels* **2011**, *25* (10), 4662-4668.
137. Iisa, K.; French, R. J.; Orton, K. A.; Yung, M. M.; Johnson, D. K.; ten Dam, J.; Watson, M. J.; Nimlos, M. R., In Situ and ex Situ Catalytic Pyrolysis of Pine in a Bench-Scale Fluidized Bed Reactor System. *Energy Fuels* **2016**, *30* (3), 2144-2157.
138. Huang, X.; Koranyi, T. I.; Boot, M. D.; Hensen, E. J. M., Catalytic Depolymerization of Lignin in Supercritical Ethanol. *ChemSusChem* **2014**, *7* (8), 2276-2288.
139. Sluiter, A.; Hames, B.; Ruiz, R.; Scarlata, C.; Sluiter, J.; Templeton, D.; Crocker, D., Determination of structural carbohydrates and lignin in biomass. *Laboratory analytical procedure* **2008**, 1617.
140. David, K.; Pu, Y.; Foston, M.; Muzzy, J.; Ragauskas, A., Cross-Polarization/Magic Angle Spinning (CP/MAS) <sup>13</sup>C Nuclear Magnetic Resonance (NMR) Analysis of Chars from Alkaline-Treated Pyrolyzed Softwood. *Energy Fuels* **2009**, *23* (1), 498-501.
141. Faix, O.; Meier, D.; Fortmann, I., Thermal degradation products of wood. Gas chromatographic separation and mass spectrometric characterization of monomeric lignin-derived products. *Holz Roh- Werkst.* **1990**, *48* (7-8), 281-9.

142. Faix, O.; Fortmann, I.; Bremer, J.; Meier, D., Thermal degradation products of wood: gas chromatographic separation and mass spectrometric characterization of polysaccharide derived products. *Holz Roh- Werkst.* **1991**, *49* (5), 213-19.
143. Anastasakis, K.; Ross, A. B., Hydrothermal liquefaction of four brown macro-algae commonly found on the UK coasts: An energetic analysis of the process and comparison with bio-chemical conversion methods. *Fuel* **2015**, *139*, 546-553.
144. Ben, H.; Ragauskas, A. J., NMR Characterization of Pyrolysis Oils from Kraft Lignin. *Energy Fuels* **2011**, *25* (5), 2322-2332.
145. Happs, R. M.; Iisa, K.; Ferrell Iii, J. R., Quantitative <sup>13</sup>C NMR characterization of fast pyrolysis oils. *RSC Adv.* **2016**, *6* (104), 102665-102670.
146. Olarte, M. V.; Burton, S. D.; Swita, M.; Padmaperuma, A. B.; Ferrell, J.; Ben, H., Determination of Hydroxyl Groups in Pyrolysis Bio-oils using <sup>31</sup>P NMR. **2016**.
147. Ragauskas, A. J.; Beckham, G. T.; Biddy, M. J.; Chandra, R.; Chen, F.; Davis, M. F.; Davison, B. H.; Dixon, R. A.; Gilna, P.; Keller, M.; Langan, P.; Naskar, A. K.; Saddler, J. N.; Tschaplinski, T. J.; Tuskan, G. A.; Wyman, C. E., Lignin Valorization: Improving Lignin Processing in the Biorefinery. *Science* **2014**, *344* (6185), 709.
148. IEA, monthly energy review. *IEA* **2016**.
149. Mahadevan, R.; Adhikari, S.; Shakya, R.; Wang, K.; Dayton, D. C.; Li, M.; Pu, Y.; Ragauskas, A. J., Effect of torrefaction temperature on lignin macromolecule and product distribution from HZSM-5 catalytic pyrolysis. *J. Anal. Appl. Pyrolysis* **2016**, *122*, 95-105.

150. Bali, G.; Khunsupat, R.; Akinosho, H.; Payyavula, R. S.; Samuel, R.; Tuskan, G. A.; Kalluri, U. C.; Ragauskas, A. J., Characterization of cellulose structure of Populus plants modified in candidate cellulose biosynthesis genes. *Biomass Bioenergy* **2016**, *94*, 146-154.
151. Meng, X.; Pu, Y.; Bali, G.; Gjersing, E.; Davis, M.; Wellington, M.; Tuskan, G.; Tschaplinski, T.; Yoo, C. G.; Li, M.; Park, D.-Y.; Ragauskas, A. J., An in-depth understanding of biomass recalcitrance using natural poplar variants as the feedstock. *ChemSusChem* **2016**.
152. Rubin, E. M., Genomics of cellulosic biofuels. *Nature (London, U. K.)* **2008**, *454* (7206), 841-845.
153. Biofuel.org.
154. Krutof, A.; Hawboldt, K., Blends of pyrolysis oil, petroleum, and other bio-based fuels: A review. *Renewable Sustainable Energy Rev.* **2016**, *59*, 406-419.
155. Meng, J.; Moore, A.; Tilotta, D. C.; Kelley, S. S.; Adhikari, S.; Park, S., Thermal and Storage Stability of Bio-Oil from Pyrolysis of Torrefied Wood. *Energy Fuels* **2015**, *29* (8), 5117-5126.
156. Lujaji, F. C.; Boateng, A. A.; Schaffer, M. A.; Mullen, C. A.; Mkilaha, I. S. N.; Mtui, P. L., Pyrolysis Oil Combustion in a Horizontal Box Furnace with an Externally Mixed Nozzle. *Energy Fuels* **2016**, *30* (5), 4126-4136.
157. Zacher, A. H.; Olarte, M. V.; Santosa, D. M.; Elliott, D. C.; Jones, S. B., A review and perspective of recent bio-oil hydrotreating research. *Green Chem.* **2014**, *16* (2), 491-515.

158. Carpenter, D.; Westover, T. L.; Czernik, S.; Jablonski, W., Biomass feedstocks for renewable fuel production: a review of the impacts of feedstock and pretreatment on the yield and product distribution of fast pyrolysis bio-oils and vapors. *Green Chem.* **2014**, *16* (2), 384-406.
159. Zhu, J. Y.; Pan, X. J., Woody biomass pretreatment for cellulosic ethanol production: Technology and energy consumption evaluation. *Bioresour. Technol.* **2010**, *101* (13), 4992-5002.
160. Carrasco, J. L.; Gunukula, S.; Boateng, A. A.; Mullen, C. A.; DeSisto, W. J.; Wheeler, M. C., Pyrolysis of forest residues: An approach to techno-economics for bio-fuel production. *Fuel* **2017**, *193*, 477-484.
161. Long, Y.; Yu, Y.; Chua, Y. W.; Wu, H., Acid-catalysed cellulose pyrolysis at low temperatures. *Fuel* **2017**, *193*, 460-466.
162. Ben, H.; Mu, W.; Deng, Y.; Ragauskas, A. J., Production of renewable gasoline from aqueous phase hydrogenation of lignin pyrolysis oil. *Fuel* **2013**, *103*, 1148-1153.
163. Hu, F.; Ragauskas, A., Pretreatment and Lignocellulosic Chemistry. *BioEnergy Res.* **2012**, *5* (4), 1043-1066.
164. Neupane, S.; Adhikari, S.; Wang, Z.; Ragauskas, A. J.; Pu, Y., Effect of torrefaction on biomass structure and hydrocarbon production from fast pyrolysis. *Green Chem.* **2015**, *17* (4), 2406-2417.
165. Pu, Y.; Hu, F.; Huang, F.; Davison, B. H.; Ragauskas, A. J., Assessing the molecular structure basis for biomass recalcitrance during dilute acid and hydrothermal pretreatments. *Biotechnol. Biofuels* **2013**, *6*, 15.

166. Vegas, R.; Kabel, M.; Schols, H. A.; Alonso, J. L.; Parajo, J. C., Hydrothermal processing of rice husks: effects of severity on product distribution. *J. Chem. Technol. Biotechnol.* **2008**, *83* (7), 965-972.
167. Garrote, G.; Dominguez, H.; Parajo, J. C., Hydrothermal processing of lignocellulosic materials. *Holz Roh- Werkst.* **1999**, *57* (3), 191-202.
168. Ruiz, H. A.; Rodriguez-Jasso, R. M.; Fernandes, B. D.; Vicente, A. A.; Teixeira, J. A., Hydrothermal processing, as an alternative for upgrading agriculture residues and marine biomass according to the biorefinery concept: A review. *Renewable Sustainable Energy Rev.* **2013**, *21*, 35-51.
169. Stephanidis, S.; Nitsos, C.; Kalogiannis, K.; Iliopoulou, E. F.; Lappas, A. A.; Triantafyllidis, K. S., Catalytic upgrading of lignocellulosic biomass pyrolysis vapours: Effect of hydrothermal pre-treatment of biomass. *Catal. Today* **2011**, *167* (1), 37-45.
170. Du, Z.; Mohr, M.; Ma, X.; Cheng, Y.; Lin, X.; Liu, Y.; Zhou, W.; Chen, P.; Ruan, R., Hydrothermal pretreatment of microalgae for production of pyrolytic bio-oil with a low nitrogen content. *Bioresour. Technol.* **2012**, *120*, 13-18.
171. Timell, T. E., Recent progress in the chemistry of wood hemicelluloses. *Wood Sci. Technol.* **1967**, *1* (1), 45-70.
172. Hu, F.; Jung, S.; Ragauskas, A., Pseudo-lignin formation and its impact on enzymatic hydrolysis. *Bioresour. Technol.* **2012**, *117*, 7-12.
173. Sannigrahi, P.; Kim, D. H.; Jung, S.; Ragauskas, A., Pseudo-lignin and pretreatment chemistry. *Energy Environ. Sci.* **2011**, *4* (4), 1306-1310.
174. Ben, H.; Ragauskas, A. J., Torrefaction of Loblolly pine. *Green Chem.* **2012**, *14* (1), 72-76.

175. Kumar, R.; Mago, G.; Balan, V.; Wyman, C. E., Physical and chemical characterizations of corn stover and poplar solids resulting from leading pretreatment technologies. *Bioresour. Technol.* **2009**, *100* (17), 3948-3962.
176. Yan, L.; Pu, Y.; Bowden, M.; Ragauskas, A. J.; Yang, B., Physiochemical Characterization of Lignocellulosic Biomass Dissolution by Flowthrough Pretreatment. *ACS Sustainable Chem. Eng.* **2016**, *4* (1), 219-227.
177. Pandey, K. K.; Pitman, A. J., FTIR studies of the changes in wood chemistry following decay by brown-rot and white-rot fungi. *Int. Biodeterior. Biodegrad.* **2003**, *52* (3), 151-160.
178. El Hage, R.; Brosse, N.; Sannigrahi, P.; Ragauskas, A., Effects of process severity on the chemical structure of Miscanthus ethanol organosolv lignin. *Polym. Degrad. Stab.* **2010**, *95* (6), 997-1003.
179. Chang, S.; Zhao, Z.; Zheng, A.; Li, X.; Wang, X.; Huang, Z.; He, F.; Li, H., Effect of hydrothermal pretreatment on properties of bio-oil produced from fast pyrolysis of eucalyptus wood in a fluidized bed reactor. *Bioresour. Technol.* **2013**, *138*, 321-8.
180. Chen, D.; Zhou, J.; Zhang, Q., Effects of Torrefaction on the Pyrolysis Behavior and Bio-Oil Properties of Rice Husk by Using TG-FTIR and Py-GC/MS. *Energy Fuels* **2014**, *28* (9), 5857-5863.
181. Branca, C.; Di Blasi, C.; Galgano, A.; Brostrom, M., Effects of the Torrefaction Conditions on the Fixed-Bed Pyrolysis of Norway Spruce. *Energy Fuels* **2014**, *28* (9), 5882-5891.

182. Zheng, A.; Zhao, Z.; Chang, S.; Huang, Z.; Wang, X.; He, F.; Li, H., Effect of torrefaction on structure and fast pyrolysis behavior of corncobs. *Bioresour. Technol.* **2013**, *128*, 370-377.
183. Hao, N.; Ben, H.; Yoo, C. G.; Adhikari, S.; Ragauskas, A. J., Review of NMR Characterization of Pyrolysis Oils. *Energy Fuels* **2016**, *30* (9), 6863-6880.
184. Fu, Q.; Argyropoulos, D. S.; Tilotta, D. C.; Lucia, L. A., Products and functional group distributions in pyrolysis oil of chromated copper arsenate (CCA)-treated wood, as elucidated by gas chromatography and a novel <sup>31</sup>P NMR-based method. *Ind. Eng. Chem. Res.* **2007**, *46* (16), 5258-5264.
185. International Energy Outlook 2016, U.S. Energy Information Administration.
186. 2016 Billion-Ton Report, U.S. Department of Energy.
187. Bezerra, T. L.; Ragauskas, A. J., A review of sugarcane bagasse for second-generation bioethanol and biopower production. *Biofuels, Bioprod. Biorefin.* **2016**, *10* (5), 634-647.
188. Tsai, W. T.; Lee, M. K.; Chang, Y. M., Fast pyrolysis of rice straw, sugarcane bagasse and coconut shell in an induction-heating reactor. *J. Anal. Appl. Pyrolysis* **2006**, *76* (1-2), 230-237.
189. Islam, M. R.; Parveen, M.; Haniu, H., Properties of sugarcane waste-derived bio-oils obtained by fixed-bed fire-tube heating pyrolysis. *Bioresour. Technol.* **2010**, *101* (11), 4162-4168.
190. Carrier, M.; Hugo, T.; Gorgens, J.; Knoetze, H., Comparison of slow and vacuum pyrolysis of sugar cane bagasse. *J. Anal. Appl. Pyrolysis* **2011**, *90* (1), 18-26.

191. Venderbosch, R. H., A Critical View on Catalytic Pyrolysis of Biomass. *ChemSusChem* **2015**, *8* (8), 1306-1316.
192. Davidsson, K. O.; Korsgren, J. G.; Pettersson, J. B. C.; Jaglid, U., The effects of fuel washing techniques on alkali release from biomass. *Fuel* **2001**, *81* (2), 137-142.
193. Wang, H.; Srinivasan, R.; Yu, F.; Steele, P.; Li, Q.; Mitchell, B., Effect of Acid, Alkali, and Steam Explosion Pretreatments on Characteristics of Bio-Oil Produced from Pinewood. *Energy Fuels* **2011**, *25* (8), 3758-3764.
194. Alvira, P.; Tomas-Pejo, E.; Ballesteros, M.; Negro, M. J., Pretreatment technologies for an efficient bioethanol production process based on enzymatic hydrolysis: A review. *Bioresour. Technol.* **2010**, *101* (13), 4851-4861.
195. Taherzadeh, M. J.; Karimi, K., Pretreatment of lignocellulosic wastes to improve ethanol and biogas production: A review. *Int. J. Mol. Sci.* **2008**, *9* (9), 1621-1651.
196. Zheng, A.; Jiang, L.; Zhao, Z.; Chang, S.; Huang, Z.; Zhao, K.; He, F.; Li, H., Effect of Hydrothermal Treatment on Chemical Structure and Pyrolysis Behavior of Eucalyptus Wood. *Energy Fuels* **2016**, *30* (4), 3057-3065.
197. Tripathi, A.; Ferrer, A.; Khan, S. A.; Rojas, O. J., Morphological and Thermochemical Changes upon Autohydrolysis and Microemulsion Treatments of Coir and Empty Fruit Bunch Residual Biomass to Isolate Lignin-Rich Micro- and Nanofibrillar Cellulose. *ACS Sustain. Chem. Eng.* **2017**, *5* (3), 2483-2492.
198. Wu, Q.; Yu, S.; Hao, N.; Wells, T.; Meng, X.; Li, M.; Pu, Y.; Liu, S.; Ragauskas, A. J., Characterization of products from hydrothermal carbonization of pine. *Bioresour. Technol.* **2017**, *244* (Part\_1), 78-83.



199. Trajano, H. L.; Engle, N. L.; Foston, M.; Ragauskas, A. J.; Tschaplinski, T. J.; Wyman, C. E., The fate of lignin during hydrothermal pretreatment. *Biotechnol. Biofuels* **2013**, *6*, 110.
200. Rezende, C. A.; Aparecida de Lima, M.; Maziero, P.; Ribeiro de Azevedo, E.; Garcia, W.; Polikarpov, I., Chemical and morphological characterization of sugarcane bagasse submitted to a delignification process for enhanced enzymatic digestibility. *Biotechnol. Biofuels* **2011**, *4*, 54.
201. Liu, W.-J.; Li, W.-W.; Jiang, H.; Yu, H.-Q., Fates of Chemical Elements in Biomass during Its Pyrolysis. *Chem. Rev. (Washington, DC, U. S.)* **2017**, *117* (9), 6367-6398.
202. Yang, H.; Yan, R.; Chen, H.; Lee, D. H.; Zheng, C., Characteristics of hemicellulose, cellulose and lignin pyrolysis. *Fuel* **2007**, *86* (12-13), 1781-1788.
203. Ben, H.; Ragauskas, A. J., One step thermal conversion of lignin to the gasoline range liquid products by using zeolites as additives. *RSC Adv.* **2012**, *2* (33), 12892-12898.
204. Bridgwater, A. V., Review of fast pyrolysis of biomass and product upgrading. *Biomass Bioenergy* **2012**, *38*, 68-94.
205. Galebach, P. H.; Thompson, S.; Wittrig, A. M.; Buchanan, J. S.; Huber, G. W., Investigation of the Reaction Pathways of Biomass-Derived Oxygenate Conversion into Monoalcohols in Supercritical Methanol with CuMgAl-Mixed-Metal Oxide. *ChemSusChem* **2018**, *11* (23), 4007-4017.
206. Carlson, T. R.; Tompsett, G. A.; Conner, W. C.; Huber, G. W., Aromatic Production from Catalytic Fast Pyrolysis of Biomass-Derived Feedstocks. *Top. Catal.* **2009**, *52* (3), 241.

207. van Dyk, S.; Su, J.; McMillan, J. D.; Saddler, J., Potential synergies of drop-in biofuel production with further co-processing at oil refineries. *Biofuels, Bioprod. Biorefin.* **2019**, *13*, 760-775.
208. Hao, N.; Lu, K.; Ben, H.; Adhikari, S.; Lacerda, T. B.; Ragauskas, A. J., Effect of Autohydrolysis Pretreatment Conditions on Sugarcane Bagasse Structures and Product Distribution Resulting from Pyrolysis. *Energy Technol.* **2018**, *6* (4), 640-648.
209. Huber, G. W.; Chheda, J. N.; Barrett, C. J.; Dumesic, J. A., Production of Liquid Alkanes by Aqueous-Phase Processing of Biomass-Derived Carbohydrates. *Science* **2005**, *308* (5727), 1446.
210. Vispute, T. P.; Zhang, H.; Sanna, A.; Xiao, R.; Huber, G. W., Renewable Chemical Commodity Feedstocks from Integrated Catalytic Processing of Pyrolysis Oils. *Science* **2010**, *330* (6008), 1222.
211. Macala, G. S.; Matson, T. D.; Johnson, C. L.; Lewis, R. S.; Iretskii, A. V.; Ford, P. C., Hydrogen transfer from supercritical methanol over a solid base catalyst: a model for lignin depolymerization. *ChemSusChem* **2009**, *2* (3), 215-217.
212. Barta, K.; Matson, T. D.; Fettig, M. L.; Scott, S. L.; Iretskii, A. V.; Ford, P. C., Catalytic disassembly of an organosolv lignin via hydrogen transfer from supercritical methanol. *Green Chem.* **2010**, *12* (9), 1640-1647.
213. Chui, M.; Metzker, G.; Bernt, C. M.; Tran, A. T.; Burtoloso, A. C. B.; Ford, P. C., Probing the Lignin Disassembly Pathways with Modified Catalysts Based on Cu-Doped Porous Metal Oxides. *ACS Sustainable Chem. Eng.* **2017**, *5* (4), 3158-3169.

214. Huang, X.; Atay, C.; Zhu, J.; Palstra, S. W. L.; Koranyi, T. I.; Boot, M. D.; Hensen, E. J. M., Catalytic Depolymerization of Lignin and Woody Biomass in Supercritical Ethanol: Influence of Reaction Temperature and Feedstock. *ACS Sustainable Chem. Eng.* **2017**, *5* (11), 10864-10874.
215. Matson, T. D.; Barta, K.; Iretskii, A. V.; Ford, P. C., One-Pot Catalytic Conversion of Cellulose and of Woody Biomass Solids to Liquid Fuels. *J. Am. Chem. Soc.* **2011**, *133* (35), 14090-14097.
216. Galebach, P. H.; McClelland, D. J.; Eagan, N. M.; Wittrig, A. M.; Buchanan, J. S.; Dumesic, J. A.; Huber, G. W., Production of Alcohols from Cellulose by Supercritical Methanol Depolymerization and Hydrodeoxygenation. *ACS Sustain. Chem. Eng.* **2018**, *6* (3), 4330-4344.
217. Yin, W.; Venderbosch, R. H.; Bottari, G.; Krawczyk, K. K.; Barta, K.; Heeres, H. J., Catalytic upgrading of sugar fractions from pyrolysis oils in supercritical mono-alcohols over Cu doped porous metal oxide. *Appl. Catal., B* **2015**, *166-167*, 56-65.
218. Cheng, S.; Wei, L.; Julson, J.; Muthukumarappan, K.; Kharel, P. R.; Boakye, E., Hydrocarbon bio-oil production from pyrolysis bio-oil using non-sulfide Ni-Zn/Al<sub>2</sub>O<sub>3</sub> catalyst. *Fuel Process. Technol.* **2017**, *162*, 78-86.
219. Duan, P.; Xu, Y.; Wang, F.; Wang, B.; Yan, W., Catalytic upgrading of pretreated algal bio-oil over zeolite catalysts in supercritical water. *Biochem. Eng. J.* **2016**, *116*, 105-112.

220. Patel, H.; Hao, N.; Iisa, K.; French, R. J.; Orton, K. A.; Mukarakate, C.; Ragauskas, A. J.; Nimlos, M. R., Detailed Oil Compositional Analysis Enables Evaluation of Impact of Temperature and Biomass-to-Catalyst Ratio on ex Situ Catalytic Fast Pyrolysis of Pine Vapors over ZSM-5. *ACS Sustain. Chem. Eng.* **2020**, *8* (4), 1762-1773.
221. Ben, H.; Ragauskas, A. J., Heteronuclear Single-Quantum Correlation–Nuclear Magnetic Resonance (HSQC–NMR) Fingerprint Analysis of Pyrolysis Oils. *Energy Fuels* **2011**, *25* (12), 5791-5801.
222. Horne, P. A.; Williams, P. T., The effect of zeolite ZSM-5 catalyst deactivation during the upgrading of biomass-derived pyrolysis vapours. *J. Anal. Appl. Pyrolysis* **1995**, *34* (1), 65-85.
223. Persson, H.; Yang, W., Catalytic pyrolysis of demineralized lignocellulosic biomass. *Fuel* **2019**, *252*, 200-209.
224. Jae, J.; Tompsett, G. A.; Foster, A. J.; Hammond, K. D.; Auerbach, S. M.; Lobo, R. F.; Huber, G. W., Investigation into the shape selectivity of zeolite catalysts for biomass conversion. *J. Catal.* **2011**, *279* (2), 257-268.
225. Carlson, T. R.; Cheng, Y.-T.; Jae, J.; Huber, G. W., Production of green aromatics and olefins by catalytic fast pyrolysis of wood sawdust. *Energy Environ. Sci.* **2011**, *4* (1), 145-161.
226. French, R.; Czernik, S., Catalytic pyrolysis of biomass for biofuels production. *Fuel Process. Technol.* **2010**, *91* (1), 25-32.
227. Sharma, R. K.; Bakhshi, N. N., Catalytic upgrading of fast pyrolysis oil over hzsm-5. *Can. J. Chem. Eng.* **1993**, *71* (3), 383-391.

228. Mukarakate, C.; Zhang, X.; Stanton, A. R.; Robichaud, D. J.; Ciesielski, P. N.; Malhotra, K.; Donohoe, B. S.; Gjersing, E.; Evans, R. J.; Heroux, D. S.; Richards, R.; Iisa, K.; Nimlos, M. R., Real-time monitoring of the deactivation of HZSM-5 during upgrading of pine pyrolysis vapors. *Green Chem.* **2014**, *16* (3), 1444-1461.
229. Jia, L. Y.; Raad, M.; Hamieh, S.; Toufaily, J.; Hamieh, T.; Bettahar, M. M.; Mauviel, G.; Tarrighi, M.; Pinard, L.; Dufour, A., Catalytic fast pyrolysis of biomass: superior selectivity of hierarchical zeolites to aromatics. *Green Chem.* **2017**, *19* (22), 5442-5459.
230. Jae, J.; Coolman, R.; Mountziaris, T. J.; Huber, G. W., Catalytic fast pyrolysis of lignocellulosic biomass in a process development unit with continual catalyst addition and removal. *Chem. Eng. Sci.* **2014**, *108*, 33-46.
231. Lappas, A. A.; Samolada, M. C.; Iatridis, D. K.; Voutetakis, S. S.; Vasalos, I. A., Biomass pyrolysis in a circulating fluid bed reactor for the production of fuels and chemicals. *Fuel* **2002**, *81* (16), 2087-2095.
232. Paasikallio, V.; Kalogiannis, K.; Lappas, A.; Lehto, J.; Lehtonen, J., Catalytic Fast Pyrolysis: Influencing Bio-Oil Quality with the Catalyst-to-Biomass Ratio. *Energy Technol.* **2017**, *5* (1), 94-103.
233. Mante, O. D.; Agblevor, F. A., Catalytic conversion of biomass to bio-synchrude oil. *Biomass Convers. Biorefin.* **2011**, *1* (4), 203-215.
234. Iisa, K.; French, R. J.; Orton, K. A.; Budhi, S.; Mukarakate, C.; Stanton, A. R.; Yung, M. M.; Nimlos, M. R., Catalytic Pyrolysis of Pine Over HZSM-5 with Different Binders. *Top. Catal.* **2016**, *59* (1), 94-108.

235. Wang, K.; Johnston, P. A.; Brown, R. C., Comparison of in-situ and ex-situ catalytic pyrolysis in a micro-reactor system. *Bioresour. Technol.* **2014**, *173*, 124-131.
236. Wan, S.; Waters, C.; Stevens, A.; Gumidyala, A.; Jentoft, R.; Lobban, L.; Resasco, D.; Mallinson, R.; Crossley, S., Decoupling HZSM-5 Catalyst Activity from Deactivation during Upgrading of Pyrolysis Oil Vapors. *ChemSusChem* **2015**, *8* (3), 552-559.
237. Luo, G.; Resende, F. L. P., In-situ and ex-situ upgrading of pyrolysis vapors from beetle-killed trees. *Fuel* **2016**, *166*, 367-375.
238. Gamliel, D. P.; Du, S.; Bollas, G. M.; Valla, J. A., Investigation of in situ and ex situ catalytic pyrolysis of miscanthus × giganteus using a PyGC–MS microsystem and comparison with a bench-scale spouted-bed reactor. *Bioresour. Technol.* **2015**, *191*, 187-196.
239. Hernando, H.; Jiménez-Sánchez, S.; Feroso, J.; Pizarro, P.; Coronado, J. M.; Serrano, D. P., Assessing biomass catalytic pyrolysis in terms of deoxygenation pathways and energy yields for the efficient production of advanced biofuels. *Catal. Sci. Technol.* **2016**, *6* (8), 2829-2843.
240. Iisa, K.; French, R. J.; Orton, K. A.; Dutta, A.; Schaidle, J. A., Production of low-oxygen bio-oil via ex situ catalytic fast pyrolysis and hydrotreating. *Fuel* **2017**, *207*, 413-422.
241. Agblevor, F. A.; Mante, O.; McClung, R.; Oyama, S. T., Co-processing of standard gas oil and biocrude oil to hydrocarbon fuels. *Biomass Bioenergy* **2012**, *45*, 130-137.

242. Thegarid, N.; Fogassy, G.; Schuurman, Y.; Mirodatos, C.; Stefanidis, S.; Iliopoulou, E. F.; Kalogiannis, K.; Lappas, A. A., Second-generation biofuels by co-processing catalytic pyrolysis oil in FCC units. *Appl. Catal. B: Environ.* **2014**, *145*, 161-166.
243. Mante, O. D.; Dayton, D. C.; Gabrielsen, J.; Ammitzboll, N. L.; Barbee, D.; Verdier, S.; Wang, K., Integration of catalytic fast pyrolysis and hydroprocessing: a pathway to refinery intermediates and “drop-in” fuels from biomass. *Green Chem.* **2016**, *18* (22), 6123-6135.
244. Agblevor, F. A.; Elliott, D. C.; Santosa, D. M.; Olarte, M. V.; Burton, S. D.; Swita, M.; Beis, S. H.; Christian, K.; Sargent, B., Red Mud Catalytic Pyrolysis of Pinyon Juniper and Single-Stage Hydrotreatment of Oils. *Energy Fuels* **2016**, *30* (10), 7947-7958.
245. Iisa, K.; Robichaud, D. J.; Watson, M. J.; ten Dam, J.; Dutta, A.; Mukarakate, C.; Kim, S.; Nimlos, M. R.; Baldwin, R. M., Improving biomass pyrolysis economics by integrating vapor and liquid phase upgrading. *Green Chem.* **2018**, *20* (3), 567-582.
246. Paasikallio, V.; Lindfors, C.; Kuoppala, E.; Solantausta, Y.; Oasmaa, A.; Lehto, J.; Lehtonen, J., Product quality and catalyst deactivation in a four day catalytic fast pyrolysis production run. *Green Chem.* **2014**, *16* (7), 3549-3559.
247. Ben, H.; Ragauskas, A. J., Pyrolysis of Kraft Lignin with Additives. *Energy Fuels* **2011**, *25* (10), 4662-4668.
248. Olarte, M. V.; Burton, S. D.; Swita, M.; Padmaperuma, A. B.; Ferrell, J.; Ben, H. *Determination of hydroxyl groups in pyrolysis bio-oils using <sup>31</sup>P NMR*; NREL/TP-5100-65887: 2016.

249. Ben, H.; Ragauskas, A. J., One step thermal conversion of lignin to the gasoline range liquid products by using zeolites as additives. *RSC Adv.* **2012**, *2* (33), 12892-12898.
250. Chiang, H.; Bhan, A., Catalytic consequences of hydroxyl group location on the rate and mechanism of parallel dehydration reactions of ethanol over acidic zeolites. *J. Catal.* **2010**, *271* (2), 251-261.
251. Mihalcik, D. J.; Boateng, A. A.; Mullen, C. A.; Goldberg, N. M., Packed-bed catalytic cracking of oak-derived pyrolytic vapors. *Ind. Eng. Chem. Res.* **2011**, *50* (23), 13304-13312.
252. Mortensen, P. M.; Grunwaldt, J.-D.; Jensen, P. A.; Knudsen, K.; Jensen, A. D., A review of catalytic upgrading of bio-oil to engine fuels. *Appl. Catal. A: Gen.* **2011**, *407* (1-2), 1-19.
253. Mullen, C. A.; Boateng, A. A.; Mihalcik, D. J.; Goldberg, N. M., Catalytic fast pyrolysis of white oak wood in a bubbling fluidized bed. *Energy Fuels* **2011**, *25* (11), 5444-5451.
254. Peralta, M. A.; Sooknoi, T.; Danuthai, T.; Resasco, D. E., Deoxygenation of benzaldehyde over CsNaX zeolites. *J. Mol. Catal. A: Chem.* **2009**, *312* (1-2), 78-86.
255. Pereira, C.; Kokotailo, G.; Gorte, R. J.; Farneth, W., Adsorption and reaction of 2-propen-1-ol in H-ZSM-5. *J. Phys. Chem.* **1990**, *94* (5), 2063-2067.
256. Lu, Y.; Li, G.-S.; Lu, Y.-C.; Fan, X.; Wei, X.-Y., Analytical Strategies Involved in the Detailed Componential Characterization of Biooil Produced from Lignocellulosic Biomass. *Int. J. Anal. Chem.* **2017**, *2017*.
257. Wang, K.; Johnston, P. A.; Brown, R. C., Comparison of in-situ and ex-situ catalytic pyrolysis in a micro-reactor system. *Bioresour. Technol.* **2014**, *173*, 124-31.



258. Carlson, T. R.; Cheng, Y.-T.; Jae, J.; Huber, G. W., Production of green aromatics and olefins by catalytic fast pyrolysis of wood sawdust. *Energy Environ. Sci.* **2011**, *4* (1), 145-161.
259. Jae, J.; Coolman, R.; Mountziaris, T. J.; Huber, G. W., Catalytic fast pyrolysis of lignocellulosic biomass in a process development unit with continual catalyst addition and removal. *Chem. Eng. Sci.* **2014**, *108*, 33-46.
260. Stanton, A. R.; Iisa, K.; Mukarakate, C.; Nimlos, M. R., Role of Biopolymers in the Deactivation of ZSM-5 during Catalytic Fast Pyrolysis of Biomass. *ACS Sustainable Chem. Eng.* **2018**, *6* (8), 10030-10038.
261. Paasikallio, V.; Kalogiannis, K.; Lappas, A.; Lehto, J.; Lehtonen, J., Catalytic Fast Pyrolysis: Influencing Bio-Oil Quality with the Catalyst-to-Biomass Ratio. *Energy Technol.* **2017**, *5* (1), 94-103.
262. Iisa, K.; Robichaud, D. J.; Watson, M. J.; ten Dam, J.; Dutta, A.; Mukarakate, C.; Kim, S.; Nimlos, M. R.; Baldwin, R. M., Improving biomass pyrolysis economics by integrating vapor and liquid phase upgrading. *Green Chem.* **2018**, *20* (3), 567-582.
263. Olarte, M. V.; Zacher, A. H.; Padmaperuma, A. B.; Burton, S. D.; Job, H. M.; Lemmon, T. L.; Swita, M. S.; Rotness, L. J.; Neuenschwander, G. N.; Frye, J. G.; Elliott, D. C., Stabilization of Softwood-Derived Pyrolysis Oils for Continuous Bio-oil Hydroprocessing. *Top. Catal.* **2016**, *59* (1), 55-64.
264. Iliopoulou, E. F.; Stefanidis, S.; Kalogiannis, K.; Psarras, A. C.; Delimitis, A.; Triantafyllidis, K. S.; Lappas, A. A., Pilot-scale validation of Co-ZSM-5 catalyst performance in the catalytic upgrading of biomass pyrolysis vapours. *Green Chem.* **2014**, *16* (2), 662-674.

265. Xu, D.; Savage, P. E., Effect of temperature, water loading, and Ru/C catalyst on water-insoluble and water-soluble biocrude fractions from hydrothermal liquefaction of algae. *Bioresour. Technol.* **2017**, *239*, 1-6.
266. Lu, J.; Liu, Z.; Zhang, Y.; Savage, P. E., Synergistic and Antagonistic Interactions during Hydrothermal Liquefaction of Soybean Oil, Soy Protein, Cellulose, Xylose, and Lignin. *ACS Sustain. Chem. Eng.* **2018**, *6* (11), 14501-14509.
267. Xu, D.; Savage, P. E., Supercritical water upgrading of water-insoluble and water-soluble biocrudes from hydrothermal liquefaction of *Nannochloropsis* microalgae. *J. Supercrit. Fluid.* **2018**, *133*, 683-689.
268. Tekin, K.; Karagöz, S.; Bektaş, S., Hydrothermal liquefaction of beech wood using a natural calcium borate mineral. *J. Supercrit. Fluid.* **2012**, *72*, 134-139.
269. Zheng, J.-L.; Zhu, M.-Q.; Wu, H.-t., Alkaline hydrothermal liquefaction of swine carcasses to bio-oil. *Waste Manage. (Oxford)* **2015**, *43*, 230-238.
270. Bach, Q.-V.; Sillero, M. V.; Tran, K.-Q.; Skjermo, J., Fast hydrothermal liquefaction of a Norwegian macro-alga: Screening tests. *Algal Res.* **2014**, *6*, 271-276.
271. Akalin, M. K.; Tekin, K.; Karagoz, S., Supercritical fluid extraction of biofuels from biomass. *Environ. Chem. Lett.* **2017**, *15* (1), 29-41.
272. Schutyser, W.; Van den Bosch, S.; Renders, T.; De Boe, T.; Koelewijn, S. F.; Dewaele, A.; Ennaert, T.; Verkinderen, O.; Goderis, B.; Courtin, C. M.; Sels, B. F., Influence of bio-based solvents on the catalytic reductive fractionation of birch wood. *Green Chem.* **2015**, *17* (11), 5035-5045.

273. Renders, T.; Van den Bosch, S.; Vangeel, T.; Ennaert, T.; Koelewijn, S.-F.; Van den Bossche, G.; Courtin, C. M.; Schutyser, W.; Sels, B. F., Synergetic Effects of Alcohol/Water Mixing on the Catalytic Reductive Fractionation of Poplar Wood. *ACS Sustain. Chem. Eng.* **2016**, *4* (12), 6894-6904.
274. Xu, C.; Etcheverry, T., Hydro-liquefaction of woody biomass in sub- and supercritical ethanol with iron-based catalysts. *Fuel* **2008**, *87* (3), 335-345.
275. Chumpoo, J.; Prasassarakich, P., Bio-Oil from Hydro-Liquefaction of Bagasse in Supercritical Ethanol. *Energy & Fuels* **2010**, *24* (3), 2071-2077.
276. Déniel, M.; Haarlemmer, G.; Roubaud, A.; Weiss-Hortala, E.; Fages, J., Optimisation of bio-oil production by hydrothermal liquefaction of agro-industrial residues: Blackcurrant pomace (*Ribes nigrum* L.) as an example. *Biomass Bioenergy* **2016**, *95*, 273-285.
277. Miller, J. E.; Evans, L.; Littlewolf, A.; Trudell, D. E., Batch microreactor studies of lignin and lignin model compound depolymerization by bases in alcohol solvents. *Fuel* **1999**, *78* (11), 1363-1366.
278. Li, W.-G.; Zhao, W.; Liu, H.-M.; Ao, L.; Liu, K.-S.; Guan, Y.-S.; Zai, S.-F.; Chen, S.-L.; Zong, Z.-M.; Wei, X.-Y., Supercritical ethanolysis of wheat stalk over calcium oxide. *Renew. Energy* **2018**, *120*, 300-305.
279. Brittain, A. D.; Chrisandina, N. J.; Cooper, R. E.; Buchanan, M.; Cort, J. R.; Olarte, M. V.; Sievers, C., Quenching of reactive intermediates during mechanochemical depolymerization of lignin. *Catal. Today* **2018**, *302*, 180-189.

280. McCallum, C. S.; Strachan, N.; Bennett, S. C.; Forsythe, W. G.; Garrett, M. D.; Hardacre, C.; Morgan, K.; Sheldrake, G. N., Catalytic depolymerisation of suberin rich biomass with precious metal catalysts. *Green Chem.* **2018**, *20* (12), 2702-2705.
281. Katahira, R.; Mittal, A.; McKinney, K.; Chen, X.; Tucker, M. P.; Johnson, D. K.; Beckham, G. T., Base-Catalyzed Depolymerization of Biorefinery Lignins. *ACS Sustain. Chem. Eng.* **2016**, *4* (3), 1474-1486.
282. De, S.; Dutta, S.; Saha, B., Microwave assisted conversion of carbohydrates and biopolymers to 5-hydroxymethylfurfural with aluminium chloride catalyst in water. *Green Chem.* **2011**, *13* (10), 2859-2868.
283. Pagán-Torres, Y. J.; Wang, T.; Gallo, J. M. R.; Shanks, B. H.; Dumesic, J. A., Production of 5-Hydroxymethylfurfural from Glucose Using a Combination of Lewis and Brønsted Acid Catalysts in Water in a Biphasic Reactor with an Alkylphenol Solvent. *ACS Catal.* **2012**, *2* (6), 930-934.
284. Tominaga, K.-i.; Mori, A.; Fukushima, Y.; Shimada, S.; Sato, K., Mixed-acid systems for the catalytic synthesis of methyl levulinate from cellulose. *Green Chem.* **2011**, *13* (4), 810-812.
285. Yang, Y.; Hu, C.-w.; Abu-Omar, M. M., Conversion of carbohydrates and lignocellulosic biomass into 5-hydroxymethylfurfural using  $\text{AlCl}_3 \cdot 6\text{H}_2\text{O}$  catalyst in a biphasic solvent system. *Green Chem.* **2012**, *14* (2), 509-513.
286. Qi, X.; Watanabe, M.; Aida, T. M.; Smith Jr, R. L., Fast Transformation of Glucose and Di-/Polysaccharides into 5-Hydroxymethylfurfural by Microwave Heating in an Ionic Liquid/Catalyst System. *ChemSusChem* **2010**, *3* (9), 1071-1077.

287. Hepditch, M. M.; Thring, R. W., Degradation of solvolysis lignin using Lewis acid catalysts. *Can. J. Chem. Eng.* **2000**, *78* (1), 226-231.
288. Zhang, X.; Qi, Z.; Long, J.; Xu, Y.; Wang, T.; Ma, L.; Li, Y., Phenolics production through catalytic depolymerization of alkali lignin with metal chlorides. *BioResources* **2014**, *9* (2), 3347-3360, 14 pp.
289. Kaminsky, W.; Zorriquetta, I.-J. N., Catalytical and thermal pyrolysis of polyolefins. *J. Anal. Appl. Pyrolysis* **2007**, *79* (1-2), 368-374.
290. Yilmaz, E. E.; Özvural, E. B.; Vural, H., Extraction and identification of proanthocyanidins from grape seed (*Vitis Vinifera*) using supercritical carbon dioxide. *J. Supercrit. Fluid.* **2011**, *55* (3), 924-928.
291. Al Bahri, M.; Calvo, L.; Gilarranz, M. A.; Rodriguez, J. J., Activated carbon from grape seeds upon chemical activation with phosphoric acid: Application to the adsorption of diuron from water. *Chem. Eng. J.* **2012**, *203*, 348-356.
292. Yang, H.; Yan, R.; Chen, H.; Lee, D. H.; Zheng, C., Characteristics of hemicellulose, cellulose and lignin pyrolysis. *Fuel* **2007**, *86* (12), 1781-1788.
293. Arita, T.; Nakahara, K.; Nagami, K.; Kajimoto, O., Hydrogen generation from ethanol in supercritical water without catalyst. *Tetrahedron Lett.* **2003**, *44* (5), 1083-1086.
294. Fringuelli, F.; Pizzo, F.; Vaccaro, L., Lewis-Acid Catalyzed Organic Reactions in Water. The Case of AlCl<sub>3</sub>, TiCl<sub>4</sub>, and SnCl<sub>4</sub> Believed To Be Unusable in Aqueous Medium. *J. Org. Chem.* **2001**, *66* (13), 4719-4722.
295. Akalın, M. K.; Tekin, K.; Karagöz, S., Hydrothermal liquefaction of cornelian cherry stones for bio-oil production. *Bioresour. Technol.* **2012**, *110*, 682-687.

296. Akalin, M. K.; Das, P.; Alper, K.; Tekin, K.; Ragauskas, A. J.; Karagoz, S., Deconstruction of lignocellulosic biomass with hydrated cerium (III) chloride in water and ethanol. *Appl. Catal., A* **2017**, *546*, 67-78.
297. del Río, J. C.; Rencoret, J.; Prinsen, P.; Martínez, Á. T.; Ralph, J.; Gutiérrez, A., Structural Characterization of Wheat Straw Lignin as Revealed by Analytical Pyrolysis, 2D-NMR, and Reductive Cleavage Methods. *J. Agric. Food. Chem.* **2012**, *60* (23), 5922-5935.
298. Martínez, Á. T.; Rencoret, J.; Marques, G.; Gutiérrez, A.; Ibarra, D.; Jiménez-Barbero, J.; del Río, J. C., Monolignol acylation and lignin structure in some nonwoody plants: A 2D NMR study. *Phytochemistry* **2008**, *69* (16), 2831-2843.
299. Tobimatsu, Y.; Chen, F.; Nakashima, J.; Escamilla-Treviño, L. L.; Jackson, L.; Dixon, R. A.; Ralph, J., Coexistence but Independent Biosynthesis of Catechyl and Guaiacyl/Syringyl Lignin Polymers in Seed Coats. *Plant Cell* **2013**, *25* (7), 2587.
300. Huang, X.; Korányi Tamás, I.; Boot Michael, D.; Hensen Emiel, J. M., Catalytic Depolymerization of Lignin in Supercritical Ethanol. *ChemSusChem* **2014**, *7* (8), 2276-2288.
301. McClelland, D. J.; Galebach, P. H.; Motagamwala, A. H.; Wittrig, A. M.; Karlen, S. D.; Buchanan, J. S.; Dumesic, J. A.; Huber, G. W., Supercritical methanol depolymerization and hydrodeoxygenation of lignin and biomass over reduced copper porous metal oxides. *Green Chem.* **2019**.
302. Hao, N.; Alper, K.; Tekin, K.; Karagoz, S.; Ragauskas, A. J., One-pot transformation of lignocellulosic biomass into crude bio-oil with metal chlorides via hydrothermal and supercritical ethanol processing. *Bioresour. Technol.* **2019**, *288*, 121500.

303. Elliott, D. C., Historical Developments in Hydroprocessing Bio-oils. *Energy Fuels* **2007**, *21* (3), 1792-1815.
304. French, R. J.; Orton, K. A.; Iisa, K., Hydrotreating of Model Mixtures and Catalytic Fast Pyrolysis Oils over Pd/C. *Energy Fuels* **2018**, *32* (12), 12577-12586.
305. Duan, P.; Savage, P. E., Catalytic hydrotreatment of crude algal bio-oil in supercritical water. *Appl. Catal. B: Environ.* **2011**, *104* (1), 136-143.
306. Wildschut, J.; Mahfud, F. H.; Venderbosch, R. H.; Heeres, H. J., Hydrotreatment of Fast Pyrolysis Oil using Heterogeneous Noble-Metal Catalysts. *Ind. Eng. Chem. Res.* **2009**, *48* (23), 10324-10334.
307. Mullen, C. A.; Boateng, A. A.; Reichenbach, S. E., Hydrotreating of fast pyrolysis oils from protein-rich pennycress seed presscake. *Fuel* **2013**, *111*, 797-804.
308. Kim, T.-S.; Oh, S.; Kim, J.-Y.; Choi, I.-G.; Choi, J. W., Study on the hydrodeoxygenative upgrading of crude bio-oil produced from woody biomass by fast pyrolysis. *Energy* **2014**, *68*, 437-443.
309. Li, X.; Gunawan, R.; Wang, Y.; Chaiwat, W.; Hu, X.; Gholizadeh, M.; Mourant, D.; Bromly, J.; Li, C.-Z., Upgrading of bio-oil into advanced biofuels and chemicals. Part III. Changes in aromatic structure and coke forming propensity during the catalytic hydrotreatment of a fast pyrolysis bio-oil with Pd/C catalyst. *Fuel* **2014**, *116*, 642-649.
310. Duan, P.; Savage, P. E., Catalytic hydrotreatment of crude algal bio-oil in supercritical water. *Appl. Catal. B: Environ.* **2011**, *104* (1-2), 136-143.
311. Tan, Z.; Xu, X.; Liu, Y.; Zhang, C.; Zhai, Y.; liu, P.; Li, Y.; Zhang, R., Upgrading bio-oil model compounds phenol and furfural within situgenerated hydrogen. *Environ. Prog. Sustain. Energy* **2014**, *33* (3), 751-755.

312. Mortensen, P. M.; Grunwaldt, J.-D.; Jensen, P. A.; Jensen, A. D., Screening of Catalysts for Hydrodeoxygenation of Phenol as a Model Compound for Bio-oil. *ACS Catal.* **2013**, *3* (8), 1774-1785.
313. Zhao, C.; Kou, Y.; Lemonidou, A. A.; Li, X.; Lercher, J. A., Highly Selective Catalytic Conversion of Phenolic Bio-Oil to Alkanes. *Angew. Chem., Int. Ed.* **2009**, *48* (22), 3987-3990, S3987/1-S3987/6.
314. Liu, D.; Chen, E. Y., Diesel and alkane fuels from biomass by organocatalysis and metal-acid tandem catalysis. *ChemSusChem* **2013**, *6* (12), 2236-9.
315. Li, Z.; Assary, R. S.; Atesin, A. C.; Curtiss, L. A.; Marks, T. J., Rapid ether and alcohol C-O bond hydrogenolysis catalyzed by tandem high-valent metal triflate + supported Pd catalysts. *J. Am. Chem. Soc.* **2014**, *136* (1), 104-7.
316. Song, H. J.; Deng, J.; Cui, M. S.; Li, X. L.; Liu, X. X.; Zhu, R.; Wu, W. P.; Fu, Y., Alkanes from Bioderived Furans by using Metal Triflates and Palladium-Catalyzed Hydrodeoxygenation of Cyclic Ethers. *ChemSusChem* **2015**, *8* (24), 4250-5.
317. Huang, X.; Morales Gonzalez, O. M.; Zhu, J.; Korányi, T. I.; Boot, M. D.; Hensen, E. J. M., Reductive fractionation of woody biomass into lignin monomers and cellulose by tandem metal triflate and Pd/C catalysis. *Green Chem.* **2017**, *19* (1), 175-187.
318. Keskiaväli, J.; Wrigstedt, P.; Lagerblom, K.; Repo, T., One-step Pd/C and Eu(OTf)<sub>3</sub> catalyzed hydrodeoxygenation of branched C<sub>11</sub> and C<sub>12</sub> biomass-based furans to the corresponding alkanes. *Appl. Catal. A: Gen.* **2017**, *534*, 40-45.
319. Ouyang, X.; Huang, X.; Hendriks, B. M. S.; Boot, M. D.; Hensen, E. J. M., Coupling organosolv fractionation and reductive depolymerization of woody biomass in a two-step catalytic process. *Green Chem.* **2018**, *20* (10), 2308-2319.



320. Zhou, J.; Zhu, R.; Deng, J.; Fu, Y., Preparation of valeric acid and valerate esters from biomass-derived levulinic acid using metal triflates + Pd/C. *Green Chem.* **2018**, *20* (17), 3974-3980.
321. Tekin, K.; Akalin, M. K.; Karagöz, S., The effects of water tolerant Lewis acids on the hydrothermal liquefaction of lignocellulosic biomass. *J. Energy Inst.* **2016**, *89* (4), 627-635.
322. Alper, K.; Tekin, K.; Karagöz, S., Hydrothermal and supercritical ethanol processing of woody biomass with a high-silica zeolite catalyst. *Biomass Convers. Bior.* **2019**, 1-12.
323. Akhtar, J.; Amin, N. A. S., A review on process conditions for optimum bio-oil yield in hydrothermal liquefaction of biomass. *Renew. Sust. Energ. Rev.* **2011**, *15* (3), 1615-1624.
324. Brown, T. M.; Duan, P.; Savage, P. E., Hydrothermal liquefaction and gasification of *Nannochloropsis* sp. *Energy Fuels* **2010**, *24* (6), 3639-3646.
325. Hronec, M.; Fulajtarová, K., Selective transformation of furfural to cyclopentanone. *Catal. Commun.* **2012**, *24*, 100-104.
326. Li, X.-L.; Deng, J.; Shi, J.; Pan, T.; Yu, C.-G.; Xu, H.-J.; Fu, Y., Selective conversion of furfural to cyclopentanone or cyclopentanol using different preparation methods of Cu–Co catalysts. *Green Chem.* **2015**, *17* (2), 1038-1046.
327. Fang, R.; Liu, H.; Luque, R.; Li, Y., Efficient and selective hydrogenation of biomass-derived furfural to cyclopentanone using Ru catalysts. *Green Chem.* **2015**, *17* (8), 4183-4188.

328. Guo, J.; Xu, G.; Han, Z.; Zhang, Y.; Fu, Y.; Guo, Q., Selective Conversion of Furfural to Cyclopentanone with CuZnAl Catalysts. *ACS Sustain. Chem. Eng.* **2014**, *2* (10), 2259-2266.
329. Li, W.; Xie, X.-a.; Sun, J.; Fan, D.; Wei, X., Investigation of cornstalk cellulose liquefaction in supercritical acetone by FT-TR and GC-MS methods. *Green Chem. Let. Rev.* **2019**, *12* (3), 299-309.
330. Jiang, W.; Kumar, A.; Adamopoulos, S., Liquefaction of lignocellulosic materials and its applications in wood adhesives—A review. *Ind. Crop. Prod.* **2018**, *124*, 325-342.
331. Yu, J.; Biller, P.; Mamahkel, A.; Klemmer, M.; Becker, J.; Glasius, M.; Iversen, B. B., Catalytic hydrotreatment of bio-crude produced from the hydrothermal liquefaction of aspen wood: a catalyst screening and parameter optimization study. *Sustain. Energy Fuels* **2017**, *1* (4), 832-841.
332. Madsen, R. B.; Bernberg, R. Z. K.; Biller, P.; Becker, J.; Iversen, B. B.; Glasius, M., Hydrothermal co-liquefaction of biomasses – quantitative analysis of bio-crude and aqueous phase composition. *Sustain. Energy Fuels* **2017**, *1* (4), 789-805.
333. Russell, J. A.; Miller, R. K.; Molton, P. M., Formation of aromatic compounds from condensation reactions of cellulose degradation products. *Biomass* **1983**, *3* (1), 43-57.
334. Jeong, S.; Jang, G. H.; Kim, D. H., Decomposition of Lignin Using MO–MgAlO<sub>y</sub> Mixed Oxide Catalysts (M= Co, Ni and Cu) in Supercritical Ethanol. *Top Catal* **2017**, *60* (9-11), 637-643.
335. Oezbay, N.; Uzun, B. B.; Varol, E. A.; Puetuen, A. E., Comparative analysis of pyrolysis oils and its subfractions under different atmospheric conditions. *Fuel Process. Technol.* **2006**, *87* (11), 1013-1019.

336. Puetuen, E.; Uzun, B. B.; Puetuen, A. E., Production of bio-fuels from cottonseed cake by catalytic pyrolysis under steam atmosphere. *Biomass Bioenerg.* **2006**, *30* (6), 592-598.
337. Onay, O.; Bayram, E.; Kockar, O. M., Copyrolysis of Seyitoemer-lignite and safflower seed: Influence of the blending ratio and pyrolysis temperature on product yields and oil characterization. *Energy Fuels* **2007**, *21* (5), 3049-3056.
338. Schnitzer, M. I.; Monreal, C. M.; Facey, G. A.; Fransham, P. B., The conversion of chicken manure to biooil by fast pyrolysis I. Analyses of chicken manure, biooils and char by <sup>13</sup>C and <sup>1</sup>H NMR and FTIR spectrophotometry. *J. Environ. Sci. Health Part B* **2007**, *42* (1), 71-77.
339. Sensoez, S.; Angin, D., Pyrolysis of safflower (*Charthamus tinctorius* L.) seed press cake in a fixed-bed reactor: Part 2. Structural characterization of pyrolysis bio-oils. *Bioresour. Technol.* **2008**, *99* (13), 5498-5504.
340. Xu, J.; Jiang, J.; Sun, Y.; Lu, Y., Bio-oil upgrading by means of ethyl ester production in reactive distillation to remove water and to improve storage and fuel characteristics. *Biomass Bioenerg.* **2008**, *32* (11), 1056-1061.
341. Yorgun, S.; Simsek, Y. E., Catalytic pyrolysis of *Miscanthus × giganteus* over activated alumina. *Bioresour. Technol.* **2008**, *99* (17), 8095-8100.
342. Acikgoz, C.; Kockar, O. M., Characterization of slow pyrolysis oil obtained from linseed (*Linum usitatissimum* L.). *J. Anal. Appl. Pyrolysis* **2009**, *85* (1+2), 151-154.
343. Ates, F.; Isikdag, M. A., Influence of temperature and alumina catalyst on pyrolysis of corncob. *Fuel* **2009**, *88* (10), 1991-1997.

344. Rout, P. K.; Naik, M. K.; Naik, S. N.; Goud, V. V.; Das, L. M.; Dalai, A. K., Supercritical CO<sub>2</sub> Fractionation of Bio-oil Produced from Mixed Biomass of Wheat and Wood Sawdust. *Energy Fuels* **2009**, *23* (12), 6181-6188.
345. Song, Q.-H.; Nie, J.-Q.; Ren, M.-G.; Guo, Q.-X., Effective Phase Separation of Biomass Pyrolysis Oils by Adding Aqueous Salt Solutions. *Energy Fuels* **2009**, *23* (6), 3307-3312.
346. Sukhbaatar, B.; Steele, P. H.; Kim, M. G., Use of lignin separated from bio-oil in oriented strand board binder phenol-formaldehyde resins. *BioResources* **2009**, *4* (2), 789-804.
347. De Sisto, W. J.; Hill, N., II; Beis, S. H.; Mukkamala, S.; Joseph, J.; Baker, C.; Ong, T.-H.; Stemmler, E. A.; Wheeler, M. C.; Frederick, B. G.; van Heiningen, A., Fast Pyrolysis of Pine Sawdust in a Fluidized-Bed Reactor. *Energy Fuels* **2010**, *24* (4), 2642-2651.
348. Naik, S.; Goud, V. V.; Rout, P. K.; Dalai, A. K., Supercritical CO<sub>2</sub> fractionation of bio-oil produced from wheat-hemlock biomass. *Bioresour. Technol.* **2010**, *101* (19), 7605-7613.
349. Puetuen, E., Catalytic pyrolysis of biomass: Effects of pyrolysis temperature, sweeping gas flow rate and MgO catalyst. *Energy (Oxford, U. K.)* **2010**, *35* (7), 2761-2766.
350. Karimi, E.; Briens, C.; Berruti, F.; Moloodi, S.; Tzanetakis, T.; Thomson, M. J.; Schlaf, M., Red Mud as a Catalyst for the Upgrading of Hemp-Seed Pyrolysis Bio-oil. *Energy Fuels* **2010**, *24* (12), 6586-6600.

351. Christensen, E. D.; Chupka, G. M.; Luecke, J.; Smurthwaite, T.; Alleman, T. L.; Iisa, K.; Franz, J. A.; Elliott, D. C.; McCormick, R. L., Analysis of Oxygenated Compounds in Hydrotreated Biomass Fast Pyrolysis Oil Distillate Fractions. *Energy Fuels* **2011**, *25* (11), 5462-5471.
352. Demiral, I.; Ayan, E. A., Pyrolysis of grape bagasse: Effect of pyrolysis conditions on the product yields and characterization of the liquid product. *Bioresour. Technol.* **2011**, *102* (4), 3946-3951.
353. Smets, K.; Adriaensens, P.; Vandewijngaarden, J.; Stals, M.; Cornelissen, T.; Schreurs, S.; Carleer, R.; Yperman, J., Water content of pyrolysis oil: Comparison between Karl Fischer titration, GC/MS-corrected azeotropic distillation and <sup>1</sup>H NMR spectroscopy. *J. Anal. Appl. Pyrolysis* **2011**, *90* (2), 100-105.
354. Strahan, G. D.; Mullen, C. A.; Boateng, A. A., characterizing biomass fast pyrolysis oils by <sup>13</sup>C NMR and chemometric analysis. *Energy Fuels* **2011**, *25* (11), 5452-5461.
355. David, K.; Ben, H.; Muzzy, J.; Feik, C.; Iisa, K.; Ragauskas, A., Chemical characterization and water content determination of bio-oils obtained from various biomass species using <sup>31</sup>P NMR spectroscopy. *Biofuels* **2012**, *3* (2), 123-128.
356. Kar, Y.; Sen, N.; Deveci, H., Usability of terebinth (*Pistacia terebinthus* L.) fruits as an energy source for diesel-like fuels production. *Energy Convers. Manage.* **2012**, *64*, 433-440.
357. Dalitz, F.; Steiwand, A.; Raffelt, K.; Nirschl, H.; Guthausen, G., <sup>1</sup>H NMR Techniques for Characterization of Water Content and Viscosity of Fast Pyrolysis Oils. *Energy Fuels* **2012**, *26* (8), 5274-5280.

358. Kim, T.-S.; Kim, J.-Y.; Kim, K.-H.; Lee, S.; Choi, D.; Choi, I.-G.; Choi, J. W., The effect of storage duration on bio-oil properties. *J. Anal. Appl. Pyrolysis* **2012**, *95*, 118-125.
359. Liu, W.-J.; Tian, K.; Jiang, H.; Zhang, X.-S.; Ding, H.-S.; Yu, H.-Q., Selectively Improving the Bio-Oil Quality by Catalytic Fast Pyrolysis of Heavy-Metal-Polluted Biomass: Take Copper (Cu) as an Example. *Environ. Sci. Technol.* **2012**, *46* (14), 7849-7856.
360. Pittman, C. U., Jr.; Mohan, D.; Eseyin, A.; Li, Q.; Ingram, L.; Hassan, E.-B. M.; Mitchell, B.; Guo, H.; Steele, P. H., Characterization of Bio-oils Produced from Fast Pyrolysis of Corn Stalks in an Auger Reactor. *Energy Fuels* **2012**, *26* (6), 3816-3825.
361. Salema, A. A.; Ani, F. N., Microwave-assisted pyrolysis of oil palm shell biomass using an overhead stirrer. *J. Anal. Appl. Pyrolysis* **2012**, *96*, 162-172.
362. Volli, V.; Singh, R. K., Production of bio-oil from de-oiled cakes by thermal pyrolysis. *Fuel* **2012**, *96*, 579-585.
363. Ben, H.; Ragauskas, A. J., Comparison for the compositions of fast and slow pyrolysis oils by NMR characterization. *Bioresour. Technol.* **2013**, *147*, 577-584.
364. Ben, H.; Ragauskas, A. J., Influence of Si/Al ratio of ZSM-5 zeolite on the properties of lignin pyrolysis products. *ACS Sustainable Chem. Eng.* **2013**, *1* (3), 316-324.
365. Chang, S.; Zhao, Z.; Zheng, A.; Li, X.; Wang, X.; Huang, Z.; He, F.; Li, H., Effect of hydrothermal pretreatment on properties of bio-oil produced from fast pyrolysis of eucalyptus wood in a fluidized bed reactor. *Bioresour. Technol.* **2013**, *138*, 321-8.
366. Paasikallio, V.; Agblevor, F.; Oasmaa, A.; Lehto, J.; Lehtonen, J., Catalytic pyrolysis of forest thinnings with ZSM-5 catalysts: Effect of reaction temperature on bio-oil physical properties and chemical composition. *Energy Fuels* **2013**, *27* (12), 7587-7601.

367. Richard, C. J.; Patel, B.; Chadwick, D.; Hellgardt, K., Hydrothermal deoxygenation of pyrolysis oil from Norwegian spruce: *Picea abies*. *Biomass Bioenerg.* **2013**, *56*, 446-455.
368. Zhang, Z.; Sui, S.; Wang, F.; Wang, Q.; Pittman, C. U., Jr., Catalytic conversion of bio-oil to oxygen-containing fuels by acid-catalyzed reaction with olefins and alcohols over silica sulfuric acid. *Energies (Basel, Switz.)* **2013**, *6* (9), 4531-4550, 20 pp.
369. Zhou, S.; Garcia-Perez, M.; Pecha, B.; McDonald, A. G.; Kersten, S. R. A.; Westerhof, R. J. M., Secondary vapor phase reactions of lignin-derived oligomers obtained by fast pyrolysis of pine wood. *Energy Fuels* **2013**, *27* (3), 1428-1438.
370. Bi, Y.; Wang, G.; Shi, Q.; Xu, C.; Gao, J., Compositional Changes during Hydrodeoxygenation of Biomass Pyrolysis Oil. *Energy Fuels* **2014**, *28* (4), 2571-2580.
371. Choudhury, N. D.; Chutia, R. S.; Bhaskar, T.; Kataki, R., Pyrolysis of jute dust: effect of reaction parameters and analysis of products. *J. Mater. Cycles Waste Manage.* **2014**, *16* (3), 449-459.
372. Chutia, R. S.; Kataki, R.; Bhaskar, T., Characterization of liquid and solid product from pyrolysis of *Pongamia glabra* deoiled cake. *Bioresour. Technol.* **2014**, *165*, 336-342.
373. Demiral, I.; Kul, S. C., Pyrolysis of apricot kernel shell in a fixed-bed reactor: Characterization of bio-oil and char. *J. Anal. Appl. Pyrolysis* **2014**, *107*, 17-24.
374. Doassans-Carrere, N.; Ferrasse, J.-H.; Boutin, O.; Mauviel, G.; Lede, J., Comparative Study of Biomass Fast Pyrolysis and Direct Liquefaction for Bio-Oils Production: Products Yield and Characterizations. *Energy Fuels* **2014**, *28* (8), 5103-5111.

375. Huang, F.; Ben, H.; Pan, S.; Pu, Y.; Ragauskas, A., The use of combination of zeolites to pursue integrated refined pyrolysis oil from kraft lignin. *Sustain. Chem. Proc.* **2014**, 2, 7/1-7/11, 11 pp.
376. Onal, E.; Uzun, B. B.; Putun, A. E., Bio-oil production via co-pyrolysis of almond shell as biomass and high density polyethylene. *Energy Convers. Manage.* **2014**, 78, 704-710.
377. Nanda, S.; Azargohar, R.; Kozinski, J. A.; Dalai, A. K., Characteristic Studies on the Pyrolysis Products from Hydrolyzed Canadian Lignocellulosic Feedstocks. *BioEnergy Res.* **2014**, 7 (1), 174-191.
378. Zhou, S.; Garcia-Perez, M.; Pecha, B.; McDonald, A. G.; Westerhof, R. J. M., Effect of particle size on the composition of lignin derived oligomers obtained by fast pyrolysis of beech wood. *Fuel* **2014**, 125, 15-19.
379. Zhang, Z.; MacQuarrie, D. J.; Clark, J. H.; Matharu, A. S., Green Materials: Adhesive Properties of Bio-oils Derived from Various Biorenewable Waste Streams: From Wood to Paper to Paper Deinking Residue. *ACS Sustain. Chem. Eng.* **2015**, 3 (11), 2985-2993.
380. Zhang, X.; Chen, L.; Kong, W.; Wang, T.; Zhang, Q.; Long, J.; Xu, Y.; Ma, L., Upgrading of bio-oil to boiler fuel by catalytic hydrotreatment and esterification in an efficient process. *Energy (Oxford, U. K.)* **2015**, 84, 83-90.
381. Saikia, R.; Chutia, R. S.; Kataki, R.; Pant, K. K., Perennial grass (*Arundo donax* L.) as a feedstock for thermo-chemical conversion to energy and materials. *Bioresour. Technol.* **2015**, 188, 265-272.



382. Ozbay, G.; Pekgozlu, A. K.; Ozcifci, A., The effect of heat treatment on bio-oil properties obtained from pyrolysis of wood sawdust. *Eur. J. Wood Wood Prod.* **2015**, *73* (4), 507-514.
383. Ly, H. V.; Kim, S.-S.; Woo, H. C.; Choi, J. H.; Suh, D. J.; Kim, J., Fast pyrolysis of macroalga *Saccharina japonica* in a bubbling fluidized-bed reactor for bio-oil production. *Energy (Oxford, U. K.)* **2015**, *93* (Part\_2), 1436-1446.
384. Krishna, B. B.; Singh, R.; Bhaskar, T., Effect of catalyst contact on the pyrolysis of wheat straw and wheat husk. *Fuel* **2015**, *160*, 64-70.
385. Hosseinneshad, S.; Fini, E. H.; Sharma, B. K.; Basti, M.; Kunwar, B., Physiochemical characterization of synthetic bio-oils produced from bio-mass: a sustainable source for construction bio-adhesives. *RSC Adv.* **2015**, *5* (92), 75519-75527.
386. Elkasabi, Y.; Mullen, C. A.; Jackson, M. A.; Boateng, A. A., Characterization of fast-pyrolysis bio-oil distillation residues and their potential applications. *J. Anal. Appl. Pyrolysis* **2015**, *114*, 179-186.
387. Boscagli, C.; Raffelt, K.; Zevaco, T. A.; Olbrich, W.; Otto, T. N.; Sauer, J.; Grunwaldt, J.-D., Mild hydrotreatment of the light fraction of fast-pyrolysis oil produced from straw over nickel-based catalysts. *Biomass Bioenerg.* **2015**, *83*, 525-538.
388. Bordoloi, N.; Narzari, R.; Chutia, R. S.; Bhaskar, T.; Kataki, R., Pyrolysis of *Mesua ferrea* and *Pongamia glabra* seed cover: Characterization of bio-oil and its sub-fractions. *Bioresour. Technol.* **2015**, *178*, 83-89.
389. Balagurumurthy, B.; Srivastava, V.; Kumar, J.; Biswas, B.; Singh, R.; Gupta, P.; Kumar, K. L. N. S.; Singh, R.; Bhaskar, T., Value addition to rice straw through pyrolysis in hydrogen and nitrogen environments. *Bioresour. Technol.* **2015**, *188*, 273-279.

390. Pradhan, D.; Singh, R. K.; Bendu, H.; Mund, R., Pyrolysis of Mahua seed (*Madhuca indica*) - Production of biofuel and its characterization. *Energy Convers. Manage.* **2016**, *108*, 529-538.
391. Krishna, B. B.; Biswas, B.; Kumar, J.; Singh, R.; Bhaskar, T., Role of Reaction Temperature on Pyrolysis of Cotton Residue. *Waste Biomass Valoriz.* **2016**, *7* (1), 71-78.
392. Cheng, T.; Han, Y.; Zhang, Y.; Xu, C., Molecular composition of oxygenated compounds in fast pyrolysis bio-oil and its supercritical fluid extracts. *Fuel* **2016**, *172*, 49-57.
393. Ben, H.; Huang, F.; Li, L.; Ragauskas, A. J., In situ upgrading of whole biomass to biofuel precursors with low average molecular weight and acidity by the use of zeolite mixture. *RSC Adv.* **2015**, *5* (91), 74821-74827.
394. Joseph, J.; Rasmussen, M. J.; Fecteau, J. P.; Kim, S.; Lee, H.; Tracy, K. A.; Jensen, B. L.; Frederick, B. G.; Stemmler, E. A., Compositional Changes to Low Water Content Bio-oils during Aging: An NMR, GC/MS, and LC/MS Study. *Energy Fuels* **2016**, *30* (6), 4825-4840.
395. Yin, W.; Kloekhorst, A.; Venderbosch, R. H.; Bykova, M. V.; Khromova, S. A.; Yakovlev, V. A.; Heeres, H. J., Catalytic hydrotreatment of fast pyrolysis liquids in batch and continuous set-ups using a bimetallic Ni-Cu catalyst with a high metal content. *Catal. Sci. Technol.* **2016**, *6* (15), 5899-5915.
396. Agarwal, S.; van Es, D.; Heeres, H. J., Catalytic pyrolysis of recalcitrant, insoluble humin byproducts from C6 sugar biorefineries. *J. Anal. Appl. Pyrolysis* **2017**, *123*, 134-143.

397. Dodge, L. A.; Kalinoski, R. M.; Das, L.; Bursavich, J.; Muley, P.; Boldor, D.; Shi, J., Sequential Extraction and Characterization of Lignin-Derived Compounds from Thermochemically Processed Biorefinery Lignins. *Energy Fuels* **2019**, *33* (5), 4322-4330.
398. Nazari, L.; Yuan, Z.; Souzanchi, S.; Ray, M. B.; Xu, C., Hydrothermal liquefaction of woody biomass in hot-compressed water: Catalyst screening and comprehensive characterization of bio-crude oils. *Fuel* **2015**, *162*, 74-83.
399. Feng, J.; Jiang, J.; Yang, Z.; Su, Q.; Wang, K.; Xu, J., Characterization of depolymerized lignin and renewable phenolic compounds from liquefied waste biomass. *RSC Adv.* **2016**, *6* (98), 95698-95707.

# APPENDIX

## APPENDIX A: TABLES

**Table 1.** Comparison of physical properties of bio-oils from thermal processing and heavy fuel oils.<sup>9-11</sup>

| <b>Properties</b>           | <b>Pyrolysis oil</b> | <b>Liquefaction oil</b> | <b>Heavy fuel oil</b> |
|-----------------------------|----------------------|-------------------------|-----------------------|
| Higher heating value, MJ/kg | 16-19                | 35                      | 40                    |
| Elemental composition, wt%  |                      |                         |                       |
| C                           | 54-58                | 73                      | 85                    |
| H                           | 5.5-7.0              | 8                       | 11                    |
| O                           | 35-40                | 16                      | 1                     |
| N                           | 0-0.2                | -                       | 0.3                   |
| ash                         | 0-0.2                | -                       | 0.1                   |
| Moisture content, wt%       | 15-30                | 5.1                     | 0.1                   |
| pH                          | 2.5                  | -                       | -                     |
| Solids, wt%                 | 0.2-1.0              | -                       | 1.0                   |
| Viscosity (50 °C), cP       | 40-100               | 15000 (at 61 °C)        | 180                   |

**Table 2.** Characteristics of bio-oil and challenges for its applications.<sup>10, 12, 14-15</sup>

| <b>Property</b> | <b>Characteristics</b>   | <b>Challenges</b>   |
|-----------------|--|---|
| Oxygen content  | Usually 35-40 wt%, depending on the original biomass source and pyrolysis parameters | High oxygen ratio results in low heating value, immiscibility with hydrocarbon fuels and instability of pyrolysis oil |
| Water content   | Affected by feedstock and pyrolysis atmosphere                                       | Lowers the heating value and delays ignition  |
| Corrosiveness   | A pH of 2-3  | Can affect carbon steel and aluminum materials; cannot be stored in some sealing materials                            |
| Viscosity       | Similar to the viscosity of crude oils in the temperature range 35-45 °C             | An appropriate preheating can facilitate pumping of bio-oil   |
| Aging           | Higher-molecular-weight compounds forming over time                                  | Makes bio-oil difficult to store and transport  |

**Table 3.** Typical bio-oil upgrading methods and characteristics.<sup>22, 28-31</sup>

| <b>Upgrading method</b>  | <b>Characteristics</b>   |
|--------------------------|--|
| Catalytic cracking       | Zeolites are commonly used as catalysts; cost effective; undesirable byproducts  |
| Hydrotreating            | Requires high pressures, moderate temperatures, a source of hydrogen and catalysts; high-quality products; high experimental instrument requirements   |
| Steam reforming          | Produces hydrogen-rich syngas; requires stable catalysts because of carbon deposition during the steam reforming process   |
| Aqueous phase processing | Converts low-boiling fractions of bio-oils into hydrogen and alkanes   |
| Esterification           | Lowers concentrations of acids and carbonyl groups in the presence of an alcohol and an acid catalyst; usually accompanied by an oxidation pretreatment of bio-oils for converting aldehydes into carbonyl acids |
| Gasification for syngas  | Compared to the gasification of solid biomass, the process pressure requirement is much lower; reduces bio-refinery system costs by utilizing extensive commercial gasification plants                           |

**Table 4.** Summary of non-catalytic and catalytic degradation of lignin in ethanol.

| Feedstock   | T (°C)  | t (min) | P <sub>int</sub> (MPa)                            | Catalyst  | Key Findings   | References |
|---|---------|---------|---|---|----------------|------------|
| Organosolv lignin   | 200-350 | 30-60   | 2-3 (H <sub>2</sub> )                             | -   | <sup>f1</sup>  | 51         |
| Protobind lignin  | 200-280 | 15-45   | -   | -   | <sup>f2</sup>  | 49         |
| Lab.prepared lignin using conc. H <sub>2</sub> SO <sub>4</sub>    | 293-350 | 30      | 2 (N <sub>2</sub> )                               | -   | <sup>f3</sup>  | 50         |
| Lab.prepared lignin from wheat straw                              | 250-450 | 0-480   | -   | -   | <sup>f4</sup>  | 52         |
| Alkali lignin   | 180-300 | 60-480  | 7.2*  | 10% NaOH  | <sup>f5</sup>  | 41         |
| Organosolv lignin   | 290     | 0-60    | -   | Metal hydroxides and metal carbonate  | <sup>f6</sup>  | 54         |
| Kraft lignin/<br>Organosolv lignin                                | 350     | 30-180  | 0.1 (N <sub>2</sub> ) or<br>0.3 (H <sub>2</sub> ) | 10 wt% catalyst: MgO loaded different supports (i.e., carbon, Al <sub>2</sub> O <sub>3</sub> , and ZrO <sub>2</sub> ) and Ru/C, and physical mixtures of Ru/C and each MgO.       | <sup>f7</sup>  | 55         |
| Alkali lignin   | 300-400 | 60      | 11.6-13.2*  | sulfated ZrO <sub>2</sub> , sulfated ZrO <sub>2</sub> supported Al <sub>2</sub> O <sub>3</sub> , and synthesized high-silica zeolites in H form and a commercial zeolite catalyst | <sup>f8</sup>  | 56         |
| Concentrated sulfuric acid hydrolysis lignin (CSAHL)/Kraft lignin | 350     | 0-60    | 21.7-35.1   | Formic acid to lignin ratio: 1.5  | <sup>f9</sup>  | 59         |
| Alkali lignin   | 440     | 300     | N/A   | Metal supported zeolites (Co, Ni and Cu in loadings 5, 10 and 30 wt% and the Si/Al <sub>2</sub> ratio of ZSM-5 (30, 50, 80 and 200).).  | <sup>f10</sup> | 334        |
| Alkali lignin   | 180-300 | 0-480   | N/A   | Raney/Ni or Rh/C catalyst   | <sup>f11</sup> | 63         |

<sup>f1</sup> The highest bio-oil yield was ~95 wt%.

<sup>f2</sup> The highest bio-oil yield was ~81 wt%.

<sup>f3</sup> The highest bio-oil yield was ~30 wt%.

<sup>f4</sup> The highest bio-oil yield was 40 wt%.

<sup>f5</sup> The highest bio-oil yield was ~67wt%. Increase in temperature resulted in increase the relative yields of phenols.

<sup>f6</sup> The lignin conversion was 93% and obtained with the use of 7.8 meq KOH. The studies with model compounds showed that EtOH-derived products incorporated into bio-oils.

<sup>f7</sup> The use of co-catalyst increased monomeric phenols. By replacing N<sub>2</sub> with H<sub>2</sub>, the molecular weight (Mw) of bio-oil decreased and monomeric phenols yield increased. Under identical conditions, bio-oil from organosolv lignin had a higher yield of aromatic monomer and lower Mw in comparison with Kraft lignin in the catalytic run (with Ru/C and MgO/ZrO<sub>2</sub> catalyst).



**Table 4. (Continued)**


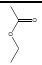




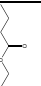
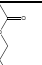
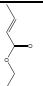
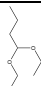
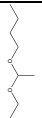
<sup>f8</sup> All catalysts gave higher conversion than that of the non-catalytic run. The highest bio-oil yield was 62.5 wt% and obtained with sulfated ZrO<sub>2</sub> catalyst. Ethanol itself degraded without and with the use of catalyst.

<sup>f9</sup> The conversion and bio-oil yields were 99% and 90 wt% for KL and 92 % and 85 wt% for CSAHL. The compounds in the bio-oil were mainly phenols, esters, furans, alcohols, and traces of aliphatic hydrocarbons.

<sup>f10</sup> The highest monoaromatic yield (98.2 wt%) was and obtained with the use of 10 wt% Cu loaded on ZSM-5 with a Si/Al<sub>2</sub> ratio of 30.

<sup>f11</sup> The highest bio-oil yield of 75wt% ca. was obtained with Raney-Ni catalyst. The use of either Raney/Ni or Rh/C catalyst increased the relative content of phenols.

**Table 5.** Yields (mg/g of lignin) of the products from ethanol degradation without and with Kraft lignin added at 280 °C for 240 min over 0.5 g Mo/Al<sub>2</sub>O<sub>3</sub> catalyst with initial 0.1 MPa of N<sub>2</sub> and 100 mL of ethanol.<sup>65</sup> (Adapted from Ref. 65 with the permission from American Chemistry Society.)

| Aliphatics |  |  |  |  |  |  |  |  |  |  |  |
|------------|---|---|---|---|---|---|--|---|---|---|---|
| Without KL | 879   | 1615  | 917   | 2   | 7   | 651   | 80   | 25  | 21  | 26  | 30  |
| With KL    | 566   | 526   | 982   | 410   | 3   | 79  | 58   | 60  | 17  | 3   | 4   |

**Table 6.** Summary of non-catalytic and catalytic degradation of lignocellulosic biomass in ethanol.

| Entry | Feed            | T (°C)  | t (min) | P <sub>int</sub> (MPa)              | Catalyst                                       | Key Findings  | References |
|-------|-----------------|---------|---------|-------------------------------------|--|---------------|------------|
| 1     | Beech wood      | 265-320 | 37-143  | 9-17* (purged with N <sub>2</sub> ) | -  | <sup>f1</sup> | 83         |
| 2     | Hawthorn stones | 280-320 | 60-120  | 1.0 (N <sub>2</sub> )               | -  | <sup>f2</sup> | 84         |
| 3     | Pine wood       | 280-400 | 0-240   | 0.4-7.5 (N <sub>2</sub> )           | -  | <sup>f3</sup> | 85         |
| 4     | Rice straw      | 275-345 | 15-30   | N/A (purged with CO <sub>2</sub> )  | -  | <sup>f4</sup> | 87         |
| 5     | Rice stalk      | 200-280 | 60      | 14-15* (N <sub>2</sub> )            | -  | <sup>f5</sup> | 88         |
| 6     | Pine wood       | 200-350 | 15-60   | 2-10 (H <sub>2</sub> )              | (FeSO <sub>4</sub> )·7H <sub>2</sub> O and FeS | <sup>f6</sup> | 58         |
| 7     | Wood sawdust    | 300-400 | 40      | 2-10 (H <sub>2</sub> )              | [BMIM]Cl/NiCl <sub>2</sub>                     | <sup>f7</sup> | 90         |
| 8     | Wood sawdust    | 320     | 40      | 2-6 (H <sub>2</sub> )               | MoO <sub>2</sub> /SiO <sub>2</sub>             | <sup>f8</sup> | 91         |

<sup>f1</sup> The highest biomass conversion and bio-oil yields were 88.5 % and 40.4 wt%.

<sup>f2</sup> The lowest and highest biomass conversion were ~55 and 83 %, respectively. The bio-oil yields were in the range from ~32 to ~41 wt%.

<sup>f3</sup> Biomass conversion were in the range ~34-98 1%. Bio-oil yield ranged from ~16 to 60 wt%.

<sup>f4</sup> In the first step, rice straw was pretreated at 200 °C for 10 min. In the second step, the temperature was raised to the desired temperature. The highest biomass conversion and bio-oil yield was ~80 % and 48 wt% , respectively.

<sup>f5</sup> The highest biomass conversion and bio-oil yields were ~78% and ~55 wt% were obtained with non-torrefied rice stalk. The torrefaction process led to decrease in biomass conversion and bio-oil yields but increased heating values.

<sup>f6</sup> The highest bio-oil yield was 63 wt% and obtained with (FeSO<sub>4</sub>)·7H<sub>2</sub>O at 350 °C. Phenolic compounds were dominant regardless the type of catalyst.

<sup>f7</sup> Biomass conversion and bio-oil yields from the non-catalytic run were ~63 % and ~33 wt%, respectively. The biomass conversion was increased to ~70 % and the bio-oil yield was 50 wt % with [BMIM]Cl/NiCl<sub>2</sub>.

<sup>f8</sup> Biomass conversion and bio-oil yields were ~79 % and 47 wt% in the non-catalytic run. Biomass conversion and bio-oil yields were ~90 % and 72 wt% in the catalytic run.

**Table 7.** NMR techniques applied in bio-oil analysis.

| Feedstock   | Pyrolysis method                 | Post pyrolysis upgrading method | Fraction analyzed by NMR  | NMR technique                             |
|---|----------------------------------|---------------------------------|---|---|
| Apricot pulp <sup>335</sup>   | Slow pyrolysis                   | -                               | Water-insoluble phase, toluene subfraction, methanol subfraction  | <sup>1</sup> H NMR                        |
| Cottonseed cake <sup>336</sup>  | Zeolite-catalyzed slow pyrolysis | -                               | Water-insoluble phase   | <sup>1</sup> H NMR                        |
| Safflower seed <sup>337</sup>   | Co-pyrolysis with lignite        | -                               | Water-insoluble phase   | <sup>1</sup> H NMR                        |
| Chicken manure <sup>338</sup>   | Fast pyrolysis                   | -                               | Light oil fraction, heavy oil fraction                            | <sup>1</sup> H, <sup>13</sup> C NMR       |
| Pine wood, pine bark, oak wood, oak bark <sup>104</sup>   | Fast pyrolysis                   | -                               | Whole bio-oil, ethyl acetate subfraction                          | <sup>1</sup> H, <sup>13</sup> C NMR       |
| Safflower <sup>339</sup>  | Slow pyrolysis                   | -                               | Whole bio-oil   | <sup>1</sup> H NMR                        |
| Rice husk <sup>340</sup>  | Fast pyrolysis                   | Reactive distillation           | Whole bio-oil   | <sup>1</sup> H NMR                        |
| <i>Miscanthus × giganteus</i> <sup>341</sup>  | Alumina-catalyzed slow pyrolysis | -                               | Water-insoluble phase   | <sup>1</sup> H NMR                        |
| Linseed <sup>342</sup>  | Slow pyrolysis                   | -                               | Water-insoluble phase   | <sup>1</sup> H NMR                        |
| Corn cob <sup>343</sup>   | Alumina-catalyzed slow pyrolysis | -                               | Water-insoluble phase   | <sup>1</sup> H NMR                        |
| Switchgrass, corn stover, alfalfa stems, guayule (whole shrub), guayule bagasse, chicken litter <sup>98</sup> | Fast pyrolysis                   | -                               | Electrostatic precipitator fraction                               | <sup>1</sup> H, <sup>13</sup> C, DEPT NMR |
| Wheat, wood sawdust <sup>344</sup>  | Fast pyrolysis                   | -                               | Crude bio-oil, supercritical-CO <sub>2</sub> -extracted fractions | <sup>1</sup> H NMR                        |
| Rice husk <sup>345</sup>  | Fast pyrolysis                   | -                               | Whole bio-oil, salt induced subfractions                          | <sup>13</sup> C NMR                       |

**Table 7.** (Continued)

| <b>Feedstock</b>  | <b>Pyrolysis method</b>             | <b>Post pyrolysis upgrading method</b> | <b>Fraction analyzed by NMR</b>  | <b>NMR technique</b>                 |
|---|-------------------------------------|--|--|--------------------------------------|
| Pine wood <sup>346</sup>  | Fast pyrolysis                      | -                                      | Whole bio-oil, pyrolytic lignin fraction   | <sup>13</sup> C NMR                  |
| Pine wood, sweetgum, loblolly pine lignin, loblolly pine lignin <sup>99</sup> | Fast pyrolysis                      | -                                      | Whole bio-oil  | <sup>31</sup> P NMR                  |
| Pine wood <sup>347</sup>  | Fast pyrolysis                      | -                                      | Electrostatic precipitator fraction, water-soluble fraction, water-insoluble fraction  | <sup>13</sup> C NMR                  |
| Wheat-hemlock <sup>348</sup>  | Fast pyrolysis                      | -                                      | Crude bio-oil, supercritical CO <sub>2</sub> extracted fractions   | <sup>1</sup> H NMR                   |
| Cotton seed <sup>349</sup>  | Magnesium-oxide-catalyzed pyrolysis | -                                      | Whole bio-oil  | <sup>1</sup> H NMR                   |
| Hemp-seed <sup>350</sup>  | Fast pyrolysis                      | Catalytic hydrotreatment               | Methanol extracts, acetone extracts, acetonitrile extracts, ethyl acetate extracts, diethyl ether extracts of crude/upgraded bio-oil | <sup>1</sup> H, <sup>13</sup> C NMR  |
| Softwood kraft lignin <sup>136</sup>  | Catalyzed slow pyrolysis            | -                                      | Heavy fraction, light fraction   | <sup>13</sup> C, <sup>31</sup> P NMR |
| Softwood kraft lignin <sup>119</sup>  | Slow pyrolysis                      | -                                      | Heavy fraction, light fraction   | <sup>13</sup> C, <sup>31</sup> P NMR |
| Pine wood, softwood lignin, cellulose <sup>101</sup>                          | Slow pyrolysis                      | -                                      | Whole bio-oil  | HSQC-NMR                             |

**Table 7.** (Continued)

| <b>Feedstock</b>  | <b>Pyrolysis method</b>          | <b>Post pyrolysis upgrading method</b> | <b>Fraction analyzed by NMR</b>     | <b>NMR technique</b>                                 |
|---|----------------------------------|--|-------------------------------------|--|
| <sup>351</sup>  | Fast pyrolysis                   | Catalytic hydrotreatment               | Distillate fractions                | <sup>13</sup> C NMR                                  |
| Grape bagasse <sup>352</sup>  | Slow pyrolysis                   | -                                      | Water insoluble fraction            | <sup>1</sup> H NMR                                   |
| Rapeseed cake, willow, cellulose, sludge, polyethylene glycol <sup>353</sup>  | Fast pyrolysis                   | -                                      | Whole bio-oil                       | <sup>1</sup> H NMR                                   |
| Oak, rye grass, barley straw, eel grass, cow manure, pennycress presscake, camelina presscake, barley DDGS <sup>354</sup> | Fast pyrolysis                   | -                                      | Electrostatic precipitator fraction | <sup>13</sup> C, DEPT NMR                            |
| Softwood kraft lignin <sup>203</sup>  | Zeolite catalyzed slow pyrolysis | -                                      | Heavy fraction, light fraction      | <sup>13</sup> C, <sup>31</sup> P, HSQC-NMR           |
| Corn stover, white oak, mixed hardwood, poplar, white oak <sup>355</sup>  | Slow pyrolysis                   | -                                      | Whole bio-oil                       | <sup>31</sup> P NMR                                  |
| Terebinth <sup>356</sup>  | Slow pyrolysis                   | -                                      | Water insoluble phase               | <sup>1</sup> H NMR                                   |
| Poplar wood, softwood lignin, cellulose <sup>105</sup>  | Slow pyrolysis                   | -                                      | Fresh bio-oil, aged bio-oil         | <sup>1</sup> H, <sup>13</sup> C, <sup>31</sup> P NMR |

**Table 7.** (Continued)

| <b>Feedstock</b>   | <b>Pyrolysis method</b>  | <b>Post pyrolysis upgrading method</b> | <b>Fraction analyzed by NMR</b> | <b>NMR technique</b>                       |
|--|--|--|---------------------------------|--|
| Corn stover, corn cobs, bagasse, maize granulates, hay, wheat bran, wheat straw, softwood, oil palm fronds, empty fruit bunches, dynamotive <sup>357</sup> | Fast pyrolysis   | -                                      | Whole bio-oil                   | <sup>1</sup> H NMR                         |
| Poplar wood <sup>358</sup>   | Fast pyrolysis   | -                                      | Aged pyrolytic lignin           | <sup>13</sup> C NMR                        |
| Fir <sup>359</sup>   | Catalytic fast pyrolysis   | -                                      | Whole bio-oil                   | <sup>1</sup> H NMR                         |
| Poplar wood <sup>113</sup>   | Fresh fluid catalytic cracking catalysts and zeolite-catalyzed pyrolysis | -                                      | Whole bio-oil                   | <sup>13</sup> C NMR                        |
| Corn stalks <sup>360</sup>   | Fast pyrolysis   | -                                      | Whole bio-oil                   | <sup>1</sup> H, <sup>13</sup> C NMR        |
| Oil palm shell <sup>361</sup>  | Microwave pyrolysis  | -                                      | Whole bio-oil                   | <sup>1</sup> H NMR                         |
| Sesame, mustard, neem de-oiled cake <sup>362</sup>   | Slow pyrolysis   | -                                      | Whole bio-oil                   | <sup>1</sup> H NMR                         |
| Softwood kraft lignin <sup>363</sup>   | Slow pyrolysis, fast pyrolysis   | -                                      | Heavy fraction, light fraction  | <sup>13</sup> C, HSQC-NMR                  |
| Softwood kraft lignin <sup>364</sup>   | Zeolite slow pyrolysis   | -                                      | Heavy fraction, light fraction  | <sup>13</sup> C, <sup>31</sup> P, HSQC-NMR |

**Table 7.** (Continued)

| <b>Feedstock</b>                                   | <b>Pyrolysis method</b>                            | <b>Post pyrolysis upgrading method</b> | <b>Fraction analyzed by NMR</b>                                    | <b>NMR technique</b>                       |
|--|--|--|--|--|
| Eucalyptus wood <sup>365</sup>                     | Fast pyrolysis following hydrothermal pretreatment | -                                      | Whole bio-oil  | <sup>13</sup> C NMR                        |
| Forest thinnings <sup>366</sup>                    | Zeolite catalyzed fast pyrolysis                   | -                                      | Whole bio-oil  | <sup>13</sup> C NMR                        |
| Norwegian spruce <sup>367</sup>                    | Fast pyrolysis                                     | Hydrothermal deoxygenation             | Whole bio-oil  | <sup>31</sup> P NMR                        |
| Pine wood <sup>368</sup>                           | Fast pyrolysis                                     | Acid-catalyzed reaction                | Whole bio-oil  | <sup>1</sup> H NMR                         |
| Pine wood <sup>369</sup>                           | Fast pyrolysis                                     | -                                      | Pyrolytic lignin   | <sup>1</sup> H NMR                         |
| Ash wood, birch wood <sup>21</sup>                 | Fast pyrolysis                                     | -                                      | Accelerated aged whole bi-oil                                      | <sup>13</sup> C NMR                        |
| Forestry residue <sup>370</sup>                    | Fast pyrolysis                                     | Hydrodeoxygenation                     | Water-insoluble phase  | <sup>1</sup> H NMR                         |
| Jute dust <sup>371</sup>                           | Slow pyrolysis                                     | -                                      | Water free bi-oil  | <sup>1</sup> H NMR                         |
| <i>Pongamia glabra</i> deoiled cake <sup>372</sup> | Slow pyrolysis                                     | -                                      | Organic phase  | <sup>1</sup> H, <sup>13</sup> C NMR        |
| Apricot kernel shell <sup>373</sup>                | Slow pyrolysis                                     | -                                      | Water-insoluble phase  | <sup>1</sup> H NMR                         |
| Beech <sup>374</sup>                               | Fast pyrolysis                                     | -                                      | Heavy fraction, light fraction, aerosol                            | <sup>1</sup> H NMR                         |
| Softwood kraft lignin <sup>123</sup>               | Microwave pyrolysis                                | -                                      | Phenols extracted from crude bio-oil, organic solvent subfractions | <sup>13</sup> C, <sup>31</sup> P NMR       |
| Softwood kraft lignin <sup>375</sup>               | Zeolite-catalyzed slow pyrolysis                   | -                                      | Heavy fraction   | <sup>13</sup> C, <sup>31</sup> P, HSQC-NMR |
| Pine wood <sup>100</sup>                           | Slow pyrolysis                                     | -                                      | Heavy fraction   | <sup>19</sup> F NMR                        |



**Table 7.** (Continued)

| <b>Feedstock</b>   | <b>Pyrolysis method</b>                     | <b>Post pyrolysis upgrading method</b>                     | <b>Fraction analyzed by NMR</b>  | <b>NMR technique</b>                                 |
|--|---|--|--|--|
| Almond shell <sup>376</sup>  | Co-pyrolysis with high-density polyethylene | -  | Organic phase  | <sup>1</sup> H NMR                                   |
| Pine wood residue, timothy grass residue, wheat straw residue <sup>377</sup> | Slow pyrolysis                              | -  | Whole bio-oil  | <sup>1</sup> H, <sup>13</sup> C NMR                  |
| Beech wood <sup>378</sup>  | Fast pyrolysis                              | -  | Pyrolytic lignin   | <sup>1</sup> H NMR                                   |
| Spruce wood chips, waste paper, paper deinking residue <sup>379</sup>        | Microwave pyrolysis                         | Curing in oven, for adhesive properties analysis           | Cured bio-oil scrapings  | <sup>13</sup> C CP/MAS NMR                           |
| Rice husk <sup>380</sup>   | Fast pyrolysis                              | Catalytic hydrotreatment and esterification                | Crude whole bio-oil, upgraded whole bio-oil  | <sup>13</sup> C NMR                                  |
| Loblolly pine wood <sup>107</sup>  | Fast pyrolysis                              | Catalytic deoxygenation of oxidized bio-oil with syngas    | Oxidized bio-oil, partial deoxygenated bio-oil, fully deoxygenated bio-oil                     | <sup>1</sup> H NMR                                   |
| <i>Arundo donax</i> L. <sup>381</sup>  | Slow pyrolysis                              | -  | Organic phase  | <sup>1</sup> H, <sup>13</sup> C NMR                  |
| <i>Fraxinus excelsior</i> L. <sup>382</sup>                                  | Slow pyrolysis following heat pretreatment  | -  | Diethyl ether extracts   | <sup>1</sup> H NMR                                   |
| Jatropha curcas cake <sup>122</sup>  | Fast pyrolysis                              | Hydrodeoxygenation, catalytic cracking with vacuum gas oil | Crude heavy fraction, deoxygenated heavy fraction, fluid catalytic cracking liquid distillates | <sup>1</sup> H, <sup>13</sup> C, <sup>31</sup> P NMR |

**Table 7.** (Continued)

| <b>Feedstock</b>   | <b>Pyrolysis method</b>                        | <b>Post pyrolysis upgrading method</b> | <b>Fraction analyzed by NMR</b>   | <b>NMR technique</b>   |
|--|--|--|---|--|
| Loblolly pine wood <sup>155</sup>  | Fast pyrolysis following torrefaction          | -                                      | Accelerated aged whole bio-oil  | <sup>13</sup> C NMR  |
| Saccharina japonica <sup>383</sup>   | Fast pyrolysis                                 | -                                      | Whole bio-oil   | <sup>1</sup> H, <sup>13</sup> C NMR  |
| Wheat straw, wheat husk <sup>384</sup>   | Slow pyrolysis, catalyzed slow pyrolysis       | -                                      | Whole bio-oil   | <sup>1</sup> H NMR   |
| Wood pallet, corn stover, miscanthus and swine manure <sup>385</sup>             | Slow pyrolysis                                 | -                                      | Water-insoluble fraction  | <sup>1</sup> H, <sup>13</sup> C NMR  |
| Switchgrass <sup>130</sup>   | Fast pyrolysis                                 | -                                      | Pyrolytic lignin  | <sup>1</sup> H- <sup>13</sup> C HSQC, <sup>1</sup> H- <sup>13</sup> C HMBS, <sup>13</sup> C DEPT |
| Switchgrass, equine manure <sup>386</sup>  | Fast pyrolysis, tail-gas reactive pyrolysis    | -                                      | Distillation residues   | <sup>1</sup> H, <sup>13</sup> C NMR  |
| Wheat straw <sup>387</sup>   | Fast pyrolysis                                 | Catalytic hydrodeoxygenation           | Light phase   | <sup>1</sup> H NMR   |
| <i>Mesua ferrea</i> seed cover, <i>Pongamia glabra</i> seed cover <sup>388</sup> | Slow pyrolysis                                 | -                                      | Organic phase, <i>n</i> -hexane extracts, toluene extracts, ethyl acetate extracts, methanol extracts | <sup>1</sup> H NMR   |
| Rice straw <sup>389</sup>  | Slow pyrolysis                                 | -                                      | Organic fraction  | <sup>1</sup> H NMR   |
| Pine wood, sugarcane bagasse <sup>106</sup>                                      | Fast pyrolysis, ZSM-5-catalyzed fast pyrolysis | -                                      | Whole bio-oil   | <sup>1</sup> H NMR   |
| Switchgrass <sup>112</sup>   | Microwave pyrolysis                            | -                                      | Liquid nitrogen trapped bio-oil   | <sup>13</sup> C NMR  |

**Table 7.** (Continued)

| <b>Feedstock</b>                 | <b>Pyrolysis method</b> | <b>Post pyrolysis upgrading method</b> | <b>Fraction analyzed by NMR</b>  | <b>NMR technique</b> |
|----------------------------------|-------------------------|--|--|----------------------|
| Mahua seed <sup>390</sup>        | Slow pyrolysis          | -                                      | Water immiscible phase   | <sup>1</sup> H NMR   |
| Cotton residue <sup>391</sup>    | Slow pyrolysis          | -                                      | Organic fraction   | <sup>1</sup> H NMR   |
| Red pine <sup>392</sup>          | Fast pyrolysis          | -                                      | Supercritical-CO <sub>2</sub> -extracted fractions   | <sup>1</sup> H NMR   |
| Spruce wood chips <sup>115</sup> | Microwave pyrolysis     | -                                      | Whole bio-oil, water-soluble extract, neutral extract, phenolic extract, organic acids extract | <sup>13</sup> C NMR  |

**Table 8.** Composition of the  $^1\text{H}$  NMR Chemical Shift Integration Regions of Bio-oil.<sup>98, 102,</sup>

104-105

| Assignments  | Chemical shift ranges (ppm) <sup>104</sup> | Assignments                                       | Chemical shift ranges (ppm) <sup>98</sup> | Assignments  | Chemical shift ranges (ppm) <sup>102</sup> |
|--|--|---|---|--|--|
| $-\text{CHO}$ , $-\text{COOH}$ ,<br>downfield $\text{ArH}$                                   | 10.0-8.0                                   | Aldehydes   | 10.1-9.5                                  | $-\text{COOH}$   | 12.5-11.0                                  |
| $\text{ArH}$ , $\text{HC}=\text{C}$ -<br>(conjugated)  | 8.0-6.8                                    | (Hetero-) aromatics                               | 8.5-6.0                                   | $-\text{CHO}$ , $\text{ArOH}$  | 11.0-8.25                                  |
| $\text{HC}=\text{C}$ - (non-conjugated)  | 6.8-6.4                                    | Methoxy, carbohydrates                            | 6.0-4.4                                   | Aromatics, conjugated – $\text{C}=\text{C}$ -                                      | 8.25-6.0                                   |
| $\text{CHO}$ , $\text{ArOH}$ ,<br>$\text{HC}=\text{C}$ - (non-conjugated)                    | 6.4-4.2                                    | Alcohols, methylene-dibenzene                     | 4.4-3.0                                   | Aliphatic $\text{OH}$ , $-\text{C}=\text{C}$ -, $\text{Ar}-\text{CH}_2-\text{O}$ - | 6.0-4.2                                    |
| $\text{CH}_3\text{O}$ , $-\text{CH}_2\text{O}$ ,<br>$\text{CHO}$                             | 4.2-3.0                                    | Aliphatics $\alpha$ to heteroatom or unsaturation | 3.0-1.5                                   | Ether, methoxy   | 4.2-3.0                                    |
| $\text{CH}_3\text{C}=\text{O}$ ,<br>$\text{CH}_3-\text{Ar}$ , $-\text{CH}_2-$<br>$\text{Ar}$ | 3.0-2.2                                    | Alkanes   | 1.5-0.5                                   | $-\text{CH}_2\text{C}=\text{O}$ ,<br>aliphatics                                    | 3.0-2.0                                    |
| $\text{CH}_2$ , aliphatic<br>$\text{OH}$   | 2.2-1.6                                    | -   | -   | Aliphatics   | 2.0-0.0                                    |
| $-\text{CH}_3$ , $\text{CH}_2$   | 1.6-0.0                                    | -   | -   | -  | -  |

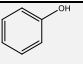
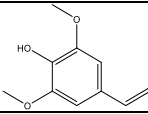
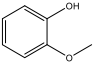
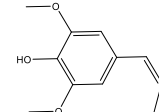
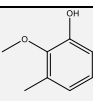
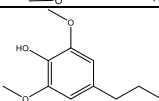
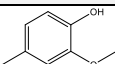
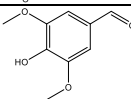
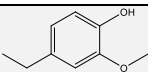
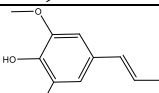
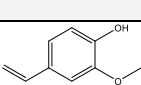
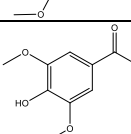
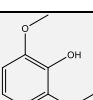
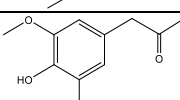
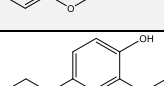
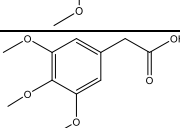
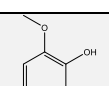
**Table 9.** Comparison of  $^{13}\text{C}$  NMR Chemical Shift Integration Regions of Bio-oil.<sup>102, 104</sup>

| Assignments      | Chemical shift ranges (ppm) <sup>102</sup> | Assignments        | Chemical shift ranges (ppm) <sup>104</sup> |
|------------------|--|--------------------|--|
| Carbonyls        | 215-163                                    | Carbonyls          | 215-163                                    |
| Aromatics        | 163-110                                    | Aromatics, alkenes | 163-103                                    |
| Carbohydrates    | 110-84                                     | Carbohydrates      | 103-70                                     |
| Methoxy/hydroxyl | 84-54                                      | Methoxy/hydroxyl   | 70-54                                      |
| General          | 54-0                                       | Alkyl              | 54-0                                       |
| Alkyl            | Mostly secondary and tertiary carbons      | 34-24              |  |
|                  | Mostly primary and some secondary carbons  | 24-6               |  |

**Table 10.** Chemical Shift Assignments for Bio-oils after Derivatization with TMDPUsing NHND as an Internal Standard in a  $^{31}\text{P}$  NMR Spectrum.<sup>119</sup>

| Assignments   |            | Chemical shifts (ppm) |
|---|------------|-----------------------|
| <i>endo-N</i> -hydroxy-5-norbornene-2,3-dicarboximide (internal standard) |            | 152.8-151.0           |
| Aliphatic OH  |            | 150.0-145.5           |
| C5-substituted condensed phenolic OH                                      | $\beta$ -5 | 144.7-142.8           |
|   | 4-O-5      | 142.8-141.7           |
|   | 5-5        | 141.7-140.2           |
| Guaiacyl phenolic OH  |            | 140.2-139.0           |
| Catechol type OH  |            | 139.0-138.2           |
| <i>p</i> -Hydroxyphenyl OH  |            | 138.2-137.3           |
| Acid-OH   |            | 136.6-133.6           |
| Water peak  |            | 133.1-131.3           |
|   |            | 16.9-15.1             |

**Table 11.** The detected monomeric phenols from the decomposition of lignin in ethanol at 350 °C.<sup>51</sup>

| Name of monomeric phenols | Structure   | Name of monomeric phenols         | Structure   |
|---------------------------|---|-----------------------------------|---|
| phenol                    |    | 4-vinylsyringol                   |    |
| guaiacol                  |    | cis-4-propenylsyringol            |    |
| 3-methylguaiacol          |    | 4-propylsyringol                  |    |
| 4-methylguaiacol          |    | syringaldehyde                    |    |
| 4-ethylguaiacol           |    | trans-4-propenylsyringol          |    |
| 4-vinylguaiacol           |   | acetosyringone                    |   |
| syringol                  |  | syringyl acetone                  |  |
| 4-propylguaiacol          |  | 3,4,5-trimethoxyphenylacetic acid |  |
| 4-methylsyringol          |  |                                   |   |

**Table 12.** Molecular weight of bio-oils from pyrolysis and liquefaction reported in the literature.

| <b>Thermochemical processing methods</b> | <b>Biomass feedstock</b>                             | <b>Catalyst applied</b>              | <b>M<sub>n</sub> (g/mol)</b> | <b>M<sub>w</sub> (g/mol)</b> |
|--|--|--------------------------------------|------------------------------|------------------------------|
| Pyrolysis                                | pine <sup>393</sup>                                  | zeolite                              | 91~170                       | 160~447                      |
| Pyrolysis                                | Miscanthus; corn stover; wood pellets <sup>385</sup> | N/A                                  | 137-192                      | 610~1035                     |
| Liquefaction                             | Swine manure <sup>385</sup>                          | N/A                                  | 1011                         | 2978                         |
| Pyrolysis                                | Pine <sup>394</sup>                                  | N/A                                  | 109-145                      | 393~632                      |
| Pyrolysis                                | Pine <sup>395</sup>                                  | Ni-Cu; Ru-C                          | N/A                          | 380~1050                     |
| Pyrolysis                                | Humin (crude; synthetic) <sup>396</sup>              | N/A                                  | 50~240                       | N/A                          |
| Pyrolysis                                | Beech wood <sup>396</sup>                            | zeolite                              | N/A                          | 321~401                      |
| Pyrolysis                                | Lignin <sup>397</sup>                                | Pd/C                                 | 467~514                      | 836~925                      |
| Liquefaction (hydrogenolysis)            | Lignin <sup>397</sup>                                | Pd/C                                 | 390~597                      | 1157~1182                    |
| Liquefaction                             | Birch wood <sup>398</sup>                            | Hydrotalcite, KOH, FeSO <sub>4</sub> | 362~383                      | 633~856                      |
| Liquefaction                             | Lignin <sup>399</sup>                                | Sulfuric acid                        | 132~371                      | 249~797                      |



**Table 13.** The proximate and ultimate analyses of the grape seeds.

|   |                           |       |
|---|---------------------------|-------|
| <b>Proximate analyses (wt %, as received)</b> | Moisture                  | 7.62  |
|   | Volatile matter           | 77.51 |
|   | Fixed carbon <sup>a</sup> | 12.30 |
|   | Ash                       | 2.57  |
| <b>Ultimate analyses (wt %, dry basis)</b>    | C                         | 51.69 |
|   | H                         | 7.51  |
|   | N                         | 1.98  |
|   | O <sup>b</sup>            | 38.83 |
|   | HHV (MJ/kg)               | 21.26 |
| <b>Component analyses (wt %)</b>              | extractives               | 17.14 |
|   | $\alpha$ -cellulose       | 17.93 |
|   | holocellulose             | 43.89 |
|   | lignin                    | 40.19 |

<sup>a,b</sup> calculated by difference

**Table 14.** The proximate and ultimate analyses of the fir woods.

|                                  |                           |       |
|----------------------------------|---------------------------|-------|
| <b>Proximate analysis (wt %)</b> | Moisture                  | 7.56  |
|                                  | Volatile matter           | 80.24 |
|                                  | Fixed carbon <sup>a</sup> | 11.35 |
|                                  | Ash                       | 0.85  |
| <b>Ultimate analysis (wt %)</b>  | C                         | 46.30 |
|                                  | H                         | 6.49  |
|                                  | N                         | 0.10  |
|                                  | Ob                        | 47.11 |
|                                  | HHV (MJ/kg)               | 16.51 |
| <b>Component analysis (wt %)</b> | Extractives               | 2.73  |
|                                  | $\alpha$ -cellulose       | 44.82 |
|                                  | Holocellulose             | 76.77 |
|                                  | Lignin                    | 26.34 |

<sup>a</sup>By difference [100 - (Moisture (%) + Volatile matter (%) + Ash (%))]

<sup>b</sup>By difference [100 - (C (%) + H (%) + N (%))]

**Table 15.** An example of the relation between the temperature and pressure during the autohydrolysis pretreatment.

| <b>Reaction temperature (°C)</b> | <b>Corresponding pressures (Pa)</b>        |
|----------------------------------|--|
| 180                              | $8.27 \times 10^5 \sim 9.65 \times 10^5$   |
| 200                              | $12.41 \times 10^5 \sim 13.79 \times 10^5$ |

**Table 16.** Comparison of the lignin and carbohydrates contents of untreated (control) and autohydrolysis pretreated pine wood (wt%).<sup>a</sup>

| <b>Sample</b> | <b>Glucose</b> | <b>Xylose</b> | <b>Galactose</b> | <b>Arabinose</b> | <b>Mannose</b> | <b>Acid insoluble lignin</b> |
|---------------|----------------|---------------|------------------|------------------|----------------|------------------------------|
| Control       | 39.88          | 5.71          | 2.11             | 1.10             | 9.71           | 32.06                        |
| Pretreated    | 42.54          | 3.47          | 0.08             | 0.51             | 3.09           | 46.11                        |

<sup>a</sup>The contents are presented as the percentages of the wood samples.

**Table 17.** Assignment of FT-IR spectra in a region of 1750 – 1000  $\text{cm}^{-1}$  for pine wood samples.

| Peak No. in<br>Figure 15 | Peak ( $\text{cm}^{-1}$ ) | Assignment                                  |
|--------------------------|---------------------------|---|
| 1                        | 1738                      | C=O in hemicellulose                        |
| 2                        | 1660                      | Absorbed O-H and conjugated C=O             |
| 3                        | 1600                      | Aromatic skeletal vibration                 |
| 4                        | 1511                      | Aromatic skeletal vibration                 |
| 5                        | 1462                      | C-H deformation in lignin and carbohydrates |
| 6                        | 1423                      | C-H deformation in lignin and carbohydrates |
| 7                        | 1375                      | Aliphatic C-H stretching in $\text{CH}_3$   |
| 8                        | 1335/1320                 | C-O stretching in syringyl derivatives      |
| 9                        | 1266                      | Guaiacyl ring breathing                     |
| 10                       | 1230/1205                 | C-O stretching                              |
| 11                       | 1162                      | C-O-C vibration                             |
| 12                       | 1110                      | Aromatic skeletal and C-O stretching        |
| 13                       | 1060                      | C-O stretch in cellulose and hemicellulose  |
| 14                       | 1032                      | Aromatic C-H in plane deformation           |

**Table 18.** Structural detection of the individual compounds in bio-oils by GC-MS analysis.

| Time [min] | Compounds  | Py-500 °C |        |        |        | Py-600 °C |        |        |        |
|------------|--|-----------|--------|--------|--------|-----------|--------|--------|--------|
|            |  | control   | 180-10 | 180-40 | 200-40 | control   | 180-10 | 180-40 | 200-40 |
| 1.95       | Acetic acid  | 3.60      | 1.49   | 0.52   | 0.63   | 3.46      | 2.08   | 0.98   | 0.61   |
| 2.20       | 2-Propanone, 1-hydroxy-                                  | 1.13      | 0.33   | 0.19   | 0.39   | 1.03      | 0.51   | 0.43   | 0.42   |
| 3.75       | 1-Hydroxy-2-butanone                                     | 0.24      | n.d.   | n.d.   | n.d.   | 0.22      | n.d.   | n.d.   | n.d.   |
| 3.84       | Acetic acid, methyl ester                                | 0.48      | n.d.   | n.d.   | n.d.   | 0.21      | n.d.   | n.d.   | n.d.   |
| 4.08       | Butanedial   | 0.43      | n.d.   | n.d.   | n.d.   | 0.19      | n.d.   | n.d.   | n.d.   |
| 4.30       | Propanoic acid, 2-oxo-, methyl ester                     | 0.61      | 0.19   | 0.12   | 0.17   | 0.39      | 0.28   | 0.23   | 0.17   |
| 5.72       | 4-Hydroxy-4-methyl-2-pentanone                           | 0.53      | n.d.   | 0.24   | 0.15   | 0.35      | 0.15   | 0.13   | 0.10   |
| 8.39       | 1,2-Cyclopentanedione                                    | 3.17      | 0.88   | 0.72   | 0.89   | 2.52      | 1.12   | 0.95   | 0.74   |
| 10.77      | 4-Hydroxy-5,6-dihydro-(2H)-pyran-2-one                   | 1.27      | 2.19   | 1.01   | 0.36   | 1.18      | 2.37   | 1.11   | 0.26   |
| 11.81      | 2-Cyclopenten-1-one, 2-hydroxy-3-methyl-                 | 1.79      | 0.68   | 1.02   | 1.09   | 1.72      | 0.73   | 0.73   | 0.78   |
| 13.51      | Furyl hydroxymethyl ketone                               | 0.11      | 0.20   | 0.15   | 0.26   | 0.22      | 0.21   | 0.19   | 0.19   |
| 14.55      | Maltol   | 0.58      | 0.32   | 0.38   | 0.40   | 0.29      | 0.34   | 0.39   | 0.27   |
| 14.72      | 2-Cyclopenten-1-one, 2-hydroxy-3-ethyl-                  | 0.56      | 0.20   | n.d.   | n.d.   | 0.38      | n.d.   | n.d.   | n.d.   |
| 15.52      | 4H-Pyran-4-one, 2,3-dihydro-3,5-dihydroxy-6-methyl-      | 0.31      | 0.30   | 0.21   | 0.32   | n.d.      | n.d.   | n.d.   | 0.17   |
| 17.20      | 4H-Pyran-4-one, 3,5-dihydroxy-2-methyl-                  | 0.24      | 1.08   | 1.80   | 3.36   | 0.38      | 1.17   | 1.71   | 2.23   |
|            | <b>Total of acid, Ketone, or aldehyde type compounds</b> | 15.05     | 7.87   | 6.35   | 8.00   | 12.54     | 8.96   | 6.86   | 5.95   |
| 5.39       | Furfural   | 0.83      | 0.76   | 0.38   | 0.47   | 0.78      | 0.74   | 0.47   | 0.39   |
| 6.20       | 2-Furanmethanol  | 1.46      | 0.25   | 0.21   | 0.16   | 1.28      | 0.13   | 0.12   | 0.22   |
| 6.54       | Acetol acetate   | 0.40      | 0.18   | 0.23   | 0.29   | 0.45      | 0.22   | 0.16   | 0.25   |
| 8.00       | 2(5H)-Furanone   | 0.75      | 0.10   | 0.11   | n.d.   | 0.63      | 0.10   | 0.14   | n.d.   |
| 9.51       | 2-Furancarboxaldehyde, 5-methyl-                         | 0.28      | 0.50   | 0.40   | 0.51   | 0.61      | 0.60   | 0.48   | 0.52   |
| 13.58      | 4-hydroxy-2,5-dimethyl-3(2H)-furanone                    | 0.26      | 0.35   | 0.55   | 0.61   | 0.46      | 0.42   | 0.45   | 0.31   |
| 18.50      | 2-Furancarboxaldehyde, 5-(hydroxymethyl)-                | 0.59      | 2.25   | 3.13   | 4.83   | 0.23      | 1.98   | 2.59   | 2.34   |
|            | <b>Total of furan type compounds</b>                     | 4.56      | 4.39   | 4.99   | 6.87   | 4.43      | 4.19   | 4.41   | 4.04   |
| 10.32      | Phenol   | 1.20      | 0.66   | 0.50   | 0.90   | 1.33      | 2.37   | 0.69   | 0.98   |
| 12.66      | Phenol, 2-methyl-  | 0.55      | 0.28   | 0.22   | 0.35   | 0.53      | 0.31   | 0.26   | 0.40   |
| 13.35      | Phenol, 4-methyl-  | 1.50      | 1.09   | 0.95   | 1.37   | 1.52      | 1.17   | 1.02   | 1.39   |

**Table 18.** (Continued)

| Time<br>[min] | Compounds                                   | Py-500 °C   |            |            |            | Py-600 °C   |            |            |            |
|---------------|---|-------------|------------|------------|------------|-------------|------------|------------|------------|
|               |   | contro<br>l | 180-<br>10 | 180-<br>40 | 200-<br>40 | contro<br>l | 180-<br>10 | 180-<br>40 | 200-<br>40 |
| 13.65         | Phenol, 2-methoxy-                          | 1.43        | 0.74       | 0.57       | 0.86       | 0.62        | 0.49       | 0.62       | 0.64       |
| 15.63         | Phenol, 2,4-dimethyl-                       | 0.38        | 0.57       | 0.40       | 0.54       | 0.43        | 0.59       | 0.54       | 0.50       |
| 16.03         | 2,3-Dihydroxybenzaldehyde                   | 0.97        | n.d.       | n.d.       | n.d.       | 0.68        | 0.26       | n.d.       | n.d.       |
| 16.21         | Phenol, 4-ethyl-                            | 2.41        | 1.11       | 0.94       | 1.74       | 2.28        | 1.23       | 1.09       | 1.83       |
| 16.32         | Phenol, 3,4-dimethyl-                       | 0.27        | 0.12       | 0.10       | 0.12       | 0.41        | 0.17       | 0.19       | 0.10       |
| 16.91         | Phenol, 2-methoxy-4-methyl-                 | 1.28        | 2.76       | 2.94       | 3.79       | 1.19        | 1.85       | 2.98       | 2.78       |
| 17.60         | 1,2-Benzenediol                             | 2.47        | 0.82       | 0.86       | 1.41       | 3.22        | 1.10       | 1.00       | 1.48       |
| 17.91         | 4-vinylphenol                               | 13.95       | 6.87       | 6.03       | 5.99       | 12.92       | 7.80       | 6.69       | 4.27       |
| 19.10         | 1,2-Benzenediol, 3-methoxy-                 | 1.24        | 0.58       | 0.89       | 1.39       | 1.14        | 0.81       | 0.94       | 0.96       |
| 19.20         | 1,2-Benzenediol, 3-methyl-                  | 0.55        | 0.22       | 0.29       | 0.73       | 0.77        | 0.34       | 0.31       | 0.51       |
| 19.49         | Phenol, 4-ethyl-2-methoxy-                  | 1.09        | 0.53       | 0.62       | 1.26       | 1.05        | 0.49       | 0.44       | 0.39       |
| 20.07         | 1,2-Benzenediol, 4-methyl-                  | 0.35        | 0.17       | 0.43       | 0.44       | 0.83        | 0.75       | 0.59       | 1.25       |
| 20.54         | 2-Methoxy-4-vinylphenol                     | 5.32        | 2.67       | 2.14       | 2.24       | 4.18        | 2.47       | 2.14       | 1.35       |
| 21.65         | Phenol, 2,6-dimethoxy-                      | 3.69        | 1.33       | 1.88       | 2.35       | 2.88        | 1.36       | 1.69       | 1.44       |
| 21.88         | Phenol, 3,4-dimethoxy-                      | 0.42        | 0.28       | 0.32       | 0.49       | 0.40        | 0.37       | 0.33       | 0.43       |
| 22.19         | Benzaldehyde, 4-hydroxy-                    | 0.91        | n.d.       | n.d.       | n.d.       | 0.85        | n.d.       | n.d.       | n.d.       |
| 22.97         | Vanillin                                    | 0.84        | 0.46       | 0.43       | 0.56       | 1.18        | 0.41       | 0.45       | 0.52       |
| 24.21         | Phenol, 4-methyl-2,6-dimethoxy              | 2.77        | 1.81       | 2.16       | 2.67       | 2.55        | 1.92       | 2.17       | 1.69       |
| 24.24         | trans-Isoeugenol                            | 0.56        | 0.24       | 0.35       | 0.39       | 0.35        | 0.21       | 0.29       | 0.35       |
| 24.55         | Homovanillin                                | 0.15        | 0.19       | 0.19       | 0.17       | 0.18        | 0.19       | 0.18       | 0.13       |
| 25.26         | Acetovanillone                              | 0.36        | 0.18       | 0.21       | 0.30       | 0.25        | 0.18       | 0.20       | 0.21       |
| 26.08         | 3,4-Dihydro-6-hydroxy-2H-1-benzopyran-2-one | 0.84        | 0.34       | n.d.       | 0.23       | 0.78        | 0.29       | 0.13       | 0.13       |
| 26.23         | Syringol, 4-ethyl-                          | 0.62        | 0.57       | 0.47       | 0.79       | 0.68        | 0.62       | 0.76       | 0.41       |
| 26.40         | Guaiacylacetone                             | 0.50        | 0.49       | 0.17       | 0.26       | 0.32        | 0.33       | 0.25       | 0.15       |
| 27.22         | Syringol, 4-vinyl-                          | 2.77        | 2.26       | 2.14       | 1.12       | 2.91        | 2.53       | 2.49       | 1.82       |
| 28.13         | Phenol, 2,6-dimethoxy-4-(2-propenyl)-       | 0.60        | 0.46       | 0.35       | 0.30       | 0.78        | 0.39       | 0.57       | 0.28       |
| 28.28         | Syringol, 4-propyl-                         | 0.28        | 0.53       | 0.39       | 0.38       | 0.32        | 0.43       | 0.45       | 0.33       |
| 29.29         | Phenol, 2,6-dimethoxy-4-(2-propenyl)-       | 0.59        | 0.33       | 0.33       | 0.36       | 0.87        | 0.50       | 0.52       | 0.36       |
| 29.56         | Benzaldehyde, 4-hydroxy-3,5-dimethoxy-      | 0.60        | 0.48       | 0.35       | 0.34       | 0.68        | 0.59       | 0.57       | 0.42       |
| 30.46         | Phenol, 2,6-dimethoxy-4-(2-propenyl)-       | 2.85        | 1.47       | 1.38       | 1.54       | 2.39        | 1.58       | 1.63       | 1.00       |
| 31.26         | Acetosyringone                              | 0.97        | 0.45       | 0.67       | 2.05       | 0.85        | 0.41       | 0.49       | 1.89       |
| 32.11         | Syringyl acetone                            | 1.17        | 0.70       | 0.71       | 0.67       | 0.84        | 0.58       | 0.63       | 0.44       |

**Table 18.** (Continued)

| Time<br>[min] | Compounds                                    | Py-500 °C   |            |            | Py-600 °C  |             |            |            |            |
|---------------|--|-------------|------------|------------|------------|-------------|------------|------------|------------|
|               |  | contro<br>l | 180-<br>10 | 180-<br>40 | 200-<br>40 | contro<br>l | 180-<br>10 | 180-<br>40 | 200-<br>40 |
|               | <b>Total of phenol type<br/>compounds</b>    | 56.47       | 31.7<br>4  | 30.3<br>7  | 38.0<br>9  | 53.16       | 35.0<br>9  | 33.3<br>1  | 30.8<br>4  |
| 14.00         | anhydrosugar(unknown<br>)                    | 1.88        | 0.25       | 0.31       | 0.42       | 1.92        | 0.25       | 0.26       | 0.32       |
| 18.82         | anhydrosugar(unknown<br>)                    | 0.18        | 1.24       | 0.81       | 0.56       | 0.33        | 1.44       | 0.69       | 0.33       |
| 19.90         | anhydrosugar(unknown<br>)                    | 0.60        | 1.48       | 2.78       | 3.37       | 1.97        | 1.59       | 0.78       | 0.60       |
| 28.00         | .beta.-D-<br>Glucopyranose, 1,6-<br>anhydro- | 10.20       | 44.8<br>9  | 46.9<br>7  | 30.7<br>3  | 14.53       | 40.6<br>1  | 45.0<br>6  | 49.1<br>1  |
| 30.80         | 1,6-Anhydro- $\alpha$ -D-<br>galactofuranose | 0.27        | 1.60       | 1.90       | 1.67       | 0.34        | 1.67       | 1.68       | 1.28       |
|               | <b>Total of other<br/>compounds</b>          | 13.13       | 49.4<br>6  | 52.7<br>7  | 36.7<br>5  | 19.08       | 45.5<br>4  | 48.4<br>7  | 51.6<br>4  |



**Table 19.** Effect of B:C ratio and upgrading temperature on molecular weight distribution of bio-oil.

|                                 |               | <b>Mn</b> | <b>Mw</b> | <b>PDI</b> |
|---------------------------------|---------------|-----------|-----------|------------|
| Effect of B:C ratio             |               |           |           |            |
|                                 | FP            | 289       | 488       | 1.69       |
| Bottom                          | 550°C B:C 1.8 | 132       | 297       | 2.25       |
|                                 | 550°C B:C 1.4 | 120       | 251       | 2.08       |
|                                 | 550°C B:C 1.0 | 108       | 197       | 1.82       |
| Top                             | 550°C B:C 1.8 | 94.5      | 141       | 1.48       |
|                                 | 550°C B:C 1.4 | 98.8      | 161       | 1.63       |
|                                 | 550°C B:C 1.0 | 90.0      | 124       | 1.38       |
| Effect of upgrading temperature |               |           |           |            |
| Bottom                          | 500°C B:C 1.4 | 131       | 291       | 2.22       |
|                                 | 550°C B:C 1.4 | 120       | 251       | 2.08       |
|                                 | 600°C B:C 1.4 | 112       | 219       | 1.96       |
| Top                             | 500°C B:C 1.4 | 96.1      | 165       | 1.71       |
|                                 | 550°C B:C 1.4 | 98.8      | 161       | 1.63       |
|                                 | 600°C B:C 1.4 | 86.6      | 122       | 1.41       |

**Table 20.** Identified compounds in bio-oils from the hydrothermal processing of grape seed without and with additive (MgCl<sub>2</sub>:TiCl<sub>4</sub>). (T=300 °C, t=30 min, PH<sub>2</sub>int.=2 MPa)

| Retention time (min) | Compounds                              | Peak area (%)    |            |            |            |
|----------------------|--|------------------|------------|------------|------------|
|                      |  | without additive | 1:1 (mmol) | 2:2 (mmol) | 4:4 (mmol) |
| 2.23                 | Acetic acid                            | 0.31             | 0.37       | -          | 0.48       |
| 3.74                 | 1,3-Diazine                            | 0.07             | -          | -          | -          |
| 3.92                 | (E)-2-Methyl-2-butenal                 | 0.06             | -          | -          | -          |
| 4.07                 | 2,4-Pentadienenitrile                  | 0.13             | -          | -          | -          |
| 5.27                 | Cyclopentanone                         | 0.26             | 0.16       | 0.1        | 0.25       |
| 6.48                 | 2-Methylpyridine                       | 0.13             | -          | -          | -          |
| 6.66                 | Methylpyrazine                         | 0.31             | 0.12       | -          | -          |
| 7.14                 | 2-Cyclopenten-1-one                    | 0.33             | 0.25       | 0.25       | 0.62       |
| 7.83                 | 3-Methylcyclopentanone                 | 0.03             | -          | -          | -          |
| 10.76                | 2-Heptanone                            | 0.05             | -          | -          | 0.12       |
| 11.67                | 2-Methyl-2-cyclopenten-1-one           | 0.76             | 0.71       | 0.61       | 1.09       |
| 12.22                | 2,5-Dimethylpyrazine                   | 0.04             | -          | -          | -          |
| 12.41                | 1-(2-Furanyl)ethanone                  | -                | -          | 0.08       | 0.06       |
| 12.60                | Butyrolactone                          | 0.31             | 0.24       | 0.28       | 0.38       |
| 17.55                | 3-Methyl-2-cyclopenten-1-one           | 0.6              | 0.38       | 0.3        | 0.44       |
| 20.52                | 1-Methyl-2-methylenecyclohexane        | 0.05             | -          | -          | -          |
| 20.73                | 2-Octanone                             | -                | -          | -          | 0.2        |
| 20.75                | 6-Methyl-2-heptanone                   | -                | 0.13       | 0.15       | -          |
| 20.87                | 4-Oxo-pentanoic acid methyl ester      | -                | -          | -          | 0.04       |
| 20.97                | 2,3-dimethyl-2-cyclopenten-1-one       | 0.13             | -          | -          | -          |
| 22.29                | Phenol                                 | 0.39             | 0.28       | 0.24       | 0.37       |
| 23.66                | Hexanoic acid                          | -                | -          | 0.25       | 0.36       |
| 24.46                | 2-Hydroxy-3-methyl-2-cyclopenten-1-one | -                | -          | -          | 0.21       |
| 24.47                | 3-Methyl-1,2-cyclopentanedione         | 0.08             | -          | 0.18       | -          |
| 24.74                | 2,3-Dimethyl-2-cyclopenten-1-one       | 0.24             | 0.18       | 0.15       | 0.18       |
| 29.64                | 2-Methoxyphenol                        | 8.11             | 6.47       | 4.65       | 4.48       |
| 29.97                | 1-Methyl-2,5-pyrrolidinedione          | 0.19             | 0.17       | -          | -          |
| 32.03                | 4-Oxo-pentanoic acid                   | -                | -          | -          | 2.49       |
| 36.95                | 2-Acetyl-cyclopentanone                | -                | -          | -          | 0.11       |
| 37.62                | 2-Methoxy-4-methylphenol               | 1.15             | 1.04       | 0.78       | 0.64       |
| 43.77                | 4-Ethyl-2-methoxyphenol                | 1.58             | 1.38       | 0.94       | 0.58       |
| 49.60                | 2-Methoxy-4-propylphenol               | 0.49             | 0.35       | 0.21       | -          |
| 57.11                | 1-(4-Hydroxy-3-methoxyphenyl)ethanone  | 0.66             | 0.37       | 0.43       | 0.3        |
| 59.75                | 4-Hydroxy-3-methoxybenzeneacetic acid  | -                | 0.65       | -          | 1.72       |
| 70.57                | 1,11-Dodecadiene                       | -                | -          | 0.22       | -          |

**Table 20.** (Continued)

| Retention time<br>(min) | Compounds                                | Peak area (%)       |               |               |               |
|-------------------------|--|---------------------|---------------|---------------|---------------|
|                         |  | without<br>additive | 1:1<br>(mmol) | 2:2<br>(mmol) | 4:4<br>(mmol) |
| 70.58                   | (Z)-Cyclodecene                          | -                   | -             | -             | 0.4           |
| 71.62                   | (E,Z)-2,4-Dodecadiene                    | -                   | -             | -             | 0.26          |
| 72.00                   | 2-Methyl-3-octyne                        | -                   | -             | -             | 0.27          |
| 80.62                   | 14-Methylpentadecanoic acid methyl ester | 0.72                | -             | 0.45          | -             |
| 80.63                   | Hexadecanoic acid methyl ester           | -                   | 0.5           | -             | 0.62          |
| 84.06                   | n-Hexadecanoic acid                      | 9.6                 | 10.53         | 11.32         | 11.98         |
| 89.29                   | 9,12-Octadecadienoic acid methyl ester   | 0.98                | 0.81          | 0.33          | -             |
| 89.52                   | 11-Octadecenoic acid methyl ester        | -                   | -             | 0.52          | -             |
| 89.53                   | E,E,Z-1,3,12-Nonadecatriene-5,14-diol    | -                   | -             | -             | 0.55          |
| 89.55                   | (Z)-9-Octadecenoic acid methyl ester     | 0.78                | 0.73          | -             | 1.04          |
| 89.82                   | 10-Octadecenoic acid methyl ester        | -                   | 0.37          | 0.54          | -             |
| 90.53                   | Octadecanoic acid methyl ester           | -                   | 0.31          | 0.54          | -             |
| 90.54                   | 16-Methylheptadecanoic acid methyl ester | 0.26                | -             | -             | 1.72          |
| 90.89                   | 5-Eicosyne                               | -                   | -             | -             | 2.22          |
| 91.87                   | Linoleic acid                            | 37.99               | 30.09         | 4.52          | 3.36          |
| 92.04                   | (E)-9-Octadecenoic acid                  | 12.64               | 17.35         | 54.07         | 41.36         |
| 92.16                   | 9-Eicosyne                               | 5.74                | -             | -             | -             |
| 92.50                   | Octadecanoic acid                        | 5.59                | 6.35          | 7.83          | 11.19         |
| 95.34                   | Dihydro-5-tetradecyl-2(3H)-furanone      | -                   | -             | -             | 1.12          |
| 95.48                   | 4-Hydroxy-3-methoxybenzeneacetic acid    | 0.5                 | 0.19          | 0.24          | -             |
| 96.04                   | Tetrahydro-6-tridecyl-2H-pyran-2-one     | -                   | -             | -             | 0.55          |
| 96.21                   | Cyclododecanone                          | -                   | -             | -             | 0.78          |
| 96.23                   | Cis-8-Methyl-1.beta-acetyl-hydrindane    | -                   | -             | 0.49          | -             |
| 96.34                   | (Z)-9,17-Octadecadienal                  | 0.39                | -             | -             | -             |
| 108.15                  | Stigmastan-3,5-dien                      | 0.38                | 0.42          | -             | -             |

**Table 21.** Identified compounds in bio-oils from the supercritical ethanol processing of grape seed without and with additive (MgCl<sub>2</sub>:TiCl<sub>4</sub>). (T=300 °C, t=30 min, PH<sub>2</sub>int.=2 MPa).

| Retention time (min) | Compounds                           | Peak area (%)    |            |            |            |
|----------------------|-------------------------------------|------------------|------------|------------|------------|
|                      |                                     | without additive | 1:1 (mmol) | 2:2 (mmol) | 4:4 (mmol) |
| 2.01                 | N-ethyl-N-methyl-ethanamine         | -                | -          | 0.15       | -          |
| 2.39                 | 1-Butanol                           | -                | 0.05       | 0.12       | 0.42       |
| 2.72                 | Triethylamine                       | -                | 0.05       | 0.11       | -          |
| 3.10                 | 2-Ethoxyethanol                     | -                | 0.13       | 0.12       | 0.09       |
| 3.31                 | Propanoic acid                      | 0.02             | -          | -          | -          |
| 3.41                 | 1,1-Diethoxyethane                  | 0.02             | 0.05       | 0.2        | 1.31       |
| 3.47                 | 1,3-Diethoxy-5-methylcyclohexan     | -                | -          | 0.01       | -          |
| 3.60                 | 3-Methyl-1-Butanol                  | -                | 0.06       | 0.08       | -          |
| 3.68                 | 2-Methyl-1-Butanol                  | 0.03             | 0.07       | 0.08       | 0.05       |
| 3.96                 | Pyridine                            | -                | 0.02       | -          | -          |
| 3.97                 | 1-Ethoxy-2-Propanol                 | -                | -          | -          | 0.03       |
| 4.21                 | Pyrrole                             | 0.02             | -          | -          | -          |
| 4.46                 | 2,2-Diethoxypropane                 | -                | 0.17       | -          | -          |
| 4.91                 | Hydroxyacetic acid ethyl ester      | -                | 0.35       | 0.19       | -          |
| 6.19                 | 2-Hydroxypropanoic acid ethyl ester | 0.25             | 1.03       | 0.84       | 0.51       |
| 6.39                 | 2-Methylpyridine                    | -                | -          | 0.04       | -          |
| 6.49                 | Methylpyrazine                      | -                | 0.09       | -          | -          |
| 7.04                 | 2-Cyclopenten-1-one                 | -                | 0.02       | 0.03       | -          |
| 8.77                 | 2-Furanmethanol                     | 0.24             | -          | -          | -          |
| 10.06                | Tetrahydro-2-furanmethanol          | -                | 0.05       | -          | -          |
| 11.64                | 2-Methyl-2-cyclopenten-1-one        | 0.03             | 0.13       | 0.16       | -          |
| 11.73                | 1,1-Diethoxybutane                  | -                | -          | -          | 0.38       |
| 11.92                | 2-Hydroxybutanoic acid methyl ester | 0.14             | -          | -          | 0.16       |
| 11.93                | 2-Hydroxybutanoic acid ethyl ester  | -                | 0.29       | 0.26       | -          |
| 12.40                | Ethylpyrazine                       | -                | 0.03       | 0.02       | -          |
| 14.43                | Butyrolactone                       | 0.09             | 0.12       | 0.11       | -          |
| 12.88                | Ethoxyacetic acid ethyl ester       | -                | 0.06       | 0.09       | 0.12       |
| 14.50                | 2-Ethylcyclopentanone               | -                | -          | 0.01       | -          |
| 16.64                | 5-Methyltetrahydro-2-furanone       | -                | -          | 0.05       | -          |
| 16.69                | Ethylhydrazone-2-propanone          | -                | -          | -          | 0.07       |
| 17.02                | 1,1-Diethoxy-3-methylbutane         | -                | 0.04       | 0.06       | -          |
| 17.69                | 3-Methyl-2-cyclopenten-1-one        | -                | 0.04       | 0.07       | -          |
| 20.90                | 2,3-Dimethyl-2-cyclopenten-1-one    | 0.03             | 0.13       | 0.18       | 0.18       |

**Table 21.** (Continued)

| Retention time<br>(min) | Compounds   | Peak area (%)       |               |               |               |
|-------------------------|---|---------------------|---------------|---------------|---------------|
|                         |   | without<br>additive | 1:1<br>(mmol) | 2:2<br>(mmol) | 4:4<br>(mmol) |
| 22.34                   | (Z)-3-Hexenoic acid ethyl ester                   | -                   | -             | 0.06          | -             |
| 22.35                   | 3-Hexenoic acid ethyl ester                       | -                   | -             | 0.06          | 0.22          |
| 22.36                   | Phenol  | 0.1                 | 0.08          | 0.08          | -             |
| 23.42                   | Bicyclo[3.2.1]octane                              | -                   | -             | 0.02          | -             |
| 24.36                   | 2-Hydroxy-3-methyl-2-cyclopenten-1-one            | 0.1                 | 0.11          | -             | -             |
| 24.42                   | 3-Methyl-1,2-cyclopentanedione                    | -                   | -             | 0.03          | -             |
| 25.80                   | Ethyl-2-hexenoate                                 | -                   | -             | 0.03          | 0.23          |
| 26.56                   | 2-Furancarboxylic acid ethyl ester                | 0.13                | 0.13          | 0.15          | 0.08          |
| 27.64                   | 4-Oxo-pentanoic acid ethyl ester                  | 0.37                | 0.7           | 0.65          | 0.49          |
| 28.40                   | Hexahydroindole                                   | -                   | 0.7           | -             | -             |
| 29.57                   | 2-Methoxyphenol                                   | 2.81                | 1.38          | 0.66          | -             |
| 29.82                   | 2-Pyrrolidinone                                   | -                   | 0.18          | 0.02          | -             |
| 30.54                   | Heptanoic acid ethyl ester                        | -                   | 0.13          | 0.12          | -             |
| 30.82                   | 4-Methylphenol                                    | -                   | -             | 0.13          | -             |
| 32.20                   | 3-Ethyl-2-hydroxy-2-cyclopenten-1-one             | 0.15                | 0.08          | -             | -             |
| 34.57                   | 2-Ethoxyphenol                                    | 0.15                | 0.58          | 0.71          | 0.58          |
| 37.35                   | Butanedioic acid diethyl ester                    | 0.95                | 1.04          | 0.98          | 0.88          |
| 37.64                   | 2-Methoxy-4-methylphenol                          | 0.74                | 0.66          | 0.37          | -             |
| 38.19                   | 1H-Pyrrole-2-carboxylic acid ethyl ester          | 0.43                | 0.38          | -             | -             |
| 38.23                   | Octanoic acid ethyl ester                         | -                   | -             | 0.3           | 0.28          |
| 39.18                   | Diethyl methylsuccinate                           | 0.12                | 0.23          | 0.16          | 0.23          |
| 41.64                   | 2-Ethoxy-4-methylphenol                           | -                   | 0.17          | 0.15          | 0.33          |
| 41.65                   | 2-Methyl-1,3-benzenediol                          | -                   | -             | 0.23          | -             |
| 43.79                   | 4-Ethyl-2-methoxyphenol                           | 2.03                | 1.16          | 0.65          | -             |
| 44.42                   | Pentanedioic acid diethyl ester                   | 0.33                | 0.35          | 0.38          | 0.44          |
| 45.21                   | Nonanoic acid ethyl ester                         | -                   | -             | 0.14          | -             |
| 48.35                   | Benzenepropanoic acid ethyl ester                 | -                   | 0.13          | 0.17          | -             |
| 49.00                   | 2-Methoxy-3-(2-propenyl)phenol                    | 0.16                | -             | -             | -             |
| 49.02                   | 2-Methoxy-5-(1-propenyl)phenol                    | -                   | 0.1           | -             | -             |
| 49.63                   | 2-Methoxy-4-propylphenol                          | 1.29                | 0.63          | 0.22          | -             |
| 51.66                   | Decanoic acid ethyl ester                         | -                   | -             | 0.14          | -             |
| 52.49                   | 2-Ethoxy-5-methoxybenzaldehyde                    | -                   | -             | 0.16          | -             |
| 53.8                    | 2-Amino-4-acetamino anisole                       | -                   | 0.11          | -             | -             |
| 54.82                   | 2-Methoxy-4-(1-propenyl)phenol                    | 0.41                | 0.12          | -             | -             |
| 55.00                   | 4-Ethyl-4H-1,2,4-triazol-3-amine                  | -                   | -             | -             | 0.77          |
| 55.16                   | 5-Ethoxy-3,4-dihydro-2H-pyrrole-2-carboxylic acid | -                   | -             | 0.4           | -             |
| 55.20                   | 5-Ethoxy-3,4-dihydro-2H-pyrrole-2-carboxylic acid | -                   | 0.35          | -             | -             |
| 55.63                   | 5-Oxo-2-pyrrolidinecarboxylic acid ethyl ester    | 2.52                | -             | 0.77          | -             |

**Table 21.** (Continued)

| Retention time<br>(min) | Compounds  | Peak area (%)       |               |               |               |
|-------------------------|--|---------------------|---------------|---------------|---------------|
|                         |  | without<br>additive | 1:1<br>(mmol) | 2:2<br>(mmol) | 4:4<br>(mmol) |
| 57.15                   | 1-(4-hydroxy-3-methoxyphenyl)ethanone              | 0.02                | -             | -             | -             |
| 59.27                   | 2-Ethoxy-5-[1-propenyl]phenol                      | -                   | -             | 0.14          | -             |
| 59.80                   | 2-Methoxy-4-(methoxymethyl)phenol                  | -                   | 0.15          | -             | -             |
| 63.03                   | 4-Hydroxy-3-methoxybenzoic acid ethyl ester        | 0.1                 | -             | -             | -             |
| 63.23                   | Diethyl suberate                                   | -                   | 0.1           | -             | -             |
| 66.22                   | Ethyl homovanillate                                | 0.12                | 0.09          | -             | -             |
| 74.13                   | Tetradecanoic acid ethyl ester                     | -                   | 0.09          | 0.17          | -             |
| 79.09                   | 9-Cedranone  | -                   | -             | 0.12          | -             |
| 80.61                   | Hexadecanoic acid methyl ester                     | 0.24                | -             | 0.12          | -             |
| 83.08                   | E-11-Hexadecenoic acid ethyl ester                 | 0.24                | 0.14          | -             | 0.31          |
| 83.09                   | Ethyl-9-hexadecenoate                              | -                   | -             | 0.15          | -             |
| 83.51                   | n-Hexadecanoic acid                                | 0.69                | -             | 0.17          | -             |
| 84.81                   | Hexadecanoic acid ethyl ester                      | 8.21                | 9.05          | 9.87          | 11.54         |
| 89.26                   | 8,11-Octadecadienoic acid methyl ester             | -                   | 0.1           | -             | -             |
| 89.27                   | 9,12-Octadecadienoic acid methyl ester             | 0.68                | -             | 0.07          | -             |
| 89.54                   | 10-Octadecenoic acid methyl ester                  | 0.43                | -             | -             | -             |
| 90.56                   | 16-Methyl-heptadecanoic acid methyl ester          | 0.14                | -             | -             | -             |
| 91.29                   | 2-Butyl-5-hexyloctahydro-1H-indene                 | -                   | -             | -             | 0.72          |
| 91.33                   | (Z,Z)-9,12-Octadecadienoic acid                    | -                   | 0.62          | -             | 0.66          |
| 91.85                   | 9,12-Octadecadienoic acid ethyl ester              | 36.32               | 32.46         | 0.09          | 10.83         |
| 91.94                   | Linoleic acid ethyl ester                          | 0.87                | 6.46          | 31.45         | 27.25         |
| 92.03                   | Ethyl Oleate                                       | 18.95               | 20.33         | 19.02         | 23.92         |
| 92.66                   | Octadecanoic acid ethyl ester                      | 4.78                | 5.36          | 5.8           | 6.28          |
| 92.69                   | 6-Tetradecyne                                      | -                   | -             | -             | 0.9           |
| 93.05                   | (R)-(-)-14-Methyl-8-hexadecyn-1-ol                 | -                   | -             | 1.21          | -             |
| 93.07                   | cis-9,trans-11-Tetradecadien-1-yl-acetate          | -                   | -             | -             | 0.6           |
| 93.26                   | Isopropyl linoleate                                | -                   | -             | 0.62          | -             |
| 93.41                   | 9-Octadecyne                                       | -                   | -             | 0.47          | -             |
| 93.70                   | Methyl 2-octylcyclopropene-1-octanoate             | -                   | -             | 0.36          | -             |
| 94.13                   | 7-Hexadecyne                                       | 2.35                | -             | -             | -             |
| 95.46                   | 4-Hydroxy-3-methoxybenzeneacetic acid methyl       | 0.65                | -             | -             | -             |
| 95.99                   | 2-Hexenylhexanoate                                 | -                   | -             | 0.16          | -             |
| 96.14                   | (Z,Z,Z)-9,12,15-Octadecatrienoic acid methyl ester | 0.13                | 0.13          | 0.17          | -             |
| 96.22                   | (E)-4-Hexadecen-6-yne                              | 0.2                 | -             | -             | -             |
| 96.23                   | (Z,Z,Z)-9,12,15-Octadecatrienoic acid ethyl ester  | -                   | 0.13          | -             | -             |
| 96.48                   | 2-Hydroxycyclopentadecanone                        | 0.27                | -             | -             | -             |
| 96.49                   | 11-Eicosenoic acid methyl ester                    | -                   | 0.12          | -             | -             |

**Table 21.** (Continued)

| Retention time<br>(min) | Compounds  | Peak area (%)       |               |               |               |
|-------------------------|--|---------------------|---------------|---------------|---------------|
|                         |  | without<br>additive | 1:1<br>(mmol) | 2:2<br>(mmol) | 4:4<br>(mmol) |
| 96.50                   | Oxacyclohexadecan-2-one                              | -                   | -             | 0.23          | -             |
| 96.59                   | 10-Oxo-octadecanoic acid methyl ester                | -                   | -             | 0.21          | -             |
| 97.04                   | Heptadecanoic acid ethyl ester                       | -                   | 0.02          | 0.31          | -             |
| 97.05                   | Eicosanoic acid ethyl ester                          | -                   | 0.28          | -             | -             |
| 97.55                   | 7,11-Hexadecadienal                                  | 0.11                | -             | -             | -             |
| 103.64                  | 2,6,10,14-Tetramethylpentadecanoic acid methyl ester | -                   | -             | 0.13          | -             |

**Table 22.** Quantitative analysis of hydroxyl groups in bio-oils produced from hydrothermal and supercritical ethanol processing.

|         |   | phenolic OH (mmol/g)                    |              |              |              |                  |              |                 |               |
|---------|---|---|--------------|--------------|--------------|------------------|--------------|-----------------|---------------|
|         |   | C <sub>5</sub> substituted condensed OH |              |              |              | Non-condensed OH |              |                 |               |
|         |   | aliphatic (mmol/g)                      | β-5          | 4-O-5        | 5-5          | guaiacyl         | catechol     | p-hydroxyphenyl | COOH (mmol/g) |
| ethanol | without additive                                  | 1.13<br>±0.3                            | 0.09<br>±0.0 | 0.05<br>±0.0 | 0.05<br>±0.0 | 0.45<br>±0.1     | 0.31<br>±0.0 | 0.14<br>±0.0    | 0.24<br>±0.0  |
|         | MgCl <sub>2</sub> :TiCl <sub>4</sub> =1mmol:1mmol | 0.75<br>±0.2                            | 0.15<br>±0.0 | 0.11<br>±0.0 | 0.09<br>±0.0 | 0.30<br>±0.0     | 0.20<br>±0.1 | 0.18<br>±0.0    | 0.11<br>±0.0  |
|         | MgCl <sub>2</sub> :TiCl <sub>4</sub> =2mmol:2mmol | 0.53<br>±0.0                            | 0.26<br>±0.0 | 0.15<br>±0.0 | 0.06<br>±0.0 | 0.29<br>±0.0     | 0.21<br>±0.1 | 0.14<br>±0.1    | 0.15<br>±0.0  |
|         | MgCl <sub>2</sub> :TiCl <sub>4</sub> =4mmol:4mmol | 0.38<br>±0.1                            | 0.28<br>±0.0 | 0.19<br>±0.1 | 0.12<br>±0.0 | 0.14<br>±0.0     | 0.14<br>±0.0 | 0.10<br>±0.0    | 0.09<br>±0.0  |
| water   | without additive                                  | 0.15<br>±0.0                            | 0.06<br>±0.0 | 0.08<br>±0.0 | 0.11<br>±0.0 | 0.81<br>±0.0     | 0.49<br>±0.0 | 0.21<br>±0.0    | 2.15<br>±0.0  |
|         | MgCl <sub>2</sub> :TiCl <sub>4</sub> =1mmol:1mmol | 0.16<br>±0.0                            | 0.07<br>±0.0 | 0.09<br>±0.0 | 0.11<br>±0.0 | 0.80<br>±0.1     | 0.46<br>±0.0 | 0.24<br>±0.0    | 2.01<br>±0.1  |
|         | MgCl <sub>2</sub> :TiCl <sub>4</sub> =2mmol:2mmol | 0.16<br>±0.0                            | 0.06<br>±0.0 | 0.16<br>±0.0 | 0.03<br>±0.0 | 0.48<br>±0.0     | 0.38<br>±0.1 | 0.16<br>±0.0    | 2.40<br>±0.0  |
|         | MgCl <sub>2</sub> :TiCl <sub>4</sub> =4mmol:4mmol | 0.07<br>±0.0                            | 0.07<br>±0.0 | 0.06<br>±0.0 | 0.04<br>±0.0 | 0.43<br>±0.1     | 0.55<br>±0.0 | 0.25<br>±0.0    | 2.22<br>±0.1  |



**Table 23.** Elemental composition (wt% and atomic ratio) of raw material, bio-oils and solid residues from the hydrothermal liquefaction of grape seed with (MgCl<sub>2</sub>:TiCl<sub>4</sub>). (T:300 °C, t=30 min, PH<sub>2</sub>int.=2 MPa)

| Additives<br>(mmol)                                   | Product<br>Type | C<br>(wt%)    | H<br>(wt%)   | N<br>(wt%)   | O <sup>a</sup><br>(wt%) | H/C  | O/C  | HHV<br>(MJ/kg) |
|---|-----------------|---------------|--------------|--------------|-------------------------|------|------|----------------|
|   | Raw Material    | 51.7<br>±0.08 | 7.5<br>±0.01 | 2.0<br>±0.02 | 38.8                    | 1.74 | 0.56 | 21.26          |
| without additive                                      | Bio-oil         | 72.1<br>±0.03 | 9.3<br>±0.01 | 1.3<br>±0.06 | 17.3                    | 1.54 | 0.18 | 34.51          |
| MgCl <sub>2</sub> :TiCl <sub>4</sub> =1<br>mmol:1mmol | Bio-oil         | 72.2<br>±0.09 | 9.4<br>±0.02 | 1.0<br>±0.05 | 17.4                    | 1.56 | 0.18 | 34.72          |
| MgCl <sub>2</sub> :TiCl <sub>4</sub> =2<br>mmol:2mmol | Bio-oil         | 72.1<br>±0.14 | 9.6<br>±0.01 | 1.1<br>±0.07 | 17.3                    | 1.60 | 0.18 | 34.98          |
| MgCl <sub>2</sub> :TiCl <sub>4</sub> =4<br>mmol:4mmol | Bio-oil         | 73.4<br>±0.11 | 9.3<br>±0.03 | 0.6<br>±0.02 | 16.7                    | 1.51 | 0.17 | 35.05          |
| without additive                                      | Solid residue   | 56.4<br>±0.04 | 5.4<br>±0.01 | 1.8<br>±0.02 | 36.4                    | 1.14 | 0.48 | 20.25          |
| MgCl <sub>2</sub> :TiCl <sub>4</sub> =1<br>mmol:1mmol | Solid residue   | 66.0<br>±0.10 | 5.2<br>±0.04 | 2.0<br>±0.03 | 26.9                    | 0.94 | 0.31 | 24.88          |
| MgCl <sub>2</sub> :TiCl <sub>4</sub> =2<br>mmol:2mmol | Solid residue   | 61.1<br>±0.06 | 5.1<br>±0.02 | 1.4<br>±0.03 | 32.4                    | 1.00 | 0.40 | 22.18          |
| MgCl <sub>2</sub> :TiCl <sub>4</sub> =4<br>mmol:4mmol | Solid residue   | 58.7<br>±0.09 | 5.0<br>±0.02 | 1.4<br>±0.09 | 34.9                    | 1.03 | 0.45 | 20.80          |

**Table 24.** Elemental composition (wt% and atomic ratio) of raw material, bio-oils, and solid residues from supercritical ethanol processing of grape seed without and with additive (MgCl<sub>2</sub>:TiCl<sub>4</sub>). (T=300 °C, t=30 min, PH<sub>2</sub>int.=2 MPa)

| <b>Additives<br/>(mmol)</b>                           | <b>Product<br/>Type</b> | <b>C<br/>(wt%)</b> | <b>H<br/>(wt%)</b> | <b>N<br/>(wt%)</b> | <b>O<sup>a</sup><br/>(wt%)</b> | <b>H/C</b> | <b>O/C</b> | <b>HHV<br/>(MJ/kg)</b> |
|---|-------------------------|--------------------|--------------------|--------------------|--------------------------------|------------|------------|------------------------|
|   | Raw Material            | 51.7<br>±0.08      | 7.5<br>±0.01       | 2.0<br>±0.02       | 38.8                           | 1.74       | 0.56       | 21.26                  |
| Without additive                                      | Bio-oil                 | 66.9<br>±0.01      | 8.8<br>±0.01       | 1.0<br>±0.01       | 23.2                           | 1.59       | 0.26       | 31.09                  |
| MgCl <sub>2</sub> :TiCl <sub>4</sub> =<br>1mmol:1mmol | Bio-oil                 | 69.1<br>±0.01      | 9.3<br>±0.01       | 1.3<br>±0.01       | 20.3                           | 1.61       | 0.22       | 32.96                  |
| MgCl <sub>2</sub> :TiCl <sub>4</sub> =<br>2mmol:2mmol | Bio-oil                 | 70.1<br>±0.01      | 9.1<br>±0.01       | 1.2<br>±0.01       | 19.6                           | 1.57       | 0.21       | 33.24                  |
| MgCl <sub>2</sub> :TiCl <sub>4</sub> =<br>4mmol:4mmol | Bio-oil                 | 72.5<br>±0.01      | 9.0<br>±0.01       | 1.6<br>±0.01       | 16.9                           | 1.49       | 0.17       | 34.35                  |
| Without additive                                      | Solid residue           | 59.5<br>±0.01      | 4.9<br>±0.01       | 2.1<br>±0.01       | 33.6                           | 0.98       | 0.42       | 21.08                  |
| MgCl <sub>2</sub> :TiCl <sub>4</sub> =<br>1mmol:1mmol | Solid residue           | 60.5<br>±0.01      | 5.1<br>±0.01       | 1.9<br>±0.01       | 32.6                           | 1.01       | 0.40       | 21.89                  |
| MgCl <sub>2</sub> :TiCl <sub>4</sub> =<br>2mmol:2mmol | Solid residue           | 55.9<br>±0.01      | 4.9<br>±0.01       | 1.5<br>±0.01       | 37.7                           | 1.05       | 0.51       | 19.17                  |
| MgCl <sub>2</sub> :TiCl <sub>4</sub> =<br>4mmol:4mmol | Solid residue           | 51.4<br>±0.01      | 5.3<br>±0.01       | 1.3<br>±0.01       | 42.0                           | 1.24       | 0.61       | 17.46                  |

**Table 25.** Boiling point distributions (wt%) of the crude bio-oils obtained from hydrothermal liquefaction and supercritical ethanol processing of grape seed without and with the additives. (T=300 °C, t=30 min, PH<sub>2int.</sub>=2 MPa)

| <b>Conversion type</b> | <b>Additives (mmol)</b> | <b>Light Naphtha</b> | <b>Heavy Naphtha</b> | <b>Light Gas Oil</b> | <b>Heavy Gas Oil</b> |
|------------------------|-------------------------|----------------------|----------------------|----------------------|----------------------|
|                        |                         | <b>&lt;93°C</b>      | <b>93-204°C</b>      | <b>204-343°C</b>     | <b>&gt;343°C</b>     |
| Hydrothermal           | without catalyst        | 2.0                  | 17.8                 | 62.6                 | 13.2                 |
|                        | 1:1                     | 1.4                  | 13.0                 | 65.8                 | 12.8                 |
|                        | 2:2                     | 1.7                  | 19.9                 | 67.9                 | 8.2                  |
|                        | 4:4                     | 2.4                  | 18.9                 | 68.2                 | 8.6                  |
| Supercritical ethanol  | without catalyst        | 1.8                  | 29.6                 | 58.4                 | 6.8                  |
|                        | 1:1                     | 1.9                  | 33.2                 | 55.9                 | 6.4                  |
|                        | 2:2                     | 2.0                  | 31.8                 | 54.1                 | 7.7                  |
|                        | 4:4                     | 2.6                  | 26.5                 | 52.3                 | 12.6                 |

**Table 26.** Bio-oil and solid residue yields produced from fir wood without and with catalyst at different concentrations of the raw material through HTL and SCEL processing. (T=300 °C, t=30 min)

| Catalyst loading            | Bio-oil (wt%) |       | Solid residue (wt%) |       |
|-----------------------------|---------------|-------|---------------------|-------|
|                             | HTL           | SCEL  | HTL                 | SCEL  |
| without catalyst            | 5.08          | 28.70 | 41.97               | 41.60 |
| Pd/C                        | 10.47         | 47.26 | 30.51               | 19.62 |
| Sm(OTf) <sub>3</sub>        | 6.80          | 30.31 | 41.78               | 40.83 |
| Pd/C & Sm(OTf) <sub>3</sub> | 9.84          | 49.44 | 30.33               | 16.93 |
| La(OTf) <sub>3</sub>        | 6.94          | 30.19 | 42.37               | 38.62 |
| Pd/C & La(OTf) <sub>3</sub> | 10.22         | 49.71 | 30.81               | 20.09 |
| Cu(OTf) <sub>2</sub>        | 6.05          | 29.51 | 43.30               | 40.69 |
| Pd/C & Cu(OTf) <sub>2</sub> | 8.75          | 46.80 | 32.50               | 18.92 |

**Table 27.** Elemental composition (wt% and atomic ratio) of raw material, bio-oils and solid residues from the HTL of fir wood without and with catalysts. (T=300 °C, t=30 min)

| Catalyst loading            | Product Type  | C     | H    | N    | O <sup>a</sup> | H/C  | O/C  | HHV (MJ/kg) |
|-----------------------------|---------------|-------|------|------|----------------|------|------|-------------|
|                             | Raw Material  | 46.30 | 6.49 | 0.10 | 47.10          | 1.68 | 0.76 | 16.51       |
| without catalyst            | Bio-oil       | 66.16 | 6.17 | 0.08 | 27.60          | 1.12 | 0.31 | 26.24       |
| Pd/C                        | Bio-oil       | 71.91 | 6.47 | 0.14 | 21.48          | 1.08 | 0.22 | 29.71       |
| Sm(OTf) <sub>3</sub>        | Bio-oil       | 67.08 | 6.20 | 0.10 | 26.62          | 1.11 | 0.30 | 26.78       |
| Pd/C & Sm(OTf) <sub>3</sub> | Bio-oil       | 72.19 | 6.50 | 0.14 | 21.17          | 1.08 | 0.22 | 29.90       |
| La(OTf) <sub>3</sub>        | Bio-oil       | 66.51 | 6.45 | 0.09 | 26.95          | 1.16 | 0.30 | 26.87       |
| Pd/C & La(OTf) <sub>3</sub> | Bio-oil       | 71.63 | 6.88 | 0.13 | 21.37          | 1.15 | 0.22 | 30.22       |
| Cu(OTf) <sub>2</sub>        | Bio-oil       | 66.70 | 6.38 | 0.12 | 26.80          | 1.15 | 0.30 | 26.87       |
| Pd/C & Cu(OTf) <sub>2</sub> | Bio-oil       | 72.62 | 6.70 | 0.17 | 20.51          | 1.11 | 0.21 | 30.46       |
| without catalyst            | Solid Residue | 53.78 | 4.91 | 0.19 | 41.13          | 1.10 | 0.57 | 17.85       |
| Pd/C                        | Solid Residue | 54.73 | 4.79 | 0.21 | 40.27          | 1.05 | 0.55 | 18.15       |
| Sm(OTf) <sub>3</sub>        | Solid Residue | 62.47 | 5.17 | 0.21 | 32.15          | 0.99 | 0.39 | 22.75       |
| Pd/C & Sm(OTf) <sub>3</sub> | Solid Residue | 50.41 | 4.71 | 0.25 | 44.63          | 1.12 | 0.66 | 15.80       |
| La(OTf) <sub>3</sub>        | Solid Residue | 60.62 | 5.14 | 0.25 | 34.00          | 1.02 | 0.42 | 21.75       |
| Pd/C & La(OTf) <sub>3</sub> | Solid Residue | 57.53 | 4.67 | 0.19 | 37.60          | 0.97 | 0.49 | 19.41       |
| Cu(OTf) <sub>2</sub>        | Solid Residue | 56.46 | 5.01 | 0.17 | 38.36          | 1.06 | 0.51 | 19.39       |
| Pd/C & Cu(OTf) <sub>2</sub> | Solid Residue | 55.41 | 4.76 | 0.24 | 39.59          | 1.03 | 0.54 | 18.46       |

**Table 28.** Elemental composition (wt% and atomic ratio) of raw material, bio-oils and solid residues from SCEL processing of fir wood without and with catalysts. (T=300 °C, t=30 min)

| Catalysts                   | Product Type  | C     | H    | N    | O <sup>a</sup> | H/C  | O/C  | HHV (MJ/kg) |
|-----------------------------|---------------|-------|------|------|----------------|------|------|-------------|
|                             | Raw Material  | 46.3  | 6.49 | 0.1  | 47.1           | 1.68 | 0.76 | 16.51       |
| without catalyst            | Bio-oil       | 61.69 | 7.78 | 0.23 | 30.3           | 1.51 | 0.37 | 26.55       |
| Pd/C                        | Bio-oil       | 71.88 | 8.13 | 0.24 | 19.75          | 1.36 | 0.21 | 32.38       |
| Sm(OTf) <sub>3</sub>        | Bio-oil       | 61.7  | 7.23 | 0.2  | 30.87          | 1.41 | 0.38 | 25.66       |
| Pd/C & Sm(OTf) <sub>3</sub> | Bio-oil       | 72.94 | 7.79 | 0.25 | 19.02          | 1.28 | 0.2  | 32.39       |
| La(OTf) <sub>3</sub>        | Bio-oil       | 63.15 | 7.11 | 0.2  | 29.54          | 1.35 | 0.35 | 26.22       |
| Pd/C & La(OTf) <sub>3</sub> | Bio-oil       | 70.52 | 7.55 | 0.24 | 21.7           | 1.28 | 0.23 | 30.74       |
| Cu(OTf) <sub>2</sub>        | Bio-oil       | 62.05 | 6.97 | 0.2  | 30.78          | 1.35 | 0.37 | 25.43       |
| Pd/C & Cu(OTf) <sub>2</sub> | Bio-oil       | 73.36 | 7.54 | 0.27 | 18.83          | 1.23 | 0.19 | 32.20       |
| without catalyst            | Solid Residue | 54.86 | 5.58 | 0.2  | 39.36          | 1.22 | 0.54 | 19.49       |
| Pd/C                        | Solid Residue | 54.95 | 5.48 | 0.12 | 39.45          | 1.2  | 0.54 | 19.36       |
| Sm(OTf) <sub>3</sub>        | Solid Residue | 58.18 | 5.73 | 0.14 | 35.96          | 1.18 | 0.46 | 21.43       |
| Pd/C & Sm(OTf) <sub>3</sub> | Solid Residue | 56.68 | 5.22 | 0.16 | 37.94          | 1.11 | 0.5  | 19.84       |
| La(OTf) <sub>3</sub>        | Solid Residue | 59.41 | 5.55 | 0.16 | 34.89          | 1.12 | 0.44 | 21.77       |
| Pd/C & La(OTf) <sub>3</sub> | Solid Residue | 54.7  | 5.15 | 0.17 | 39.98          | 1.13 | 0.55 | 18.7        |
| Cu(OTf) <sub>2</sub>        | Solid Residue | 58.01 | 5.73 | 0.14 | 36.11          | 1.19 | 0.47 | 21.35       |
| Pd/C & Cu(OTf) <sub>2</sub> | Solid Residue | 52.77 | 5.19 | 0.07 | 41.96          | 1.18 | 0.6  | 17.76       |

**Table 29.** Boiling point distributions (wt%) of the crude bio-oils obtained from HTL and SCEL processing of fir wood without and with catalysts. (T=300 °C, t=30 min)

| Conversion type | Catalysts                   | Light Naphtha | Heavy Naphtha | Light Gas Oil | Heavy Gas Oil |
|-----------------|-----------------------------|---------------|---------------|---------------|---------------|
|                 |                             | <93 °C        | 93-204 °C     | 204-343 °C    | >343 °C       |
| HTL             | without catalyst            | 3.1           | 34.0          | 39.3          | 13.9          |
|                 | Pd/C                        | 4.8           | 32.2          | 38.8          | 20.7          |
|                 | Sm(OTf) <sub>3</sub>        | 2.6           | 31.4          | 41.9          | 15.7          |
|                 | Pd/C & Sm(OTf) <sub>3</sub> | 2.6           | 27.5          | 41.1          | 23.6          |
|                 | La(OTf) <sub>3</sub>        | 4.2           | 40.8          | 32.6          | 12.3          |
|                 | Pd/C & La(OTf) <sub>3</sub> | 3.0           | 28.7          | 39.0          | 23.1          |
|                 | Cu(OTf) <sub>2</sub>        | 3.5           | 35.1          | 37.3          | 14.6          |
|                 | Pd/C & Cu(OTf) <sub>2</sub> | 4.5           | 32.0          | 38.2          | 21.6          |
| SCEL            | without catalyst            | 7.1           | 39.2          | 30.1          | 16.4          |
|                 | Pd/C                        | 4.5           | 28.3          | 38.8          | 20.3          |
|                 | Sm(OTf) <sub>3</sub>        | 3.1           | 30.3          | 38.5          | 18.6          |
|                 | Pd/C & Sm(OTf) <sub>3</sub> | 5.2           | 28.8          | 37.4          | 20.3          |
|                 | La(OTf) <sub>3</sub>        | 3.6           | 30.9          | 36.0          | 17.4          |
|                 | Pd/C & La(OTf) <sub>3</sub> | 4.4           | 30.5          | 37.9          | 19.5          |
|                 | Cu(OTf) <sub>2</sub>        | 4.6           | 38.0          | 37.5          | 14.6          |
|                 | Pd/C & Cu(OTf) <sub>2</sub> | 4.3           | 29.9          | 37.3          | 18.6          |

**Table 30.** Identified compounds in bio-oils from the HTL of fir wood without and with catalysts. (T=300 °C, t=30 min)

| Name of compound                            | Retention time (min) | area %           |      |                             |                             |                             |
|---|----------------------|------------------|------|-----------------------------|-----------------------------|-----------------------------|
|   |                      | without catalyst | Pd/C | Pd/C & Sm(OTf) <sub>3</sub> | Pd/C & La(OTf) <sub>3</sub> | Pd/C & Cu(OTf) <sub>2</sub> |
| <b>Acid</b>                                 |                      |                  |      |                             |                             |                             |
| Acetic acid                                 | 2.18                 | 0.64             | -    | -                           | 0.27                        | -                           |
| 4-hydroxy-3-methoxybenzeneacetic acid       | 66.46                | 4.90             | 7.09 | 6.97                        | 5.31                        | 6.28                        |
| 3-(4-Hydroxy-3-methoxyphenyl)propanoic acid | 71.78                | -                | 0.34 | 0.32                        | 0.56                        | -                           |
| Octadecanoic acid                           | 91.55                | -                | 0.14 | 0.17                        | -                           | -                           |
| <b>Ketone</b>                               |                      |                  |      |                             |                             |                             |
| 3-Hydroxy-2-butanone                        | 3.18                 | 0.78             | -    | 0.56                        | 0.56                        | 0.57                        |
| (E)-6,10-Dimethyl-5,9-dodecadien-2-one      | 8.36                 | -                | -    | 0.34                        | 0.18                        | -                           |
| 2-Cyclohexen-1-one                          | 13.75                | 0.28             | -    | -                           | -                           | -                           |
| 2,5-Hexanedione                             | 14.35                | 5.21             | 1.77 | 1.87                        | 2.06                        | 2.11                        |
| γ-Valerolactone                             | 16.73                | 0.92             | -    | -                           | 0.20                        | 0.20                        |
| 2,3-Dimethyl-4-hydroxy-2-butenolactone      | 31.15                | -                | -    | -                           | -                           | 0.31                        |
| 2,5-Octanedione                             | 31.58                | -                | -    | -                           | 0.11                        | -                           |
| 1-Cyclohexylethanone                        | 33.53                | -                | 0.15 | 0.16                        | -                           | -                           |
| 4-(1-Methylethyl)-2-cyclohexen-1-one        | 41.60                | -                | 0.73 | -                           | -                           | -                           |
| 5Alpha-androstan-17-one                     | 96.91                | -                | -    | 0.16                        | -                           | -                           |
| <b>Cyclopentenone</b>                       |                      |                  |      |                             |                             |                             |
| Cyclopentanone                              | 5.16                 | 0.35             | 2.70 | 2.29                        | 2.09                        | 2.30                        |
| 2-Cyclopenten-1-one                         | 7.07                 | 3.50             | -    | -                           | 0.10                        | 0.16                        |
| 2-Methylcyclopentanone                      | 7.32                 | -                | 0.93 | 0.81                        | 0.71                        | 0.77                        |
| 3-Methylcyclopentanone                      | 7.72                 | 0.11             | 0.13 | 0.11                        | 0.12                        | 0.12                        |
| 2-Methyl-2-cyclopenten-1-one                | 11.63                | 4.16             | 3.31 | 3.32                        | 3.12                        | 3.49                        |
| 3-Methyl-2-cyclopenten-1-one                | 17.59                | 3.44             | 1.60 | 1.64                        | 1.65                        | 1.75                        |
| 3,4-Dimethyl-2-cyclopenten-1-one            | 20.34                | 0.54             | 0.32 | 0.28                        | 0.34                        | 0.40                        |
| 2,3-Dimethyl-2-cyclopenten-1-one            | 20.85                | 0.67             | 0.41 | 0.40                        | 0.54                        | 0.51                        |
| 2-Hydroxy-3-methyl-2-cyclopenten-1-one      | 24.39                | 0.25             | -    | -                           | 0.48                        | 0.51                        |
| 3-Methyl-1,2-cyclopentanedione              | 24.55                | -                | 3.26 | -                           | -                           | -                           |
| 3,4-Dimethyl-2-hydroxycyclopent-2-en-1-one  | 27.36                | -                | -    | -                           | 0.30                        | -                           |



**Table 30.** (Continued)

| Name of compound                           | Retention time (min) | area %           |       |                             |                             |                             |
|--|----------------------|------------------|-------|-----------------------------|-----------------------------|-----------------------------|
|  |                      | without catalyst | Pd/C  | Pd/C & Sm(OTf) <sub>3</sub> | Pd/C & La(OTf) <sub>3</sub> | Pd/C & Cu(OTf) <sub>2</sub> |
| 2-Hydroxy-3,5-dimethylcyclopent-2-en-1-one | 27.40                | 0.67             | 0.43  | 0.42                        | -                           | 0.45                        |
| 3-Ethyl-2-cyclopenten-1-one                | 28.02                | -                | 0.23  | 0.21                        | 0.19                        | 0.27                        |
| 3-Ethyl-2-hydroxy-2-cyclopenten-1-one      | 32.14                | 0.54             | -     | -                           | -                           | 0.08                        |
| 2-Acetyl-cyclopentanone                    | 36.96                | -                | 0.89  | 0.84                        | 0.53                        | 0.72                        |
| <b>Alcohol</b>                             |                      |                  |       |                             |                             |                             |
| 1,2-Butanediol                             | 5.64                 | 0.80             | -     | -                           | -                           | 0.64                        |
| (E)-3-Methyl-2-penten-4-yn-1-ol            | 9.03                 | 0.18             | -     | -                           | -                           | -                           |
| Homovanillyl alcohol                       | 59.65                | -                | 2.71  | 2.74                        | 2.87                        | 2.52                        |
| <b>Aromatics</b>                           |                      |                  |       |                             |                             |                             |
| Phenol                                     | 21.69                | 1.45             | 0.84  | 0.85                        | 0.89                        | 0.96                        |
| 2-Methylphenol                             | 28.09                | 0.40             | 0.24  | 0.25                        | 0.32                        | 0.23                        |
| 2-Methoxyphenol                            | 29.66                | 25.10            | 12.24 | 12.02                       | 10.85                       | 12.11                       |
| 4-Methylphenol                             | 29.85                | 0.82             | 1.23  | 1.26                        | 0.60                        | 1.36                        |
| 2-Methoxy-4-methylphenol                   | 36.22                | 5.10             | 8.51  | 8.40                        | 8.18                        | 8.58                        |
| 4-Ethylphenol                              | 36.70                | -                | 0.32  | 0.32                        | 0.36                        | 0.36                        |
| 4-Ethyl-2-methoxyphenol                    | 43.57                | 3.11             | 10.19 | 9.59                        | 9.69                        | 11.00                       |
| 2,6-Dimethoxyphenol                        | 48.60                | 0.61             | 0.48  | 0.48                        | 0.48                        | 0.62                        |
| 2-Methoxy-4-propylphenol                   | 49.37                | 0.98             | 16.13 | 15.86                       | 16.73                       | 16.91                       |
| 4-Hydroxy-2-methoxybenzaldehyde            | 51.62                | -                | 0.23  | -                           | -                           | -                           |
| Vanilin                                    | 51.79                | 4.26             | -     | -                           | -                           | -                           |
| 3-Acetylphenol                             | 53.04                | 0.78             | 0.16  | 0.17                        | 0.37                        | -                           |
| 2-Methoxy-4-acetylphenol                   | 57.01                | 1.63             | 0.61  | 0.70                        | 0.62                        | 0.64                        |
| 4-(4-Hydroxy-3-methoxyphenyl)-2-butanone   | 66.04                | 0.55             | 0.15  | 0.16                        | -                           | -                           |
| 3,5-Diisopropylphenol                      | 69.30                | -                | 0.17  | 0.18                        | -                           | -                           |
| <b>Furan</b>                               |                      |                  |       |                             |                             |                             |
| 1-(2-furanyl)ethanone                      | 12.14                | 1.03             | 0.44  | 0.41                        | 0.42                        | 0.46                        |
| 2-Methylbenzofuran                         | 30.19                | -                | 0.26  | -                           | -                           | 0.25                        |

**Table 31.** Identified compounds in bio-oils from the SCEL processing of fir wood without and with catalysts. (T=300 °C, t=30 min, PH<sub>2int.</sub>=2 MPa)

| Name of compound                           | Retention time (min) | area %           |      |                             |                             |                             |
|--|----------------------|------------------|------|-----------------------------|-----------------------------|-----------------------------|
|  |                      | without catalyst | Pd/C | Pd/C & Sm(OTf) <sub>3</sub> | Pd/C & La(OTf) <sub>3</sub> | Pd/C & Cu(OTf) <sub>2</sub> |
| <b>Acid</b>                                |                      |                  |      |                             |                             |                             |
| 3-Hydroxy-4-methoxycinnamic acid           | 65.63                | 0.14             | -    | -                           | -                           | -                           |
| 4-Hydroxy-5-methoxyphenylacetylformic acid | 66.02                | -                | 0.55 | -                           | -                           | -                           |
| <b>Ether</b>                               |                      |                  |      |                             |                             |                             |
| 1-Methoxy-2-methylpropane                  | 3.11                 | -                | 1.16 | -                           | -                           | -                           |
| 1-Ethoxybutane                             | 5.49                 | -                | -    | 0.38                        | -                           | -                           |
| 4-Ethyl-1,2-dimethoxybenzene               | 46.83                | -                | -    | 0.12                        | 0.08                        | -                           |
| <b>Ketone</b>                              |                      |                  |      |                             |                             |                             |
| 1-Hydroxy-2-propanone                      | 2.48                 | -                | 1.08 | -                           | 1.43                        | -                           |
| 3-Hydroxy-2-butanone                       | 3.10                 | 0.21             | -    | 0.57                        | 0.76                        | 0.68                        |
| 2-Hydroxycyclohexanone                     | 20.32                | -                | -    | -                           | -                           | 0.39                        |
| cyclopentenone                             |                      |                  |      |                             |                             |                             |
| 2-Cyclopenten-1-one                        | 6.97                 | 0.28             | -    | -                           | -                           | -                           |
| 2-Methylcyclopentanone                     | 7.17                 | -                | 0.34 | 0.29                        | 0.31                        | 0.22                        |
| 1-Hydroxy-2-pentanone                      | 8.37                 | -                | -    | -                           | -                           | 0.76                        |
| 2-Methyl-2-cyclopenten-1-one               | 11.44                | 0.29             | -    | -                           | -                           | -                           |
| 2-Ethylcyclopentanone                      | 14.30                | -                | 0.59 | 0.69                        | 0.48                        | 0.52                        |
| 3-Methyl-2-cyclopenten-1-one               | 17.40                | 0.16             | -    | -                           | -                           | -                           |
| 2,3-Dimethyl-2-cyclopenten-1-one           | 20.72                | 0.24             | 0.45 | 0.5                         | 0.59                        | 0.33                        |
| 3-Methyl-1,2-cyclopentanedione             | 24.55                | 0.7              | -    | -                           | 0.05                        | -                           |
| 2-Hydroxy-3-methyl-2-cyclopenten-1-one     | 25.10                | 1.09             | -    | -                           | -                           | -                           |
| 3-Ethyl-2-hydroxy-2-cyclopenten-1-one      | 32.51                | 1.67             | 0.41 | 0.2                         | 0.35                        | 0.37                        |
| 2-Hydroxy-3-propyl-2-cyclopenten-1-one     | 38.89                | 0.22             | -    | -                           | -                           | -                           |
| 3,5-Diethyl-2-hydroxycyclopent-2-en-1-one  | 40.67                | -                | -    | -                           | 0.1                         | -                           |
| <b>Alcohol</b>                             |                      |                  |      |                             |                             |                             |
| 1,2-Ethanediol                             | 3.61                 | 1.26             | -    | -                           | 1.03                        | -                           |
| Propylene glycol                           | 4.34                 | -                | -    | -                           | 0.74                        | -                           |
| 1,2-Butanediol                             | 8.49                 | -                | 0.5  | -                           | -                           | 0.39                        |
| 3-Ethyl-4-octanol                          | 30.30                | -                | -    | 0.63                        | -                           | -                           |
| 1-Octyn-4-ol                               | 30.41                | -                | -    | -                           | -                           | 0.65                        |
| <b>Aromatics</b>                           |                      |                  |      |                             |                             |                             |
| 2-Methoxyphenol                            | 29.64                | 5.52             | 2.2  | 1.84                        | 1.81                        | 1.8                         |
| 2-Ethoxyphenol                             | 34.39                | 0.22             | -    | -                           | -                           | -                           |
| 2-Methoxy-3-methylphenol                   | 36.25                | 0.42             | -    | -                           | -                           | -                           |
| 4-Ethylphenol                              | 37.01                | 0.21             | -    | 0.26                        | -                           | -                           |

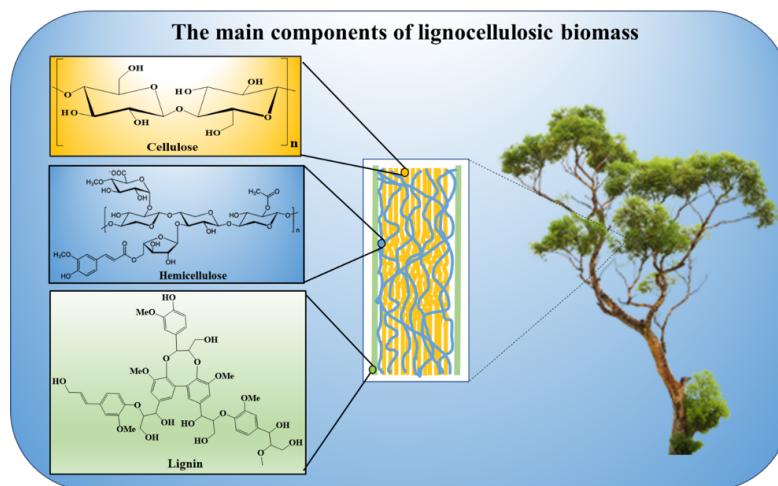
**Table 31.** (Continued)

| Name of compound                                   | Retention<br>time<br>(min) | area %              |       |                                |                                |                                |
|--|----------------------------|---------------------|-------|--------------------------------|--------------------------------|--------------------------------|
|  |                            | without<br>catalyst | Pd/C  | Pd/C &<br>Sm(OTf) <sub>3</sub> | Pd/C &<br>La(OTf) <sub>3</sub> | Pd/C &<br>Cu(OTf) <sub>2</sub> |
| 2-Ethylphenol                                      | 37.07                      | -                   | -     | -                              | -                              | 0.25                           |
| 2-Methoxy-4-methylphenol                           | 37.67                      | 3.08                | 1.71  | 1.58                           | 1.13                           | 1.34                           |
| 4-Propylphenol                                     | 43.21                      | -                   | -     | -                              | 0.09                           | -                              |
| 4-Ethyl-2-methoxyphenol                            | 43.78                      | 5.05                | 8.66  | 9.07                           | 6.8                            | 7.91                           |
| 2-Methoxy-3-(2-propenyl)phenol                     | 48.97                      | 1.51                | -     | -                              | -                              | -                              |
| 2-Methoxy-4-propylphenol                           | 49.74                      | 7.58                | 4.92  | 5.93                           | 6.32                           | 5.16                           |
| Vanilin  | 51.81                      | 0.33                | -     | -                              | -                              | -                              |
| 2-Methoxy-4-(1-propenyl)phenol                     | 52.09                      | 3.36                | -     | -                              | -                              | -                              |
| 1-(4-Hydroxy-3-methoxyphenyl)ethanone              | 57.18                      | 0.37                | -     | -                              | -                              | -                              |
| Ethyl homovanillate                                | 66.11                      | 0.45                | -     | 0.15                           | -                              | -                              |
| 4-(Ethoxymethyl)-2-methoxyphenol                   | 66.57                      | -                   | -     | 4.53                           | -                              | -                              |
| 4-Hydroxy-3-methoxybenzeneacetic acid              | 66.64                      | 2.82                | 28.99 | 21.6                           | 16.8                           | 26.08                          |
| Ethyl-3-(4-hydroxy-3-methoxyphenyl)propionate      | 71.57                      | 0.36                | 0.38  | 0.51                           | 0.41                           | 0.41                           |
| <b>Furan</b>                                       |                            |                     |       |                                |                                |                                |
| 2-Furanmethanol                                    | 8.83                       | 1.8                 | -     | -                              | -                              | -                              |
| 3-Furanmethanol                                    | 9.18                       | -                   | -     | -                              | -                              | 0.61                           |
| Tetrahydro-2-furanmethanol                         | 10.07                      | 0.39                | 4.59  | 4.08                           | 3.73                           | 4.25                           |
| Tetrahydro-2-methylfuran                           | 12.33                      | -                   | 0.38  | -                              | -                              | -                              |
| Tetrahydro-2-(methoxymethyl)furan                  | 16.90                      | -                   | -     | 0.24                           | -                              | -                              |
| 2,5-Diethoxytetrahydrofuran                        | 23.20                      | 0.1                 | -     | -                              | -                              | -                              |
| 2-Furancarboxylic acid ethyl ester                 | 26.38                      | 0.32                | 0.28  | 0.19                           | 0.25                           | 0.14                           |
| <b>Ester</b>                                       |                            |                     |       |                                |                                |                                |
| 2-Hydroxypropanoic acid ethyl ester                | 6.39                       | 3.85                | 1.44  | 1                              | 0.92                           | 0.77                           |
| 2-Hydroxybutanoic acid ethyl ester                 | 11.89                      | -                   | 1.59  | -                              | -                              | -                              |
| 2-Hydroxybutanoic acid methyl ester                | 11.96                      | 1.68                | -     | -                              | -                              | -                              |
| Butyrolactone                                      | 12.59                      | 0.45                | 0.51  | 0.45                           | 0.39                           | 0.54                           |
| Ethoxyacetic acid ethyl ester                      | 12.79                      | 0.15                | -     | -                              | -                              | -                              |
| 4-Oxopentanoic acid ethyl ester                    | 27.68                      | 1.46                | -     | 0.44                           | -                              | 0.42                           |
| Ethyl-2-hydroxyhexanoate                           | 30.24                      | -                   | 0.58  | -                              | -                              | -                              |
| Benzoic acid ethyl ester                           | 35.58                      | -                   | -     | -                              | 0.04                           | -                              |
| 5-Oxohexanoic acid ethyl ester                     | 36.05                      | -                   | -     | 0.18                           | -                              | 0.15                           |
| Butanedioic acid diethyl ester                     | 37.43                      | 1.78                | 0.81  | 0.81                           | 0.59                           | 0.93                           |
| Diethyl methylsuccinate                            | 39.08                      | 0.42                | -     | -                              | -                              | 0.25                           |
| Pentanedioic acid diethyl ester                    | 44.28                      | -                   | 0.75  | 0.7                            | 0.7                            | 0.88                           |
| Hexanedioic acid diethyl ester                     | 51.24                      | 0.21                | 0.29  | 0.34                           | 0.4                            | 0.28                           |
| 4-Hydroxy-3-methoxybenzeneacetic acid methyl ester | 60.81                      | -                   | 0.51  | 0.83                           | 0.41                           | -                              |

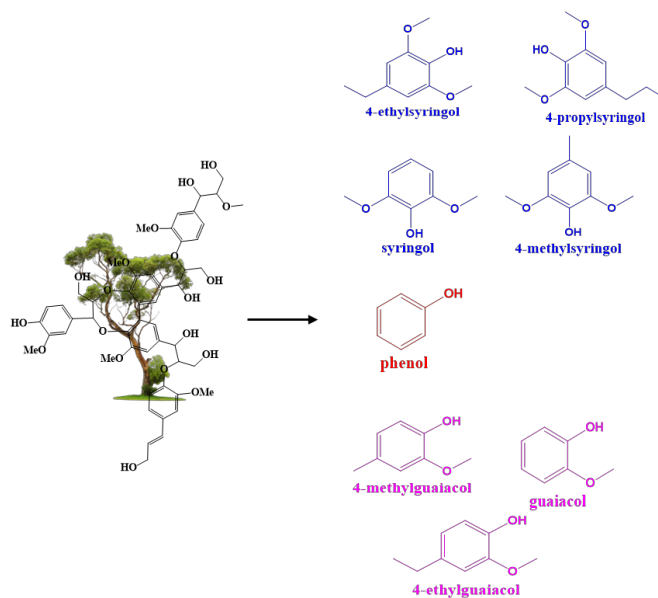
**Table 31.** (Continued)

| Name of compound                            | Retention<br>time<br>(min) | area %              |      |                                |                                |                                |
|---|----------------------------|---------------------|------|--------------------------------|--------------------------------|--------------------------------|
|   |                            | without<br>catalyst | Pd/C | Pd/C &<br>Sm(OTf) <sub>3</sub> | Pd/C &<br>La(OTf) <sub>3</sub> | Pd/C &<br>Cu(OTf) <sub>2</sub> |
| 4-Hydroxy-3-methoxybenzoic acid ethyl ester | 62.94                      | 0.89                | 0.3  | 0.29                           | 0.35                           | 0.46                           |
| Diethylphthalate                            | 63.20                      | 0.17                | -    | -                              | -                              | -                              |
| Hexadecanoic acid ethyl ester               | 84.19                      | 0.23                | -    | -                              | 0.06                           | -                              |
| Heptadecanoic acid ethyl ester              | 88.02                      | 0.4                 | -    | -                              | -                              | -                              |
| Linoleic acid ethyl ester                   | 91.31                      | 0.34                | -    | -                              | -                              | -                              |
| Ethyl Oleate                                | 91.52                      | 0.51                | -    | -                              | -                              | -                              |
| Octadecanoic acid ethyl ester               | 92.33                      | 0.24                | 0.49 | 0.47                           | 0.39                           | 0.5                            |
| Methyldehydroabietate                       | 95.54                      | 0.38                | 0.31 | 0.29                           | 0.24                           | 0.35                           |

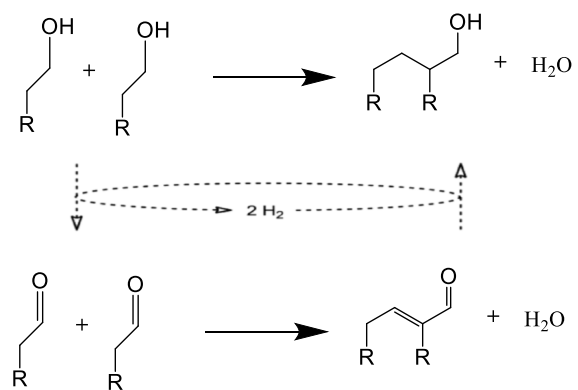
## APPENDIX B: FIGURES



**Figure 1.** The main components of lignocellulosic biomass.<sup>6</sup> (Reproduced from Ref. 6 with permission from John Wiley & Sons)

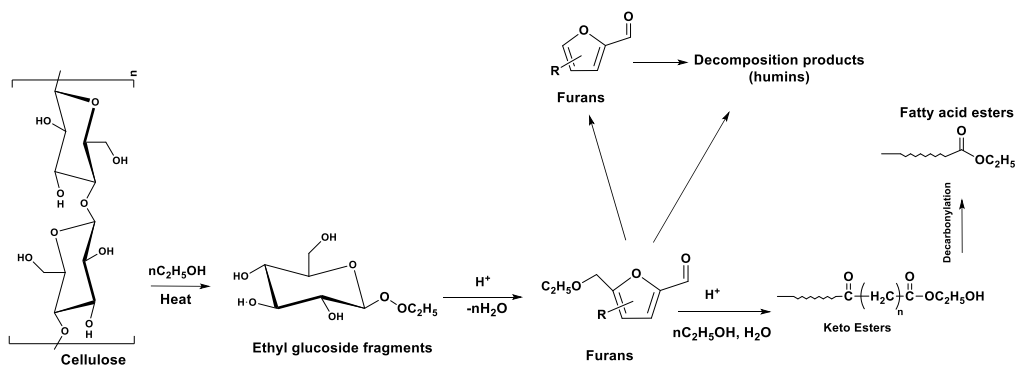


**Figure 2.** Monomeric phenols from degradation of lignin in ethanol.<sup>6</sup> (Reproduced from Ref. 6 with permission from John Wiley & Sons)



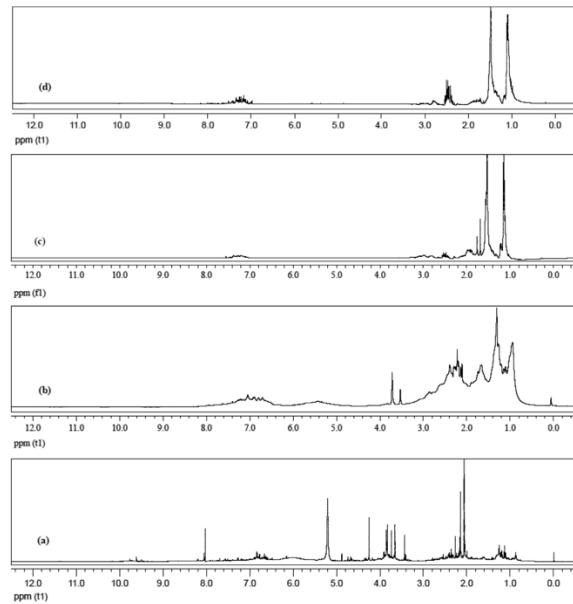
**Figure 3.** Schematic representation of the Guerbet reaction for primary alcohols.<sup>71</sup>

(Reproduced from Ref. 71 with permission from The Royal Society of Chemistry)

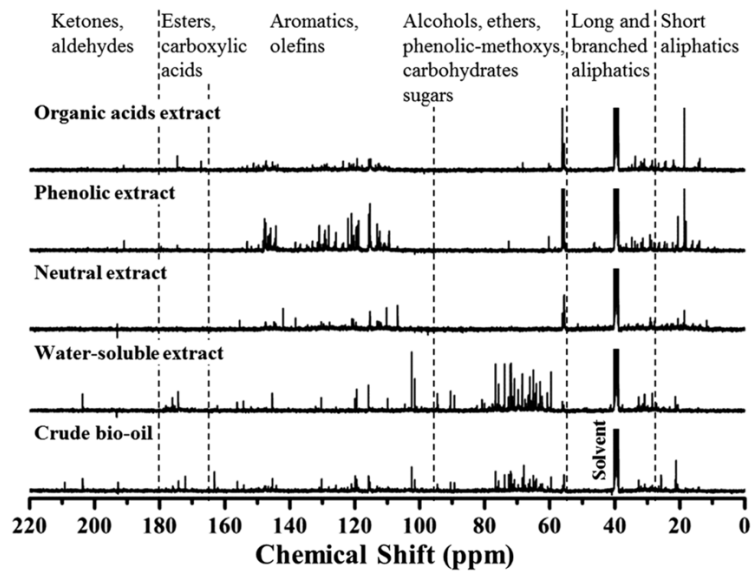


**Figure 4.** Acid-catalyzed decomposition of cellulose in ethanol.<sup>78</sup> (Reproduced from Ref. 78 with permission from Elsevier)

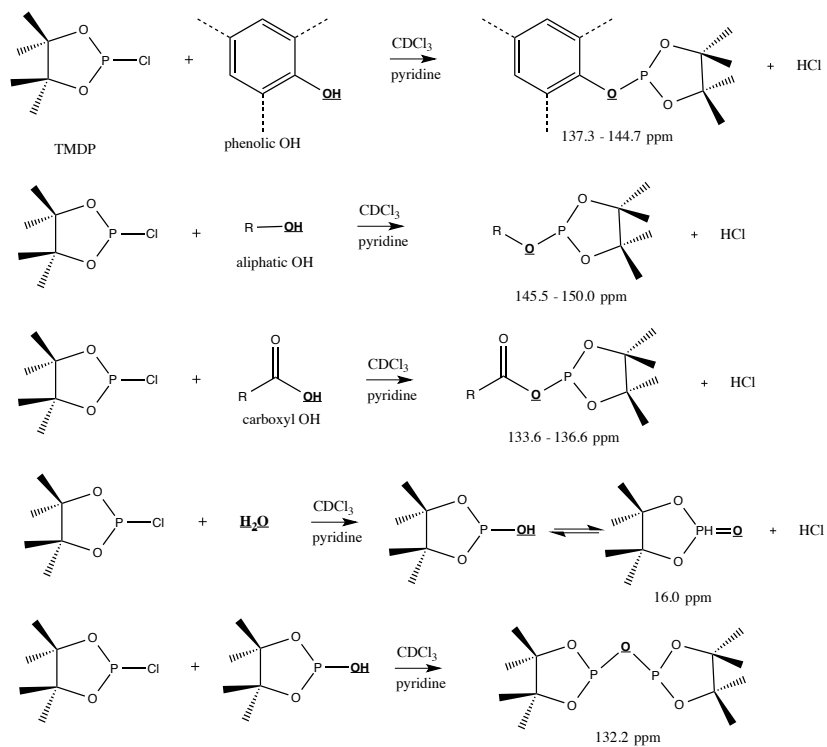




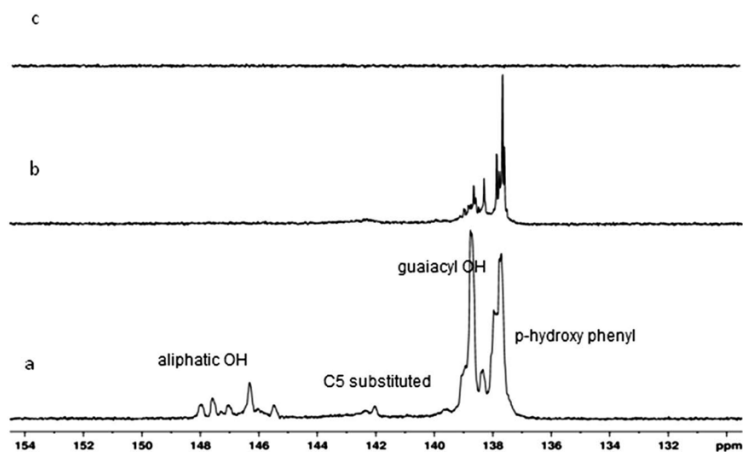
**Figure 5.**  $^1\text{H}$  NMR spectra of a) oxidized bio-oil, b) partially deoxygenated bio-oil, c) fully deoxygenated bio-oil, and d) a commercial gasoline-jet fuel-diesel mixture.<sup>107</sup>  
(Reproduced from Ref. 107 with permission from Elsevier)



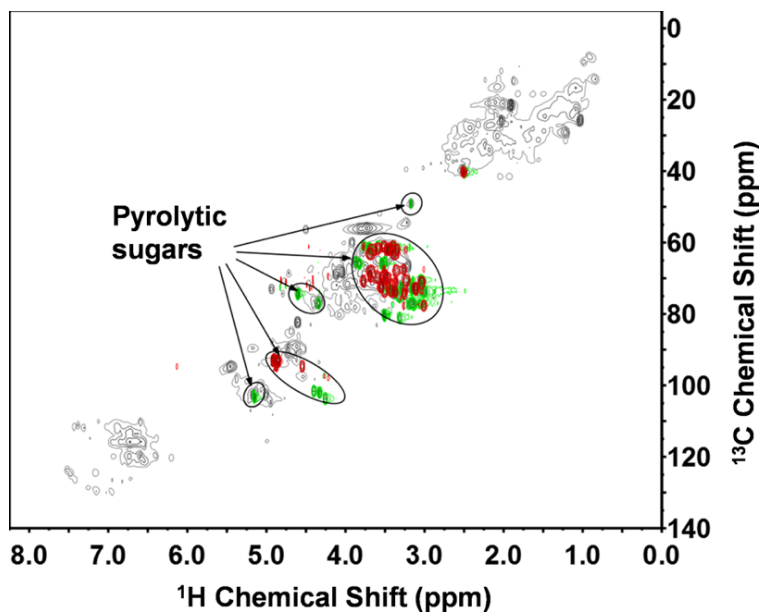
**Figure 6.**  $^{13}\text{C}$  NMR spectra of the crude bio-oil, water-soluble extract, neutral extract, phenolic extract, and organic acids extract.<sup>115</sup> (Reproduced from Ref. 115 with the permission from The Royal Society of Chemistry)



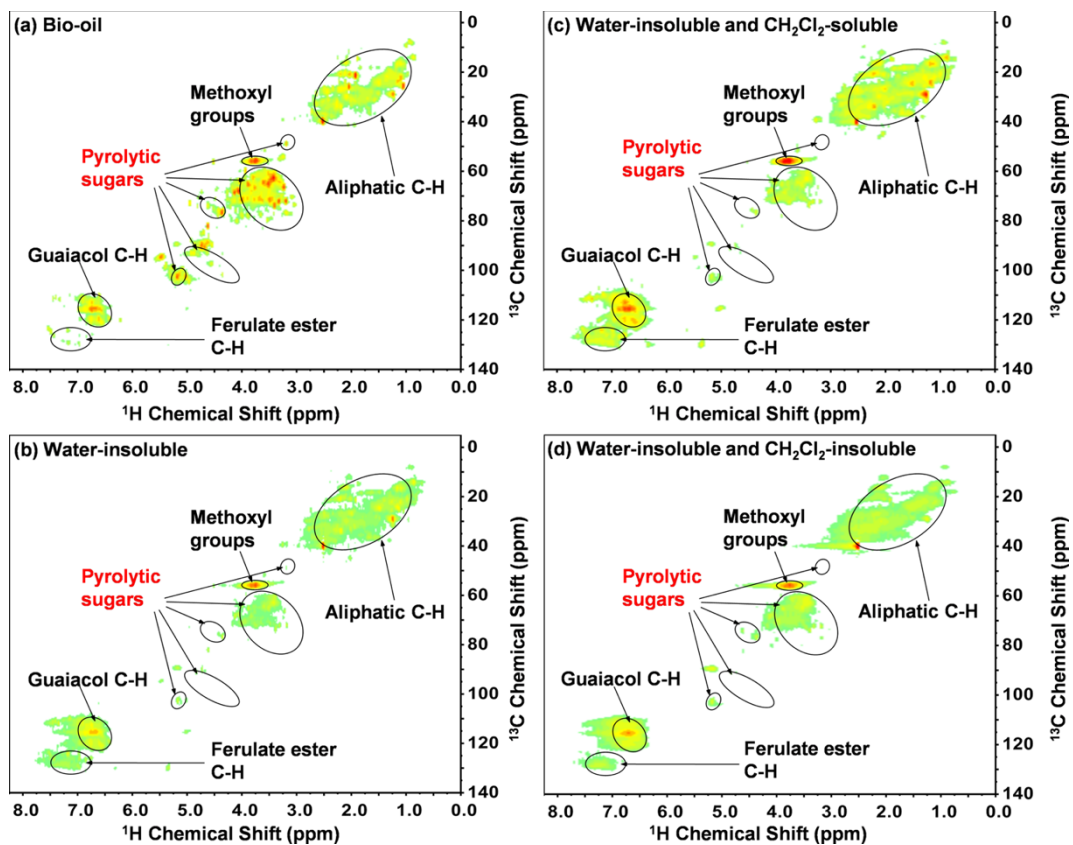
**Figure 7.** Reactions between TMDP and various hydroxyl functional groups and the <sup>31</sup>P NMR assignment of phosphitylated compounds.<sup>119</sup> (Reprinted from Ref. 119 with permission from American Chemistry Society)



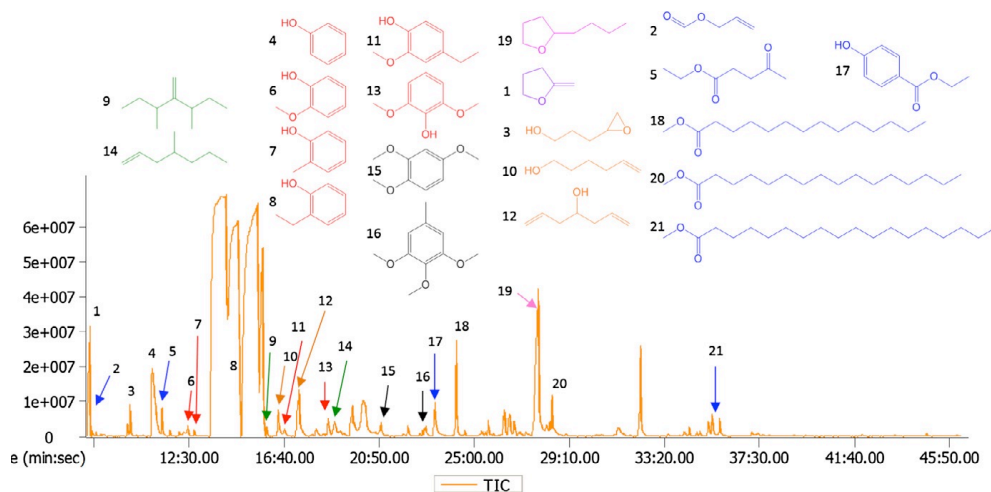
**Figure 8.** Quantitative  $^{31}\text{P}$  NMR spectra of a) the crude oil, b) the bio-oil upgraded at 250 °C and c) the bio-oil upgraded at 300 °C.<sup>122</sup> (Reproduced from Ref. 122 with permission from The Royal Society of Chemistry)



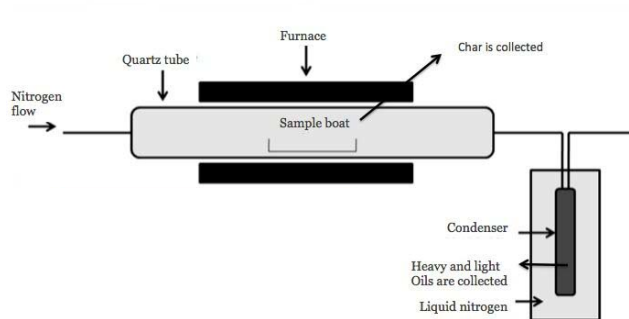
**Figure 9.** HSQC spectra of bio-oil, sugar monomer standards, and anhydrosugar standards. Gray: bio-oil; Red: sugar monomer standards (i.e., glucose, galactose, mannose, xylose, and arabinose; Green: anhydrosugars (i.e., levoglucosan, cellobiosan, and cellotriosan).<sup>131</sup> (Reprinted from Ref. 131 with the permission from American Chemical Society)



**Figure 10.** HSQC spectra of bio-oil and its fractions. (a) raw bio-oil; (b) water-insoluble fraction; (c) water-insoluble and  $\text{CH}_2\text{Cl}_2$ -soluble fraction; (d) water-insoluble and  $\text{CH}_2\text{Cl}_2$ -insoluble fraction.<sup>131</sup> (Reprinted from Ref. 131 with the permission from American Chemical Society)

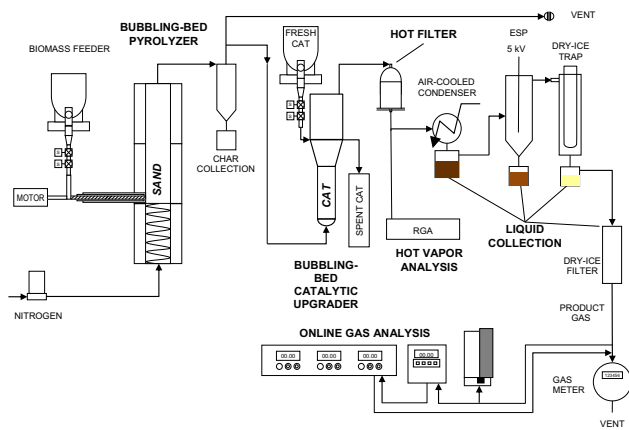


**Figure 11.** Total ion chromatogram of bio-oil produced after 30 min at 350 °C with a formic acid to lignin mass ratio of 1.5. The lignin source was CSAHL.<sup>59</sup> (Reprinted from Ref. 59 with permission from Elsevier)

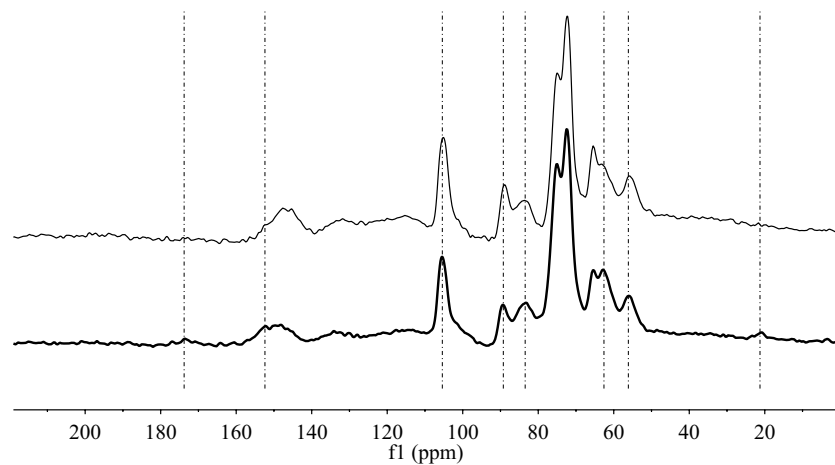


**Figure 12.** Illustration of the bench-top small scale pyrolysis unit.<sup>136</sup> (Adapted from Ref. 136 with permission from American Chemistry Society)

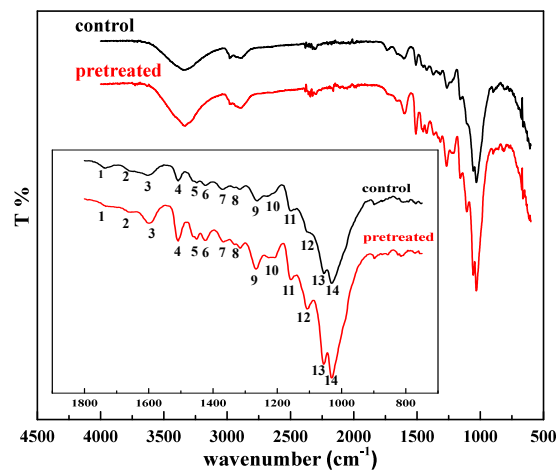




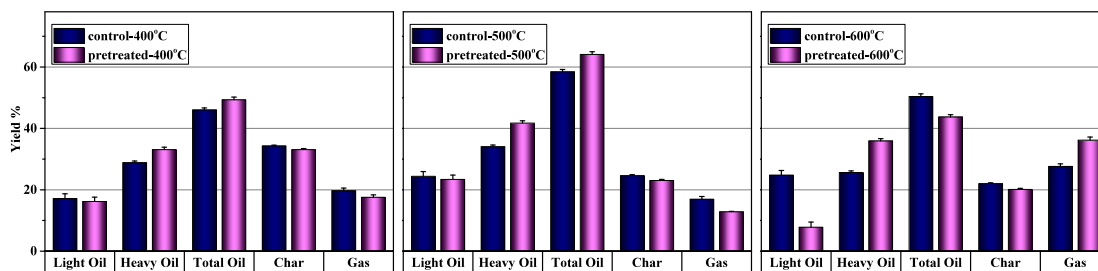
**Figure 13.** Illustration of the fluidized bed reactor system.<sup>137</sup> (Reproduced from Ref. 137 with permission from American Chemistry Society)



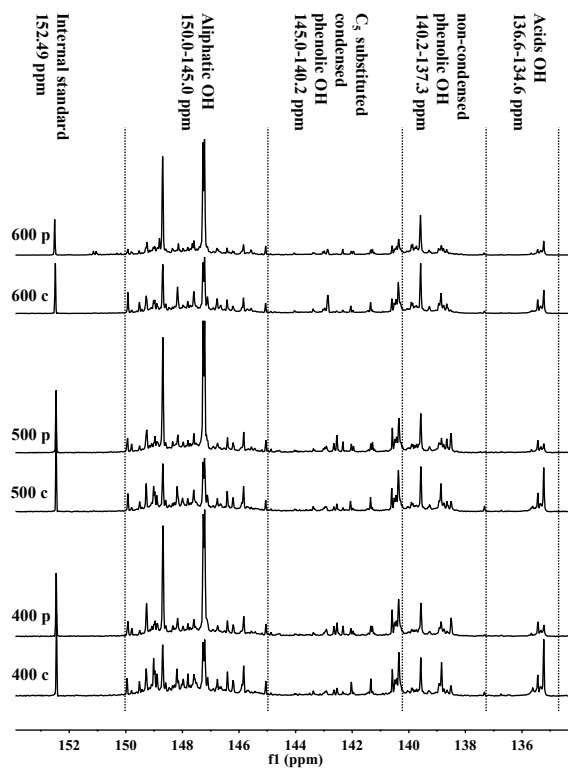
**Figure 14.** CP/MAS  $^{13}\text{C}$  NMR spectra of untreated pine wood (bottom) and autohydrolysis pretreated pine wood (top) samples.



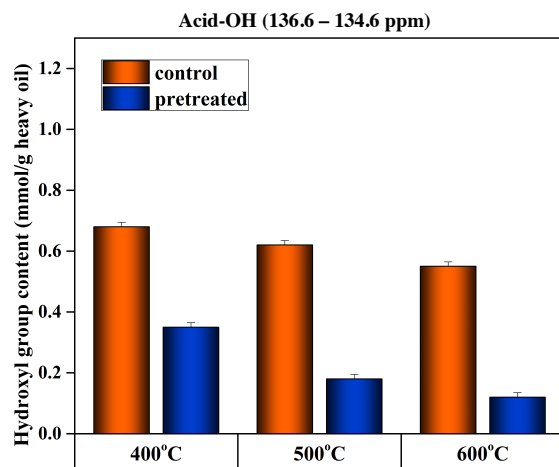
**Figure 15.** FTIR spectra of untreated pine wood and autohydrolysis pretreated pine wood samples.



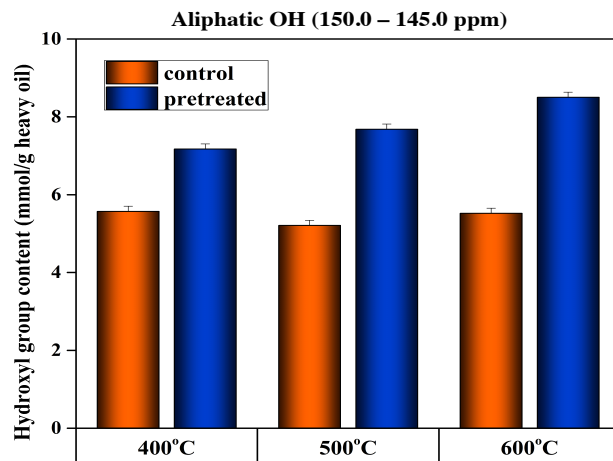
**Figure 16.** Yields distributions of pyrolysis products obtained from untreated and autohydrolysis pretreated pine wood samples under 400 °C, 500 °C, and 600 °C (wt%).



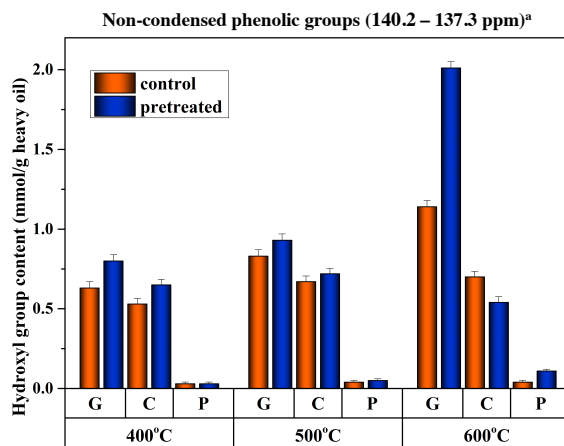
**Figure 17.**  $^{31}\text{P}$  NMR spectra of heavy oils produced from untreated and autohydrolysis pretreated pine wood at 400°C, 500°C, and 600°C. (the c denotes control, the p denotes pretreatment)



**Figure 18.** Acid-OH contents in heavy oils obtained from untreated and autohydrolysis pretreated pine wood samples under 400 °C, 500 °C, and 600 °C.

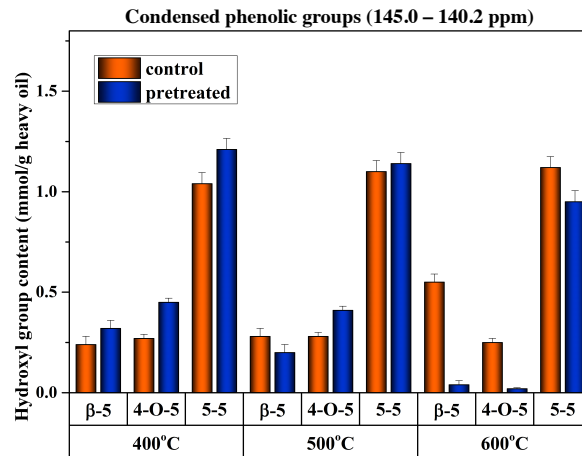


**Figure 19.** Aliphatic-OH contents in heavy oils obtained from untreated and autohydrolysis pretreated pine wood samples under 400 °C, 500 °C, and 600 °C.

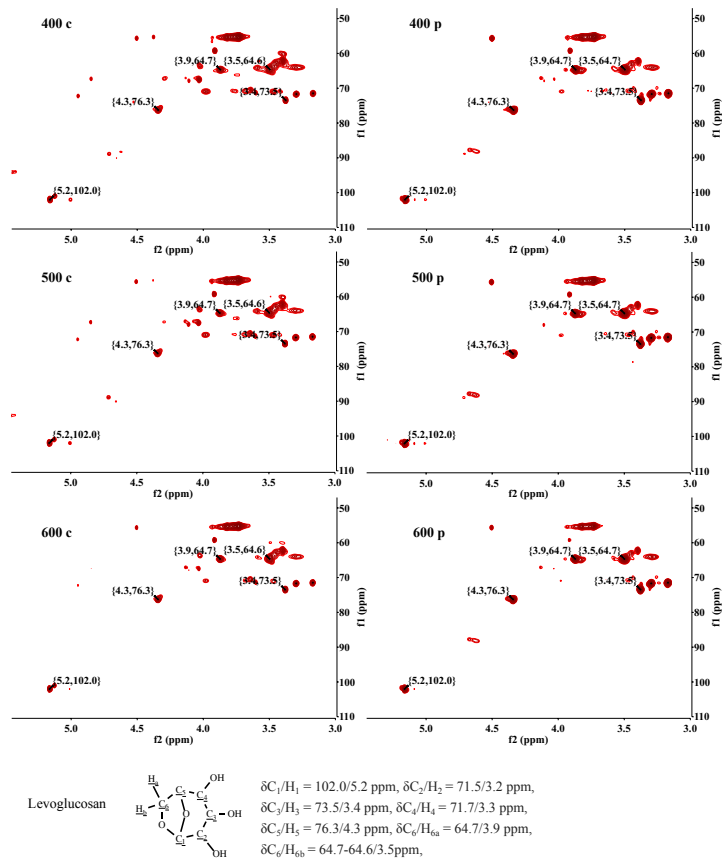


**Figure 20.** Non-condensed hydroxyl group contents in heavy oils obtained from untreated and autohydrolysis pretreated pine wood samples under 400 °C, 500 °C, and 600 °C. (<sup>a</sup>: G: guaiacyl type phenolic OH; C: catechol type phenolic OH; P: *p*-hydroxy-phenyl OH)

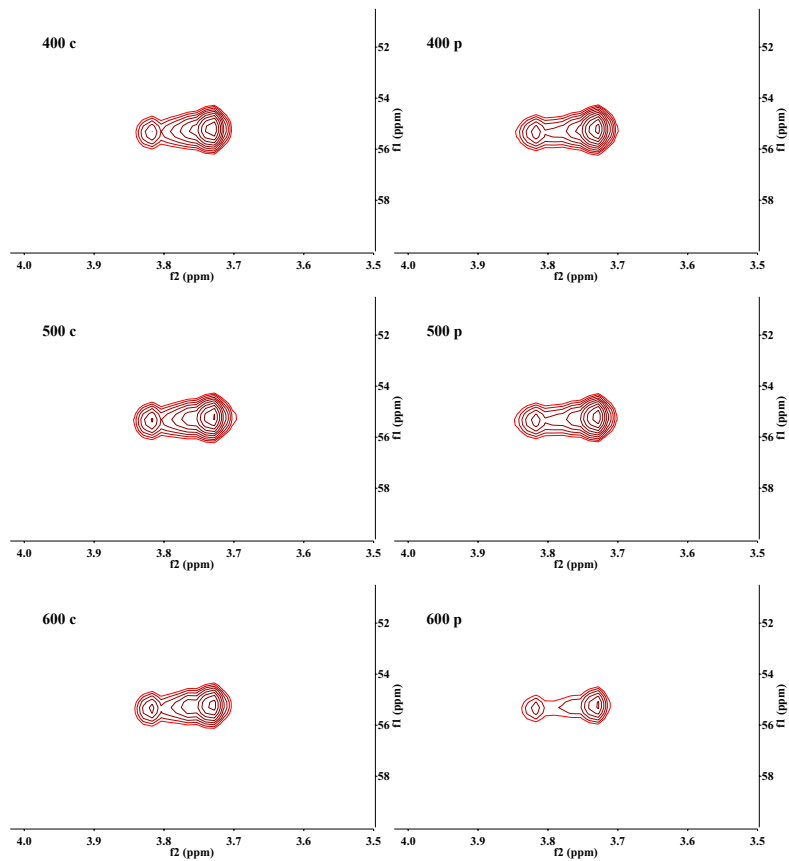




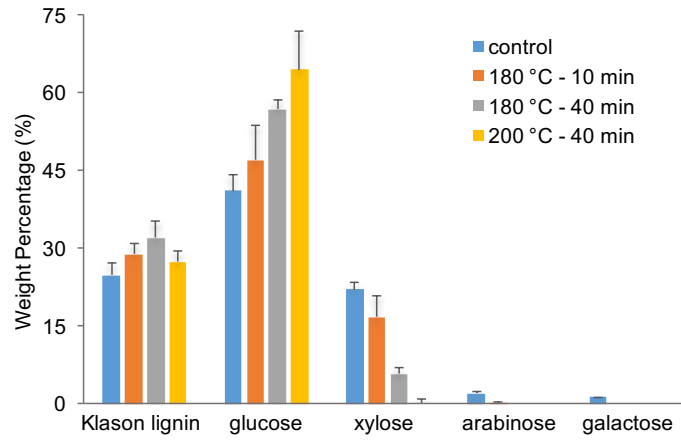
**Figure 21.** C<sub>5</sub> substituted condensed hydroxyl group contents in heavy oils obtained from untreated and autohydrolysis pretreated pine wood samples under 400 °C, 500 °C, and 600 °C.



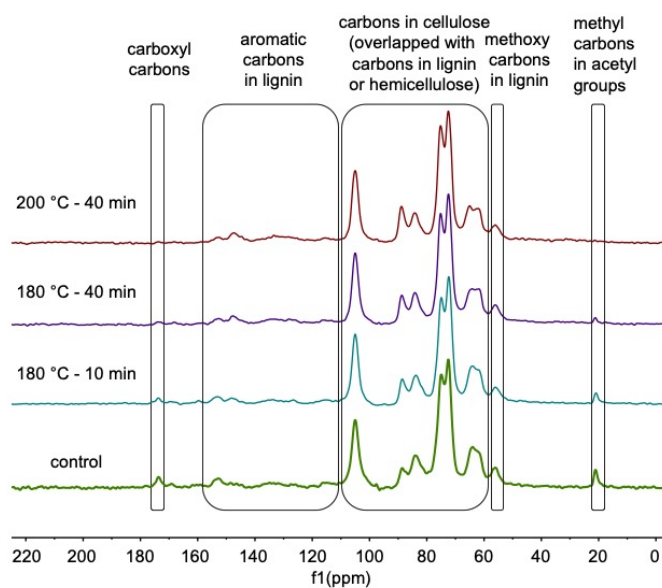
**Figure 22.** HSQC spectra of levoglucosan contents in bio-oils.



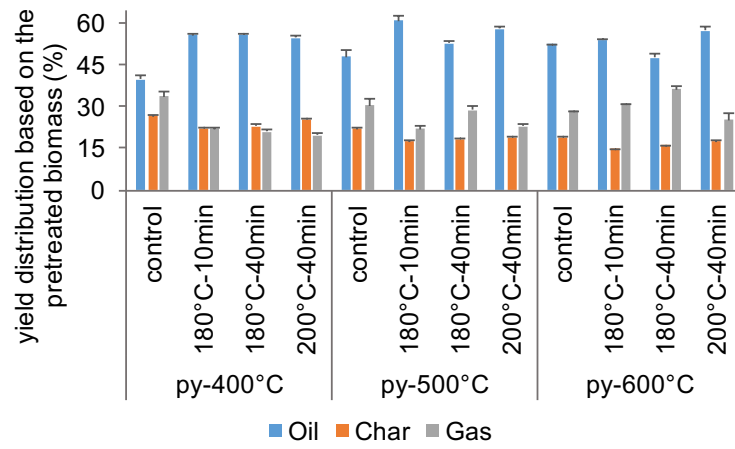
**Figure 23.** HSQC spectra of methoxy groups in bio-oils.



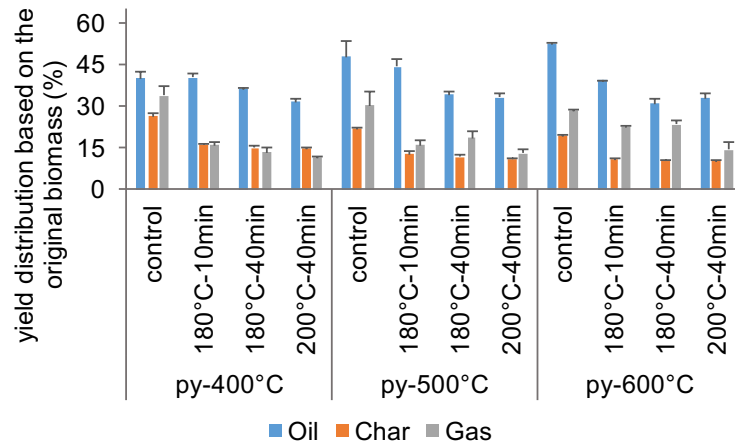
**Figure 24.** Compositional analysis of the sugarcane bagasse before and after the autohydrolysis pretreatment.



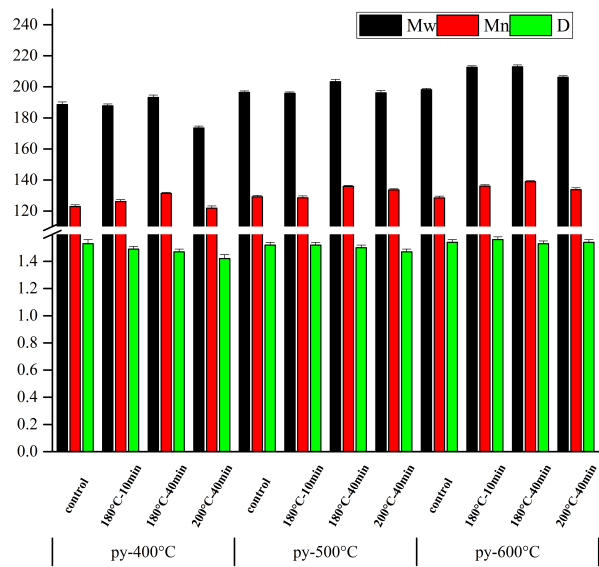
**Figure 25.** CP/MAS  $^{13}\text{C}$  NMR spectra (from bottom to top) of untreated sugarcane bagasse and sugarcane bagasse samples pretreated for 180 °C -10 min, 180 °C -40 min, 200 °C -40 min. (\*the signals in cellulose region 105-62 ppm overlap with the signals from lignin and hemicellulose)



**Figure 26.** Yield distribution of the bio-oils from the untreated and pretreated sugarcane bagasse pyrolyzed at 400, 500, and 600 °C based on the mass of pretreated biomass.

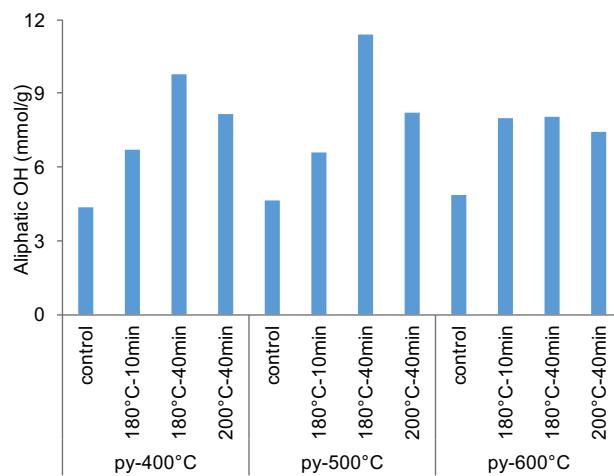


**Figure 27.** Yield distribution of the bio-oils from untreated and pretreated sugarcane bagasse pyrolyzed at 400, 500, and 600 °C based on the mass of original biomass. (mass yields of the three pretreatment conditions 180 °C – 10 min, 180 °C - 40 min, 200 °C - 40 min are 72.50%, 64.40%, and 57.29%, respectively)

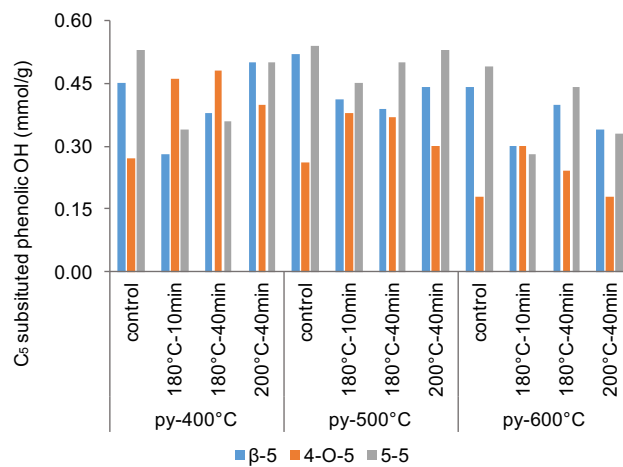


**Figure 28.** Molecular weight distribution of the bio-oils pyrolyzed from the untreated and pretreated sugarcane bagasse.

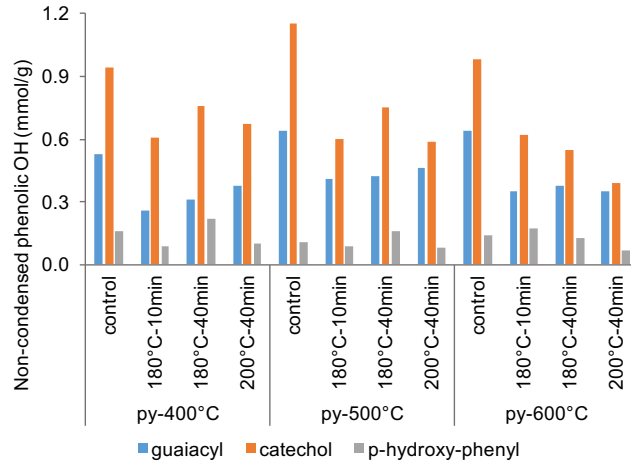




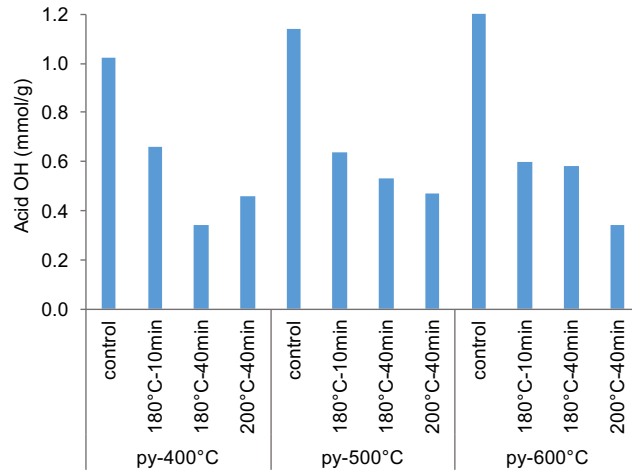
**Figure 29.** Aliphatic OH contents in the bio-oils pyrolyzed from the untreated and pretreated sugarcane bagasse.



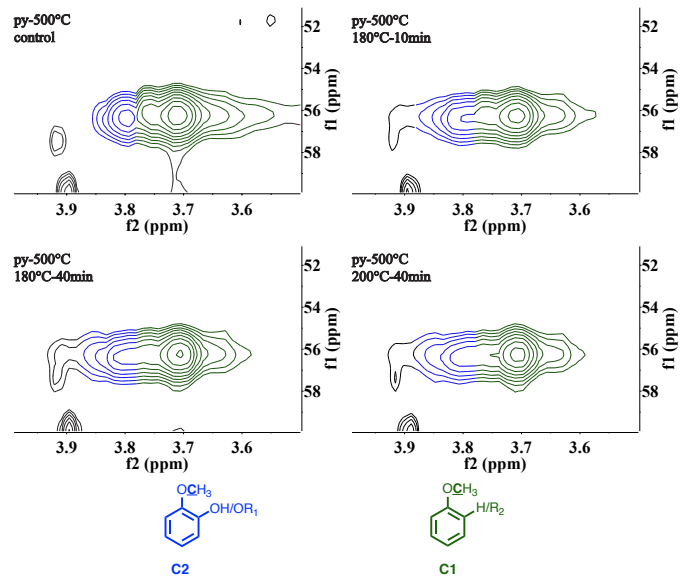
**Figure 30.** C<sub>5</sub> substituted phenolic OH contents in the bio-oils pyrolyzed from the untreated and pretreated sugarcane bagasse.



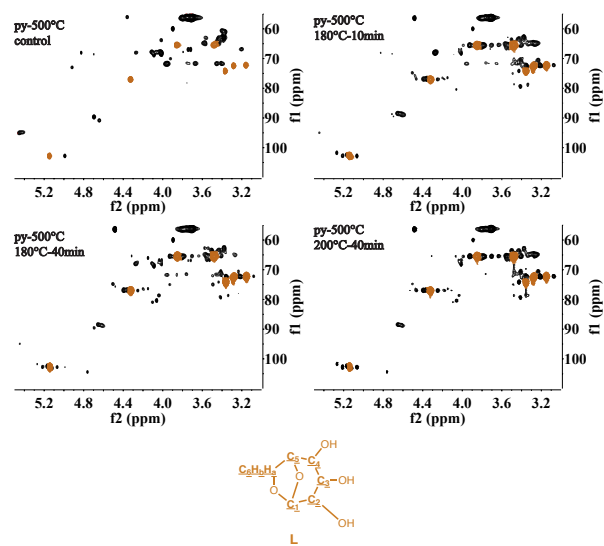
**Figure 31.** Non-condensed phenolic OH contents in the bio-oils pyrolyzed from the untreated and pretreated sugarcane.



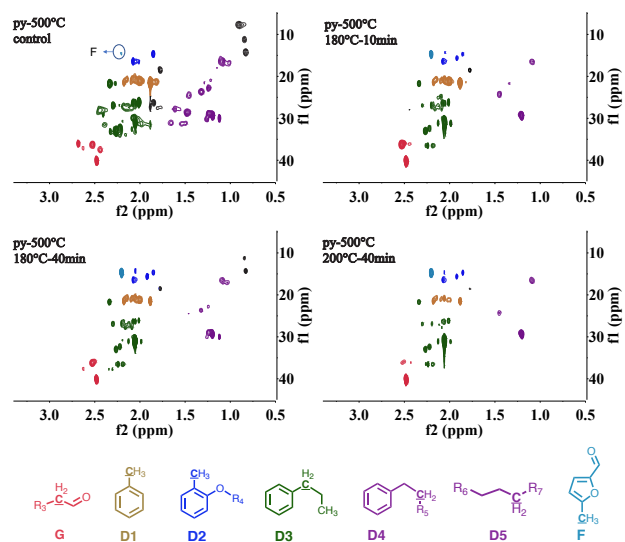
**Figure 32.** Acid contents in the bio-oils pyrolyzed from the untreated and pretreated sugarcane bagasse.



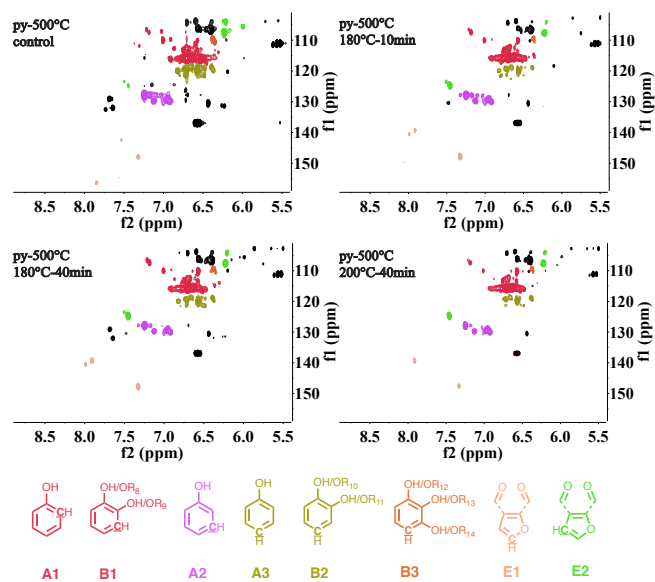
**Figure 33.** HSQC NMR spectra and assignments of methoxy groups in the sugarcane bagasse bio-oils pyrolyzed at 500 °C. (black area: unassigned)



**Figure 34.** HSQC NMR spectra and assignments of each C-H bond of levoglucosan in the sugarcane bagasse bio-oils pyrolyzed at 500 °C. (black area: unassigned)

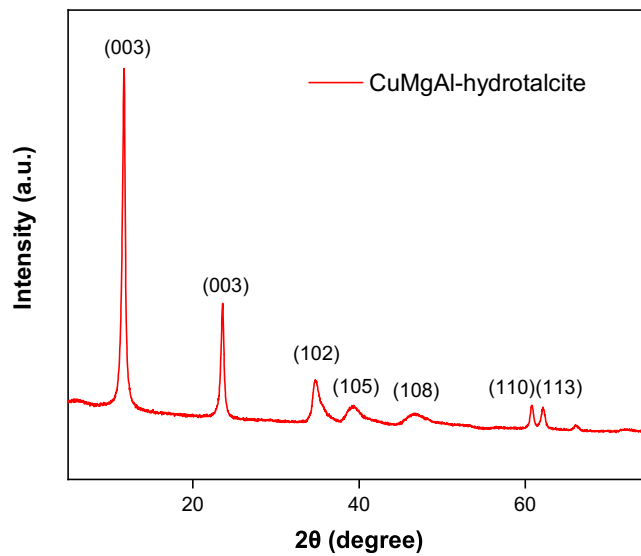


**Figure 35.** HSQC NMR spectra and assignments of aliphatic C-H bonds in the sugarcane bagasse bio-oils pyrolyzed at 500 °C. (black area: unassigned)

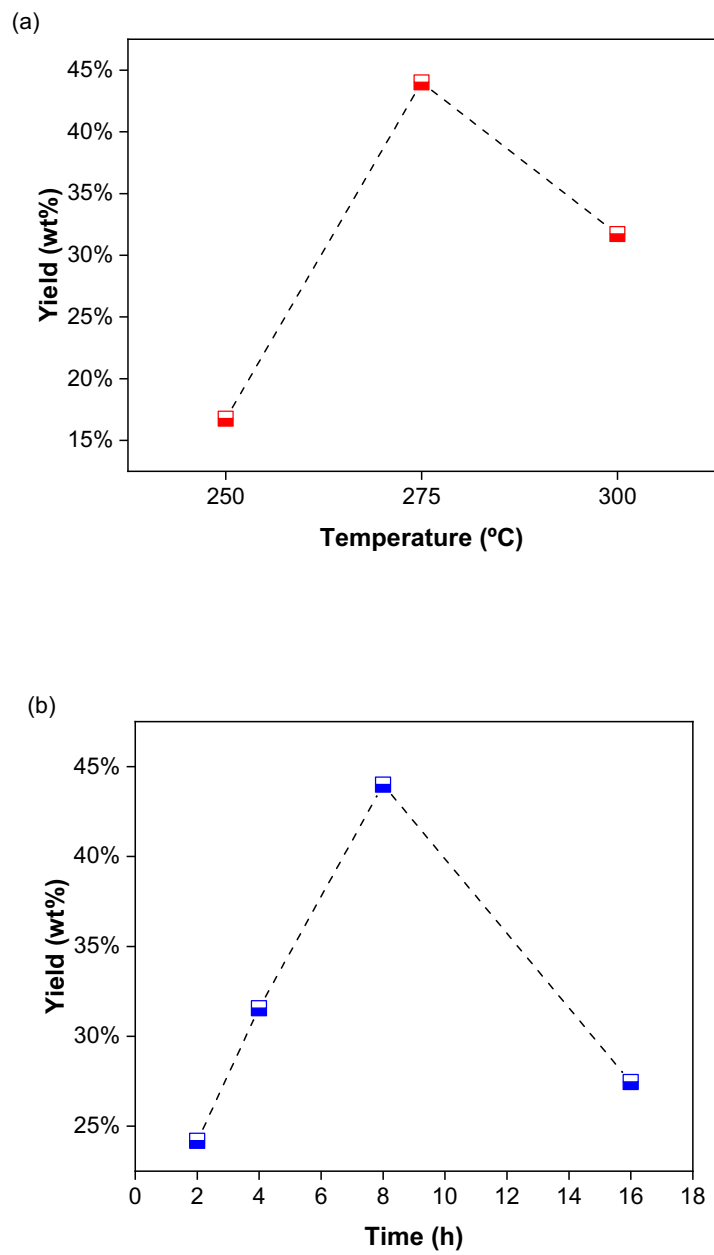


**Figure 36.** HSQC NMR spectra and assignments of aromatic C-H bonds in the sugarcane bagasse bio-oils pyrolyzed at 500 °C. (black area: unassigned)

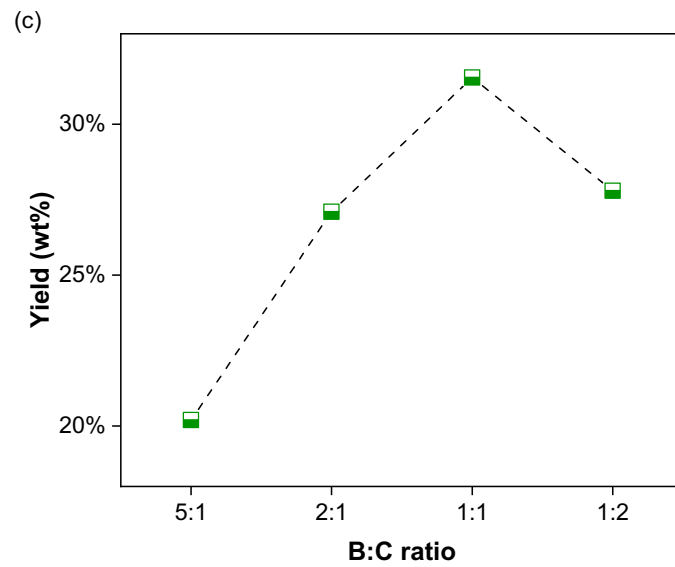




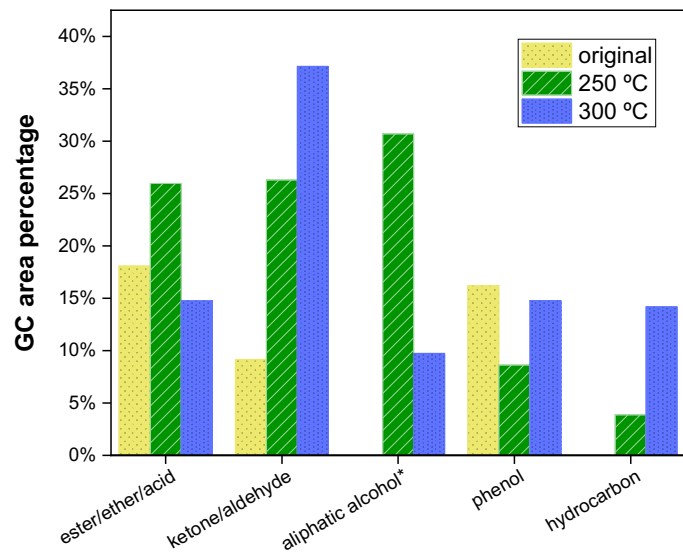
**Figure 37.** X-ray spectra of the copper doped hydrotalcite precursor.



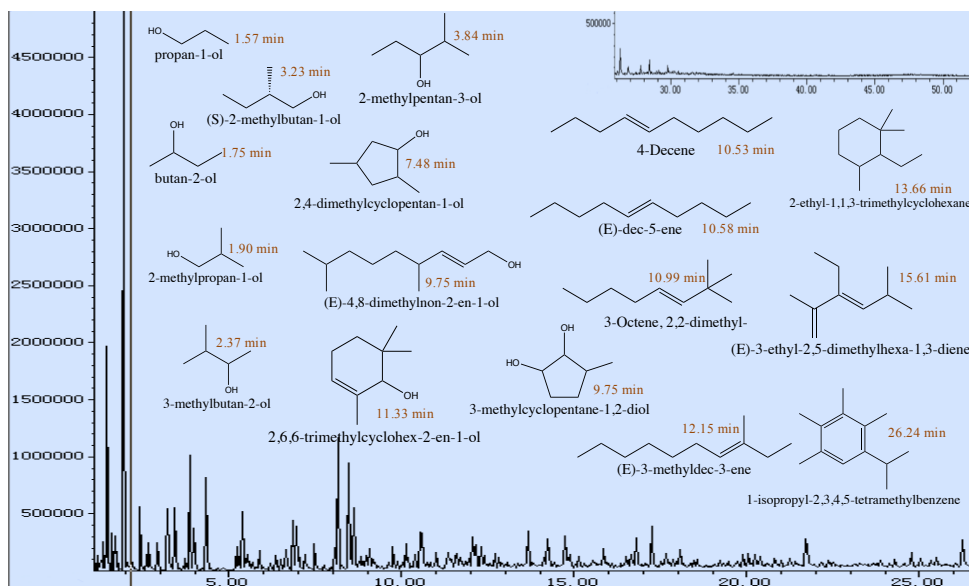
**Figure 38.** Effect of (a) varied reaction temperature, 8 h, B:C = 1:1; (b) varied reaction time, 275 °C, B:C = 1:1; (c) varied B:C ratio, 275 °C, 8h.



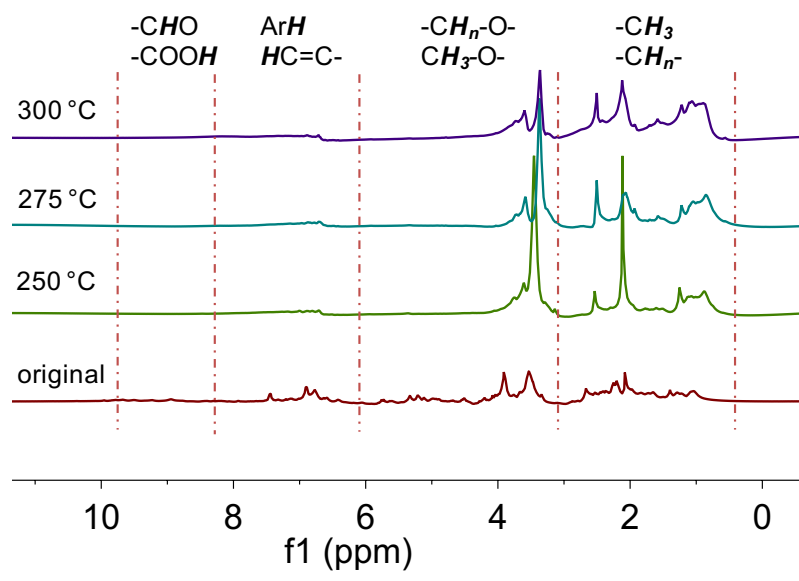
**Figure 38.** (Continued)



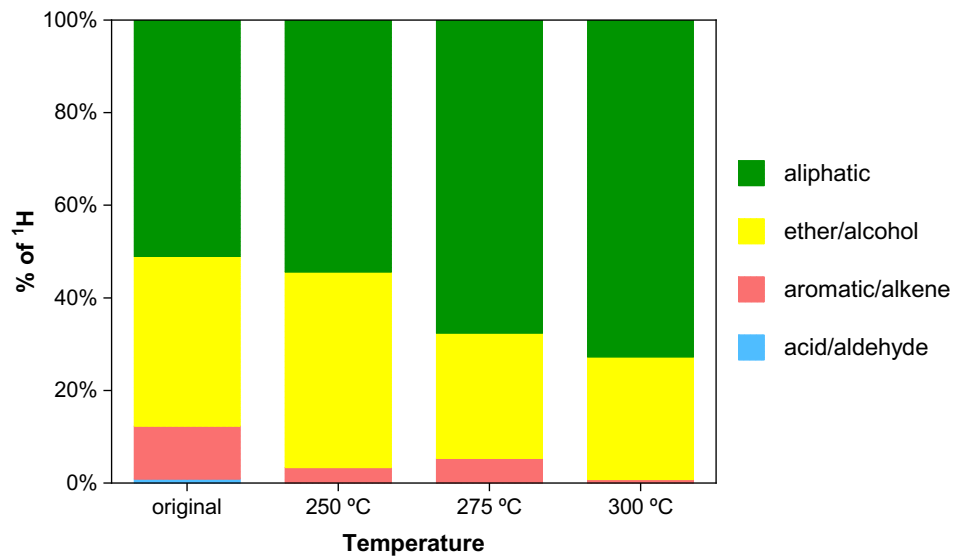
**Figure 39.** GC-MS results of the bio-oils at 250 °C and 300 °C (8 h, B:C = 1:1).



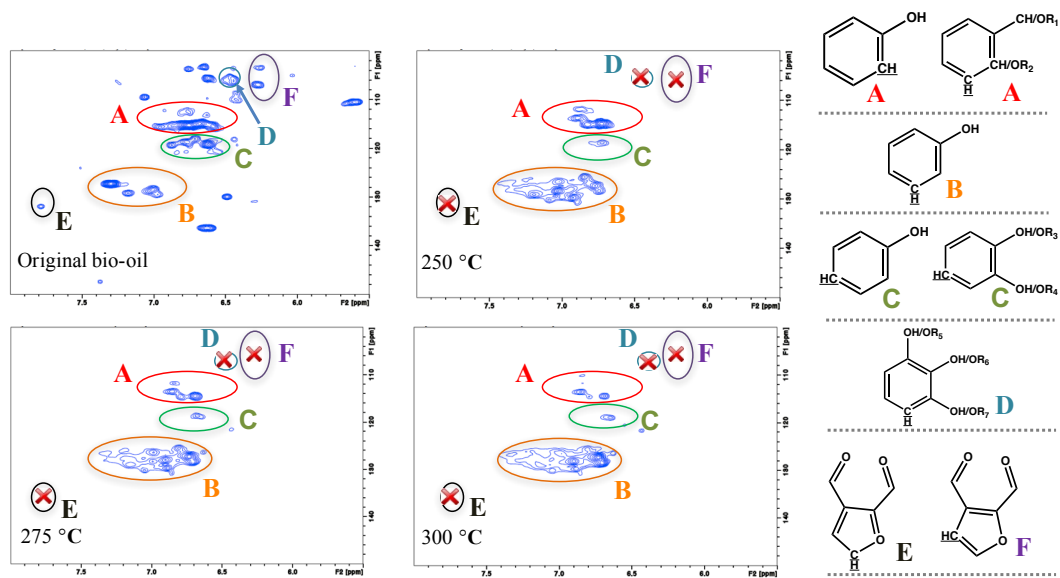
**Figure 40.** An example of the GC spectra of the upgraded bio-oil (300 °C, 8 h, B:C = 1:1).



**Figure 41.** <sup>1</sup>H NMR analysis of bio-oils (8 h, B:C = 1:1).

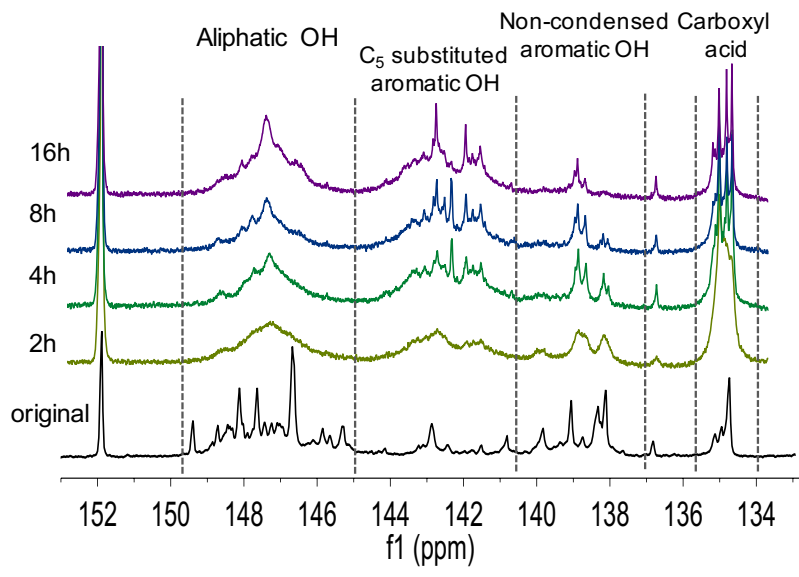


**Figure 42.** <sup>1</sup>H NMR integration results of bio-oils (8 h, B:C = 1:1).

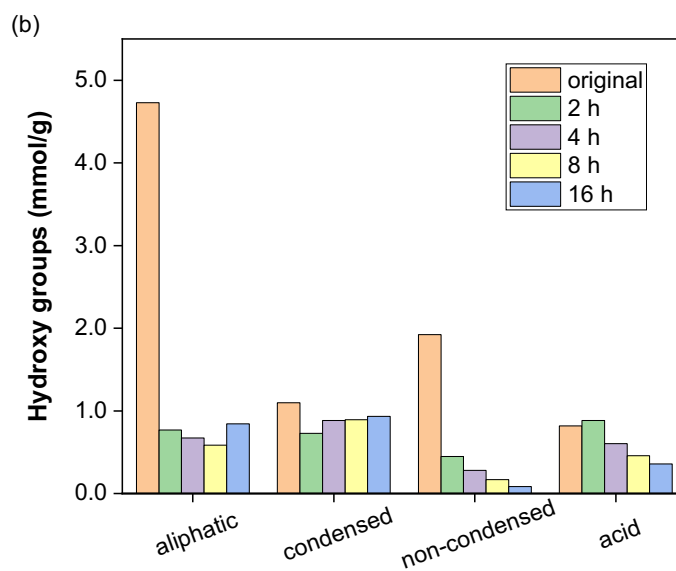
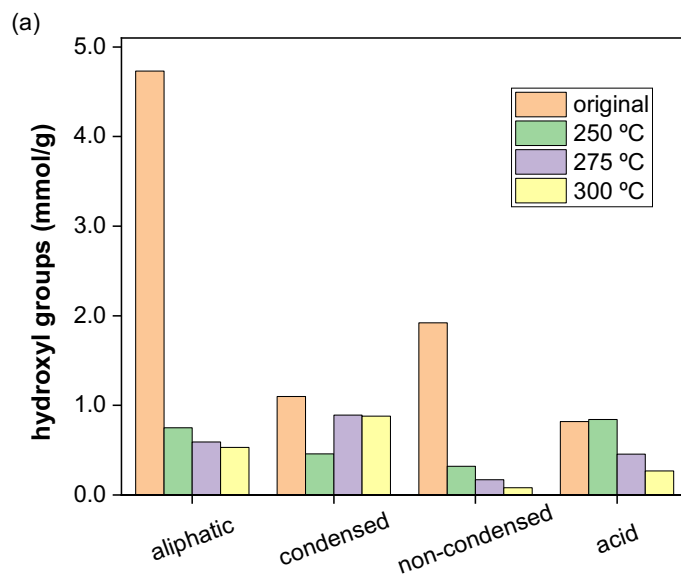


**Figure 43.** HSQC NMR analysis of bio-oils (8 h, B:C = 1:1).

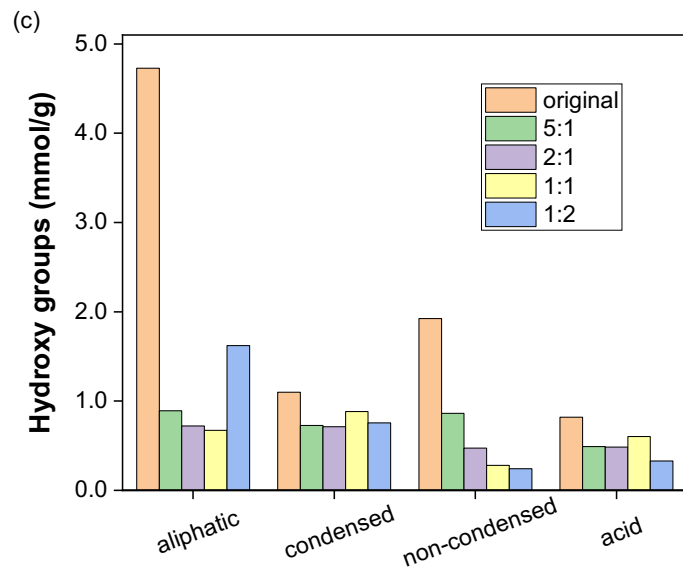




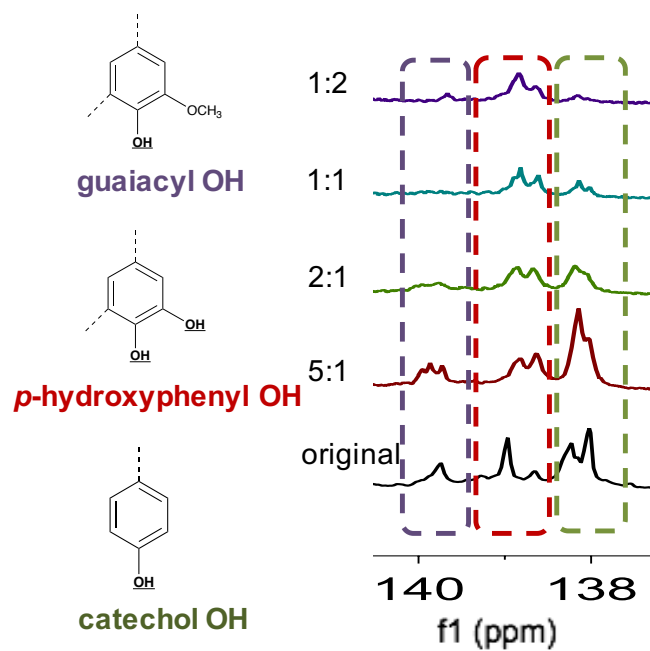
**Figure 44.**  $^{31}\text{P}$  NMR analysis of bio-oils (275 °C, B:C = 1:1).



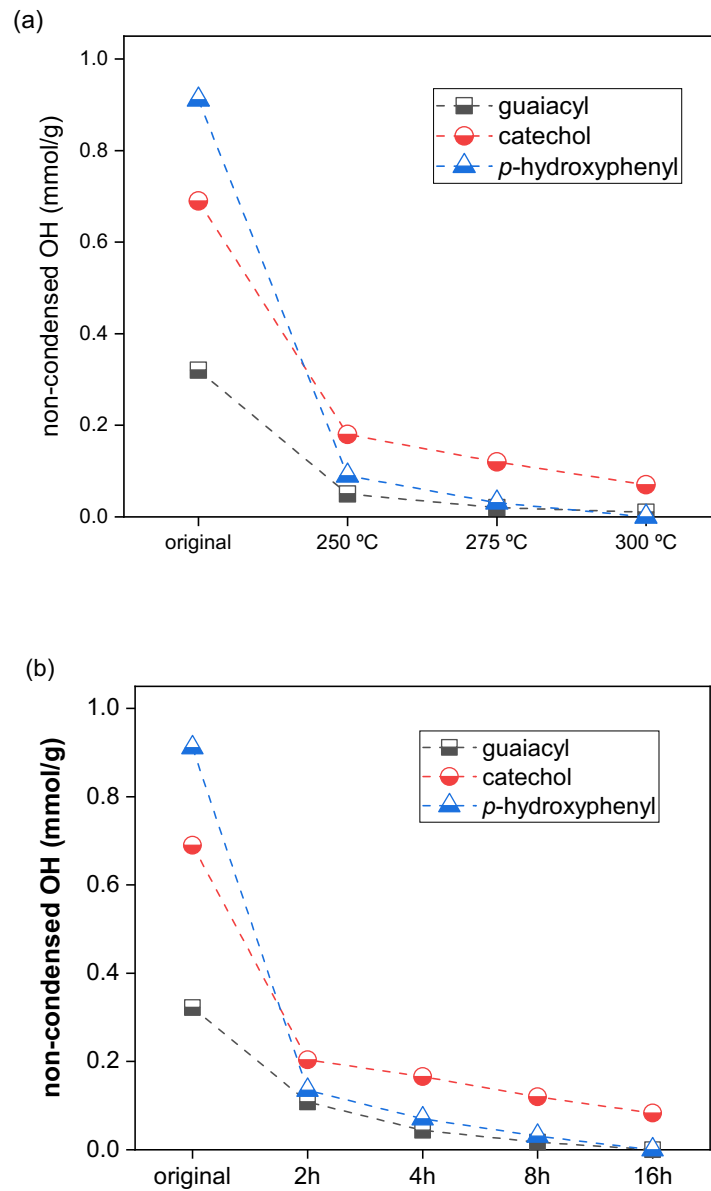
**Figure 45.**  $^{31}\text{P}$  NMR integration results of bio-oils (a) 8 h, B:C = 1:1; (b) 275 °C, B:C = 1:1; (c) 275 °C, 4h.



**Figure 45.** (Continued)



**Figure 46.** Non-condensed OH of bio-oils (275 °C, B:C = 1:1, 4h).



**Figure 47.**  $^{31}\text{P}$  NMR integration results of non-condensed OH (a) 8 h, B:C = 1:1; (b) 275 °C, B:C = 1:1; (c) 275 °C, 4h.

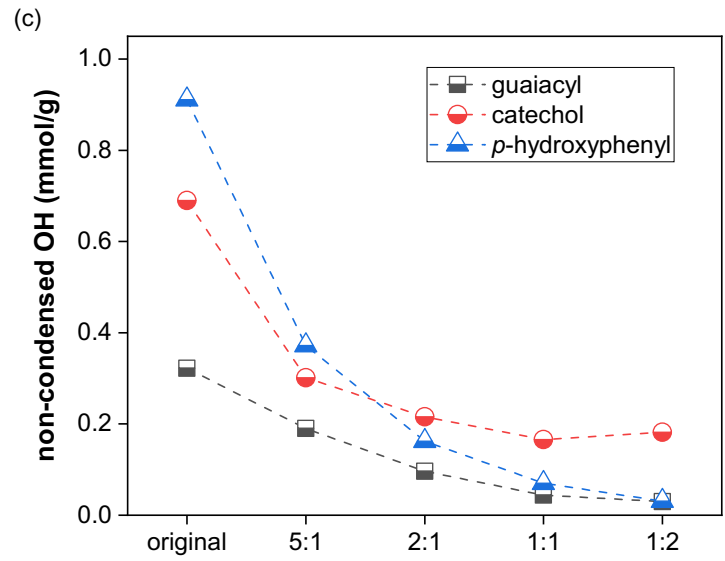
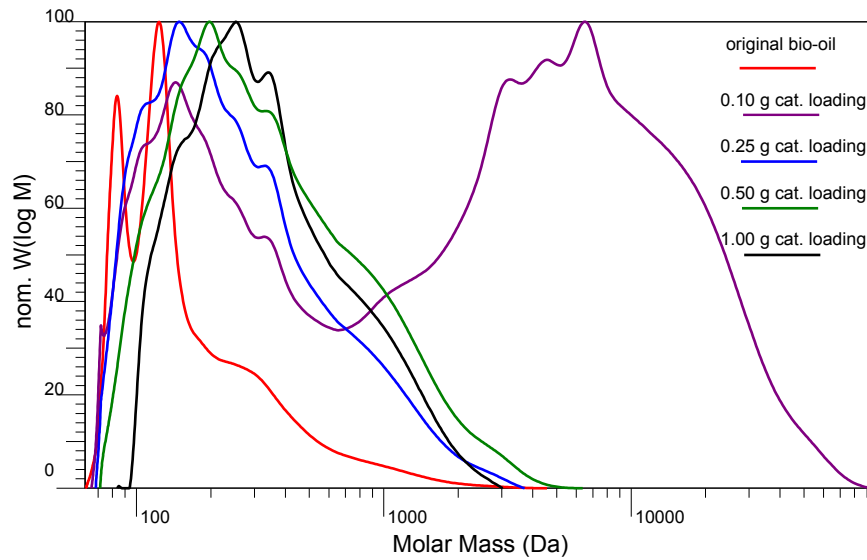
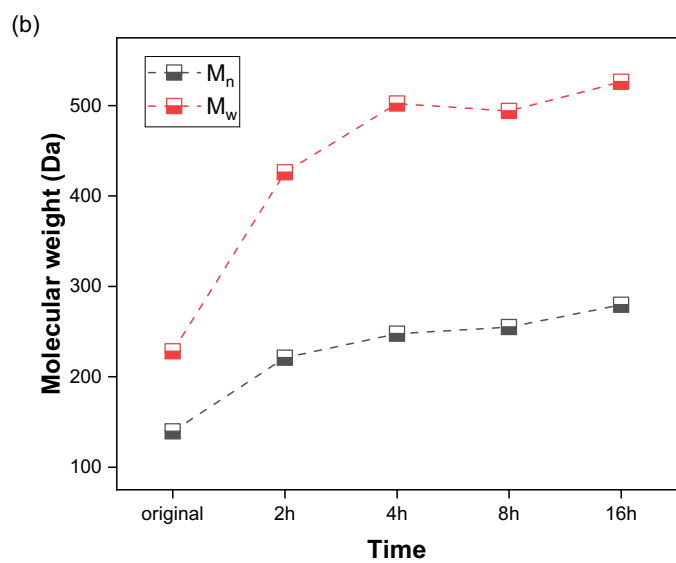
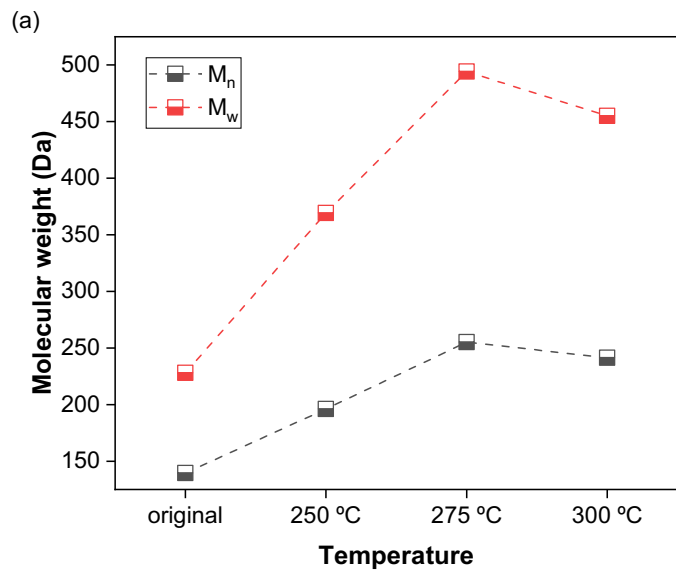


Figure 47. (Continued)

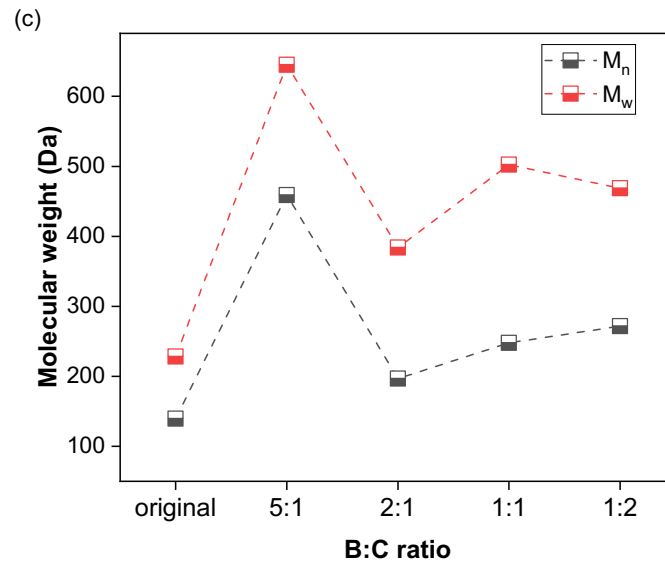


**Figure 48.** GPC curve of bio-oils. (275 °C, B:C = 1:1, 4h).

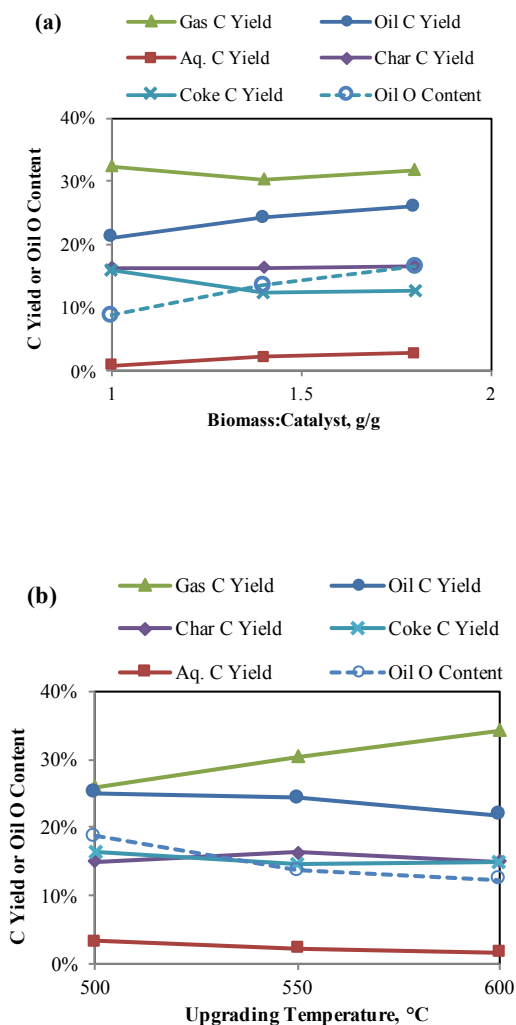


**Figure 49.** GPC curve of bio-oils (a) 8 h, B:C = 1:1; (b) 275 °C, B:C = 1:1; (c) 275 °C, 4h.

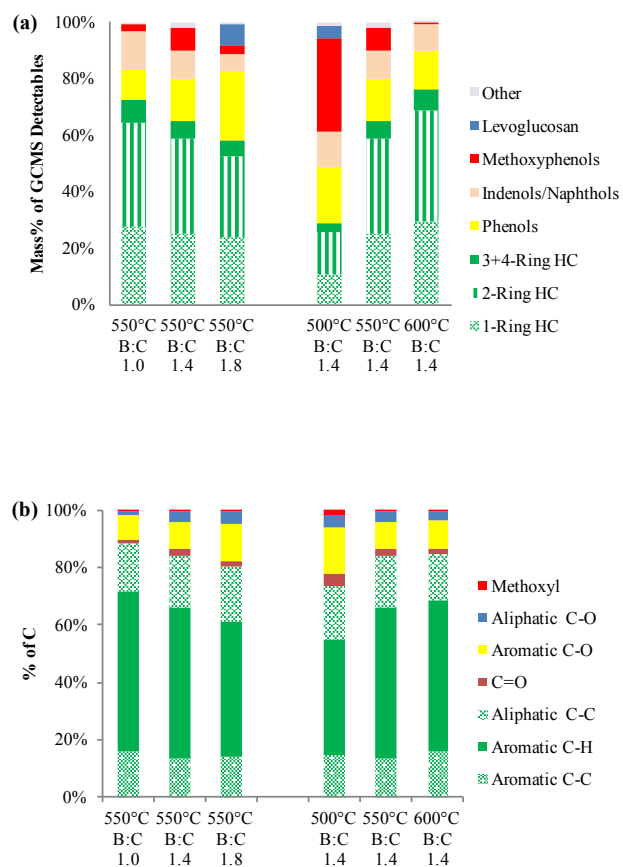




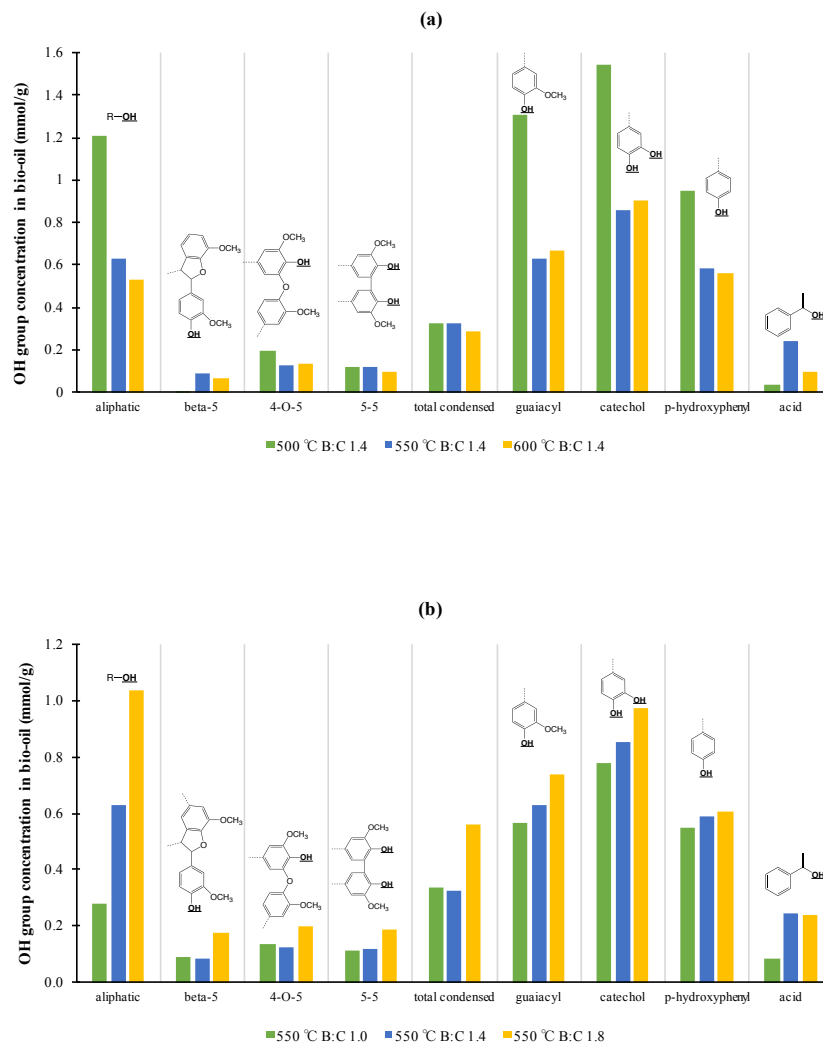
**Figure 49.** (Continued)



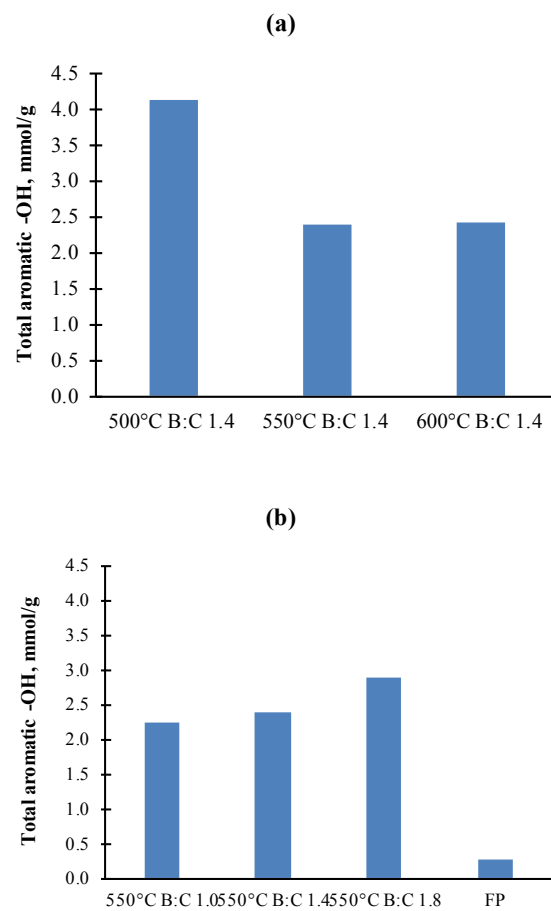
**Figure 50.** Carbon yields (g C in product/g C in feed) for CFP products and oil organic oxygen content. (a) function of the biomass-to-catalyst mass (B:C) ratio with upgrading temperature of 550°C, and b) function of the upgrading temperature ratio with B:C of 1.4. Two of the experiments were repeated (550° and 600°C at B:C 1.4) and the average is shown for these experiments. The replicate carbon yields for all products were within one percentage point of the average.



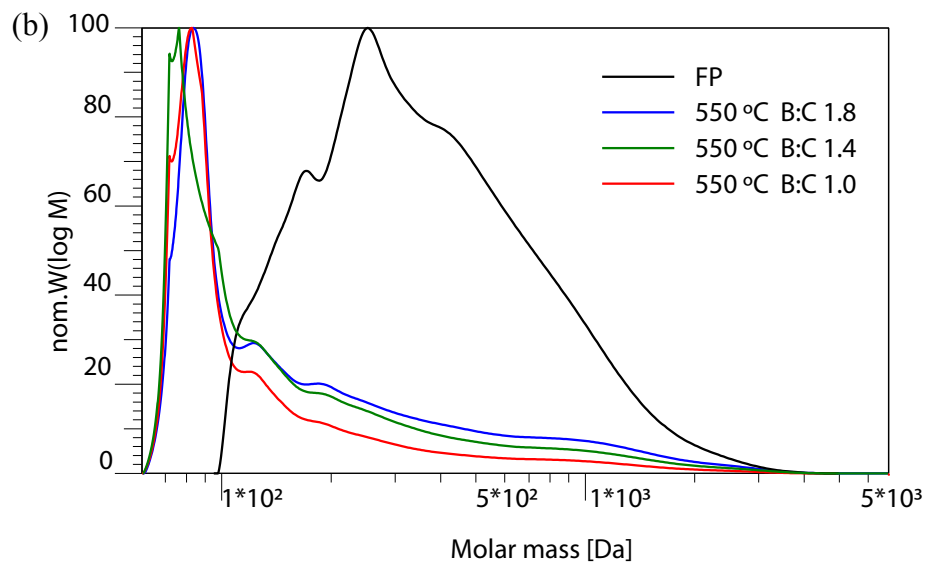
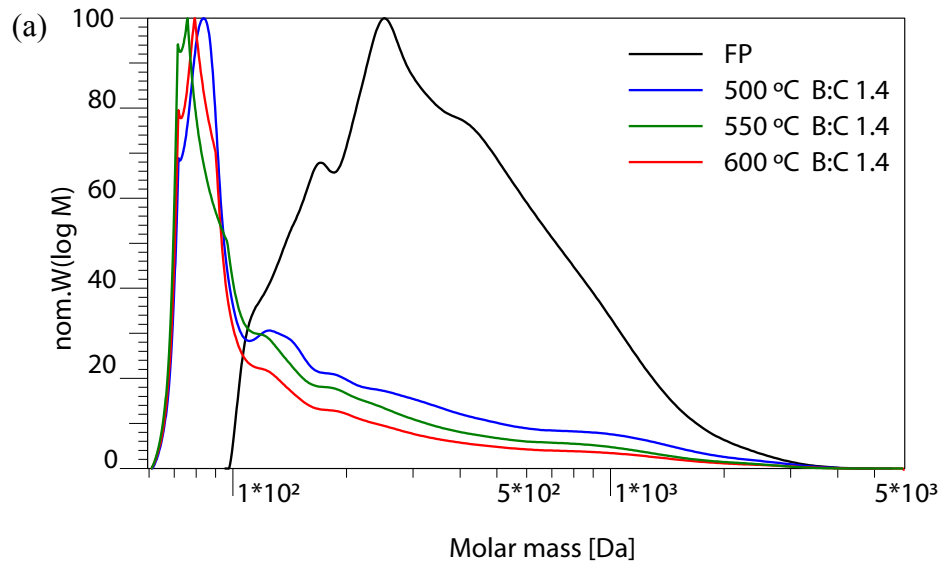
**Figure 51.** a) GC-MS analysis and b)  $^{13}\text{C}$  NMR analysis of the oils. The values are weight-averaged results of analyses of bottom and top oils. The GC-MS analysis shows the mass selectivity of the identified fraction, and the identified compounds constituted 25-43% of the oil. Other in GC-MS includes peaks for furans and ketones.



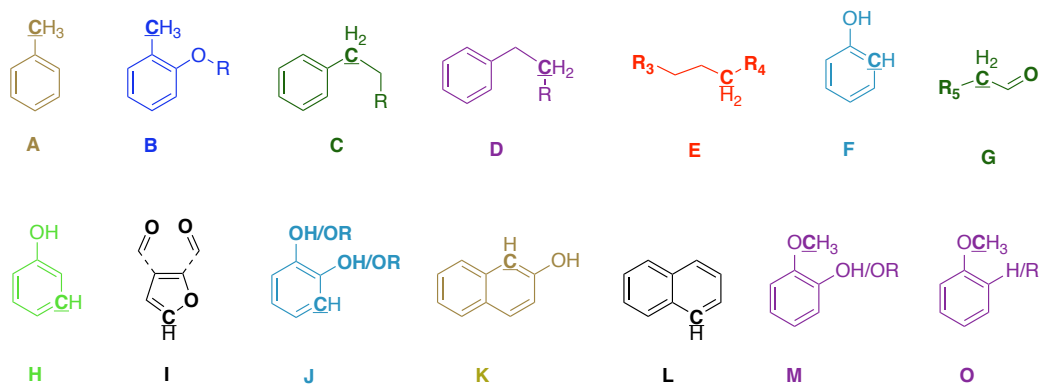
**Figure 52.** The effect of (a) upgrading temperature, and (b) B:C ratio on various hydroxyl groups of bio-oil. The values are weight-averaged results of analyses of bottom and top oils.



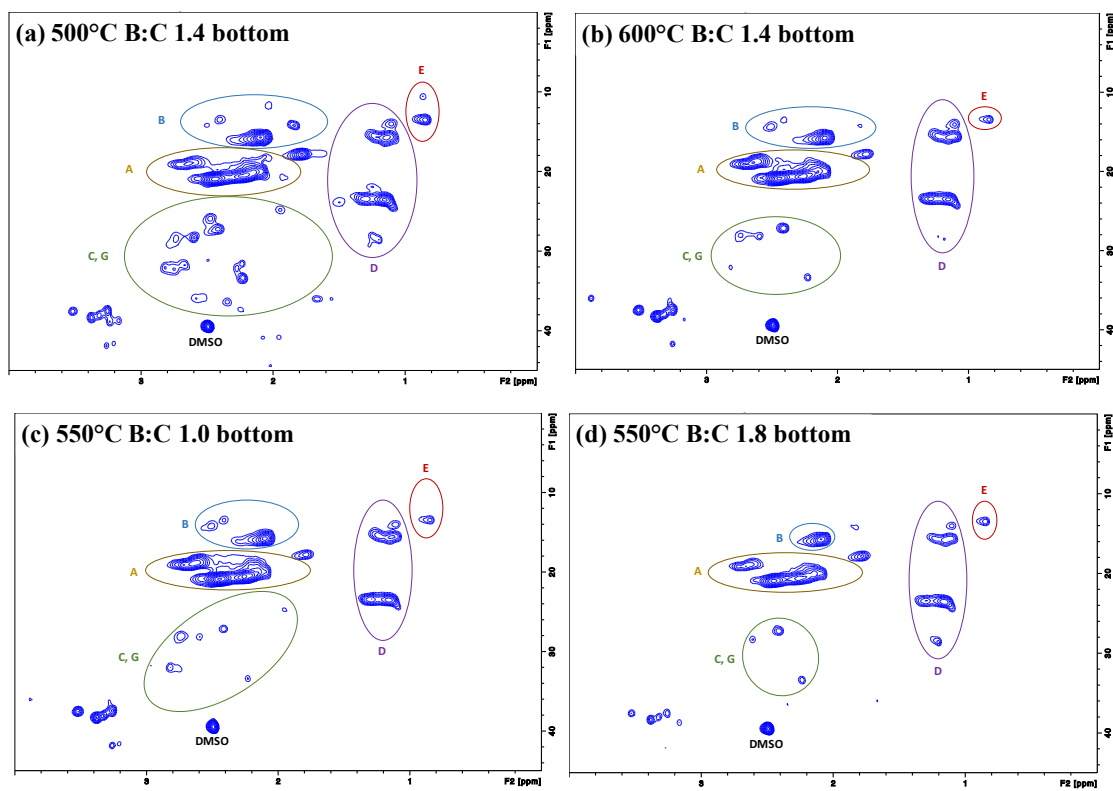
**Figure 53.** The effect of (a) upgrading temperature, and (b) B:C ratio on total aromatic hydroxyl groups in bio-oil. The values are weight-averaged results of analyses of bottom and top oils.



**Figure 54.** Molecular weight distributions for non-catalytic fast pyrolysis oil (FP) and bottom CFP oils. (a) different upgrading temperatures, and (b) for different biomass:catalyst (B:C) ratios.

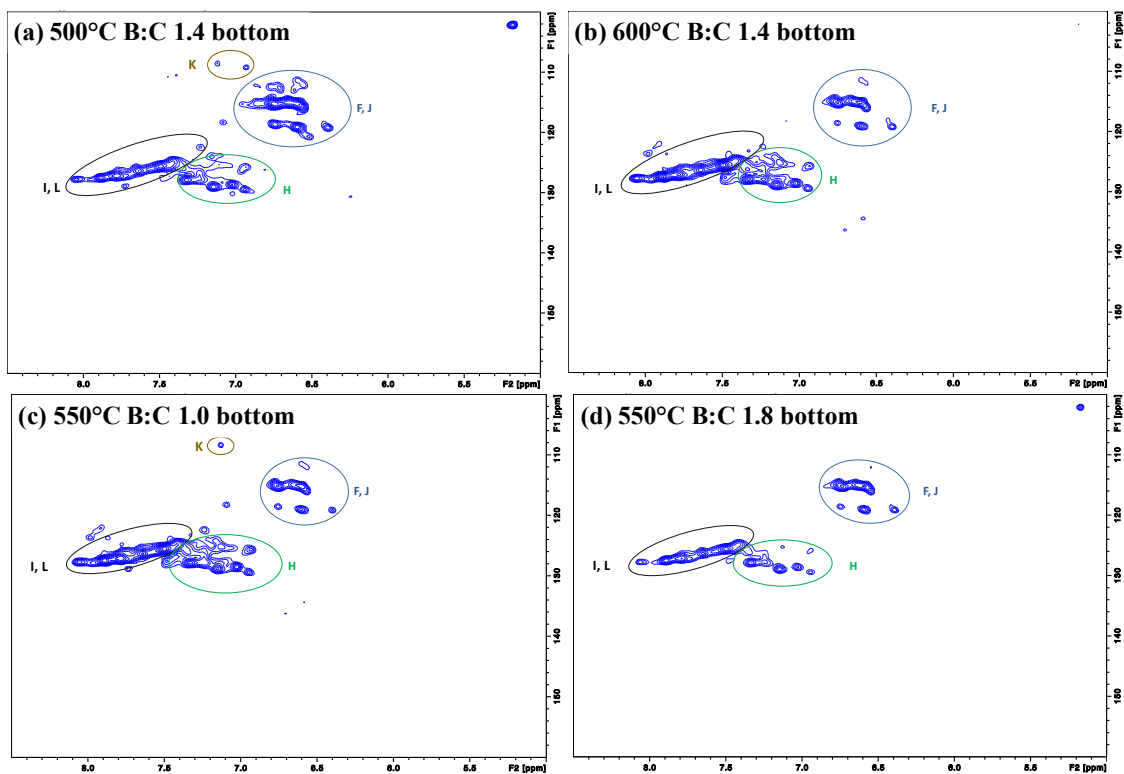


**Figure 55.** Detailed structures of assignments for HSQC-NMR analysis of bio-oil.

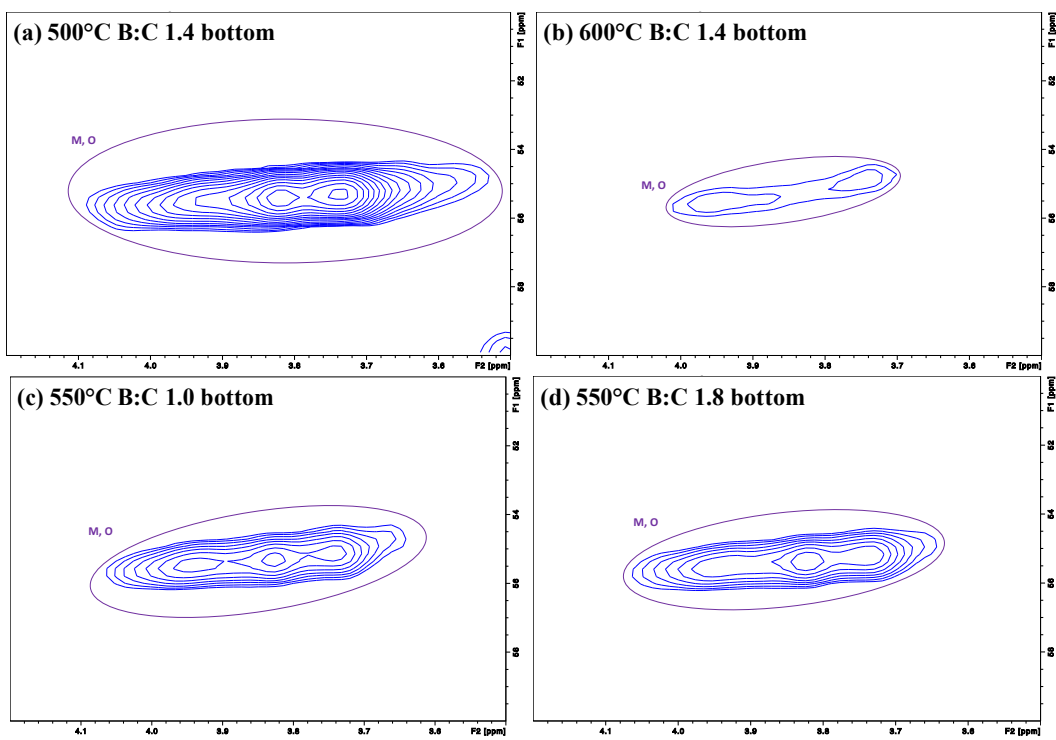


**Figure 56.** The aliphatic C-H bonds in the HSQC NMR spectra for selected bottom fractions of CFP oils. (a) 500°C B:C 1.4 bottom, (b) 600°C B:C 1.4 bottom, (c) 550°C B:C 1.0 bottom, (d) 550°C B:C 1.8 bottom.

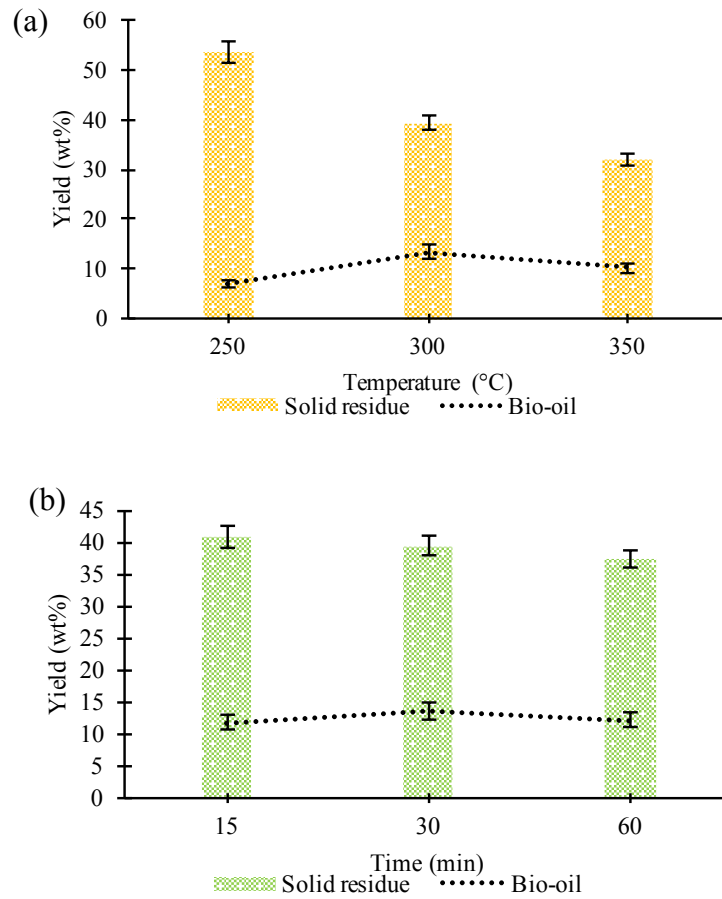




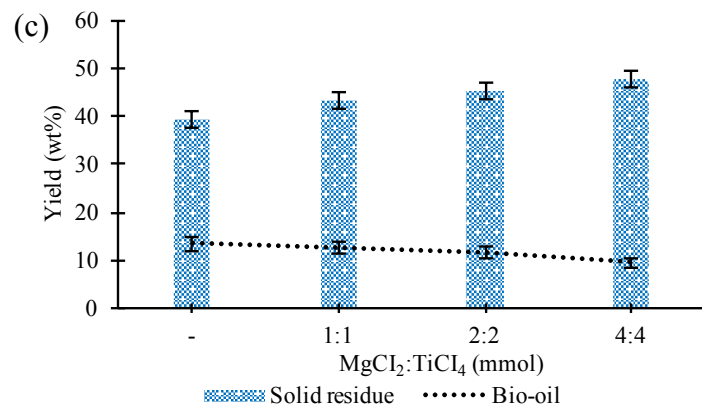
**Figure 57.** Aromatic C-H bonds in the HSQC NMR spectra. (a) 500°C B:C 1.4 bottom, (b) 600°C B:C 1.4 bottom, (c) 550°C B:C 1.0 bottom, (d) 550°C B:C 1.8 bottom.



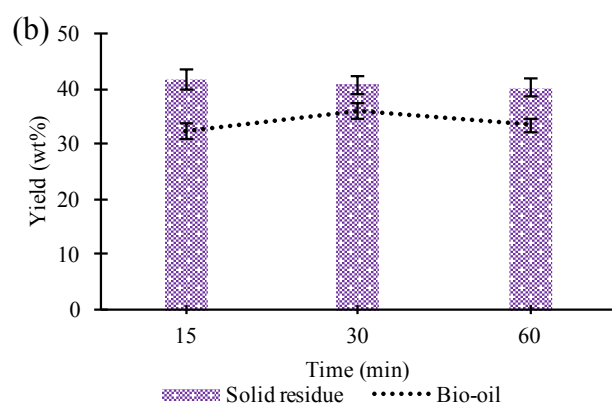
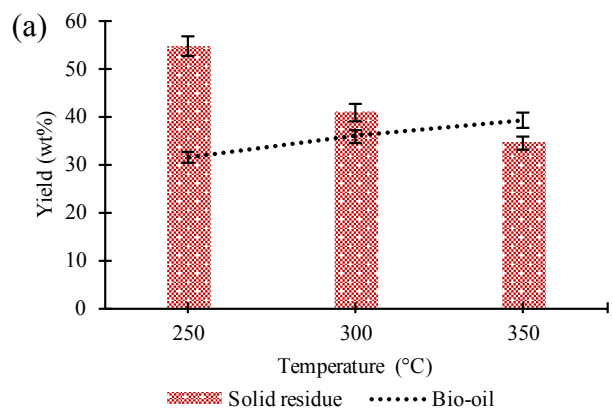
**Figure 58.** Methoxyl group in the HSQC NMR spectra. (a) 500°C B:C 1.4 bottom, (b) 600°C B:C 1.4 bottom, (c) 550°C B:C 1.0 bottom, (d) 550°C B:C 1.8 bottom.



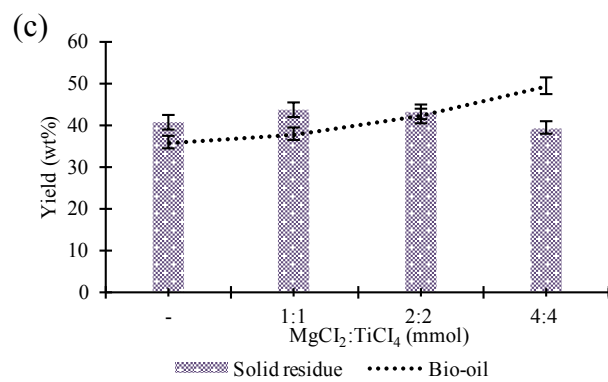
**Figure 59.** Bio-oil and solid residue yields obtained in hydrothermal medium. (a) residence time=30 min, without additives; (b) T=300 °C, without additives; (c) T=300 °C, residence time=30 min, with and without additives.



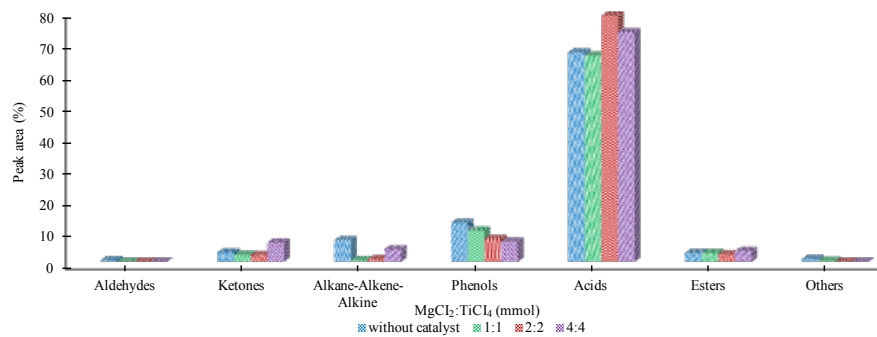
**Figure 59.** (Continued)



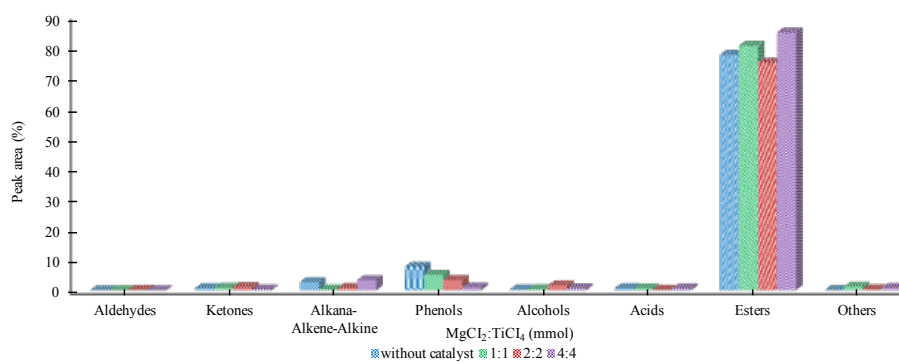
**Figure 60.** Bio-oil and solid residue yields obtained in supercritical ethanol.(a) residence time=30 min, without additives; (b) T=300 °C, without additives; (c) T=300 °C, residence time=30 min, with and without additives.



**Figure 60.** (Continued)

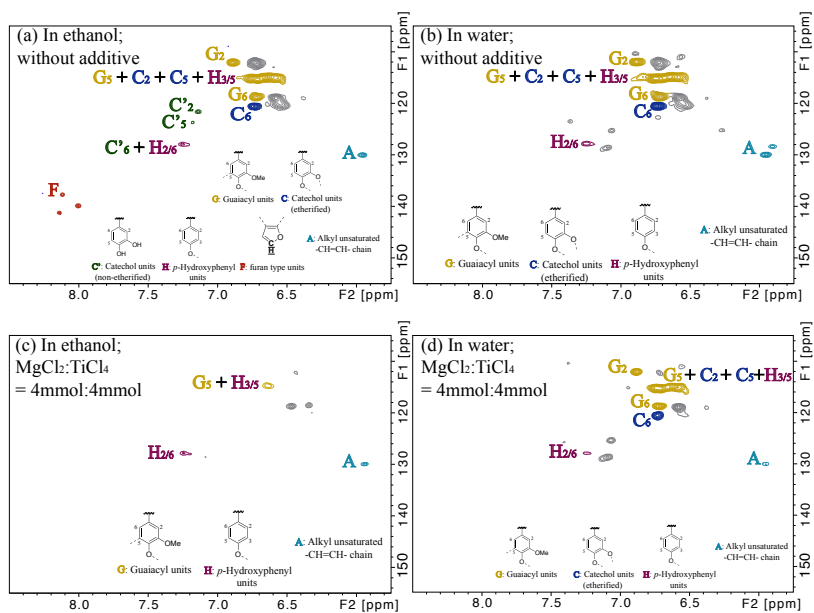


**Figure 61.** Chemical class composition of identified compounds in bio-oils from the hydrothermal processing of grape seed without and with  $\text{MgCl}_2:\text{TiCl}_4$ . ( $T=300\text{ }^\circ\text{C}$ ,  $t=30\text{ min}$ ,  $\text{PH}_2\text{int.}=2\text{ MPa}$ )

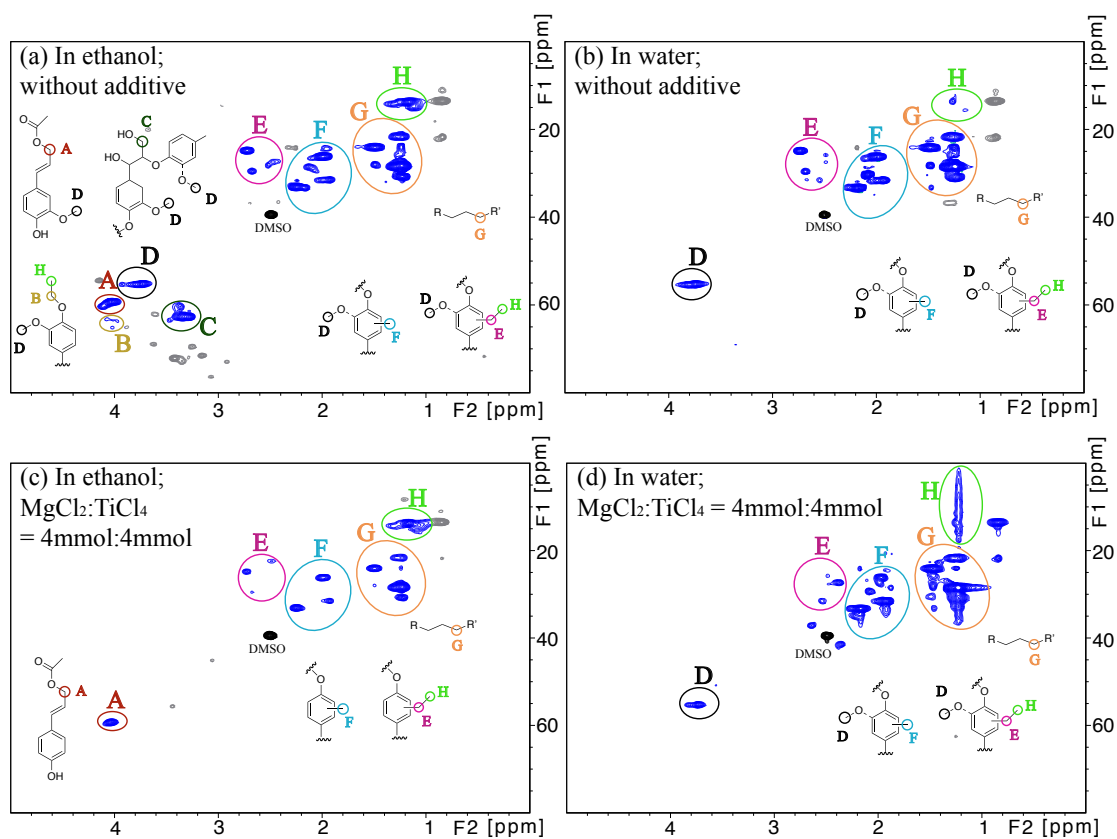


**Figure 62.** Chemical class composition of identified compounds in bio-oils from the supercritical ethanol processing of grape seed without and with  $\text{MgCl}_2:\text{TiCl}_4$ . ( $T=300\text{ }^\circ\text{C}$ ,  $t=30\text{ min}$ ,  $\text{PH}_2\text{int.}=2\text{ MPa}$ )

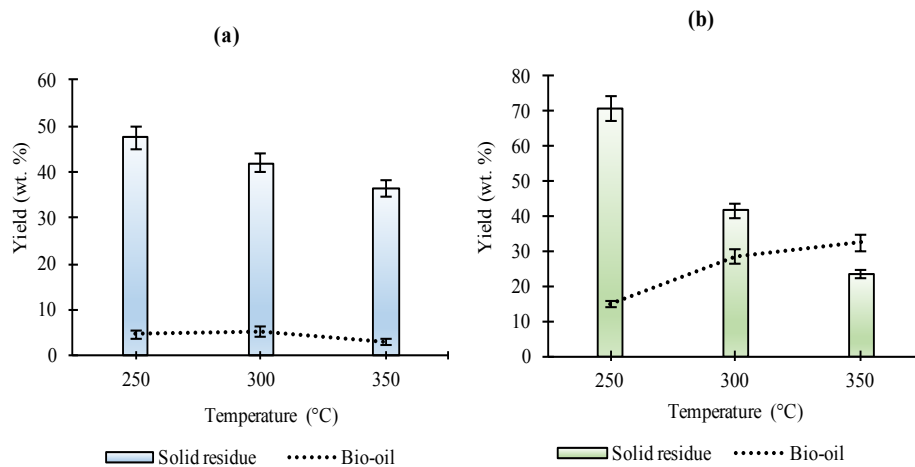




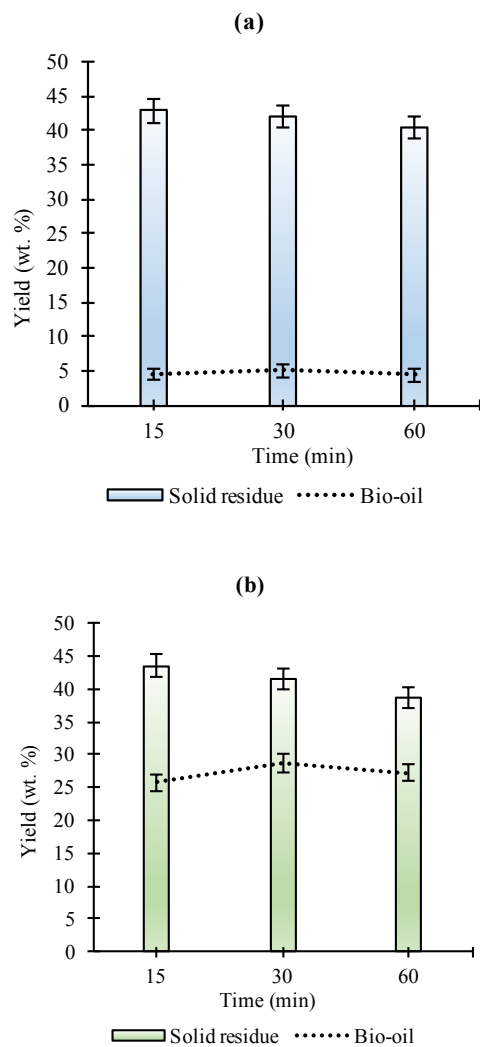
**Figure 63.** Comparison of the aromatic regions of the HSQC NMR spectra of the deconstruction products. (a) non-additive ethanol processing; (b) non-additive hydrothermal processing; (c) ethanol processing with 4 mmol MgCl<sub>2</sub>/TiCl<sub>4</sub>; (d) hydrothermal processing with 4 mmol MgCl<sub>2</sub>/TiCl<sub>4</sub>.



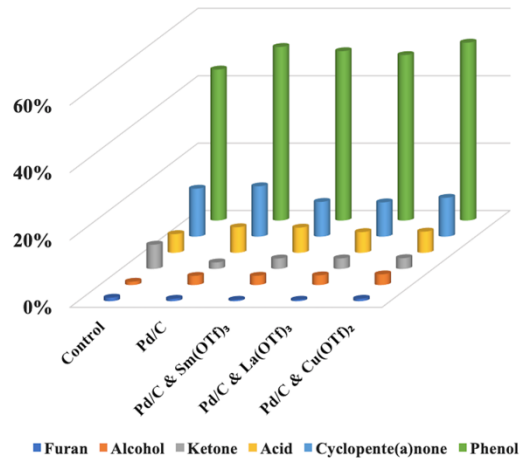
**Figure 64.** Comparison of the aliphatic regions of the HSQC NMR spectra of the deconstruction products. (a) non-additive ethanol processing; (b) non-additive hydrothermal processing; (c) ethanol processing with 4 mmol  $\text{MgCl}_2/\text{TiCl}_4$ ; (d) hydrothermal processing with 4 mmol  $\text{MgCl}_2/\text{TiCl}_4$ .



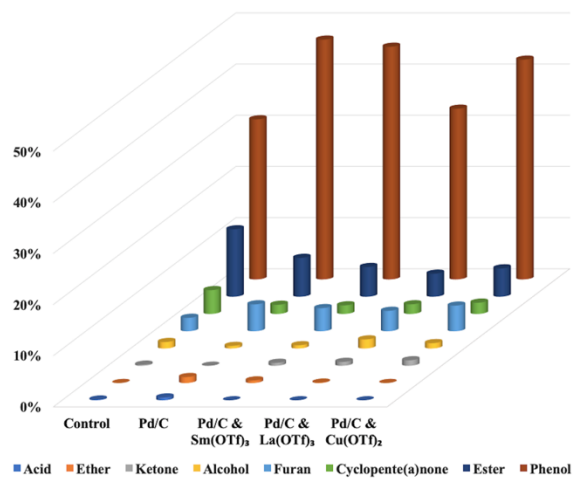
**Figure 65.** Effect of liquefaction temperature on bio-oil and solid residue yields derived from non-catalytic liquefaction of fir wood. (a) HTL media, and (b) SCEL media ( $P_{H_2int.}=2$  MPa,  $t=30$  min)



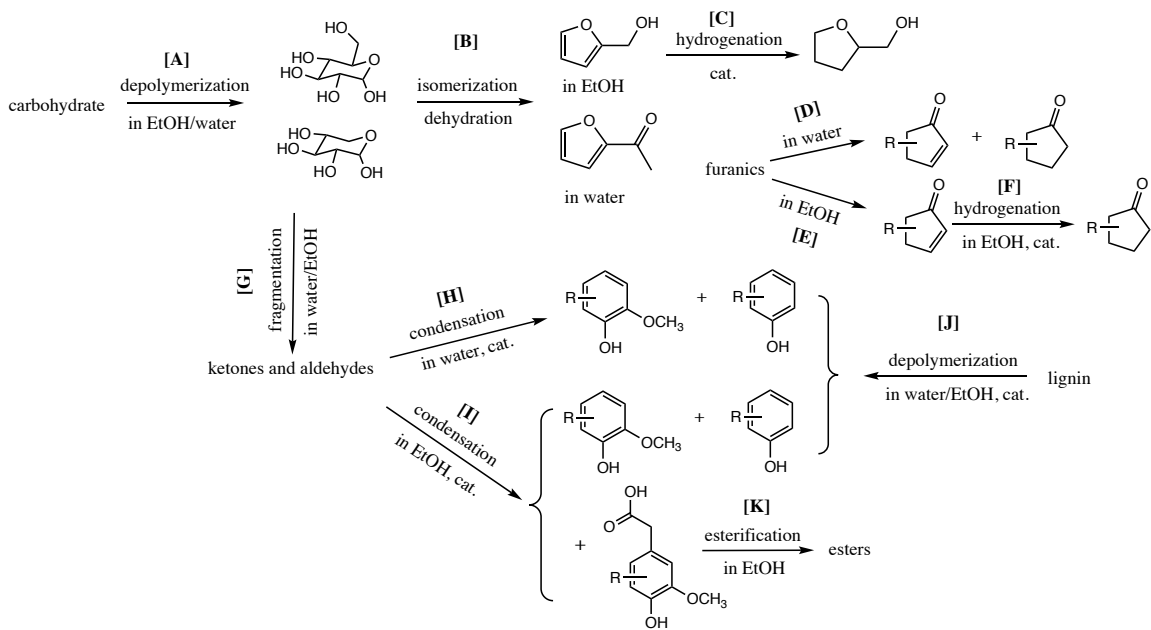
**Figure 66.** Effect of residence time on bio-oil and solid residue yields derived from non-catalytic liquefaction of fir wood. (a) HTL media, and (b) SCEL media. (T=300 °C, PH<sub>2int.</sub>=2 MPa)



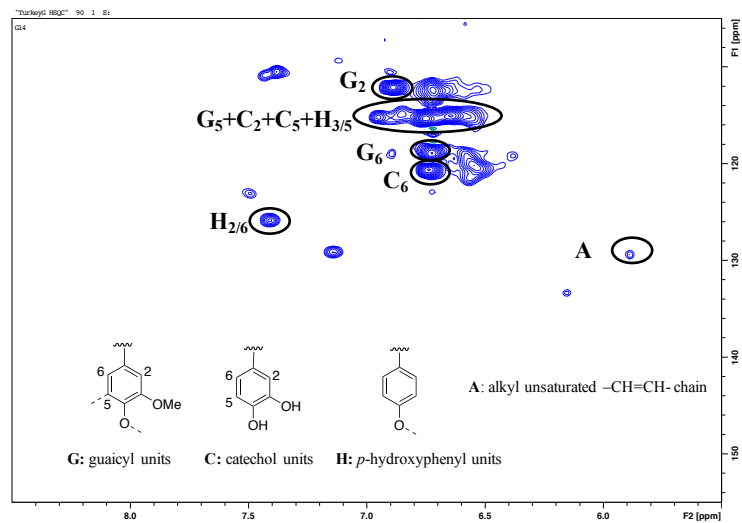
**Figure 67.** Chemical class composition of the identified compounds in the bio-crudes from HTL.



**Figure 68.** Chemical class composition of the identified compounds in the bio-crudes from SCEL.

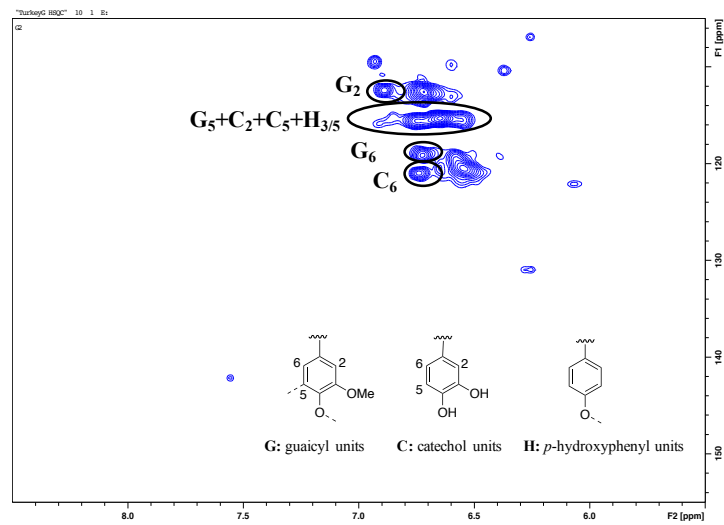


**Figure 69.** Plausible major reaction pathways for the liquefaction of lignocellulose in water and ethanol.

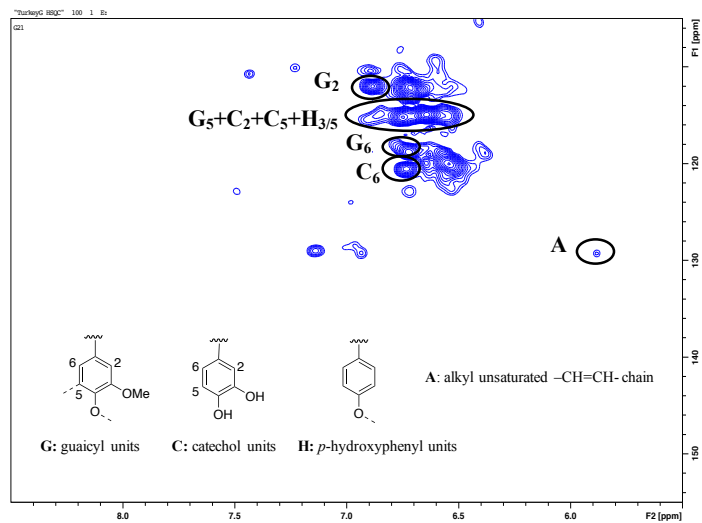


**Figure 70.** Aromatic C-H bonds in bio-oils from control HTL.

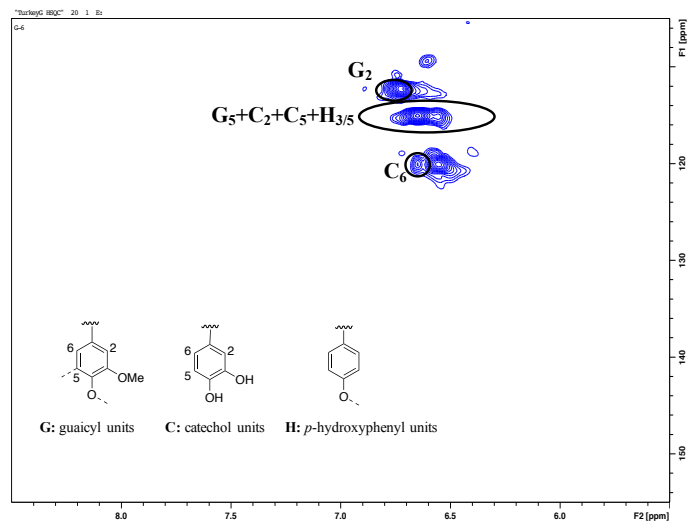




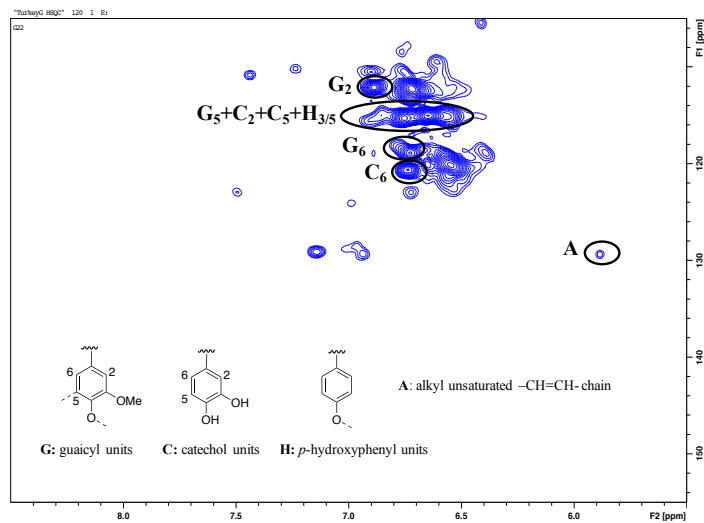
**Figure 71.** Aromatic C-H bonds in bio-oils from control SCEL.



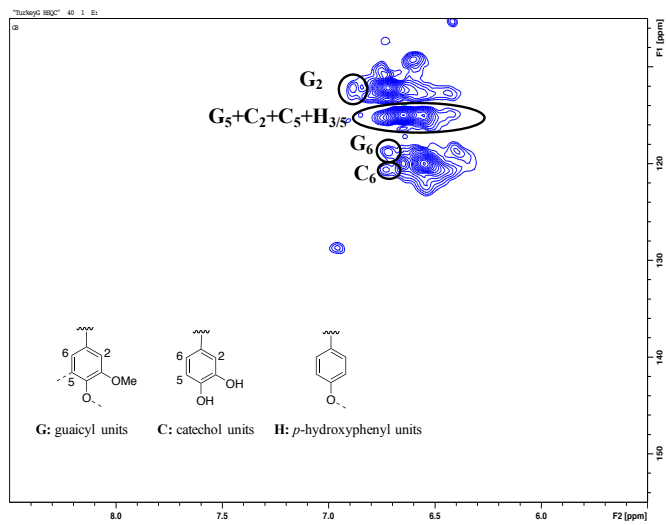
**Figure 72.** Aromatic C-H bonds in bio-oils from HTL over Pd/C.



**Figure 73.** Aromatic C-H bonds in bio-oils from SCEL over Pd/C.



**Figure 74.** Aromatic C-H bonds in bio-oils from HTL over Pd/C + Sm(OTf)<sub>3</sub>.



**Figure 75.** Aromatic C-H bonds in bio-oils from SCEL over Pd/C + Sm(OTf)<sub>3</sub>.

## VITA

Naijia Hao was born in Hefei, Anhui, China in 1992. After completion of high school education in Hefei No.8 High School, she moved north to Dalian University of Technology in 2010. She majored in Chemical Engineering in Dalian University of Technology and worked as an undergraduate research assistant in an organic synthesis lab. In 2014, She went to University of Tennessee, Knoxville to pursue her Ph.D. in Chemical Engineering under the guidance of Dr. Arthur Ragauskas. She successfully completed her dissertation defense in Feb 2020.